Department of Engineering

PhD Thesis

Advanced Laser Forming of Metallic Components

Thesis submitted in accordance with the requirements of The University of Liverpool for the degree of Doctor in Philosophy

By

HUI GAO

November 2021

HUI GAO
Laser Group
Department of Engineering
The University of Liverpool
Liverpool, UK
L69 3GH
Email: sghgao@liv.ac.uk

DECLARATION

I hereby declare that all of the work contained within this thesis has not been submitted for any other qualification.

Signed: Hui Gao

Date: 26/11/2021

Abstract

The work presented in this thesis mainly focuses on two manufacturing applications of laser forming technology, which are controlled direct laser forming of single and double curved metallic components.

Laser forming is a flexible incremental forming technology that can be applied for shaping or the correction of distortion in metallic components through the application of laser radiation, without the need for permanent dies or tools. The non-contact nature of the process has the advantage of no tool-wear, as well as sharing the high degree of flexibility associated with other laser-based processes such as cutting, marking and welding. A defocused laser beam as a heat source is employed to irradiate a material to thermally induce stresses in a component, the plastic deformation will occur when the induced thermal stress exceeds the temperature dependent yield stress. Laser thermal forming operations employ localized heating, this minimises any potential effects on other areas of a component, therefore a range of size and type of materials can be formed. Laser forming has the potential for applications in many manufacturing industries, such as automotive industry and shipbuilding.

The first study presented in this thesis is to develop an advanced scanning strategy to improve the controllability of the process and produce a two-dimensional component independent of material and process variability and this study is also to prove the manufacturing capabilities of the LF process at attempt was made to produce an actual car body component, which is linked to the Audi commercial project. The required ‘U’

shaped component with three different bending angles 20°, 40° and 60° from Audi AG was identified as an ideal candidate for laser forming.

For practical industrial applications, in addition to single curved shapes, most components have a double curved geometry, such as ship hulls, pillow shape, saddle shape etc. Therefore, it is necessary to consider 3D laser forming in order to advance the application of laser forming in the actual manufacturing environment. The second study presented in this thesis is the investigation of 3D laser forming. The component with a ship hull geometry was chosen for 3D laser forming investigation in this thesis, which is supplied by a ship building company.

Publications to Date by the Author

H. Gao, G. Sheikholeslami, G. Dearden, S. P. Edwardson

"Development of scan strategies for controlled 3D laser forming of sheet metal components" 9th International Conference on Photonic Technologies - LANE 2016

Gao, H, Sheikholeslami, G, Dearden, G and Edwardson, SP

"Reverse analysis of scan strategies for controlled 3D laser forming of sheet metal"
17TH INTERNATIONAL CONFERENCE ON SHEET METAL (SHEMET17)

H. Gao, G. Dearden, S. P. Edwardson

"LASER FORMING USING A HIGH BEAM QUALITY COMPACT FIBRE LASER"
2ND INTERNATIONAL CONFERENCE ON TEST, MEASUREMENT AND COMPUTATIONAL METHOD (TMCM 2017)

Acknowledgements

The author is extremely grateful and appreciative of all the contributions made and advice given that has made this work possible. In particular acknowledgements are given to the following people and organisations.

Firstly, I would like to thank my supervisors/advisors Dr Edwardson and Prof Geoff Dearden for initially accepting my application for a PhD student and through their continuing support throughout my studies.

I would also like to thank the laser lab manager Mr Andy Snaylam for all his hard work in setting up of experiment and in the preparation of samples.

To all the members of the Liverpool Laser Group thank you for making the time spent studying in the group a pleasurable experience.

And finally, a special thank you to the parents and wife of the author for their constant support and unwavering faith throughout the authors PhD and all past studies.

Contents

List of Figures

List of Tables

List of Symbols

Physical Quantities

C_p	Specific heat capacity
D	Laser beam diameter
D_L	Laser beam diameter before focus lens
D_t	Thermal diffusivity
d_s	Scan-line distance
E	Young's modulus
E_1	Pyrometer one
E_2	Pyrometer two
F_0	Fourier number
f	Focal length
H	Standoff distance
h	Convective heat transfer coefficient
K	Thermal diffusivity
L	Length of workpiece
L_h	Half-length of the heating zone
M^2	Beam quality factor
N	Number of passes
P	Laser power
P_0	Probability
q	Thermal heat flux density of laser beam
r	Radius of the laser beam
R^2	Coefficient of determination
SF	Flexural strength
T/t	Thickness of the workpiece
t_h	Thickness of heated volume
T_a	Ambient temperature
T_{max}	Maximum temperature
T_{pred}	Maximum predicted temperature
T_s	Sheet surface temperature
V/v	Laser scanning speed
w	Width of workpiece
W_0	Laser beam waist
α_b	Bending angle
α_{ave}	Average bending angle
α_{max}	Maximum bending angle
α_{min}	Minimum bending angle
α_{bpi}	Predicted bending angle
α_{bti}	Target bending angle
α_{th}	Coefficient of thermal expansion
β	Tolerance parameter
η	Absorptivity
ε_{max}	Maximum plastic strain of the heated surface

ρ	Density
μ	Poisson's ratio
σ_y	Yield stress
λ	Wavelength

List of Abbreviations

ANN	Artificial Neural Network
BM	Buckling Mechanism
CMM	Coordinate Measuring Machine
CNC	Computer Numerical Control
CO_2	Carbon dioxide
CW	Continuous Wave
DOF	Degree of Freedom
EDS	Energy Dispersive X-Ray Spectroscopy
FE	Finite element
FEA	Finite element analysis
FEM	Finite element method
FESEM	Field Emission Scanning Electron Microscopy
FSP	Friction stir process
FSW	Friction stir welding
HAZ	Heat affected zone
MLP	Multilayer perceptron
MSS	Mean Sum of Squares
Nd:YAG	Neodymium-doped yttrium aluminum garnet
OA	Orthogonal array
RBF	Radial basis function
RMS	Root mean squared
RVBA	Relative variation in bend angle
SS	Sum of Squares
TGM	Temperature Gradient Mechanism
UM	Upsetting Mechanism
BM	Buckling Mechanism
CM	Coupling Mechanism
UTM	Universal Testing Machine

Chapter 1

Introduction

The study presented in this thesis mainly focuses on two manufacturing applications of laser forming technology, which are controlled direct laser forming of single and double curved metallic components.

Laser forming is an incremental non-contact forming process used for flexible fabrication of metallic or non-metallic components of different shapes and shape correction by the controlled defocused laser beam induced thermal stress without any external load and tools [1].

In thermodynamics, the thermal stress is the mechanical stress generated by any change in temperature of the material. This stress can lead to plastic deformation of the material. The temperature gradients, thermal expansion or contraction are the factors that can lead to thermal stress, which is highly dependent on the thermal expansion coefficient of material. In general, the greater the temperature change, the higher the level of thermal stress will be generated [2].

The laser forming process is realised by introducing thermal stresses into the surface of a workpiece by heating the surface with a laser beam. These internal stresses induce plastic strains that result in local elastic-plastic buckling of the workpiece. Laser forming is a flexible incremental forming technology that can be applied for shaping or the correction of distortion in workpiece through the application of laser radiation,

without the need for expensive stamping dies or tools, which can reduce the cost of small batch production. In contrast with conventional forming techniques no mechanical contact is required for this process promoting the idea of 'virtual tooling'. The noncontact nature of the process has the advantage of no tool-wear, as well as sharing the high degree of flexibility integrated with other laser-based processes such as cutting, marking and welding, laser forming offers process the programmability and the possibility of automation. A defocused controlled laser beam as a heat source is employed to irradiate a material to thermally induce stresses in a component, the plastic deformation will occur when the induced thermal stress exceeds the temperature dependent yield stress [1,3,4,5].

Laser thermal forming operations employ localized heating, this minimises any potential effects on other areas of a component, therefore a range of size and type of materials can be formed, such as mild steel, stainless steel, titanium alloys, and aluminium alloys etc. [6,7,8,9,10]. These materials are widely used in the shipbuilding industry, automobile manufacturing industry, and aerospace industry where the implementation of laser forming as a replacement of existing manufacturing processes is under investigation [11,12,13,14].

In addition to the features mentioned above, the infrared thermometer or shape measuring instrument can be integrated in the laser forming system, enabling the laser forming to achieve full closed-loop control, thereby ensuring the quality of the workpiece and improving the production environment [15].

The overall deformation of laser forming of the workpiece is dependent on the heat input, geometry of workpiece, laser scanning strategy, and material properties. Heat input includes laser power, scan speed, spot size, absorptivity of the material etc. The parameters related to the workpiece geometry are length, width and thickness. Laser scanning strategy includes number of laser scans, scanning sequence in multi-scan process and scanning pattern. The performance of the process also depends on the temperature dependent thermal and mechanical properties of the material. The related thermal properties are coefficient of thermal expansion, thermal conductivity, specific heat etc. and mechanical properties are density, Young's modulus, Poisson's ratio, yield stress etc. [15,16].

Before the laser forming technology was invented, flame bending has been widely used in the profiling and straightening of heavy engineering components in the construction and shipbuilding industries. In flame bending the thermal stress is induced into the workpiece through the oxyacetylene torch. This process is completely manual, so the quality of the processing heavily relies on the skill of the operator. In addition, the heat of the flame is difficult to focus on a spot to create a steep thermal gradient, but the laser can produce a focused heating area on the surface of the workpiece, thereby greatly decreasing this problem [17,18,19]. Comparing the two heat sources, it can be seen that the flame is difficult to achieve precise control. However, the laser has a high energy density and degree of control, which can be used to form both larger and small size components. Therefore, the laser forming technology has great potential to instead of conventional flame bending in the construction and shipbuilding industry [3].

In the automotive industry, the deep drawing process is usually used to bend sheets and the high deformations rates can easily lead to cracks and ruptures in the bending area. Due to the temperature dependence of the yield strength, forming of the material will become easier at elevated temperature. Since forming only takes place at a local area of the workpiece, selective heating is sufficient and advantageous in most cases [20]. Laser selective heating offers the possibility of heating only the areas of the workpiece where the deformations are required. In addition, laser forming is a much more flexible process than deep drawing process with the ability to form any required bending angles at different positions on the workpiece only by programming the code of the Computer Numerical Control (CNC) machine tool and laser processing parameters [21]. However, like many other manufacturing processes, laser forming has also got some limitations, such as the process is somewhat slow, and not suitable for forming the deep and complicated products and components [22].

There are three main mechanisms of laser forming, which are the temperature gradient mechanism (TGM), the buckling mechanism (BM) and the upsetting or shortening mechanism (UM) [4]. The TGM produces a maximum bending angle of 0.1~3 degree per pass and the bending direction is always towards the laser [6]. For BM much larger bending angle of 1~15 degree per pass can be produced [6], however, when forming with this mechanism it is more difficult to control the magnitude and direction of the bends accurately [4,23]. If the workpiece is prevented from bending by either external forces or the geometry of the workpiece the UM can occur causing the workpiece to shorten in length and thicker along thickness direction in the laser

irradiated region [23]. For accuracy and consistency, the TGM is the most popular mechanism in laser forming. This is the main mechanism used in this thesis.

Based on the advantages and characteristics of laser forming described above, it can be seen that laser forming technology has great application potential in the fields of shipbuilding, automobile, aerospace, etc. However, up to date, the laser forming process appears to see very limited use by industry today compared to laser cutting, laser welding, and additive manufacturing due to that the reliability has not been completely verified.

The work presented in this thesis on 2D and 3D laser forming aims to prove the viability of this technique as a direct manufacturing tool. To date there has been a considerable amount of work carried out on two-dimensional laser forming, such as using multi-pass scanning strategies to produce a single curved shape. However, there is a limited understanding related to accuracy control the forming process to produce a target component.

Therefore, presented in this thesis are results of investigations into the 2D and 3D laser forming of metallic components. The first work presented in this thesis is to develop an advanced scanning strategy to improve the controllability of the process by controlling the bending angle rate to produce a two-dimensional component independent of material and process variability. A 2D laser sensor was employed to measure the bending angle after each pass and so an appropriate bending angle rate or the processing speed can be selected for the next pass based on the difference between the current and target bending angle. In addition, the study also proved the

manufacturing capabilities of the laser forming process at attempt was made to produce an actual car body component, which is linked to the Audi commercial project. The required 'U' shaped component with three different bending angles 20°, 40° and 60° from Audi AG was identified as an ideal candidate for laser forming.

For practical industrial applications, in addition to simple 2D shapes, most components have a double curved 3D geometry, such as ship hulls, pillow shape, saddle shape etc. Therefore, it is necessary to consider 3D laser forming in order to advance the application of laser forming in the actual manufacturing environment. The second work presented in this thesis is the investigation of 3D laser forming. The component with a double curved geometry was given by a shipbuilding company, the details of the size of the component was presented in the chapter 3, which was chosen for 3D laser forming investigation in this thesis. In theory, laser can be used as a heat source to form any size of plate, which is depending on the laser power and beam spot size. For a given shape with large deformation, one-off single pass would be extremely difficult to predict and control. Therefore, the purpose of the second study presented in this thesis is to develop a more sensible method to produce an accurate repeatable 3D shape independent of residual stress distribution and non-uniformity absorption of the laser radiation and to take account of any unwanted distortion either caused by above two factors or process variability.

Chapter 2

Literature Review

Recently, the laser forming technology and potential applications has been investigated by various researchers. This chapter presents the review of literature on the laser forming process. It contains the literature study on laser forming mechanisms, state of art in parametric study in laser forming, state of art in mechanical and microstructural properties study in laser forming, state of art in edge effect study, state of art in modelling of laser forming process, state of art in 2D and 3D laser forming, and previous laser forming research within the laser group at the University of Liverpool.

2.1 Laser Forming Mechanisms

Because of the good control offered by the laser beam, through control of process parameters (laser power, scanning speed and laser spot diameter) according to the workpiece geometry and material properties, different types of temperature fields can be generated, yielding different laser forming mechanisms and bending results. Laser forming is usually associated with three main forming mechanisms: the temperature gradient mechanism (TGM), the buckling mechanism (BM) and the upsetting mechanism (UM). There is a fourth mechanism, the coupling mechanism as a combination of TGM and UM identified by Shi et al. is also discussed here [23].

2.1.1 Temperature Gradient Mechanism

Geiger and Vollertsen proposed the temperature gradient mechanism (TGM) in 1993, which is defined by inducing a steep temperature gradient through the thickness of the material [4]. TGM is the most common mechanism in laser forming. It is generated when the laser beam diameter is the same order of the workpiece thickness and coupled with high scanning speeds resulting in a steep temperature gradient across the thickness of the workpiece [24,25,26,27,28]. The mechanism can be described in two stages, viz., heating, and natural cooling of the workpiece, as shown in Figure 2.1.1. The first stage is the heating stage, in which the heat is introduced at the surface of the material by using a laser.

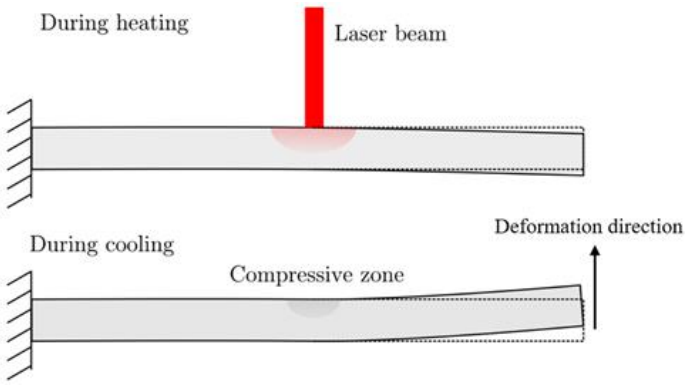

Figure 2.1.1 The two stages of the temperature gradient mechanism (TGM) [29]

Heating stage: During heating, a localized thermal expansion occurs in the heated region at the top surface of the workpiece, which results in a bending of the workpiece away from the laser beam termed counter bending. The localized expansion is resisted by the surrounding colder material. This resistance creates plastic compressive strains in the heated region.

Cooling stage: When the laser is removed, the workpiece begins to cool down and the bending direction is towards the laser beam. This is due to the contraction of the local expansion, but the plastic compressive state remains, which cause the workpiece to bend towards the laser beam.

A keynote of the temperature gradient mechanism is the steep temperature gradient that exists through the thickness during the heating phase.

Lawrence et al. [6] conducted the experiments on single-pass laser forming. They observed that in a single pass, the range of the bending angle was between 0.1° to 3°. Wang et al. [30] studied the thickening phenomenon of a metal laminates (stainless steel/carbon steel laminates (SCLP)) during the laser bending process. The SCLP is composed of the matrix layer of a carbon steel, whose both sides are covered by stainless steel layers. They observed that for stainless steel layer on the top, its thickness size changed from 91 to 102μm after laser bending, and for carbon steel layer, the thickness size changed from 630 to 657-714 μm at 10º to 40º bending angles. Researchers argued that the thickening phenomenon is caused by the thermal and plastic deformation effect.

2.1.2 Buckling Mechanism

The buckling mechanism (BM) was developed in 1993 by Geiger and Vollertsen [4], which is achieved by using large beam diameters relative to workpiece thicknesses (approximately ten times of the sheet thickness) [26] coupled with low scanning speeds typically result in a small temperature gradient across the thickness of the workpiece

and elastic-plastic buckling resulting in the bending of the workpiece towards or away from the laser beam [23,26,31], as shown in Figure 2.1.2. BM also occurs when a thin sheet with higher thermal conductivity is scanned by using slow scanning speed with a relatively high power, resulting in a high thermo-elastic strain in the material [32,33].

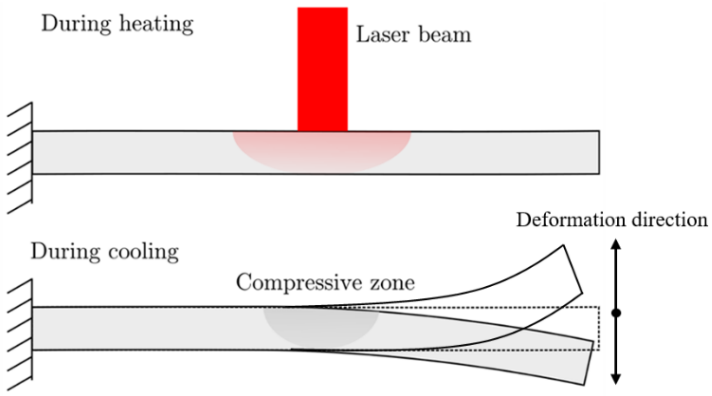

Figure 2.1.2 The two stages of the buckling mechanism (BM) [29]

The bending process in BM comprises the following steps:

Heating stage: During heating, a larger localized expansion occurs through the thickness of the material. This produces in compressive stresses in the heated region due to constrains by the bulk of the material. If the heated region is large enough, a small deviation from perfect flatness in the workpiece creates instability.

Cooling stage: As the laser is removed, the material begins to cool down. The expanded material contracts, yet the plastic compressive state remains. Due to the larger compressive zone, a buckling instability can occur, which can cause bending both towards and away from the laser beam. The direction of the bending is determined by a number of factors, such as laser parameters, workpiece geometry, internal and external stresses (gravitation forces), the pre-bending of the sheet and the relaxation of residual stresses [34,35,36,37].

Chakraborty et al. [38] performed experiments and finite element (FE) modeling to form the 25mm diameter, 1mm thick AISI 304 stainless steel flat circular plates to the bowl shape by using a 2 kW Yb fiber laser. The irradiation time was varied from 1 to 4 s, the laser beam diameter was varied from 6 to 12mm and keeping the laser power as 300 W. They observed that the plates bent more with longer irradiation time and larger laser beam diameter at constant laser power. The longer irradiation time and larger laser beam diameter resulted in a small temperature gradient across the thickness of the plate and elastic-plastic buckling, which activated the buckling mechanism.

2.1.3 Upsetting Mechanism

The upsetting mechanism (UM) was introduced in 1993 by Geiger and Vollertsen [4] and it is activated when the laser beam diameter is of the same order or greater than the plate thickness, the scanning speed is low, and the geometry of the part does not allow buckling of the material [39]. In addition, a relatively high thermal conductivity material facilitates the activation of UM [22]. In the upsetting mechanism, the workpiece is heated nearly homogeneously across its thickness by using a low scanning speed [40]. The heating and cooling stages of the upsetting mechanism can be seen in Figure 2.1.3.

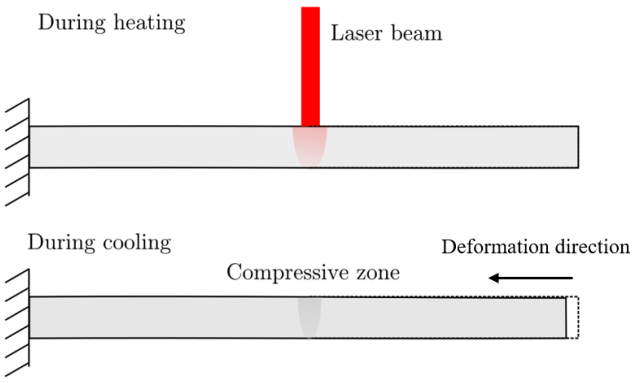

Figure 2.1.3 The two stages of the upsetting mechanism (UM) [29]

In the heated region, the flow stress decreases with increasing of the temperature and the thermal expansion approaches the elastic limit of the material. Since the free expansion of heated material is restricted by the surrounding material, further heating will lead to plastic compression. Therefore, a large amount of the thermal expansion is converted into plastic compression. The plastic compression then remains during cooling causing the heated region to contract with an almost constant strain along the thickness due to a nearly homogeneous temperature field across the plate thickness, which results in a localised shortening and an increase of local thickness. Hence, upsetting mechanism is also known as shortening mechanism [6,23,26,28]. Shi et al. [40] proposed that a more uniform temperature gradient through the thickness can be created by heating both upper and lower surface with identical settings.

It is worth noting that as a temperature gradient is impossible to be avoided in practice by using a single laser heat source, this mechanism will always result in a small amount of bending.

2.1.4 Coupling Mechanism

The coupling mechanism (CM) was introduced by Shi et al. in 2006 [23] and it is a special mechanism as it is a combination of TGM and UM. Under TGM of laser forming generate out-of-plane deformation or bending, and UM-induced laser scans produce in-plane shortening. It is worth noting that it is not possible to achieve pure TGM and UM under typical conditions [23,36]. The heating and cooling stages of the coupling mechanism can be seen in Figure 2.1.4.

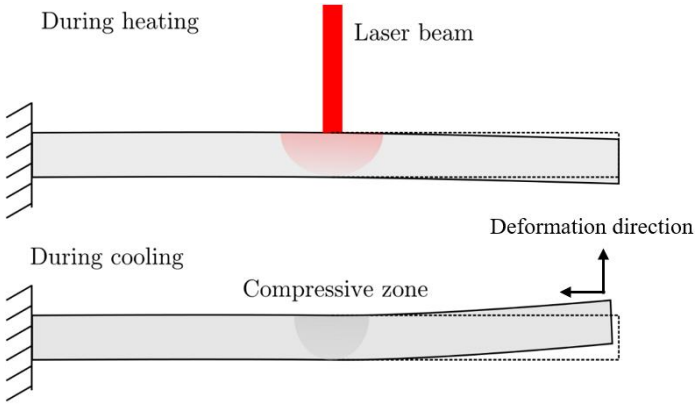

Figure 2.1.4 The two stages of the coupling mechanism (CM) [29]

Heating stage: A localized expansion through the thickness of the material will be generated during heating. The localized expansion is largest at the surface, but also occurs through the thickness. The expansion is hindered by the surrounding colder material, which creates plastic compressive strains in the heated region.

Cooling phase: As the laser is removed, the material begins to cool down causing the expansion to contract, yet the plastic compressive state remains during cooling. Due to the higher temperature at the upper surface, bending occurs towards the laser beam. As there is also a compressive state at the bottom, shrinkage (upsetting) is also achieved.

The different laser forming mechanisms are dependent on the type of process parameters used. Thus, in laser forming, the appropriate forming mechanism needs to be determined in order to choose the process parameters according to the geometry of the workpiece and the target shape. Fourier's number is an important value to predict the process parameters settings under certain forming mechanisms, which is a value combined of thermal diffusivity of the material, laser beam diameter, plate thickness and laser scanning speed.

2.1.5 Fourier's number

Fourier number is the dimensionless quantity used in the calculation of unsteady-state heat transfer, which is the ratio of the rate of heat conduction to the rate of heat stored in a body [41]. In the laser forming process, the Fourier's number can be used to differentiate between TGM and BM or UM [23,42]. For continuous mode laser, the Fourier's number is given by Shi et al. [23] and Chakraborty et al. [42] as:

$$F_0 = \frac{kd}{t^2 v}$$

Equation 2.1.1

where k, d, t and v are the thermal diffusivity, the laser beam diameter, the thickness of the workpiece and the laser scanning speed respectively.

In laser forming, TGM dominates when $F_0 < 1$, and BM or UM dominates when $F_0 > 1$. It can be noted that the Fourier's number cannot differentiate between BM or UM by itself, however the laser beam diameter can be used as a rule of thumb to differentiate between BM and UM. BM dominates in larger laser beam diameters (d)

approximately ten times of the sheet thickness (t), and UM dominates when the beam diameter is approximately the same order of the sheet thickness [26,42,43].

From Equation 2.1.1 it can be found that in the process of laser forming of a given workpiece, the different mechanisms can be converted to each other by changing the beam diameter or the scanning speed.

2.2 State of Art in Parametric Study in Laser Forming

The laser forming process is affected by various factors and process parameters. Many researchers have studied the effects of the process parameters on laser forming [44-88]. These process parameters can be classified into four categories:

1. Laser process parameters: The laser process parameters include laser power, scanning speed, laser beam diameter and number of laser passes. Laser forming process is strongly influenced by laser process parameters because this process is associated with heating by laser, and different parameters setting provide different heat input.
2. Workpiece geometry parameters: The type of the process parameters setting can be predicted according to the size of the workpiece and the target shape, and the size of the workpiece will influence the bending results under the same process parameters. The most important parameters are length, width and thickness.
3. Material properties parameters: The material properties of the workpiece play a key role in the laser forming process, which includes the mechanical and thermal properties as well as absorptivity.

4. External constraint parameters: The external constraint parameters include forced cooling, external mechanical load, and clamps.

2.2.1 Laser Power

In general, the bending angle is increased with increasing of the laser power for a given beam diameter and scanning speed [44,45,46], however after attaining a saturation point, the bending angle decreases with further increasing of the laser power [6]. The reduction in bending angle is due to two possible reasons. Firstly, a too great heat across the thickness of the material will be built up with further increasing of the laser power, which will reduce the temperature gradient between the surfaces. This reduction in the temperature gradient will trigger the BM instead of the TGM [47]. Another possible reason is the coating interaction since at higher power the absorptive graphite coating may degrade or burn off more readily, which will cause insufficient heat transfer to the substrate. Therefore, the process efficiency will be decreased, and the workpiece will be melted rather than plastic deformation with further increasing of the laser power [17,48]. In addition, Lawrence et al. [6] and Edwardson [15] suggested that a threshold heat input was need in the process, below which no bending occurs.

2.2.2 Scanning Speed

The scanning speed is one of the key parameters to control the heat input in the laser forming process. Vollertsen and Rodle [24] indicated that the heat input per unit length and the temperature variation through the thickness of the workpiece can be controlled

by the scanning speed. The heat input per unit length decreases with the increasing of the scanning speed for a given laser power, which will lead to the reduction in the bending angle. The reason for this is that the high scanning speed gives a shorter interaction time between the surface of the workpiece and the laser beam. The short interaction time leads to the reduction in the peak temperature and plastic deformation in the heated region [49,50].

Chen and Xu [44] conducted the laser forming experiments on 100μm thickness of full-hard 301 stainless steel to analyse the effect of the scanning speed on the bending angle. They found that the bending angle decreased from 0.06° to 0.02° with increasing of the scanning speed from 7mm/s to 27mm/s. The reduction in bending angle was attributed to decreasing of the energy per unit time transferred to the metallic workpiece.

Li and Yao [51] conducted the experiments on low carbon steel AISI 1010 to study the effect of different combinations of laser power and scan speed on bending angle under the constant line energy of 10 J/mm and the constant peak temperature of 1030℃ at the top surface of the workpiece, respectively. They observed that the bending angle was larger at higher scanning speed when the line energy (the ratio of the laser power to the scanning speed) was kept constant. The bending angle increased from 0.65° to 2° with increasing of the scanning speed from 40mm/s to 140mm/s. They also found that the peak temperature at the top surface of the workpiece increased from 675℃ to 1350℃ with increasing of the scanning speed from 40mm/s to 138mm/s when keeping the line energy constant, and the temperature difference between the top and bottom surfaces increased from 275℃ to 900℃. In addition, they observed that the bending

angle decreased from 1.4° to 1° with increasing of the scanning speed from 80mm/s to 160mm/s when keeping the peak temperature constant at the top surface of the workpiece. This is because that under the condition of constant peak temperature, the laser power still increase with increasing of the scanning speed but does not increase as fast as under the condition of constant line energy [51].

Barletta et al. [52] analysed the effect of scanning speed on the bending angle in Al_2O_3 coated and uncoated AA6082-T6 thin sheets. They observed that the bending angle increased with increasing of the scanning speed at high laser power. The reason for this is that the AA6082-T6 has relatively high thermal conductivity (180 W/mK) and the workpiece is very thin (0.1mm), thus if the slow scanning speed is employed which gives a longer interaction time between the surface of the material and the laser beam. The long interaction time leads to the thermal energy dispersing through the depth of the material, which in turn leads to a greater decrease in temperature gradient through the thickness of the sample. This leads to the BM dominates in the process instead of the more desirable TGM resulting in the reduction in the efficiency of the process [52].

2.2.3 Laser Beam Diameter and Geometry

The geometry of the laser beam is one of the important parameters for controlling the heat flux density. The geometry of the laser beam includes the area and shape of the laser beam spot. The laser beam shape can be circular, which is a very common laser beam, but also line, rectangle, triangle, star, donut, d-shape, cross, etc. through beam

shaping. The power density (the ratio of the power to laser beam area) is inversely proportional to the laser beam diameter. The power density decreases with increasing of laser beam diameter for a given power. Kant et al. [43] and Chen et al. [44] studied the effects of different laser beam diameters in laser forming process under the condition of TGM through experiments and FE Modelling. They observed that the bending angle decreased with increasing of laser beam diameter at a constant laser power and scanning speed. This is because that the energy input decreases with increasing of the beam diameter for a given laser power and scanning speed.

Safdar et al. [53] investigated the effects of circular, rectangular, triangular, and donut beam shapes on laser bending of tubes through experiments and finite element modelling. They found that the maximum temperature attained was for the triangular laser beam (1520 K) followed by circular laser beam (1517 K) and the rectangular laser beam (1337 K). This is because that the triangular laser beam has longer dimension in the scanning direction with respect to its lateral dimension, attained higher temperature for the same power density due to longer interaction time. However, the thermal behavior of the donut laser beam is quite different from other laser beam shapes, which allows the material to cool during the scanning cycle due to its hollow core. As the laser beam scans the temperature starts to rise when the solid portion of the laser beam moves on the material and then the temperature drops when the hollow part moves on the material and then rises again when the solid portion of the laser beam interacts with the material again.

Sheikh and Li [54] studied the effect of non-conventional laser beam geometry on material processing by finite-element modelling. They found that the specific laser beam geometry had an advantage for the specific laser material processing, such as the triangular and rectangular laser beams were beneficial for the laser transformation hardening process due to the lower heating rates; the rectangular laser beam was beneficial for the laser melting/brazing process due to the uniform cross-sectional melt pool profile; the triangular laser beam was beneficial for the laser glass cutting process due to the minimum cut path deviation.

Jamil et al. [55] studied the effects of different laser beam geometries on laser bending of sheet metal under the condition of temperature gradient mechanism. They observed that the bending angle, radius of bending edge (radius of curvature) and edge effect can be controlled significantly by the geometry of the laser beam. The square laser beam produces the highest bending angle followed by rectangular, triangular. This is because that the laser beams with a narrow leading edge are preferable to produce bending angle compared to the ones with wider leading edge. In terms of the scanning line curvatures, rectangular laser beam produces the highest distortion. This is because that a wider beam produces bending with a large bend radius, while a narrower beam produces a smaller bend radius. The triangular laser beam can be used to reduce the edge effect in the laser forming process, which is seen as the best beam for the high accuracy tolerance needed applications. The detailed discussion of the edge effects is presented in the section 2.4.

2.2.4 Number of Laser Scans

As mentioned earlier, the typical bending angle per pass is in the range of 0.1° to 3° under the condition of TGM [6]. Therefore, multiple scanning is required for achieving large bending angle in the laser forming process. Lawrence et al. [6] and Edwardson et al. [56] observed that the cumulative bending angle increases with increasing of the number of scans. However, the bending angle per pass increased at a high rate initially, and then gradually drops off, but has an amount of fluctuation between each pass. Wu et al. [57] conducted the experiments and simulation on laser bending of silicon sheet with three different thicknesses (0.1mm, 0.2mm and 0.3mm) and had the similar observation. They indicated that the falloff in the bending angle per pass could be attributed to a number of factors including strain hardening in the HAZ (a thicker material is harder to form), section thickening along the bending region (reducing the ductility of the material), absorptive coating degradation (reducing the absorption of laser radiation) and laser beam geometrical changing [15,16,45]. As the workpiece deforms the outside of the bend cold works and the orientation of the dislocations in the material are changed, which results in strain hardening [15,16]. In the laser forming process, the plastic compression leads to the upper layer thicken along the bending region [19,58]. The surface coatings as graphite will burn off with increased laser beam interaction time or multiple passes over the same track, which will reduce the absorption of laser radiation resulting in decreasing of the bending angle per pass [5,15]. In the multi-pass laser forming process, it is important to select the appropriate process parameters and cooling conditions to obtain good bending results.

Otherwise, the surface of the workpiece may melt due to the accumulation of the temperature after each pass [59]. Griffiths et al. [60] observed that the changing in absorptive coating and laser beam geometry become dominant on bending results as the number of laser scans increases. On the other hand, Kant and Joshi [61] studied the multi-pass laser forming of M1A magnesium alloy sheets by experiments and numerical simulation. They found that although the peak temperature on the upper surface of the sheet increases with increasing of the number of laser scans, the temperature difference between upper and lower surface decreases. This is due to insufficient cooling time between two consecutive laser passes.

2.2.5 Workpiece Geometry

The geometrical parameters such as the length, width and thickness of the workpiece will influence the bending results, of which the thickness is the most critical parameter, it will directly determine the temperature variation along thickness of the workpiece. A number of researchers have reported the effects of workpiece geometry on laser bending results [4,42,45,62,63,64,65,66].

Chakraborty et al. [42] developed a process to form both concave and convex sides of the mechanically bent stainless steel specimens by using a laser through experiments and numerical simulations. They observed that the bending angle was prominently larger while applying the laser on the convex side than on the concave side.

Geiger et al. [4] and Lee et al. [62] found that the bending angle changed approximately inversely proportional to the square of the workpiece thickness, and the

three laser forming mechanisms were related to the thickness, such as increasing in the thickness of the workpiece results in the transition of buckling mechanism to temperature gradient mechanism for a given process parameters setting [4,62]. Zahrani and Marasi observed that the thickness of the workpiece would affect the edge effect, such as the edge effect increased with increasing of the thickness of the workpiece [63]. Wu et al. [45] and Chen et al. [64] found that the length of the workpiece (perpendicular to the scanning path) had little effect on the laser bending angle, since the thermal field was not visibly affected with varying the length of the workpiece [45,64].

Cheng et al. [65] studied the effects of the size of the workpiece on laser forming of low-carbon steel sheet by experiments and numerical simulation. They observed that the bending angle increased with increasing of the width of the workpiece (the dimension along the scanning direction) at the fixed length and thickness, which was attributed to the larger thermal stress caused by the larger constraint from the cold material. Wu et al. [45], Chen et al. [64] and Shi et al. [66] had the similar observations.

2.2.6 Absorptivity on Laser Forming

The absorptivity of the material plays a vital role in the laser forming process. The energy input into the workpiece increases with increasing of the absorption of the laser radiation. The high reflective materials not only result in significant power loss but also damaging the optical elements due to backscattering light. A number of methods can be used to enhance the absorptivity of the material, such as using short wavelength laser, surface roughing or surface coating [6,52,67,68,69,70,71,72,73,74]. The detailed

description of absorptive coating is presented in section 3.1.3.

2.2.7 Thermal Properties of the Material

The thermal properties, such as thermal conductivity, specific heat capacity and coefficient of thermal expansion of the material, will affect the temperature distribution in the workpiece during laser forming process. The peak temperature on the upper surface of the workpiece and the temperature gradient along the thickness of the workpiece will increase with decreasing of the thermal conductivity of the material, since the less heat dissipation in relatively low thermal conductive material [26,28,75]. Guan et al. [76] studied the effect of the material properties on laser bending angle. They observed that the bending angle was inversely proportional to the specific heat capacity and thermal conductivity of the material, while proportional to the coefficient of thermal expansion of the material. Guan et al. [77] found that the thermal conductivity and specific heat capacity of the material decreased with increasing of the temperature due to the temperature dependent of the material, which resulted in the increasing of the plastic deformation and bending angle.

2.2.8 Forced Cooling

To produce a target shape with large deformation, the scanning strategy should be to increment towards the target shape with a number of passes (multi-pass scanning strategy). In multi-pass laser forming process, the temperature gradient along the thickness of the workpiece may decrease and the surface of the workpiece may melt

due to the fact that the thermal conductivity of material increases at higher accumulation of the temperature after each pass, which may influence the efficiency of the process and the quality of the forming results [59,78]. Therefore, the forced cooling should be taken into account in the multi-pass laser forming process in order to improve the efficiency of the process and the quality of the forming results.

Cheng and Yao [78] carried out experiment of laser forming of low carbon steel AISI 1010 to study the effects of forced air cooling on multi-pass laser forming process. They found that the forced air cooling not only would reduce the dwell time in between each pass but also improve the microstructure and mechanical properties of the material. The metallurgic results obtained from the study of Cheng and Yao showed that the case with forced air cooling exhibited a finer grain structure than the one without cooling. This is due to that the nucleation rate of new grains under cooling is higher than that under no cooling condition. In addition, the yield strength of the material under laser forming with forced air cooling was found higher than that without cooling. This is because of that the microstructure of the material under cooling shows a finer grain size and a finer bainite phase as compared with no cooling. Therefore, the strength of the material with cooling is higher than without cooling after laser forming [78].

Lambiase et al. [79] conducted an experimental investigation on passive water cooling in laser forming process, in which the workpiece was partially immersed into the stationary water during the process. They observed that the passive water cooling would greatly short the cooling time in between each irradiation and quickly reduce the temperature to prevent excessive oxidation and melting of the scanned surface.

Kant and Joshi [80] studied the effects of forced cooling on multi-pass laser forming process by using finite element modelling. They found that the melting of the surface of the workpiece, long dwell time in natural cooling and reduced bending angle per pass would be solved by application of forced cooling after each laser irradiation.

Shen et al. [81] studied the effects of water cooling on bending angle through experiments. The size of the stainless steel 304 workpiece was 100mm×50mm×1mm. They observed that the highest bending angle was achieved when keeping the upper surface in air and immersing the lower surface in the water. This is attributed to the efficient cooling of the bottom surface during the laser forming process. Water can prevent heat accumulation by absorbing the extra heat due to its high specific heat capacity with respect to the air. Therefore, it can increase and prolong the temperature gradient across the thickness of the workpiece resulting in larger bending.

2.2.9 External Load

Laser forming can be classified to laser direct forming and laser-assisted forming. Laser direct forming is a non-contact forming process without any external loads, which is achieved by introducing the thermal stress into the surface of a workpiece with a laser beam. As the thermal stress is over the yield stress of the material the plastic buckling will occur [3]. Laser-assisted forming is combination of the mechanical forming with laser assistance [20]. During the mechanical forming processes, the high deformation rates can lead to cracks and rupture very easily. Especially brittle materials like titanium or magnesium make difficulties in forming. Due to the dependence of the yield strength

on temperature, forming at elevated temperatures eases processing of such materials. Since forming takes place only at localized areas of the workpiece in most cases, selective laser heating is sufficient and advantageous, which can precisely heat and soften the areas of the workpiece where the strongest deformations are required [20,33,82,83].

Guan et al. [76] preloaded a mechanical load on the lower surface at the free end of the cantilever sheet to bend the workpiece toward the laser beam, as shown in Figure 2.2.1. They observed that the bending angle increased significantly with increasing of the preloading.

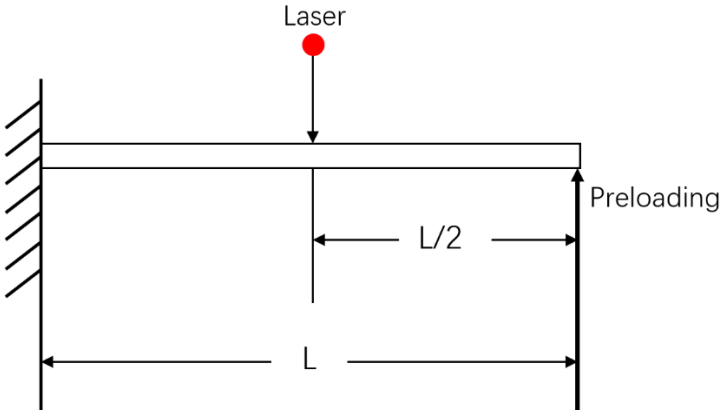

Figure 2.2.1 Laser-assisted bending by applying a load at the end of a cantilevered sheet [76]

Bammer et al. [84] successfully performed laser-assisted bending of 1-2.5mm thickness of Mg alloys (AZ31, ZE10), 1-2.5mm thickness of Al alloys (7075, Titanal), 2-12.7mm thickness of Ti alloys (Titan grade 2, WL3.7164) and 1-3mm thickness of Steels (M85, St52, Hardox).

Kant et al. [47] developed a laser-assisted bending method applying a mechanical load at the free end of the workpiece and moving in a path parallel and synchronous to that of the laser beam, as shown in Figure 2.2.2.

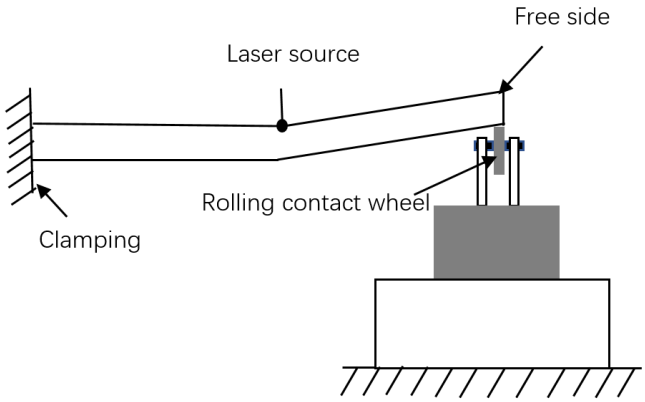

Figure 2.2.2 Laser-assisted bending by moving mechanical load [47]

Mueller et al. [85] combined mechanical load and laser to rapidly formed the three-dimensional objects, in which a defocused laser beam was applied on the bending lines to soften the bending region. Gisario et al. [86] developed a pneumatic tool with selective laser heating assistance to successfully bend the Grade2 CP Titanium and AA7075-T6 sheets.

2.2.10 Clamping

The workpiece clamping is one of the key factors to influence the laser forming results, which provides the mechanical constraint to the workpiece during the laser forming process.

Birnbaum et al. [87] studied the effects of edge clamped and unclamped conditions on laser forming of a squared sheet with the size of 80mm×80mm×0.89mm, as shown in Figure 2.2.3. Both the clamped and unclamped samples were laser irradiated at the distances of 40mm, 25mm, and 10mm to the left edge, as shown in Figure 2.2.4. They observed that the bending angles for the edge clamped workpiece were greater than those for the unclamped workpiece under the given process parameters setting. This is

due to the Poisson's effect stemming from the presence of the clamp, which acts to inhibit the displacement in the Z direction thereby increasing the stress in the Y direction. This would suggest that the presence of the external constraint would increase the total constraint, thus resulting in an increasing in bending angle.

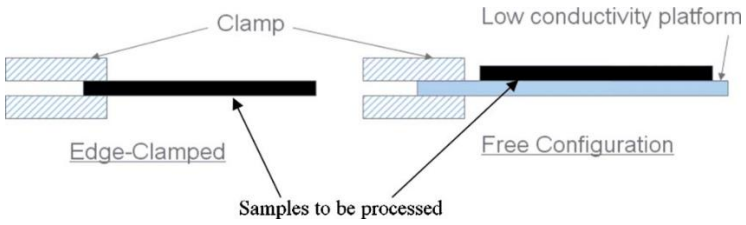

Figure 2.2.3 Schematic of clamped and unclamped workpiece [87]

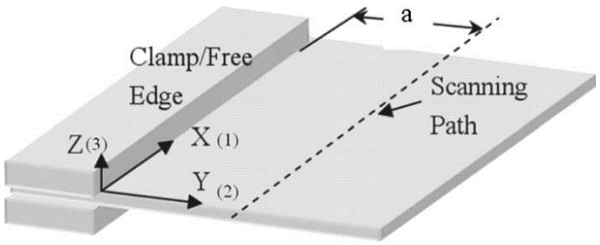

Figure 2.2.4 Schematic of clamped specimen specifying coordinate system and operating distance a=40mm, 25mm, 10mm [87]

Kant and Joshi [88] studied the effects of four different sheet clamping methods on laser forming process through finite element modelling, which were edge clamping, center clamping, corner clamping, and unclamping, respectively. They found that the maximum edge effect occurred for the unclamped condition, and it was the minimum for the edge clamping.

Hu et al. [89] studied the effects of two types of clamping conditions on laser forming process, which were edge clamping and point clamping at the start and end points of laser scanning path. The minimum edge effect was obtained for the point clamping at the start and end points of laser scanning path.

2.3 State of Art in Mechanical and Microstructure Properties Study in Laser Forming

The elevated surface temperature and localized plastic deformation will occur in the heated region during the laser forming process, which may cause the strain hardening, dynamic recrystallization and phase transformation resulting in the changing of the mechanical and microstructural properties of the material in the heated region [16].

2.3.1 Mechanical Properties of the Material

There is various research of the mechanical properties after laser forming summarized in the literature. The compressive strain and tensile strain, residual stress and hardening will be generated in the laser forming process, which will affect the mechanical properties of the material, such as the tensile strength, fatigue strength, hardness, and ductility. Laser irradiation will cause the difference in hardness between the base material and the material in the heated region.

Merklein et al. [25] investigated the changes in microstructural and mechanical properties of AA1050 and AA6082-T4/T6 undergo during the process of laser forming. They observed that the universal hardness (HU) in the heated region of AA1050 after 30 irradiations increased about 15-30% in comparison to the initial hardness of $342 \pm 9 N/mm^2$, and there was a variation in hardness along the thickness of the heated region. The increase in hardness on the irradiated surface was less than that on the lower surface of the sheet. This is because that the initial state of AA1050 has a grain structure with a dislocation substructure. After 30 irradiations (approximately 50° bending angle),

an inhomogeneous subgrain structure is produced and almost all dislocations are situated in the subgrain borders, without any dislocations in the inner area of the subgrains, which leads to work hardening and increasing in dislocation density. However, the hardness in the heated region of AA6082-T6 decreased about 10-30% in comparison to the initial hardness of $1400 \pm 28 N/mm^2$. This is because that the initial state of AA6082-T6 has a microstructure with semi-coherent precipitations, which causes the plastic strains inside the crystal lattice, and these precipitations are dissolved after one irradiation in the heated region. After 30 irradiations, an inhomogeneous subgrain structure is produced in the heated region below the irradiated surface up to 500μm, and the dislocation density inside the subgrains is low [25].

Thomson and Pridham [90] studied the changes in material property associated with laser forming of mild steel components. They observed that as the laser energy input increased, the effective yield strength of the material enhanced and ductility dropped, which would induce a higher degree of laser forming per pass. This is because that the higher laser energy input will lead to an appreciable temperature rise and hence result in a drastically increased carbon diffusion rate. Thus, the effects of deformation by bending may be swamped by the diffusion of carbon atoms back to the dislocation sites resulting in an increased yield strength.

Majumdar et al. [7] carried out experiments of laser forming of AISI 304 stainless steel with 2 kW continuous wave CO_2 laser. They observed that microhardness along the cross-section of the laser-irradiated zone was 220VHN to 375VHN, which was increased approximately 16% to 97% as compared to the base material (190VHN). The

increased microhardness is attributed to the grain refinement (grain size varying from 1.5 μm to 2.5 μm) associated with the rapid quenching during the laser forming process.

McGrath and Hughes [91] studied fatigue performance of laser-formed high-strength low-alloy (HSLA) steel plate by using 5 kW continuous wave CO_2 laser. Metal fatigue refers to the weakened condition induced in metal parts by repeated stresses or loadings, ultimately resulting in fracture under a stress much weaker than that necessary to cause fracture in a single application. They observed that the fatigue performance of the laser-formed samples was better than the stock plate and mechanically formed samples. This observation is attributed to the surface (work) hardening and the compressive residual stresses induced in the component after the laser forming application, both of which would result in a longer fatigue life [92].

2.3.2 Microstructure of the Material

There are many studies about the microstructure changes of the material after laser forming process been published.

Cheng and Yao [93] analysed the microstructure of low carbon steel (AISI 1012) after multi-scan laser forming process by finite element modelling. They observed that the flow stress was more significantly influenced by the microstructure changes. This is because that the softening effects due to recovery and recrystallization are out weighted by the hardening effects due to the martensite transformation near the upper surface in the laser forming process, which will lead to the microstructure change of

the low carbon steel resulting in an increasing of the flow stress.

Fan et al. [94] investigated the effect of phase transformations on mechanical behavior of AISI 1010 steel in laser forming. They observed that a dual α & γ phase region existed in the HAZ for the laser forming process, and the refined grains (around 10μm) in the HAZ were much smaller than those (average 25μm) in the base material. This is because that at the upper surface, the predominant phase is the martensite because in this area the peak temperature is above the nonequilibrium phase transformation temperature A_{3ne}(1120K), so the ferrite was completely transformed to the austenite during heating stage, and then the austenite was completely transformed into the martensite during cooling stage due to the high cooling rate. In the middle of the HAZ, since the temperature is about 997K during heating stage, only part of the ferrite was transformed into the austenite, so after cooling a mixture of remained ferrite and martensite was obtained. At the bottom, only very little of ferrite was transformed the austenite during heating, so the remained ferrite was the main phase after cooling.

Cheng et al. [95] investigated the microstructure and mechanical property of the microscale copper foils (thickness of 15μm) after laser dynamic forming (LDF). LDF is a new hybrid forming process, which combines the laser shock peening and metal forming, with an ultra-high strain rate forming utilizing laser shock waves. They found that the refined grain (much smaller and more uniform) and substructure were obtained after LDF with heating. From the results obtained by Cheng et al., it can be seen that before LDF, the grain size is about 15μm to 25μm with the standard deviation of 0.42. After LDF, the microstructure is dominated by high dislocation density and subgrain

structures. The subgrain size is reduced to about 0.15μm to 0.22μm with the standard deviation of 0.31. And the large compressive stress generated after LDF was benefit for the mechanical property of the copper foil, which was strengthened significantly due to the refined structure and large dislocation density.

Liu et al. [96] studied the effect of single direction raster scanning (SDRS) and cross direction raster scanning (CDRS) on microstructures and mechanical properties of laser solid formed nickel-base superalloy Inconel 718 respectively. They observed that the as-deposited microstructure of SDRS sample was composed of columnar dendrites growing epitaxially along the deposition direction; but in respect of CDRS sample, the continuous directional growth of columnar grains was inhibited and an orientation deviation of dendrites in two adjacent layers increased. The grains of the recrystallized CDRS sample were finer than the recrystallized SDRS sample. The ultimate tensile strength of SDRS sample and CDRS sample was similar, and the ductility of the SDRS sample was worse than the CDRS sample due to inhomogeneity of grain size of the SDRS sample.

Palani et al. [97] performed the experiments on laser forming of 8mm FE-410 plate by using 3 kW CO_2 laser. They observed that the microstructure for upper layers of the irradiated region has transformed into bainite and ferrite, and the depth of the bainitic formation was around 0.6 to 0.8mm into the sheet thickness. The gains in the lower layers were coarsened and elongated. The microstructure of the heat affected region was similar to that of the unaffected region, only slight coarsening of the grains in the heat affected region. The microhardness of the irradiated region (159HV-167HV) and

heat affected region (264HV) were reduced considerably in comparison to the unaffected region (340HV).

2.4 State of Art in Edge Effect Study

In the laser forming process, the main deformation occurs perpendicular to the laser scanning path, but a small amount of deformation may occur along the laser scanning path. The effect is most obvious at the edges of the workpiece, hence the term 'edge effect'. The edge effect in laser forming is contributed by the variation in the bending angle along the laser scanning path [98,99]. The curved bending edge (see Figure 2.4.1) in laser forming was contributed by several simultaneously occurring factors including the temperature difference along the laser scanning path, the mechanical constraint differences along the laser scanning path, and the shrinkage of material in the direction of laser scanning path [13,14,100,101]. There are various of studies on reducing the edge effect during laser forming process, which can be classified into three categories, as the process parameters studies, the scanning strategies studies, and the different clamping methods studies [14].

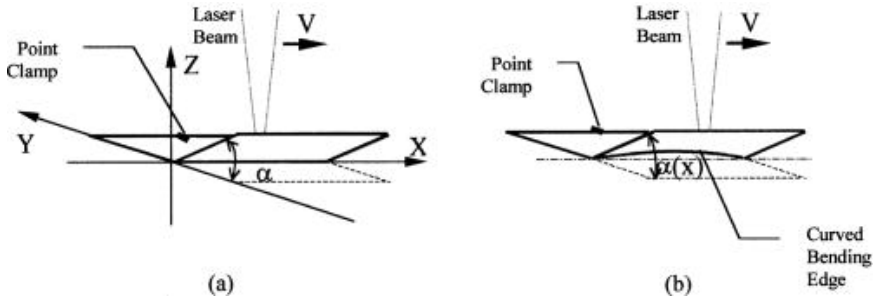

Figure 2.4.1 Schematic of straight-line laser bending (a). showing no edge effects, (b). showing edge effects characterized by the curved bending edge and non-uniform bending angle varying along the scanning path α(x) [101]

2.4.1 Process Parameter Study

Cheng and Yao [78] studied the effects of forced cooling on multi-pass laser forming. They found that the forced cooling could be used to reduce the longitudinal and tangential plastic strain differences to the laser scanning path direction resulting in reduction of the edge effect.

Jamil et al. [102] studied the influence of non-conventional laser beam profile on edge effects in laser forming of AISI304 stainless steel plate through numerical simulation. They found that the triangular laser beam could reduce the variation in the bending angle along the laser scanning path.

2.4.2 Scanning Strategy Study

Jha et al. [103] studied the edge effect and multi-curvature in laser forming of AISI 304 stainless steel. They found that the variation in the bending angle along the laser scanning path could be decreased as the number of passes was increased, thereby minimizing the edge effect. This behaviour can be attributed to the complex residual stresses developed during subsequent laser scanning.

Magee et al. [13] used different laser scanning speeds to change the heat input over the laser scanning path to reduce the edge effect. The results showed that a scanning strategy of 20-40-28mm/s could improve the edge effect compared to a constant scanning speed of 30mm/s. Shen et al. [104] performed a similar scanning strategy to Magee et al. to reduce the edge effect. They used seven different laser scanning speeds 20-25-30-32-35-33-30-28mm/s over the laser scanning path (see Figure 2.4.2) and

found that the scanning strategy of varying the scanning speed was effective for reducing the edge effect. The bending angle variation reduced from 1.29° of a constant scanning speed (30mm/s) to 0.38° of the scanning strategy of varying the scanning speed and the corresponding relative bending angle variation reduced from 16% to 5.6%. This is because that more deformation will occur near the edges by reducing the laser scanning speed near the edges, which can reduce the differences in bending angle.

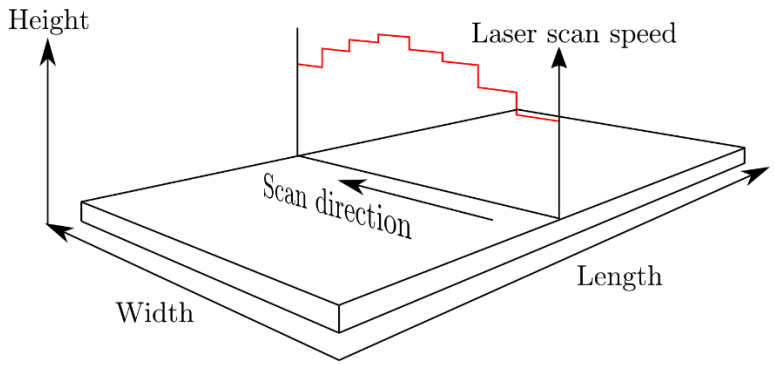

Figure 2.4.2 A schematic of the variable speed increments for reducing edge effects [104]

Safari and Farzin [105] studied the effects of different scanning strategies on laser forming of tailor machined blanks, which were variable speed method (VSM), variable power method (VPM) and variable beam diameter method (VBDM). The results showed that VSM was the best scanning strategy for laser bending of tailor machined blanks, which could reduce the differences in bending angles and curvatures of two sections in tailor machined blanks, followed by VPM. The VBDM scanning strategy was not a suitable method for laser forming of tailor machined blanks in comparison with VPM and VSM.

Shi et al. [106] studied the forming accuracy in multi-scanning laser forming of low carbon steel DC01. They tested four different scanning strategies to control the variation in bending angle along the scanning path, see Figure 2.4.3. They found that the variation in the bending angle along the scanning path was mainly dependent on the temperature distribution along the scanning path. And the results showed that the variation in the bending angle along the scanning path with the scanning strategy 3 and 4 was smaller than the scanning strategy 1 and 2, as shown in Figure 2.4.4 (a). The relative variations in the bending angle were 16.22%, 13.51%, 9.61% and 8.53% by using of the scanning method 1 to 4, respectively. This is because that the relatively symmetrical temperature distribution can be obtained by using of the scanning method 3 and 4, as can be seen in Figure 2.4.4 (b).

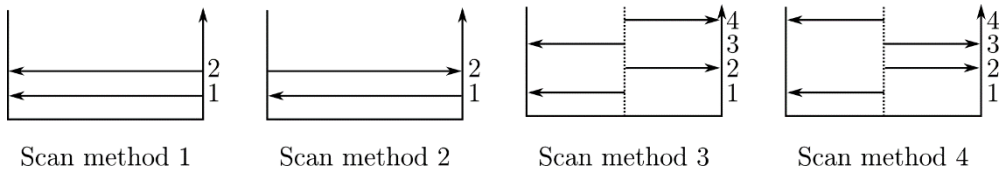

Figure 2.4.3 Four different scanning methods [106]

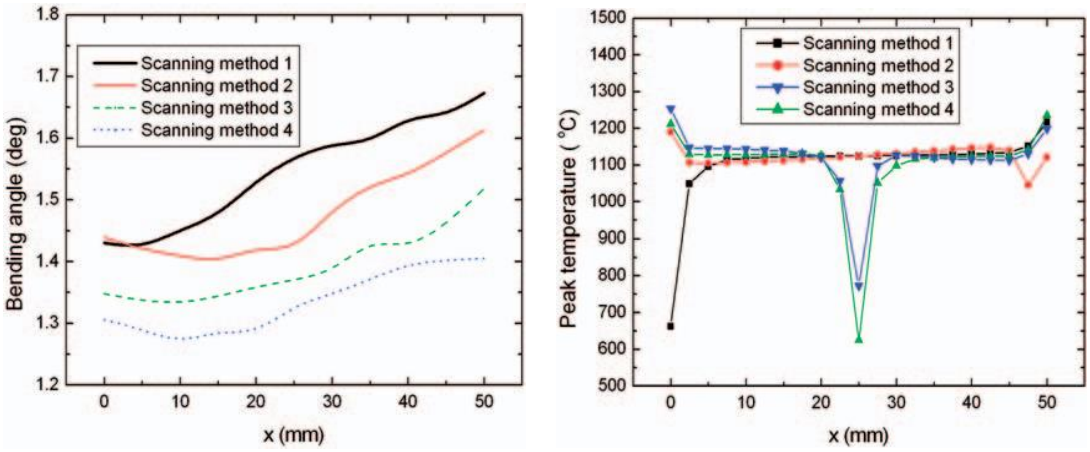

(a) (b)

Figure 2.4.4 (a). Comparison of the bending angle along the heating line with different scanning methods, (b). The temperature distribution on the top surface along the heating line with different scanning methods [106]

2.4.3 Different Clamping Methods Study

Hu et al. [89,107] investigated the effect of the constraint conditions on edge effect in the laser forming process. The edge clamping and sides clamping were employed in the laser forming process respectively, as shown in Figure 2.4.5. They found that the edge effect was reduced by clamping the two sides of the laser scanning path in comparison to the conventional edge clamping. This is because that by using of the conventional edge clamping, the plastic strain at the two ends of the scanning path is smaller than the other regions, and the strain difference between the upper and lower surface is relatively large at the two ends, which leads to a curved bending edge, as can be seen in Figure 2.4.6. However, by clamping the two sides of the laser scanning path the plastic strain distribution along the whole scanning line is more uniform than the edge clamping. This is because that the two ends of the scanning path are fully constrained, which produces more plastic strain. The uniform plastic strain distribution would lead to small variation in the bending angle along the scanning path resulting in a reduction of edge effect.

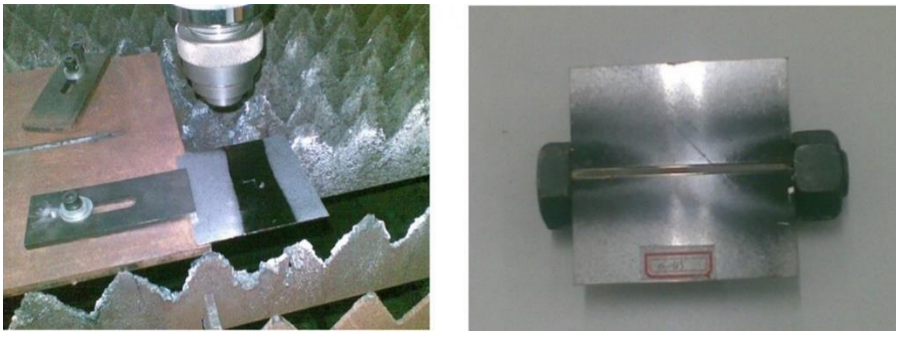

(a) (b)

Figure 2.4.5 (a). Edge clamping, (b). Clamping the two sides of the laser scanning path [89,107]

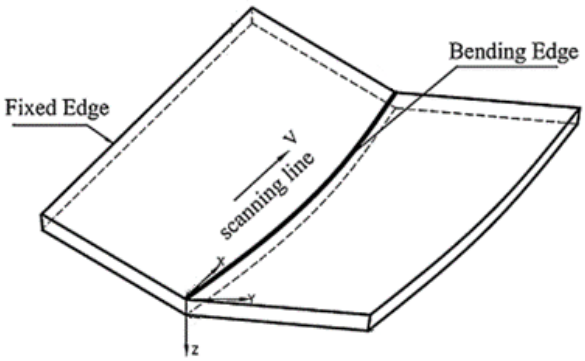

Figure 2.4.6 Edge effect characterized by the curved bending edge [89,107]

2.5 State of Art in Modelling of Laser Forming Process

The modelling research on the laser forming process has been carried out for nearly 20 years, which can provide the theoretical basis for prediction of the results and process parameters in the laser forming process. In this section, the literature review for the modelling of the laser forming process is classified into three categories, which are analytical modelling, numerical simulation, and soft computing, respectively.

2.5.1 Analytical Models

Laser forming is an advanced forming method to use laser beam heating to deform the workpiece. This process can be applied for rapid prototyping and deforming the metals, non-metals, and brittle materials. Various analytical models have been developed to explain the mechanism of the laser forming process and to predict the bending angle, stress, and temperature distribution in the workpiece. This subsection briefly reviews the analytical model of the linear laser forming process.

One of the simplest analytical models of laser forming was proposed by Vollertsen [108]. In this model, the bending angle is proportional to the laser power and

inversely proportional to the scanning speed of the laser beam and the square of the workpiece thickness. The yield strength and elastic modulus of the material are not taken into account in this model, and the analytical expression is given by

$$\alpha_b = \frac{3\alpha_{th}\eta P}{\rho C_p v t^2}$$

Equation 2.5.1

where α_b is the bending angle, α_{th} is the coefficient of thermal expansion, P is the laser power, η is the absorptivity of the material, ρ is the density, C_p is the specific heat capacity, v is the scanning speed, and t is the thickness of the workpiece.

The Vollertsen's model does not consider the effect of the yield strength and Young's modules of the material on the bending angle. Yau et al. [109] added the yield strength and Young's modulus of the material on the basis of Vollertsen's model, and the analytical expression is given by

$$\alpha_b = \frac{21\alpha_{th}\eta P}{2\rho C_p v t^2} - \frac{36 L_h \sigma_y}{tE}$$

Equation 2.5.2

where E is the Young's modulus, σ_y is the yield stress, and L_h is the half-length of the heating region.

From Equation 2.5.2 it can be found that although Yau et al. consider the effect of yield strength and elastic modulus, the model is only suitable for prediction of the bending angle in the linear range between bending angle and line energy ($\eta P/v$).

Lambiase [110] developed a two-layer model based on the elastic bending theory, in which the plastic deformation during heating and cooling stages was not considered. In Lambiase's model the thickness of the heated layer depends on the effective

temperature distribution along the thickness of the workpiece. The analytical expression is given by

$$\alpha_b = \frac{3\eta P(t - t_h)\alpha_{th}}{\rho v C_p t(t^2 - 3tt_h + 3t_h)}$$

Equation 2.5.3

where t and t_h represent the thickness of the workpiece and the thickness of the heated volume respectively, which are always estimated empirically.

Shi et al. [111] developed a model for estimating the bending angle in the plane axis perpendicular to the laser scanning path. At the heating stage, the thermal expansion not only occurs perpendicular to the laser scanning path, but also along the laser scanning path, and the thermal expansion of the upper surface is greater than that of the lower surface. At the cooling stage, the upper layer contracts, which leads to a bending perpendicular to the scanning path. The analytical expression is given by

$$\alpha_b = \frac{6.92\eta P\alpha_{th} w r^{\frac{1}{2}}}{\pi^{\frac{3}{2}} L^2 t(\rho C_p k v)^{\frac{1}{2}}}$$

Equation 2.5.4

where w is the width of the workpiece, L is the length of the workpiece, and k is the thermal conductivity.

Vollertsen et al. [32] developed an analytical model to estimate the relationship between the bending angle and the sheet thickness, laser power, laser scanning speed, elastic modulus and flow stress. The strain near the center of the laser beam is plastic, while the strain far away from the center of the laser beam is considered elastic. The analytical expression is given by

$$\alpha_b = \left[36 \frac{\alpha_{th}\sigma_y}{C_p \rho E} \frac{\eta P}{v} \frac{1}{t^2}\right]^{\frac{1}{3}}$$

Equation 2.5.5

Ueda et al. [112] derived an empirical expression to evaluate the influence of the workpiece temperature, laser beam diameter and the thickness of the workpiece on the bending angle. They found that the bending angle was in proportion to the parameter $[(D)^{1.4}(T_s)^{1.5}(h)^{-1.7}]$, in which D is the laser beam diameter, T_s is the upper surface temperature of the workpiece, and h is the thickness of the workpiece. Meanwhile, they also found that there was a linear relation between the temperature difference ΔT between the upper and lower surfaces of the workpiece and the upper surface temperature T_s, so that the bending angle could be estimated by the easily measurable upper surface temperature T_s.

Gollo et al. [113] performed the statistical analysis of the effects of material parameter, laser power, scanning speed, laser beam diameter, thickness of the workpiece, number of passes, and pulse duration, on bending angle in laser forming process by pulsed laser. They found that the factors which had most significant effect on bending angle were number of passes, material parameter, thickness of the workpiece, scanning speed, and laser beam diameter. The other factors, such as laser power and pulse duration, had less effect on bending angle. The mathematical expression is given by

$$\alpha_b = 15.1 - 0.477M + 0.0012P - 0.84V + 7.66S - 7.86T + 4.01N - 1.74D + 0.000002P^2 + 0.070V^2 - 2.38S^2 + 2.43T^2 - 0.554N^2 + 0.0552D^2$$

Equation 2.5.6

where M is the material parameter, P is laser power, V is the scanning speed, S is the laser beam diameter, T is the thickness of the workpiece, N is the number of passes, and D is the pulse duration.

It is worth noting that in Equation 2.5.6 the material parameter M is a nondimensional material parameter, which is given by

$$M = \frac{k_{METAL}\alpha A\sigma_y}{k_{SHG}\rho C_p}$$

Equation 2.5.7

where k_{METAL} is the thermal conductivity of the material of the workpiece, α is the coefficient of thermal expansion, A is the absorptivity, σ_y is the yield stress, k_{SHG} is the thermal conductivity of the shielding gas, ρ is the density of the material of the workpiece, and C_p is the specific heat capacity.

Eideh et al. [114] proposed a simple analytical model for estimating bend angle during laser forming of the sheet based on elastic-plastic theory. They indicated that the average error between the predicted and experimental results was normally between about 20% to 50%. However, the present model provided a very good agreement with the experimental results and the prediction error was reduced to 10%, and the model could also be used for the estimating of the yield stress. The analytical expression is given by

$$\alpha_b = \frac{2d\sigma_y(1-\nu^2)}{\sqrt{3}Ec}$$

Equation 2.5.8

where d is the laser beam diameter, σ_y is the yield stress, ν is the Poisson's ratio, E is the Young's modulus, and c is the distance from neutral axis to elastic plastic boundary.

Temperature distribution has great influence on the results of laser forming. Therefore, several analytical models have been developed to estimate the temperature distribution during the laser forming process by various researchers.

Woo and Cho [115] developed a new analytical solution to predict transient temperature distributions in a finite thickness plate during laser surface hardening. This analytical solution was obtained by solving a transient three-dimensional heat conduction equation with convection boundary conditions at the surfaces of the workpiece.

Cheng and Lin [116] developed an analytical model to describe the three-dimensional temperature field for a finite plate with a Gaussian heat source moving at a constant scanning speed. They observed that the distance between the center of the laser beam and the local peak temperature increased slightly as the laser beam diameter and the scanning speed increased. In addition, the peak temperature around the location that was being heated increased as the power and the scanning speed increased, whilst the lowest temperature decreased as the power and the scanning speed increased. The three-dimensional transient temperature T (x, y, z) is represented as

$$T - T_0 = \frac{\eta P}{4\rho C_p[\pi\alpha(t-\tau)]^{1.5}} \times \exp\left[\frac{(x-x')^2 + (y-y')^2 + (z-z')^2}{4\alpha(t-\tau)}\right]$$

Equation 2.5.9

where T_0 is the transformed room temperature, η is the absorptivity, α is the thermal diffusivity, ρ is the density, C_p is the specific heat capacity, and P is the laser power generated at the point P (x', y', z') at the time τ.

Shen et al. [117] developed an analytical method for treating the problem of laser induced heating and melting in solids by suggesting a simple temperature profile. They applied the analytical method to aluminum, titanium, copper, silver and fused quartz. A discontinuity in the temperature gradient was obviously observed due to the latent heat of fusion and the increment in thermal conductivity in solid phase. The effect of laser power density on the melt depths for four metals were obtained. They found that titanium needed least time to reach the fusion temperature and the vaporization temperature among these four metals due to its low thermal conductivity although it has relatively high fusion and vaporization temperatures.

Shi et al. [118] estimated the temperature field during laser forming by developing an analytical model using convection and radiation boundary conditions. They used a one-dimensional heat conduction model and only considered the variation of temperature in the thickness direction to estimate the temperature during the laser forming process. They indicated that this analytical model is more convenient for practical applications compared with other analytical models of the temperature field, because it does not include differential and integral calculus and does not need to consider the temperature dependence of the material.

Kumar and Dixit [119] developed an empirical model to estimate the maximum top surface centre-point temperature during laser forming process. The empirical model for prediction of the maximum temperature of the sheet is given by

$$T_{pred} = 0.954 \frac{\eta P}{D_t^{0.72} C_p^{1.0372} v^{0.4} D^{1.15} t^{0.1}} + T_{amb}$$

Equation 2.5.10

where T_{pred} is the predicted temperature, η is the absorptivity, P is the laser power, D_t is the thermal diffusivity, C_p is the specific heat capacity, v is the scanning speed, D is the laser beam diameter, t is the thickness, and T_{amb} is the ambient temperature.

2.5.2 Numerical Simulation of Laser Forming

The numerical simulation can improve the basic understanding of the laser forming process. Numerical models have been developed since the early 1990s. Ji and Wu [49] carried out FE Modelling of transient temperature field formed in the laser forming process. Kyrsanidi et al. [50] developed a 3D finite element modelling. The modelling can be used for the non-linear transient coupled thermal–structural analysis, in which the temperature dependent thermal and mechanical properties of the material are taken into account. A sine shape was formed from a flat sheet by using this 3D finite element modelling. Hu et al. [120] developed a 3D FE Modelling that includes a nonlinear transient indirect coupled thermal-structural analysis accounting for the temperature-dependent thermal and mechanical properties of the materials. The distribution of stress–strain, residual stress, temperature and bending angle were obtained from modelling. Vollertsen et al. [121] analysed temperature variation and bending angles in

the laser forming process by finite difference method (FDM) and finite element method (FEM). Zhang and Xu [122] developed a finite element modelling based on the uncoupled thermal and thermo-mechanical theory for simulation of the pulsed laser forming involving melting and solidification. They assumed that the laser beam is uniform along the scanning path. Thus, a 2D thermal-stress model can be applied, which greatly reduces the computational time. Safdar [123] studied the influence of the different scanning strategies on the laser forming process by FE Modelling.

Several researchers carried out FE Modelling of the laser forming process by using of commercially FEM packages, such as ABAQUS®, ANSYS®, COMSOL® etc. For example, Holzer et al. [124] performed the FE Modelling for analysing BM by using of ABAQUS®. Chen and Xu [44] developed a 3D FE Modelling to simulate the laser forming process under the temperature gradient mechanism. They studied the thermal and the mechanical properties of the material of the workpiece through the nonlinear finite element solver, ABAQUS®. Edwardson et al. [56] performed the numerical simulation by using of COMSOL® MultiPhysics of the multi-pass laser forming of mild steel, Ti-6Al-4V and AA5251 by CO_2 laser. Labeas [125] developed a FE Modelling for laser forming of aluminum alloy workpieces based on ANSYS® and it was experimentally validated by single pass and multiple passes scanning strategy. For validation of the thermal model, a deviation of about 7.6% was observed between the experimentally measured temperatures and the simulated results, which indicated a very good correlation. For validation of the mechanical model, a deviation of about 2% to 8% was observed between the experimentally bending angle and the simulated

results, which also indicated a very good correlation. Yilbas and Akhtar [126] predicted the surface temperature, bending angle, and residual stress of the AISI 304 steel sheet at 1mm in thickness by using the commercially ABAQUS® FEM package. It was found that the prediction of the temperature, residual stress, and bending angle had a good agreement with the experimental data, as can be seen in Figure 2.5.1.

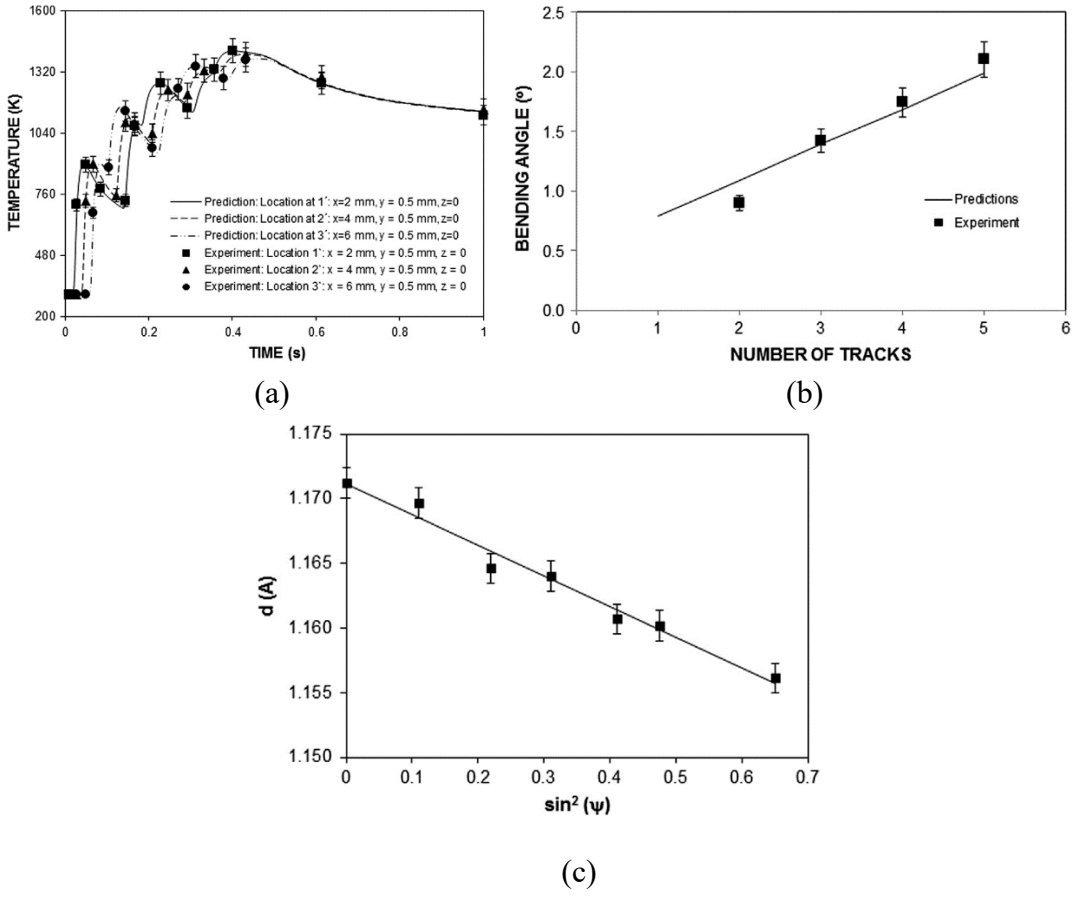

Figure 2.5.1 (a). Temporal variation of predicted surface temperature along the scanning path and thermocouple data, (b). Predicted bending angles and experimental results, (c). Linear dependence of d (211) with $\sin(\psi)^2$ [126]

The finite element modelling can provide good predictions of the results in laser forming process; however, the computational time is large for some special cases, such as the modelling of the coupled thermo-mechanical process with multi-pass scanning strategy, which always runs one day to one week. In order to solve this problem, a

number of researchers proposed various methods to reduce the computational time. It is crucial of appropriate mesh refinement and time step to obtain accurate results within a reasonable calculation time.

Pitz et al. [127] carried out numerical simulation of the laser forming process with moving meshes for large aluminium plates (100mm×100mm×2mm). The modelling was accomplished applying the FE-software COMSOL Multiphysics. They indicated that the Moving Mesh Method reduced the pure error to about 6% while it leaded to a reduction to less than about 28% of the computing time and the larger the laser path the more efficient became the Moving Mesh Method. The Moving Mesh Method allows maintaining a high mesh resolution in areas with a high amount of material agitation by moving along with the feed of the laser beam. The mesh is generated in base position by meshing one domain in laser scanning direction finely. When the process starts the finely meshed area is shifted to the boundary where the laser beam appears on the plate compressing the coarse mesh on its left to a fine mesh as well and stretching the mesh on its right. As soon as the laser beam reaches a defined position within the finely meshed area the whole mesh proceeds synchronously to the laser beam. When the laser beam has nearly completely crossed the plate the mesh stops having stretched one part of the mesh and compressed the other where the laser will still move through. Thus, the relevant zone and its close surroundings constantly show a high mesh resolution acquiring a sufficient amount of data during the process.

Yu et al. developed [128] a finite element modelling to analyse the effects of the refinement of mesh size on temperature distribution and final distortion, and the

rezoning meshes technique was adopted in the FE modelling. They developed an algorithm to generate rezoning meshes for rectangular plate, where it read the necessary information for the mesh to be generated from an input file, and the output file from the thermal and mechanical analysis in the previous step, and then generated the input file for analysis in the next step. It can be found that the rezoning meshes could not only reduce the computational time, but also had a good agreement with the experimental results.

Zhang et al. [129] developed an efficient method for computing pulsed laser bending. During pulsed laser bending, thousands of laser pulses are irradiated onto the workpiece, thus, the computational time will be very large if simulating the thermos-mechanical effect of all the laser pulses. However, Zhang et al. only used a few laser pulses in the FE modelling. It was found that the total computational time was greatly reduced, and the results were agreed with those obtained using the conventional computation method. In addition, the experimental data and computational results were consistent.

Zhang et al. [130] developed a 3D FE Modeling of laser forming to investigate the minimum requirements of temporal and spatial discretization and mesh density on the angular deformation of the plate to reduce the computational time of the modelling, in which the spatial discretization is expressed as the number of the required elements within the radius of laser beam, which will determine the total number of degree of freedom; the temporal discretization is expressed as the number of required time increments for a laser to move through a laser beam radius, which will determine the

total time increments required; and the meshing density through thickness is expressed as the number of elements in the thickness direction. Zhang et al. suggested that to reduce the computational time caused by excessive degrees of freedom and obtain an accurate solution for a 3D finite element model, the temporal discretization required at least four time increments per radius and the spatial discretization required at least two elements per radius and three elements through the thickness, which represented the minimum requirements of FE modelling for the laser forming process.

Hu et al. [131] proposed a simple, robust, and accurate method for laser bending modelling using multi-layered shell elements. The workpiece was divided into three zones, heating zone, diffusion zone and cooling confinement zone in their model. Under the TGM, the temperature gradient in the heating zone was relatively steep, but in the other two zones were almost equal to zero. The element sizes were different in different areas. They used three different models of solid, solid-shell and multilayered shell. The simulation efficiency of the solid-shell model and the multi-layered shell model was greatly improved due to the reduction of nodes and elements. The total number of nodes reduced by 26.34% and elements by 20% in the solid-shell layer. The total number of nodes reduced by 70.24%, and elements by 66.67% in the multilayered shell model.

2.5.3 Self-Computing Models

Self-computing refers to the use of self-learning methods, such as neural networks; approximate reasoning methods, such as fuzzy set theory; and evolutionary optimization techniques, such as genetic algorithms. Many efforts have been made to

use artificial neural networks (ANN) for laser forming. Artificial neural network (ANN) is a computational model that consists of several processing elements that receive inputs and deliver outputs based on their predefined activation functions [15].

Barletta et al. [132] conducted a comparative study of various neural network models of a hybrid forming (mechanical bending along with laser scanning to reduce springback) using RBF, generalized feed forward (GFF), and MLP. They found that MLP provided the best performance.

Palani et al. [97] developed an artificial neural network model based on the experimental data for parametric investigation and prediction of the bending angles in the laser forming process. The experiments were performed on 8mm FE-410 steel sheets using CO_2 Laser with maximum power of 3 kW. In the parametric study, various parameters were varied namely power (2 kW to 3 kW), number of passes (1 to 210), scanning speed (10mm/s to 30mm/s), laser beam diameter (9mm to 13mm), and frequency (500Hz to 20000Hz). The bending angle of the sheet was measured after every 10 passes. The proposed artificial neural network model gave good results in predicting the bend angle value with a mean square error of 0.005647 compared with the experimental values.

Cheng et al. [133] proposed three supervised learning methods that used neural networks to predict the bending angle in laser forming. A feed-forward back-propagation multilayer perceptron (MLP) neural network was divided into hyperbolic tangent activation function and logistic transfer function. And the third method was the radial basis function (RBF) neural network, with which the best performance could be

obtained. Dragos et al. [134] proposed the use of ANN for predicting bending angles in laser forming based on the experimental data. Casalino [135] proposed a feed forward MLP-ANN model with back propagation for laser forming. In an iterative process, the number of hidden layer neurons varied from 6 to 20. Maji et al. [136] predicted the bending angle in laser forming by using neural network and performed inverse analysis. Maji et al. [137] conducted the similar studies on the pulsed laser forming and dome surface laser forming.

Maji et al. [138] carried out forward analysis and inverse analysis of laser forming process using both genetic-neural network (GA-NN) and genetic adaptive neuro-fuzzy inference system (GA-ANFIS). In the forward analysis, the laser power, scanning speed, laser beam diameter, and number of passes were set as input values, and the bending angle was set as the output value. The results obtained from the forward analysis showed that both the GA-NN and GA-ANFIS methods were able to predict the bending angles in the laser forming process, which gave an average absolute percent deviation of 7.98% to 9.55% compared to the experimental data. In the inverse analysis, the bending angle was set as the input value, and the laser power, scanning speed, laser beam diameter, and number of passes were set as output values. The results obtained from the inverse analysis showed that both the GA-NN and GA-ANFIS methods were also able to predict the process parameters in the laser forming process. In comparison to the experimental data, these two self-computing methods gave an average absolute percent deviation of predicted laser power from 5.34% to 5.44%, scanning speed from 2.93% to 3.09%, laser beam diameter from 12.29% to 12.36%, and number of passes

from 12.42% to 16.31%. In addition, the GA-NN method was a slightly superior to the GA-ANFIS method, which was due to the reason that the GA faced a more difficult task for determining optimal knowledge base of ANFIS model compared to that of the NN model.

The training and test data were divided randomly in all the above works. The whole data in the work presented by Barletta et al. [132] were divided into 60% training, 15% cross-validation, and 25% testing data. A large amount of experimental data in the work proposed by Dragos et al. [134] were equally divided into two halves each for training and testing respectively.

Maji et al. [136,137,138] randomly divided 1000 data into two subsets of equal size, in which a part of the 1000 date were the experimental values, and the remaining data were generated by the regression model. One of the subsets was used for training and testing the ANN, and the other subset was used for verification. The training and testing data were interchanged to ensure the participation of both data in the training.

Pérez et al. [139] used MATLAB to develop an adaptive neuro-fuzzy inference system (ANFIS) model for laser surface heat treatment, which could be used to predict the maximum surface temperature of the workpiece at a particular sampling time from the input parameters, viz. the laser power and the previous measured temperature.

Jovic et al. [140] used an adaptive neuro-fuzzy inference system (ANFIS) and variable selection procedure to determine the parameters influence on the bending and thickening of the shaped surface. The selection procedure was done to obtain the found the process parameters which had the most influence on the bending and thickening of

the shaped surface.

Cheng and Yao [141] determined the optimal process parameters for laser forming of a desired shape based on genetic algorithm (GA). They indicated that the control parameters, including laser power, scanning speed, length of the scanning line, and type of fitness function, had significant effects on GA results. However, a large number of iterations were needed to achieve convergence when the number of decision variables was close to 30. Investigations showed that the algorithm control parameters and the fitness function type had significant effects on the GA synthesis results. The selection of a suitable fitness function is essential to achieve the balance among competing objectives, such as forming time, geometric accuracy, and energy consumption.

Du et al. [142] improved the back propagation network (BPN) based on the double-strand quantum genetic algorithm (DCQGA) to improve the accuracy of bending angle prediction. And, the BPN-DCQGA network was trained and verified through the sample experimental data. Moreover, this proposed network can be used to enhance the rate of convergence and obtain higher training efficiency.

2.5.4 Inverse Model

In broad terms, an inverse modelling is the process of calculating from a set of observations the causal factors that produced them, which starts with the effects and then calculates the causes, such as calculating the density of the Earth from measurements of its gravity field [143]. In laser forming, the inverse modelling can be used to predict the process parameters and laser scanning strategy based on the required

strain field or the target deformation.

Maji et al. [136] modeled and optimized the pulsed laser forming process based on the response surface methodology. Eideh and Dixit [144] developed an inverse modelling by measuring the temperature at two locations based on heuristic methods in order to minimize the combined error between the predicted temperature and the measured temperature at the two locations. Romer and Maijer [145] used inverse modelling to calculate the power density distribution of the laser beam. Kim and Oh [146] evaluated the heat transfer coefficient during heat treatment by the inverse heat transfer formula of a two-dimensional finite element model. Woodfield et al. [147] used the analytical inverse solution of unsteady one-dimensional heat conduction based on two-point temperature measurement and semi-infinite boundary conditions to determine the thermal diffusivity of solids. Shidfar et al. [148] used the conjugate gradient method (CGM) to estimate the pulse parameter of the time-exponentially varying laser pulse to obtain the surface temperature of the workpiece. Mishra and Dixit [149] determined the absorptivity, thermal diffusivity, and laser beam diameter by using the inverse thermal conduction method. They measured the temperature at one location at the center of the lower surface of the workpiece at different time intervals and used this measured temperature to estimate the thermal properties. Xu et al. [150] used a combination of experimental and simulation results to estimate the absorptivity of the material of the workpiece.

2.6 State of Art in 2D and 3D Laser Forming

The laser forming process is famous for its incremental free forming, however, from the point of view of the process control, these aspects of increased freedom become more difficult to deal with. The number of options makes the problem ill-posed, as a target shape can be implemented with various input parameters.

The literature presented in this section is divided into two categories. The first category relates to the type of laser forming, treating the laser forming as two-dimensional (2D) laser forming and three-dimensional (3D) laser forming. The 2D laser forming process is commonly used for fabricating the shapes with single curvatures, while the 3D laser forming process is commonly used for the shapes with double curvatures. The second category reviews the type of control, as the open and closed loop control. Open loop control is defined by planning the entire process before it starts. Closed loop (also denoted as feedback control) requires monitoring of the process so that the process can be adjusted by changing the input parameters in real time [151-167].

In the laser forming process, the description of the shape is usually divided into the target shape, initial shape, current shape, and final shape. The target shape is the ideal or required shape for the laser forming process to achieve; the initial shape is the starting or blank shape before any laser forming has been conducted; the current formed shape is an intermediate shape between the initial and target shape, which needs to be measured in a closed loop control; and the final formed shape is the shape obtained from a specific irradiation strategy.

2.6.1 2D Laser Forming

The 2D surface is associated with the formation of a V-bends, as shown in Figure 2.6.1. These types of shapes are usually produced using traditional mechanical press brakes. Although laser forming is unlikely to completely replace traditional mechanical press brakes, there are many benefits to be gained from the experiments on laser forming of the simple V-bends, such as the laser scanning path can be simplified to a straight line from side to side, and irradiation strategy is given by the spacing between adjacent paths, number of laser scans over each path, and energy input. Meanwhile, the evaluation of laser forming result for a V-bends is relatively simple and can often be reduced to comparison of the current bending angle to the target bending angle. Therefore, it is easier to study the laser forming process using a simple V-bends.

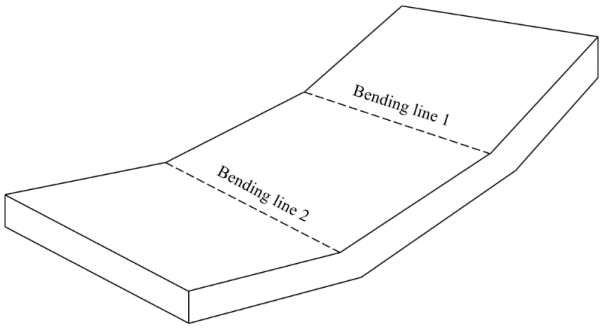

Figure 2.6.1 A simple V-bends

2.6.1.1 Open Loop Control

Liu and Yao [151] used response surface methodology (RSM) to optimize a set of parameters, including laser scanning paths, laser power, and scanning speed for laser forming on a rectangular plate and a quarter-circle plate, as show in Figure 2.6.2. The propagation of error technique was built into the design of the process as an additional

response to be optimized via desirability function and hence make the design robust. Response surface methodology (RSM) is a statistical technique useful for developing, improving, and optimizing the process, which explores the relationships between several explanatory variables and one or more response variables. The main idea of RSM is to use a sequence of designed experiments to obtain an optimal response [152].

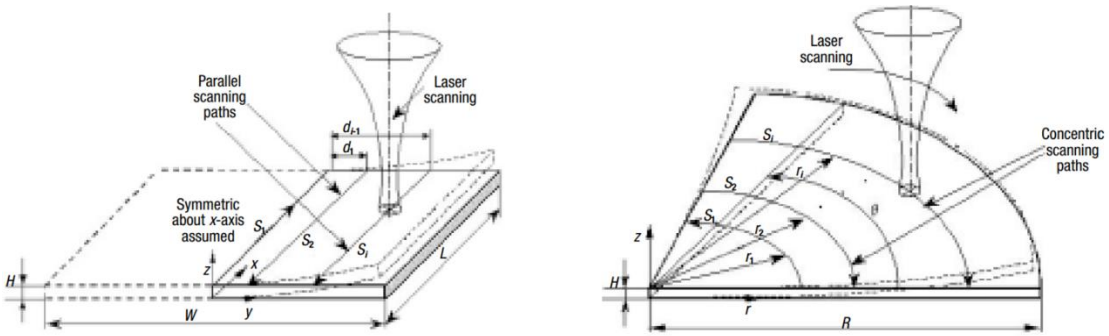

(a) (b)

Figure 2.6.2 (a) Linear parallel scanning paths on a rectangular plate and (b) Concentric paths on a quarter-circle plate [151]

Kim and Na [153] used distance-based criterion algorithm and angle-based criterion algorithm to determine the spacing between adjacent laser scanning paths in laser forming of a given sine curved shape, as shown in Figure 2.6.3.

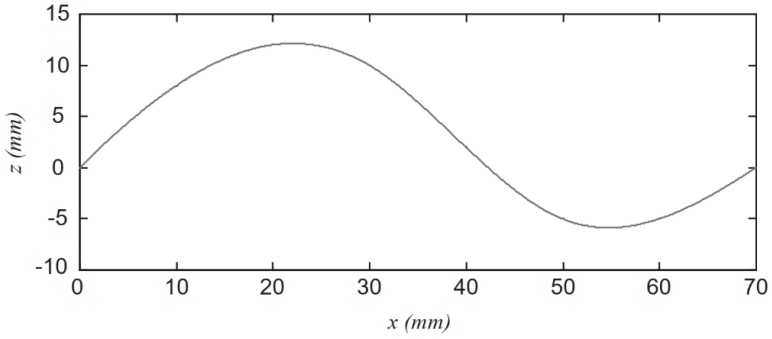

Figure 2.6.3 Target sine curved shape [153]

The distance-based criterion algorithm uses the maximum distance between the given sheet metal and the target shape as a criterion for a new forming point. If the maximum distance is larger than the offset distance, the point at the maximum distance is adopted as a new forming point. The angle-based criterion algorithm uses angles between tangent lines as a criterion for making a forming point. The angle gradually increases as the radius of the curvature decreases, so that more forming points can be generated in a highly curved surface. The results obtained from this study showed that the final formed shapes by these two algorithms were similar to the target shape, as can be seen in Figure 2.6.4. However, Kim and Na compared the advantages and disadvantages of the two algorithms, which were summarized in Table 2.6.1.

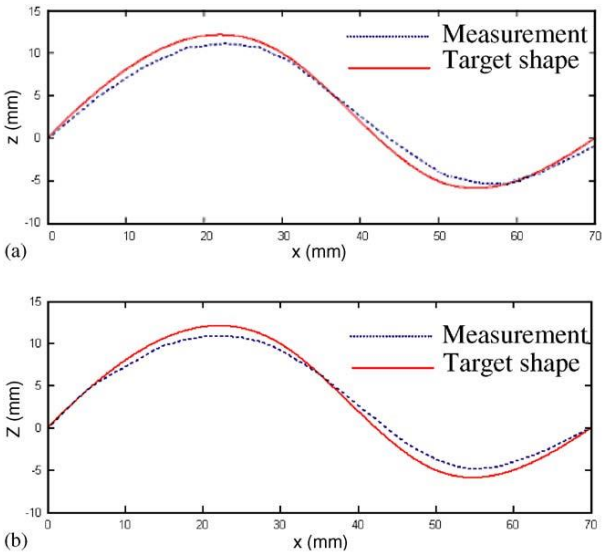

Figure 2.6.4 Results of measurements of the final formed shape: (a). distance-based algorithm, (b) angle-based algorithm [153]

Distance-based criterion algorithm		Angle-based criterion algorithm	
Advantage	Disadvantage	Advantage	Disadvantage
Smaller maximum error ~0.35mm	Needs parameter control (bending angles are not constant)	No need for parameter control (bending angles are constant)	Larger maximum error ~0.6mm

Table 2.6.1 Advantages and disadvantages of each algorithm [153]

Shen et al. [154] performed the laser forming of plates by using two laser beams scanning simultaneously along the two parallel lines through numerical simulation, as shown in Figure 2.6.5.

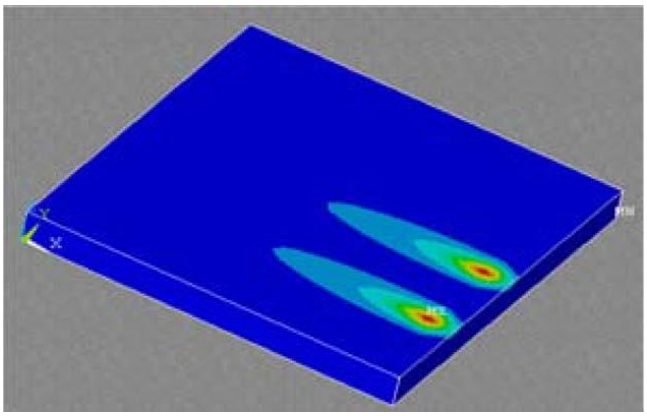

Figure 2.6.5 Numerical simulation of two laser beams scanning simultaneously along the two parallel lines [154]

The results obtained from this study showed that more deformation could be achieved by using two simultaneous scans along the two parallel lines than by using a single sequential scan along the same lines if the distance between the two parallel lines was smaller than two times beam diameter, and if the distance between the two scanning lines was larger than two times beam diameter then the plastic deformations would be the same for the simultaneously laser scans and for the single sequential scan. It can be explained from two aspects.

From the point of view of the temperature field, when the spacing between the two scanning lines are larger than two times beam diameter the temperatures generated by the two laser beams are almost independent and the two temperature fields do not interfere with each other. However, when the spacing between the two scanning lines are within two times beam diameter, the two temperature fields interfere with each other, and the temperature at the upper surface is higher than that at the lower surface. The steep temperature gradient through the thickness of the plate will lead to more bends of the plate towards the laser beam [154].

From the point of view of the plastic strains field, when the spacing between the two scanning lines are larger than two times beam diameter the plastic strains generated by each laser beam do not interfere with each other. The plastic strains developed in each plastic zone are the same as those provided by the single sequential scan along the same lines. In contrast, when the spacing between the two scanning lines are within two times beam diameter, the plastic zones generated by each laser beam are overlapped in some part and the corresponding plastic strain values are also larger. This indicates that more plastic deformation will be generated by using two laser beams simultaneously scanning along the two parallel lines than by using a single sequential laser beam scanning along the same lines [154].

2.6.1.2 Closed Loop Control

Thomson and Pridham [155] were the first to recognize the necessity of the feedback control in the laser forming process. They developed a feedback control system, which

relied on the sensors to monitor the degree of deformation of the workpiece, then compared it to a target value and adjusted the process parameters accordingly. They decided that the best method was to use scanning speed as the control parameter due to the limitation of the hardware. Adjusting the scanning speed could be achieved easily and reliably during the laser forming process. A rule-based system was used to determine the laser scanning speed in increments depending on the error between the current deformation and the target value, and they suggested using fuzzy logic and artificial intelligence to improve the rule-based system.

Kim and Na [156] modified the previous method [153] to improve the accuracy in 2D free curve laser forming. A feedback control for each single bending angle was employed in this study by incorporating a statistical method. They indicated that the statistical method was an appropriate feedback control algorithm for single bending angles, which was very effective and accurate. However, the inevitable small remaining errors in the laser forming process have an accumulating effect in a multi-pass laser forming process, which will cause the overall shape to deviate slightly from the target shape. Consequently, feedback control algorithms for 2D free curve laser forming were proposed to improve the accuracy of the final formed shape. The main objective of feedback control of multi-pass forming is to recalculate the forming points and corresponding angles based on the previous forming error. Figure 2.6.6 shows the results of the experiment with the feedback control, in comparison to the results presented in Figure 2.6.4, the accuracy is greatly improved.

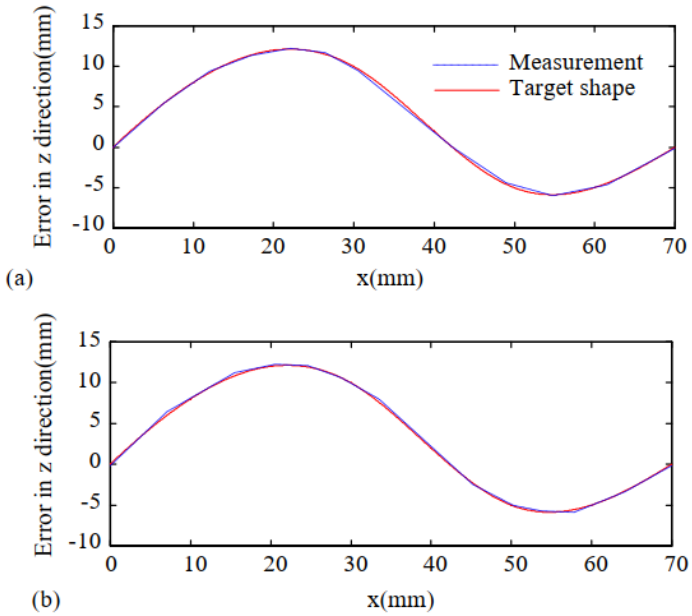

Figure 2.6.6 Results of experiments with feedback control: (a). distance-based algorithm, (b). angle-based algorithm [156]

2.6.2 3D Laser Forming

For fabrication of the 3D shapes, such as ship hull components, airplane fuselages and automotive bodies, 2D laser forming is limited. Therefore, in order to advance process for realistic applications, the investigation of the 3D scanning strategies becomes essential. 3D surfaces are characterized by double curvature. To date there has been a lot of research on 3D laser forming, most of which focused on investigation of laser forming of the dome and saddle shapes, since they are the typical double curved surface, as shown in Figure 2.6.7 [157].

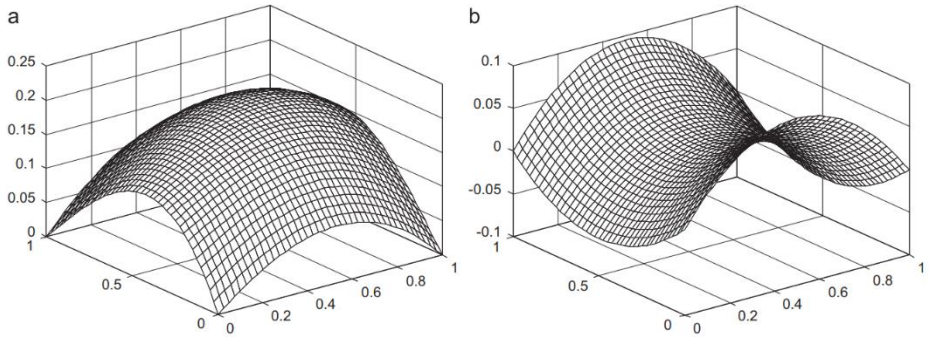

Figure 2.6.7 The typical double curved surfaces, (a). Dome shape, (b). Saddle shape [157]

Both single and double curved surface can be defined by Gaussian curvature, and the expression [158] is given by

$$K = k_1 k_2$$

Equation 2.6.1

where K is Gaussian curvature, k_1 and k_2 are principal curvatures.

From Equation 2.6.1, it can be found that if both principal curvatures are of the same sign ($k_1 k_2 > 0$), then the Gaussian curvature is positive, and the surface is said to have an elliptic point. At such points, the surface will be a dome shape; if the principal curvatures have different signs ($k_1 k_2 < 0$), then the Gaussian curvature is negative, and the surface is said to have a hyperbolic point. At such points, the surface will be a saddle shape; if one of the principal curvatures is zero ($k_1 k_2 = 0$), the Gaussian curvature is zero, and the surface is said to have a parabolic point. At such points, the surface will be a single curved surface [158].

The single curved surface is the developable surface, which can be folded from a flat surface without stretching or compression. Typically, the TGM should be the dominant mechanism used to produce plastic bending strains and out of plane deformation for a single curved developable surface. However, in comparison to the

single curved surface, most of the double curved surfaces are the non-developable surface, which cannot be produced from a plane surface without stretching or compression or tearing. In order to laser form a non-developable surface such as the dome and saddle shapes (assumed to be non-developable) significantly more in-plane plastic strain must be induced than out of plane bending strain, which means that the UM should be employed [12,15,34].

The three important factors need to be taken into account in 3D laser forming, are scanning pattern, number of passes over the scanning pattern, and energy input. In addition, the evaluation of 3D laser forming result is relatively difficult compared to the 2D laser forming, the feature values need to be selected from the formed shape to compare with the target values, such as the deflection of the points on the formed shape or the curvature of the formed shape. The different strategies of the 3D laser forming presented in the literature are summarized in the following subsections.

2.6.2.1 Open Loop Control

Kim and Na [157] performed the study of 3D laser forming of dome and saddle shapes based on the geometrical information. The overall procedure of the 3D laser forming process included three steps. In the first step, a group of small flat plane patches were decomposed from the given double curved surface, which was an expansion of Kim and Na's geometrical approach used in 2D laser forming study as mentioned before [153]. In the second step, the amount of shrinkage and the bending angle were calculated by the planar development procedure, and the laser scanning paths were

determined as the intersection lines between each plane patch. The final step was to determine the process parameters from the data maps obtained by FE modelling, which was matched to the bending and shrinkage data. Kim and Na indicated that the calculation time was reduced significantly with this method compared to the stress–strain analysis method and it was very easy to control the error bound by changing the number of patches.

Liu et al. [159] developed an optimal approach to determine the laser scanning paths and heating condition for laser forming of doubly curved shapes (pillow and saddle shapes). In their study, the overall procedure of laser forming of the given doubly curved shapes included three steps, which were determination of the required strain field, determination of the scanning paths (scanning pattern), and determination of the heating condition. In the first step, the required strain field to form the given doubly curved shapes was obtained by developing the given double curved shapes into a planar shape through numerical modelling. After the required strain field was determined, the next step was to determine the scanning paths. They placed the scanning paths perpendicular to the direction of the principal strains due to that in the laser forming process, the highest compressive strains occur perpendicular to the scanning path and in-plane orientation. The final step was to determine the heating condition. In their study, the heating condition that needed to be determined were only laser power and scanning speed, since the dimension of the workpiece and the laser beam diameter were given. The relationship between the average principal in-plane strain, laser power, and

scanning speed was created through FE modelling of single straight-line laser scanning of a plate with the above material and dimension.

Gao et al. [160,161] proposed a finite element method-based methodology to determine the laser scanning pattern and heating condition for laser forming of ship hull shape. In their study, a large-deformation model was used to obtain the required strain field to form the desired shape because the desired shape had a large deflection (30mm) relative to its thickness (1.5mm). And the elastic FEM was utilized because the development of a strain field from one shape to another was primarily a geometrical problem and was independent of the material properties [141], which can simplify the computation without altering the problem. The required strain field to form the given ship hull shape was obtained by developing the flat sheet into the desired shape through large-deformation modelling. Firstly, the top surface of the flat sheet was decomposed into a group of sixteen patches with 25 nodal points, then gave different displacement constraints on the points, which was corresponding to the height of the desired shape.

Kim and Na [157] performed the study of 3D laser forming of dome and saddle shapes based on the geometrical information. The overall procedure of the 3D laser forming process included three steps. In the first step, a group of small flat plane patches were decomposed from the given double curved surface, which was an expansion of Kim and Na's geometrical approach used in 2D laser forming study as mentioned before [153]. In the second step, the amount of shrinkage and the bending angle were calculated by the planar development procedure, and the laser scanning paths were determined as the intersection lines between each plane patch. The final step was to

determine the process parameters from the data maps obtained by FE modelling, which was matched to the bending and shrinkage data. Kim and Na indicated that the calculation time was reduced significantly with this method compared to the stress–strain analysis method and it was very easy to control the error bound by changing the number of patches.

For forming of a given shape, there can be many different scanning patterns, as shown in Figure 2.6.8, such as that Kim and Na [157] used cross paths to create both dome and saddle shape. Shen et al. [162] used parallel scanning paths to create both dome and saddle shape. Shen et al. [163] used discrete scanning paths to create the dome and saddle shape. Maji et al. [137] and Yang et al. [164] used cross spider scanning pattern to create the dome shape. Magee et al. [13] used concentric circular scanning pattern to create the saddle shape. Safari and Farzin [165] created the saddle shape by spiral scanning pattern. Gollo et al. [166] used spiral scanning pattern to create the dome shape.

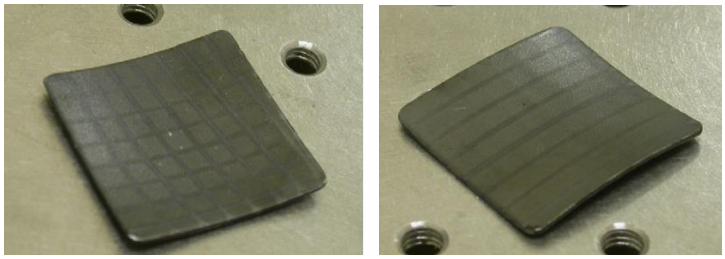

(a) Cross paths irradiation pattern

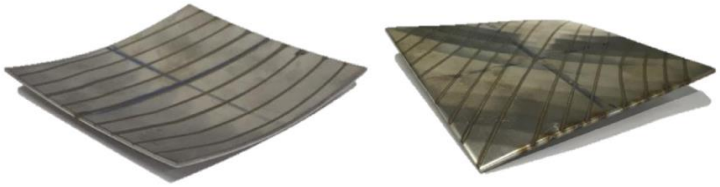

(b) Parallel paths irradiation pattern

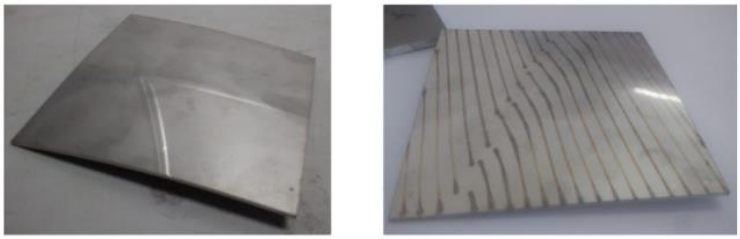

(c) Discrete paths irradiation pattern

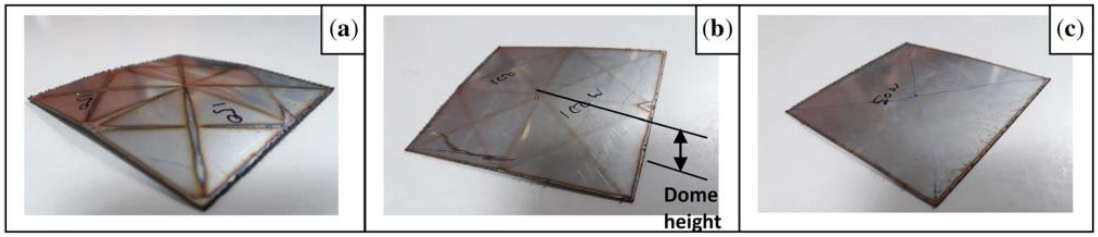

(d) Spider paths irradiation pattern

Figure 2.6.8 Examples of producing the dome and saddle shape by different irradiation patterns [157,162,163,137]

2.6.2.2 Closed Loop Control

Abed et al. [167] developed a predictive and adaptive approach to closed loop control the 3D laser forming of aluminium alloy AA5251 sheet into a desired shape with the maximum deflection of 40mm, as shown in Figure 2.6.9. Abed et al. proposed that a strategy of a one-off single pass to produce a required geometry with large deflection

would be extremely difficult to predict and control. A more sensible method of producing a required geometry would be to increment towards it over a number of passes, taking surface measurements with online monitoring system after each pass so as to have the ability to take account of any errors due to unwanted distortion.

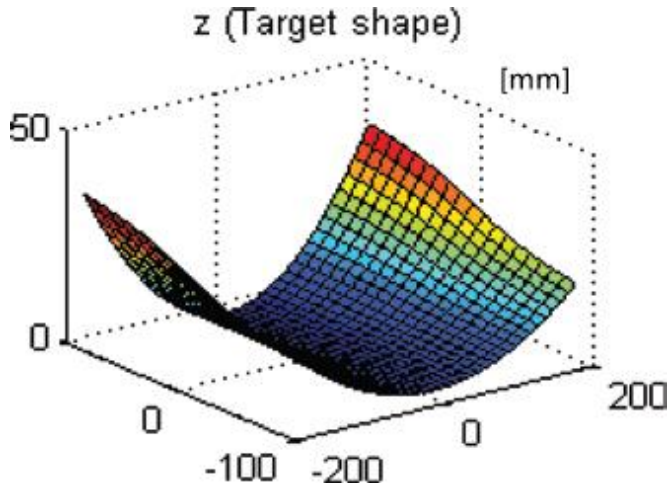

Figure 2.6.9 Interpolated points defining the desired shape [167]

The scanning strategy prediction in the study of Abed et al. was geometry based the error between the current formed shape and the desired shape, which could allow for the correction of the current formed shape if the desired shape was not formed by the scanning strategy prediction in the previous pass. The forming rate and distribution of the magnitude of forming across the surface were controlled in the closed loop by the scanning speed. The results obtained from the study of Abed et al. showed that using an iterative approach based on the error between the current and desired surfaces was possible to produce a component to within a reasonable degree of accuracy, here, the maximum error was -5mm and +3mm between the final formed shape and the desired shape.

2.7 Previous Laser Forming Research within the Laser Group at the University of Liverpool

2.7.1 Laser Forming Research in Macro Scale

The laser forming research in macro scale within the Laser Group at the University of Liverpool were mainly contributed by Magee, Edwardson, Abed, Carey, and Griffiths.

Magee [168] performed extensive empirical laser forming studies on aerospace alloys, such as AL2024-T3 aluminium alloy and Ti6Al4V titanium alloy. Parametric studies were carried out into the effects of the scanning strategy (single-pass and multi-pass) and beam size on 2D laser forming of these materials, and also developed a laser forming demonstrator for laser forming of part cylinder and initial prediction of the required irradiation paths required for 3D forming. The studies on titanium alloy found that both large and small beam size produced a TGM due to the low thermal conductivity of the material. From the aluminium alloy study, it was found that BM was induced with low scanning speed whereas higher scanning speed a TGM process was prevalent, since the material has relatively high thermal conductivity. Magee indicated that the thickening effect had greater influence on falloff in bending angle rate as the number of scans increased. The edge effect was also mentioned in Magee's studies. Magee indicated that it was attributed to the changing in mechanical restraint on the workpiece, temperature dependent material properties, and contraction in the laser moving direction. The effect could be minimized by reducing the energy input at the edges of the workpiece.

Edwardson [15] carried on a number of empirical laser forming studies and FE modelling on mild steel (CR4), titanium (TiAl4V), and aluminium alloy (AA1050 and AA6061 0/T4/T6) of various thicknesses from 0.9 to 1.6 mm. The process maps for each material were obtained by using of various beam diameters, laser powers and laser scanning speeds, which also revealed the unique forming characteristics of each material and concluded that the thermal conductivity, material strength and material thickness were the major factors for the variation in the process out comes. The effect of the dwell time between scans was investigated and it was found that too long dwell time between scans lead to a reduction in thermal gradient along the thickness, but too short a pause did not reduce the flow stresses present.

3D laser forming work carried out by Edwardson consisted of empirical studies and the development of an adaptive 3D laser forming system based on the geometry-based model through Matlab. A number of different techniques were employed in Edwardson's 3D laser forming studies, such as Bezier surface patch technique and contour lines of constant high, which was found to give reasonable prediction of the scanning strategy for the production of the target shapes.

Abed [169] studied the effect of the edge clamping and V-clamping on multi-pass laser forming process. It was concluded that the method of clamping had an effect on the current bending angle and the bending rate per pass. Abed found that the area of the beam was distorted with increasing of the bending angle using traditional edge clamping, which would reduce the energy density and result in the reduction of the efficiency of the laser forming process. However, it was found that after 25 passes no

reduction in bending rate per pass was observed using V-clamping, which was due to that the laser beam was kept perpendicular to the bending region during the laser forming process if using this type of clamping.

Most of Abed's work concentrated on the development of a closed-loop controlled 3D laser forming based on the geometry model. Abed proposed that a strategy of a one-off single pass to produce a required geometry with large deflection would be extremely difficult to predict and control. A more sensible method of producing a required geometry would be to increment towards it over a number of passes, taking surface measurements with online monitoring system after each pass so as to have the ability to take account of any errors due to unwanted distortion. The scanning strategy prediction was geometry based the error between the current formed shape and the desired shape, which could allow for the correction of the current formed shape if the desired shape was not formed by the scanning strategy prediction in the previous pass. The forming rate and distribution of the magnitude of forming across the surface were controlled in the closed loop by the scanning speed.

Carey [170] carried out the experimental and numerical studies into the laser forming of Fibre Metal Laminate materials (FML) with low power Nd:YAG laser (35 W). Carey identified that the effect of the FML parameters on laser forming process could be split into two main aspects, the stacking sequence and the fibre orientation.

From the aspect of stacking sequence, the cumulative bending angle decreased with increasing number of layers in the laminate due to laser forming mechanism occurring only in the top layer of the laminate, therefore the amount of force required to mechanically form the lower layers also increased as the number of layers increased.

Since there was a finite amount of force generated by the laser forming process for a given set of parameters, the bending angle produced was reduced. In addition, the bending process was affected by the increasing number of layers in the laminate in various ways. The spring-back occurred when number of layers in the composite was low (1:1 and 2:1). This was due to the lower effective Young's modulus of the laminate.

From the aspect of fibre orientation, Carey found that both cumulative bending angle and bending rate per pass reduced as fibres were orientated away from the direction of forming, which was consistent with offaxial loading of composites. Carey also found that the effect of fibre orientation on the bending process was to reduce the springback of 1:1 laminate and introduced a large counterbend, which was due to the increased effect of thermal contraction occurring during the curing cycle.

Griffiths [171] performed a study on laser forming of square section mild steel AISI 1010 tubes for the automotive industry through experimental study and numerical simulation. The FE modelling was used to develop the scanning strategy and predict the optimal process parameters for axial bending of the tube. From Griffiths's study, it was concluded that the scanning strategy for laser bending of the tube was to induce an in-plane shortening mechanism on three sides of the tube using the process parameters associated with the buckling or upsetting mechanism, the optimal scanning strategy can be seen in Figure 2.7.1. A tapered compression was generated around a central axis, which resulted in the tube bending towards the laser beam.

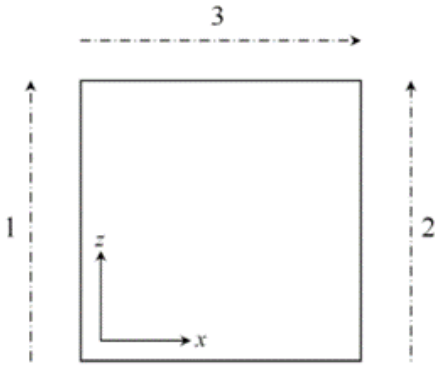

Figure 2.7.1 The optimal scanning strategy for bending of the square section tube. Dashed-dot lines represent irradiation path and direction, number represents the scanning sequency [171]

2.7.2 Laser Forming Research in Micro Scale

The laser forming research in micro scale within the Laser Group at the University of Liverpool were mainly contributed by Griffiths.

Griffiths [171] developed a novel technique for thermal laser micro forming of micro scale actuator style components (50μm and 75μm thick AISI 302 stainless steel sheet) using picosecond laser. A localised heat build-up on the top surface of micro-scale components was generated by using of the picosecond laser due to its ultra-short pulse duration and high repetition rates, which achieved for controlled and repeatable micro-adjustment.

Griffiths identified that a relatively large range of deformation was found to be produced through a combination of hatched and single line scanning paths with varying laser power and scanning speeds.

Griffiths indicated that the pulse duration was an important factor in laser micro forming. This is because that too short pulse duration would cause significant material removal by ablation, thus, an appropriate pulse duration needed to be determined in

order to limit the heat diffusion depth to within a suitable range on the top surface of the component. In addition, Griffiths also found that the repetition rate and pulse overlap must be high enough to ensure sufficient build up in temperature on the surface of the component for thermal forming.

2.8 Synopsis for Present Research

The information gathered from the literature review in this chapter reveals that to date there has been a considerable number of studies carried out on 2D and 3D laser forming. However, the laser forming process has less actual industrial applications compared to laser cutting, laser welding, and additive manufacturing. Moreover, there is limited research related to accuracy control the forming process to produce a target component. This means that the laser forming process still needs to be further studied.

The first work presented in this thesis is to develop an advanced scanning strategy to improve the controllability of the process and produce a two-dimensional component independent of material and process variability and this work is also to prove the manufacturing capabilities of the LF process at attempt was made to produce an actual car body component, which is linked to the Audi commercial project. The required ‘U’ shaped component with three different bending angles 20°, 40° and 60° from Audi AG was identified as an ideal candidate for laser forming.

For practical industrial applications, in addition to single curved shapes, most components have a double curved geometry, such as ship hulls, pillow shape, saddle shape etc. Therefore, it is necessary to consider 3D laser forming in order to advance

the application of laser forming in the actual manufacturing environment. The second work presented in this thesis is to develop an advanced 3D laser forming methodology for producing a double curved shape to within a small degree of error to the target shape. The component with a ship hull geometry was chosen for 3D laser forming investigation in this thesis, which is supplied by a ship building company.

Chapter 3

Experimental and Simulation Procedures

This chapter covers the general experimental set-up, finite element modelling, and procedures for separate investigations, such as investigations of 2D and 3D laser forming undertaken for this thesis.

3.1 General Experimental Set-up

This section describes the general experimental set-up used throughout this thesis. It contains the laser system, workstation, the use of absorptive coatings and the materials used in the experimental studies.

3.1.1 Laser System

3.1.1.1 The PRC 1.5kW CO_2

The laser used for all the laser forming processes performed in this thesis was a 1.5 kW CO_2 (wavelength 10.6μm) fast axial flow (FAF) continuous wave (CW) laser with a Class 4 safety designation manufactured by PRC. This laser has a folded cavity to conserve space and increase the cavity length (Figure 3.1.1). A general rule with the cavity is that the longer the cavity is the more power output it can produce. The cavity is housed in the lasers casing (Figure 3.1.2) along with the vacuum pump, blower, heat

exchanger and power supply.

Figure 3.1.1 PRC 1.5kW CO_2 Laser

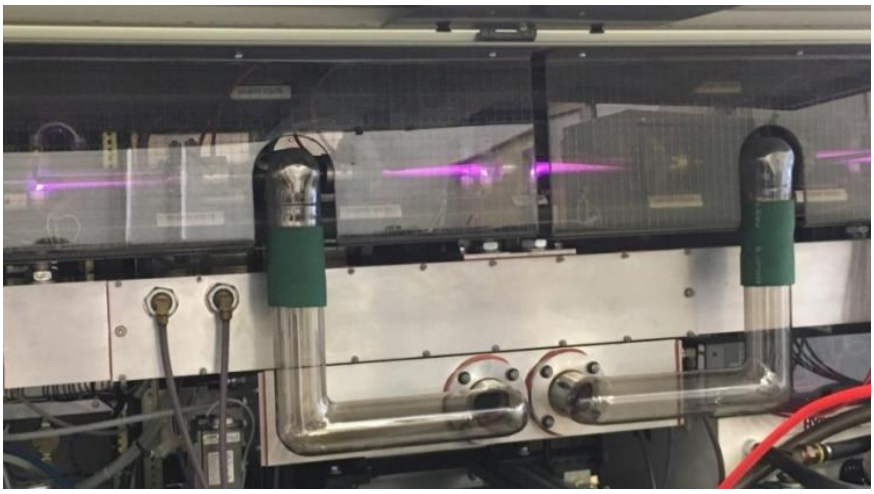

Figure 3.1.2 Laser Cavity, Heat Exchanger and Cavity Discharge

The active medium in CO_2 laser is carbon dioxide gas. The carbon dioxide molecule is made up of a carbon atom covalently bonded to two oxygen atoms. While constrained by the atomic bonds between them, these atoms naturally oscillate about each other as a result of thermal energy. The working principle of the CO_2 laser is that a photon of 10.6μm wavelength is produced as the CO_2 molecule transforms from an upper energy state to a lower level. The production of carbon dioxide molecules in the various energy states is achieved in the cavity by subjecting the gas to a high voltage

electric discharge. The nitrogen is added to the carbon dioxide in order to maintain a high population of upper laser level molecules due to that nitrogen has one excited state and the energy level of this excited state is very close to that of the upper energy state of carbon dioxide. Hence, a transition directly to the upper energy state of carbon dioxide will occur when the excited nitrogen molecules collide with unexcited state of carbon dioxide. However, the carbon dioxide must be kept cool in order for this transformation to take place. This is achieved by adding helium to the cavity gas mixture due to its high heat conductivity. The helium is used to absorb energy by collision with the carbon dioxide molecules in the bottleneck intermediate state and transfer this energy as heat to the walls of the laser cavity and remove it [15].

The three constituent gases are fed into the laser cavity from three large gas bottles, each with its own flowmeter to ensure an accurate gas mixture, a high voltage (HV) power supply and cooled water from central water-cooling system to cool the heat exchangers and optics. The optimum gas mixture in the laser cavity is around 78% helium (He); this is for good conduction and stabilisation of the plasma, 13% N_2, for the exciting of cold CO_2 to the upper energy state, and 10% CO_2 as the active medium.

The laser used in this thesis has an M^2 of approximately 2.5. M^2 is a measure of laser beam quality, which represents the degree of variation of a beam from an ideal Gaussian beam ($M^2 = 1$). M^2 is related to wavelength of the laser, the beam radius at the beam waist after the focus lens, and the divergence angle. Therefore, M^2 can be measured by placing an array detector or scanning-slit profiler at multiple positions within the beam after focusing it with a lens of high optical quality and known focal

length [172]. The laser used in this thesis has a ‘top hat’ energy distribution which is advantageous in laser forming as a larger area of the surface can be heated equally minimising the melting on the centre of the irradiation track.

3.1.1.2 Selection of Beam Diameter

As mentioned earlier, a defocused laser beam needs to be employed in the laser forming process, of which the diameter is related to the focus lens to workpiece stand-off (Z position), the lens focal length of the focus lens, the M^2 of the laser, the wavelength of the laser, and the diameter of the parallel beam before the focus lens [16]. In this thesis, the defocused beam diameters were determined using burn prints in plywood at various focus lens to workpiece stand-off. The z-axis was moved up 5mm after a burn print has been created, which allowed a measurement of the beam diameter to be taken at 5mm intervals. The actual effective beam diameter is taken as the inner ring of higher intensity and not the overall diameter due to the slight halo of lower intensity of the “top hap” beam profile. A large diameter nozzle and a small amount of compressed air is delivered coaxially to cool the lens and protect against debris for this test and throughout the laser forming studies. An example of burn prints in plywood is given in Figure 3.1.3. It needs to be noted that although the defocus beam diameters can be obtained directly in this way, there is a testing error, therefore the advanced optical testing device can be used to measure the defocus beam diameters, such as CCD, Beam Watch and Focus Monitor.

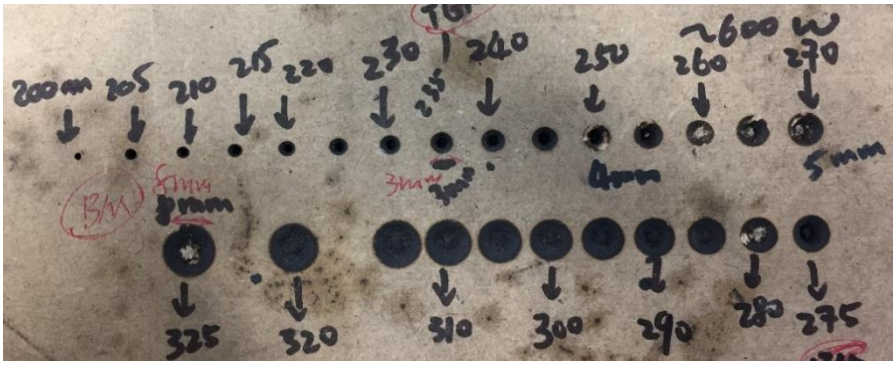

Figure 3.1.3 Burn prints in wood at 5mm Z steps, focus lens with 190mm focal length, 200mm – 325mm stand-off

3.1.1.3 Selection of Laser Power

The power of the laser is selected manually on a handheld control box. The reading of the power is based on a calibrated thermocouple measurement from the back mirror of the cavity. This reading is the laser power leaving the cavity at the output window but not for the power at the workpiece. This is due to a number of mirrors used to guide the beam to the workstation there is some power loss each time the beam is turned, the mirrors and lens absorb some of the incident energy (the optics heat up and hence have to be water cooled). Because of this a power reading is taken at the sample for varying powers at the laser. This reading is taken using a power puck. A power puck is a calibrated device whereby the temperature rise, in a coated black metal block exposed to a laser beam, is directly proportional to the incident laser power. A graph to correlate the relationship is then plotted as shown in Figure 3.1.4. This graph is then used to determine the power required on the laser to achieve the required power at the surface of the workpiece.

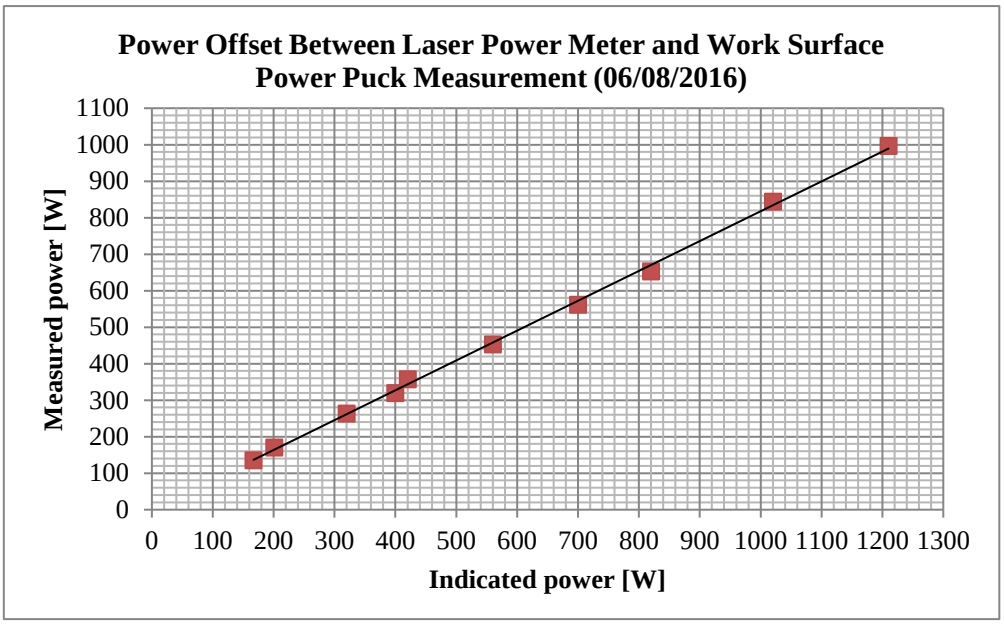

Figure 3.1.4 Power offset calibration graph

3.1.1.4 Beam Delivery

The laser beam was delivered approximately 3.5m to the processing head via three gold coated copper turning mirrors (45° fixed) and enclosed in flight tubes. The processing head contains a water-cooled zinc selenide (ZnSe) coated focus lens and the co-axial nozzle arrangement as shown in Figure 3.1.5.

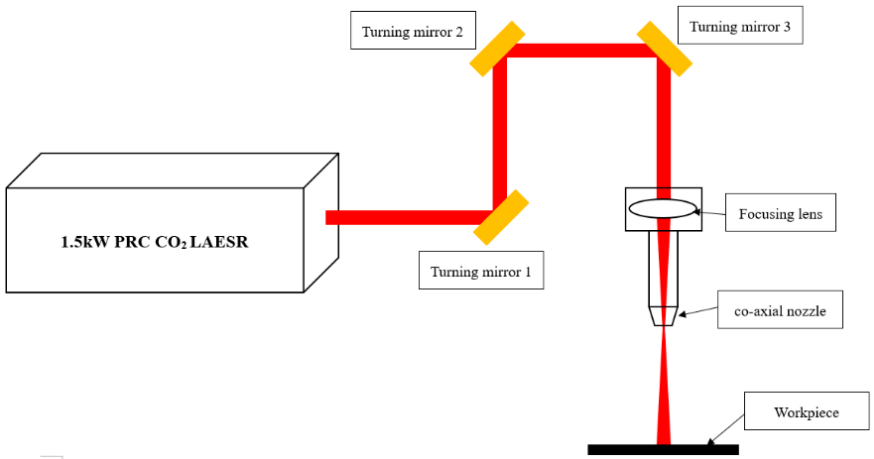

Figure 3.1.5 The schematic of the beam delivery system, a defocused beam placed on the upper surface of the workpiece

3.1.2 Workstation

3.1.2.1 Part Manipulation

The workstation consists of a 3 axis CNC moving stage driven by linear motor. The tables and control system are based around the Aerotech, Inc., A3200 Software-Based Machine Controller. Aerotech PRO115LM-300 Mechanical-Bearing Direct-Drive Linear Stage is for x & y-axis movement under the laser with the maximum travel speed of 300mm/s, accuracy of ±1.5μm and maximum 300mm of travel. ATS150-200 Mechanical Bearing, Screw-Driven Linear Stage has the maximum 300mm of travel is for z-axis movement with the maximum travel speed of 115mm/s and accuracy of ±1 μm, which provides the focus control and various beam size selection. The CNC moving stage is placed in a completely enclosed system within an interlocked cabinet with an observation double door as shown in Figure 3.1.6.

Figure 3.1.6 The CNC moving stage placed in an interlocked cabinet

3.1.2.2 Control System

The CNC moving stages are controlled by an A3200 Software-Based Machine Controller as mentioned before. The A3200 is software-based (no PC slots required) and marries a robust, high performance motion engine with I/O in one unified programming environment that is programmable in native RS-274 G-code. All of the external signals including encoder and I/O are fed directly into the drive, allowing one cable to be used between the PC and the drive. Drives are networked together with a single cable. The Operator Interface provides a traditional CNC look and feel for operating a machine running G code as shown in Figure 3.1.7. The interface provides a multi-axis readout with position, velocity shown in user units, immediate command, Manufacturing Operations Optimizer (MFO), program scan during execution, modal status, and a multi-axis jog screen. Typical cycle start, stop, feed-hold, and system stop buttons are included. The operator can open and load a new program, watch status, and manually control the machine. The CNC programs (G code and M code) for controlling the moving stage and laser were all generated in Alphacam as can be seen in Figure 3.1.8.

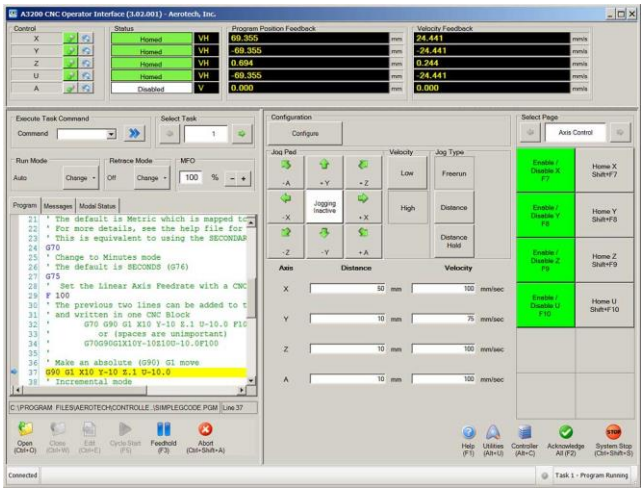

Figure 3.1.7 A3200 CNC Operator Interface

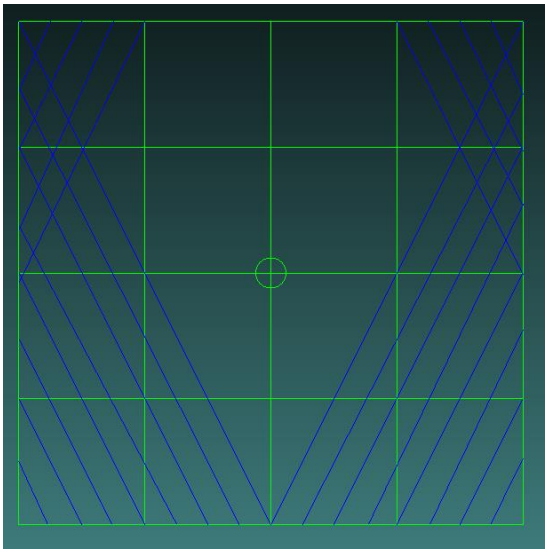

```
ENABLE X Y Z ;Turn On Servo Loop Control for the Axes
HOME Z
HOME X Y
G71 ;Metric
G76 ;Feed Speeds Units/Second
G90 ;Absolute
M52 ; CW Mode
M60 ; Beam On
M66 ; Ramp Up Laser
F$FEED ;Feed Speed mm/Second
G54 X$DATUM_X Y$DATUM_Y Z$DATUM_Z
G0 X-44.33 Y-49.839
G0 Z0.
M300 ;Gas 1 On
M100 ;Shutter Open
G1 X-50.093 Y-37.294
M101 ;Close Shutter
G0 X43.651 Y-49.839
G0 Z0.
M100 ;Shutter Open
G1 X50.093 Y-36.786
M101 ;Close Shutter
G0 X-43.75 Y50.
G0 Z0.
M100 ;Shutter Open
G1 X-49.935 Y36.318
M101 ;Close Shutter
G0 X43.75 Y50.
G0 Z0.
M100 ;Shutter Open
G1 X50.028 Y35.437
M101 ;Close Shutter
G0 X-37.5 Y-50.
G0 Z0.
M100 ;Shutter Open
```

Figure 3.1.8 The CNC programs (G code and M code) for controlling the moving stage and laser shutter open or close generated in Alphacam

3.1.2.3 Measurement System

The MICRO-EPSILON scanCONTROL2700-100 laser scanner with a measuring range of 100mm and a resolution of 15μm for 2D/3D measurements is integrated with the system for all of the studies in the thesis. The sensor is mounted on the z moving stage. The operating principle of the laser scanner is based on the laser triangulation principle for two-dimensional profile acquisition of a height profile of various target

surfaces. A laser line is projected onto the target surface via a linear optical system onto the target surface. A high-quality optical system projects the diffusely reflected light of this laser line back onto a highly sensitive sensor matrix. In addition to the calibrated distance information (z-axis vertical height from ground), the controller, integrated into the sensor head, uses this matrix image to calculate the position along the laser line (x/y-axis). This generates calibrated matched measurement values (z, x/y) which are than output as a precise line profile. Regardless of the position or angle the profile data are absolute calibrated data sets in a two-dimensional coordinate system that is fixed in respect to the sensor. In the case of moving objects or a traversing sensor, it is therefore possible to obtain a precise 3D image of the target as well as an intensity image at the same time. The measurements for 2D bending angle and 3D profile can be seen in Figure 3.1.9 and Figure 3.1.10.

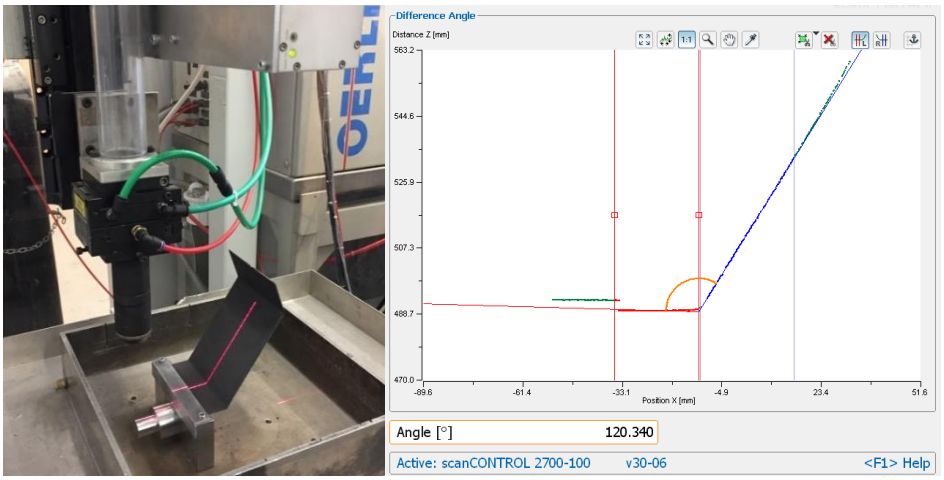

Figure 3.1.9 Bending angle measurement by laser scanner

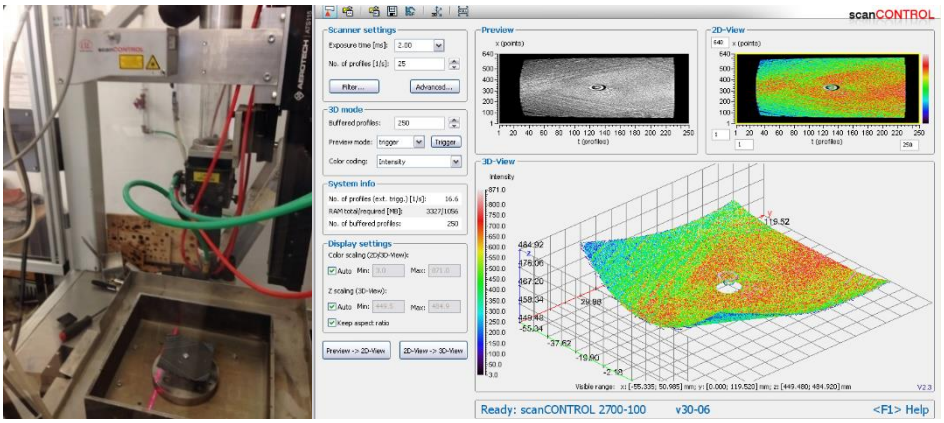

Figure 3.1.10 Surface measurement by laser scanner

3.1.2.4 Workpiece Constraints

The workpiece clamping is one of the important factors in laser forming, which provides a mechanical constraint during the heating process. Therefore, different methods of clamping will affect the final deformation of the workpiece [42,45] . There are two different methods of clamping the workpiece in the investigations carried out in this thesis. An edge clamping is used for laser forming of single curved shape (2D laser forming) (Figure 3.1.11 (a)). It is the simplest method of constraint and doesn't require a hole to be drilled into the workpiece. For laser forming of double curved component (3D laser forming) a centre clamping (Figure 3.1.11 (b)) is used, which requires a hole to be drilled into the centre of the workpiece. Although drilling the workpiece will generate additional pre-stressing, fixing the workpiece was essential to avoid any unwanted movement. In addition, any problems with the weight of the workpiece limiting the amount of forming available can be alleviated by raising the workpiece off the working bench.

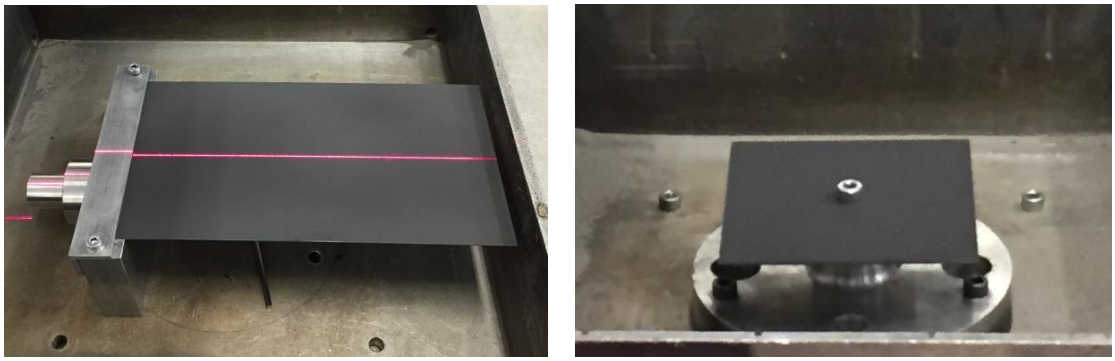

(a). Edge clamping for 2D laser forming (b). Centre clamping for 3D laser forming

Figure 3.1.11 Different types of clamping

3.1.3 Absorptive Coating

The absorptivity of the material plays a vital role in laser material processing, and the energy input to the material will increase as the absorptivity increases. It can be seen in Figure 3.1.12, the absorptivity of the metals decreases as the wavelength increases, especially when the wavelength exceeds 10μm, the absorptivity of the material is extremely low.

In metals, the radiation is predominantly absorbed by free electrons in an "electron gas". These free electrons are free to oscillate and reradiate without disturbing the solid atomic structure. As a wave front arrives at a surface of the target then all the free electrons in the surface vibrate in phase generating an electric filed 180° out of phase with the incoming beam creating "electron gas". This "electron gas" within the metal structure means that the radiation is unable to penetrate metals to any significant depth, only one to two atomic diameters or free paths, thus metals are opaque and they appear shiny [15,16].

There are many ways to increase the absorptivity of the material, such as using a shorter wavelength laser, increasing the power density, and changing the surface conditions. However, as mentioned earlier, the CO_2 laser with the wavelength of 10.6μm was used throughout in this study, and the power density involved in laser forming was relatively low (10^2-10^4 Wcm^{-2}) compared to laser cutting (>10^7 Wcm^{-2}) [14,16]. Therefore, changing the surface conditions is usually required when using this laser type in laser forming process [52,69,70,71,72,73,74].

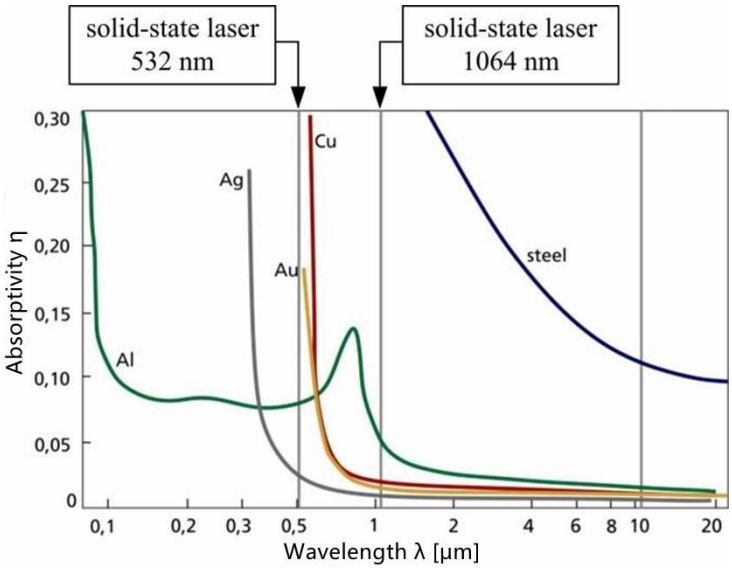

Figure 3.1.12 Wavelength dependence of the absorptivity of different metals [173]

There are many methods can be applied to change the surface conditions of materials, such as roughening of the surface, which includes sandpaper roughened and sandblasted, oxidising the surface, and coating the surface [16]. Typical values of the reflectivity and absorptivity of various surfaces to 10.6μm radiation for perpendicular laser beam incidence is summarised in Table 3.1.1.

		Reflectivity %			Absorptivity %
		Direct	Diffuse	Total	Total
Roughening	Sand Paper roughened (1μm)	90	2.7	92.7	7.3
	Sandblasted (19μm)	17.3	14.5	31.8	68.2
	Sandblasted (50μm)	1.8	20	21.8	78.2
Oxidising	Oxidised	1.4	9.1	10.5	89.5
Coating	Graphite	19.1	3.6	22.7	77.3
	Molybdenum disulfide	5.5	4.5	10	90

Table 3.1.1 Typical values of the reflectivity of various surfaces to 10.6um radiation for perpendicular laser beam incidence [16]

Absorptive coatings are the most common means to increase the absorption of CO_2 laser radiation and widely used in industry. The coating layer absorbs laser energy and transfers the released heat to the workpiece [16].

The coating used throughout the studies in this thesis is graphite, which is quoted to have an absorptivity of 77.3 % (Table 3.1.1). Since graphite is manually sprayed onto the surface of the workpiece through a spray can, the uniformity and consistency of the coating layer cannot be guaranteed, which will cause the non-uniform heat transmission to the surface of the workpiece. It is possible to evenly cover the smaller samples, but for larger samples, it is very difficult. In order to make graphite have good and uniform adhesion on the surface of the workpiece, the sample will be cleaned with acetone to remove any surface contaminants before coating.

The uneven coating layer thickness will cause non uniform heat transfer to the metal substrate, thus affecting the accuracy and stability of the process. In addition, it can be seen from Figure 3.1.13 that the longer laser interaction time and the higher intensity of the laser beam will cause the degradation of the coating more seriously

resulting in the reduction of heat transmission to the workpiece. However, re-coating was not used throughout the studies in this thesis, this is because that normally for optimum adhesion a surface should be cleaned with acetone first, however, this was thought to be not suitable for the current experimental conditions. Because there is no visual positioning system, once the workpiece is removed from the clamping for re-coating, it is difficult to ensure the alignment of the laser for the next pass.

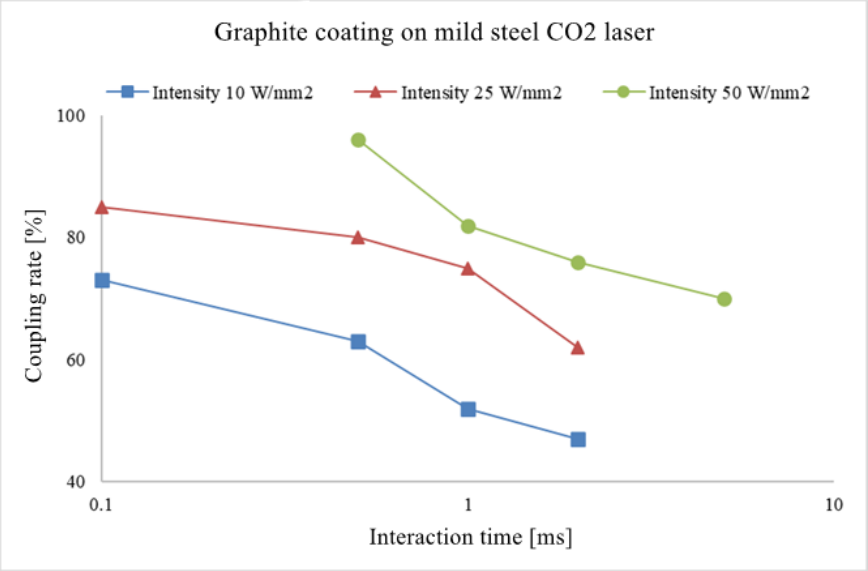

Figure 3.1.13 Dependence of coupling rate of coated surfaces on interaction time and incident intensity [5]

3.1.4 Materials used in this Thesis

There are three materials used for the studies in this thesis, which are mild steel DC01, AA6061-T6 and mild steel S275, in which mild steel DC01 and AA6061-T6 (supplied by Audi) were used for 2D laser forming studies, mild steel S275 was used for investigation of 3D laser forming.

3.1.4.1 Mild Steel DC01

The first material used in the investigation of 2D laser forming is 0.89mm thick mild steel DC01, a European standard cold-rolled quality low-carbon steel flat product for cold forming. It can be noted that D means (Drawing) flat products for cold forming, C means Cold rolled and 01 means Drawing quality. The main application areas of the DC01 includes automotive industry, construction industry, electronic equipment and home appliance industry, decorative purposes, food canning, etc. [174]. Technical data on this material is listed in the following tables:

Composition	Fe%	C%	S%	P%	Mn%
Weight	99.19 min	0.12 max	0.045 max	0.045 max	0.60 max

Table 3.1.2 Material composition in weight percentage of Mild Steel DC01 [174]

Density [kg/m3]	Young's Modulus [GPa]	Tensile Strength [MPa]	Yield Strength [MPa]	Shear Modulus [GPa]	Bulk Modulus [GPa]	Hardness [HV]
7870	205	365	305	80	140	108

Table 3.1.3 Mechanical Properties of Mild Steel DC01 [174]

Melting point [°C]	1515
Thermal Conductivity [W/m K]	49.8
Coefficient of Thermal Expansion [10^{-6}/K] 20 °C	12.2
Coefficient of Thermal Expansion [10^{-6}/K] 250 °C	13.5

Coefficient of Thermal Expansion [10^{-6}/K] 500 °C	14.2
Specific Heat Capacity [J/kg K] 50-100 °C	448
Specific Heat Capacity [J/kg K] 250-300 °C	536
Specific Heat Capacity [10^{-6}/K] 400-450 °C	649
Specific Heat Capacity [10^{-6}/K] 650-700 °C	825

Table 3.1.4 Thermal Properties of Mild Steel DC01 [174]

3.1.4.2 Aluminum Alloy 6061 (AA6061)

The second material used in the investigation of 2D laser forming is 1mm thick AA6061, a non-ferrous wrought and age hardenable 6000 series aluminium alloy. AA6061 is a general-purpose structural alloy. The main alloying elements are magnesium (Mg) and silicon (Si). The temper designations mainly have O, T4, and T6. O denotes that the alloy is annealed, and T indicates that the alloy is thermally treated to produce stable tempers. In addition, T is always followed by one or two numbers which shows the exact type of heat treatment, and more details of the processing of the alloy. The lowest strength temper for wrought products is obtained by the O temper; AA 6061-O is in the softest possible condition because the strain hardening form cold working is reduced by annealing. AA6061 in both of the T4 and T6 temper are solution heat treated and cold worked. The main difference between these two tempers is that the T4 temper is naturally aged to a substantially stable condition after solution heat treatment, but the

T6 temper is artificially aged. Generally speaking, an alloy in the T4 temper owns higher ductility and lower strength than the same alloy in the T6 temper. Because AA6061 is easy to extrude, which can provide a variety of product forms such as sheet, strip, plate, rod, forgings, tubes, pipes, wires, extruded parts and structural shapes. In addition, AA6061 has good corrosion resistance, mechanical properties, formability, weldability, and machinability, whose applications range from food and beverage packaging, electronic products and home appliances, architectural decoration, automotive to aerospace components [175]. Technical data on this material is listed in the following tables:

Composition	**Al%**	**Mn%**	**Fe%**	**Mg%**	**Si%**
Weight	96.2 min	0.15 max	0.7 max	0.8-1.2	0.4-0.8
Composition	**Cu%**	**Zn%**	**Ti%**	**Other (Each)%**	**Other (Total)%**
Weight	0.15-0.4	0.25 max	0.15 max	0.05 max	0.15 max

Table 3.1.5 Material composition in weight percentage of AA6061 [175]

Temper	**Density [kg/m3]**	**Young's Modulus [GPa]**	**Tensile Strength [MPa]**	**Yield Strength [MPa]**	**Shear Modulus [GPa]**	**Hardness [HV]**
O	2700	69	125	55	80	32
T4	2700	69	249	145	165	71
T6	2700	69	310	275	205	102

Table 3.1.6 Mechanical Properties of AA6061 in various tempers [175]

	O	T4	T6
Melting Range [°C]	582-652	582-652	582-652
Thermal Conductivity [W/m K]	180	154	166.9
Coefficient of Thermal Expansion [10^{-6}/K] 20 °C	23.6	23.6	23.6
Coefficient of Thermal Expansion [10^{-6}/K] 250 °C	25.2	25.2	25.2
Specific Heat Capacity [10^{-6}/K] 20 °C	896	896	896

Table 3.1.7 Thermal Properties of AA6061 in three different tempers [175]

3.1.4.3 Mild Steel S275

The material used in the investigation of 3D laser forming is 1.5mm thick mild steel S275, a non-alloy structural steel. Structural steels are used in many ways and their application can be diverse. They are particularly useful because they are strong, tough, ductile, formable, weldable, and equally as important, affordable [176]. Technical data on this material is listed in the following tables:

Composition	Fe%	Si%	C%	S%	P%	Mn%
Weight	98.01 min	0.05 max	0.25 max	0.05 max	0.04 max	1.60 max

Table 3.1.8 Material composition in weight percentage of Mild Steel S275 [176]

Density [kg/m3]	Young's Modulus [GPa]	Tensile Strength [MPa]	Yield Strength [MPa]	Shear Modulus [GPa]	Bulk Modulus [GPa]	Hardness [HV]
7900	200	370	275	79.3	140	147

Table 3.1.9 Mechanical Properties of Mild Steel S275 [176]

Melting point [°C]	1460
Thermal Conductivity [W/m K]	50
Coefficient of Thermal Expansion [10^{-6}/K] 20 °C	11.2
Coefficient of Thermal Expansion [10^{-6}/K] 250 °C	13.1
Coefficient of Thermal Expansion [10^{-6}/K] 500 °C	14.1
Specific Heat Capacity [J/kg K] 20 °C	450
Specific Heat Capacity [J/kg K] 250 °C	530
Specific Heat Capacity [10^{-6}/K] 500 °C	720
Specific Heat Capacity [10^{-6}/K] 700 °C	830

Table 3.1.10 Thermal Properties of Mild Steel S275 [176]

3.2 Finite Element Modelling

In this thesis, the FE modelling of the laser forming process was carried out in COMSOL Multiphysics version 5.2a, which is mainly focus on investigation of the effect of scanning path spacing on laser forming process, which can provide the

theoretical support for prediction of the scanning pattern in 3D laser forming study.

The following modules in COMSOL were used for FE modelling of laser forming process: Geometry Module, which was used to create 3D geometric parts and define laser scanning paths; Structural Mechanics Module, which was used for analysing mechanical behaviour of solid structures, such as strain levels; deformations etc.; Heat Transfer Module, which supports the fundamental mechanisms of heat transfer; conduction, convection and radiation; and Material Library, which contains data for 3870 materials including the materials used in the thesis, and so the properties of the material (mild steel S275) used in FE modelling, such as the thermal expansion coefficient (α_{th}), Young's modulus (E), Poisson's ratio (υ), specific heat capacity (C_p), thermal conductivity (k), density (ρ) and yield stress (σ_{ys}) were all sourced from COMSOL's built in materials library.

The heat transfer theory and FE model development of laser forming process are presented in the following subsections. Most of the details are sourced from COMSOL Multiphysics Users Guide 5.2a [177].

3.2.1 Heat Transfer

3.2.1.1 Conductive heat flux

Conduction is a process in which transfer of heat takes place between objects by direct contact due to temperature difference, which occurs in solids through molecular collisions [41]. The basic law of heat conduction is the Fourier heating equation. The heat transferred through a unit cross-sectional area in a unit time is proportional to the

temperature gradient in the normal direction of the cross-section, namely:

$$\nabla . q = -\rho C_p \frac{\partial T}{\partial t}$$

Equation 3.2.1

$$q = -k\nabla T$$

Equation 3.2.2

where ρ is the density (kg/m^3), C_p is the specific heat capacity (J/kgK), T is the temperature (K), t is the time (s), and k is the thermal conductivity (W/mK). q is the conductive heat flux vector (W/m^2). The term ∇ is the differential or gradient operator for three-dimensional Cartesian co-ordinate systems.

3.2.1.2 Convection and Radiation heat flux boundary conditions

The inward heat flux, q_0, is often a sum of contributions from convection and radiation. The special case $q_0 = 0$ is called thermal insulation.

$$q_0 = q_{conv} + q_{rad}$$

Equation 3.2.3

$$-n . q = q_0$$

Equation 3.2.4

where n is the normal vector on the boundary, q_0 is the inward heat flux (W/m^2), normal to the boundary.

3.2.1.2.1 Convection heat flux

Convection refers to the form of heat transfer, in which energy transition occurs within the fluid due to density difference, which occurs in fluids by actual flow of matter [41].

A common type of convective heat flux boundary conditions can be seen in Equation 3.2.5.

$$q_{conv} = h(T_{ext} - T)$$

Equation 3.2.5

where h is the heat transfer coefficient (W/m^{2}K), T_{ext} is the temperature (K) far away from the modelled domain.

The overall heat transfer coefficient refers to the degree of which heat is conducted through over a series of resistant mediums. It is influenced by the thickness and thermal conductivity of the mediums through which heat is transferred. The larger the coefficient, the easier heat is transferred from its source to the product being heated [41]. In laser forming, the workpiece with fluid flow, which is air in this thesis, on each side of it can be considered as a heat exchanger. Therefore, the overall heat transfer coefficient, U, can be calculated as:

$$\frac{1}{UA} = \frac{1}{h_i A_i} + \sum \left(\frac{s_n}{k_n A_n}\right) + \frac{1}{h_0 A_0}$$

Equation 3.2.6

where U is the overall heat transfer coefficient (W/m^{2}K), k_n is the thermal conductivity (W/mK) of material in layer(n), $h_{I,0}$ is the inside or outside wall individual fluid convection heat transfer coefficient (W/m^{2}K), s_n is the thickness of layer n (m), A is the wall area (m^2).

In laser forming, a plane wall with equal area in one layer and the fluid on each side is typically air, so the Equation 3.2.6 can be simplified to

$$\frac{1}{U} = \frac{1}{h_a} + \frac{s_0}{k} + \frac{1}{h_a}$$

Equation 3.2.7

where h_a is the heat transfer coefficient of the air (W/m^2K), s_0 is the thickness of the workpiece, k is the thermal conductivity of material (W/mK).

The overall heat transfer co-efficient can be calculated as:

$$U = \frac{1}{\frac{2}{h_a} + \frac{s_0}{k}}$$

Equation 3.2.8

3.2.1.2.2 Radiative heat flux

In addition to conduction and convection, the third mechanism for heat transfer is radiation. Thermal radiation denotes the stream of electromagnetic waves emitted from a body at a certain temperature [41]. The object is fully opaque in this thesis. The Surface-to-Surface Radiation Interface theory is described in this section. The total incoming radiative flux is called irradiation and denoted G (W/m^2). The total outgoing radiative flux is called radiosity and denoted J (W/m^2). This radiosity is the sum of diffusively reflected and emitted radiation as depicted in Figure 3.2.1.

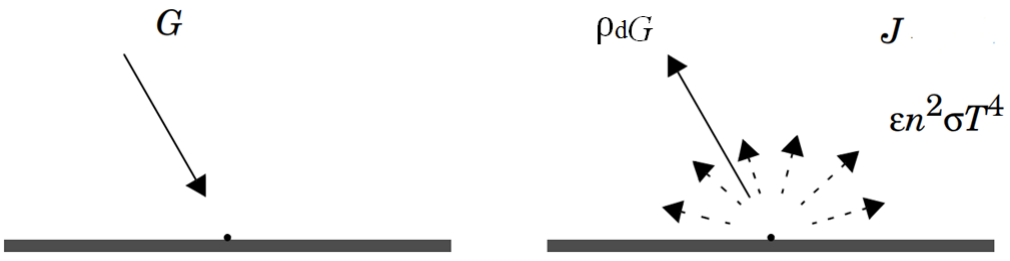

Figure 3.2.1 Incoming irradiation (left), outgoing radiosity (right)

$$J = \rho_d G + \varepsilon n^2 \sigma T^4$$

Equation 3.2.9

where ρ_d is diffuse reflectivity, ε is the surface emissivity, n is the refractive index, σ is the Stefan Boltzmann constant (5.67×10^{-8} W/m^{2}K^4), T is the surface temperature (K).

Laser forming process was in the air throughout the numerical modelling in this thesis, so the refractive index n is 1, so the Equation 3.2.9 can be simplified to

$$J = \rho_d G + \varepsilon \sigma T^4$$

Equation 3.2.10

Therefore, the net inward radiative heat flux, q_{rad} is then given by the difference between the irradiation and the radiosity:

$$q_{rad} = G - J$$

Equation 3.2.11

Using Equation 3.2.10 and Equation 3.2.11, J can be eliminated, and a general expression is obtained for the net inward heat flux into the opaque body based on G and T.

$$q_{rad} = (1 - \rho_d) G - \varepsilon \sigma T^4$$

Equation 3.2.12

Most opaque bodies behave as ideal grey bodies, whose absorptivity of a surface does not vary with variation in temperature and wavelength of the incident radiation [41]. For a grey body, the absorptivity and emissivity are equal, and no radiation is transmitted through the body, therefore the relationship between absorptivity, emissivity and reflectivity is described by Equation 3.2.13.

$$\alpha = \varepsilon = 1 - \rho_d$$

Equation 3.2.13

Thus, for ideal gray bodies, q_{rad} is given by:

$$q_{rad} = \varepsilon(G - \sigma T^4)$$

Equation 3.2.14

Since $G = \sigma T_{amb}^4$, Equation 3.2.14 can be expressed as

$$q_{rad} = \varepsilon\sigma(T_{amb}^4 - T^4)$$

Equation 3.2.15

3.2.2 FE Modelling of Laser Forming Process

FE modelling presented in this section consists of three steps. The first step is to create a heat source, the second step is to determinate meshing and solving time step, and the third step is validation by experiment. It can be noted that a number of assumptions have been made in developing the FE modelling, which includes:

- The initial temperature is constant.
- The material is isotropic and homogeneous.
- The thermal and mechanical properties of the materials will not be influenced by the temperature.
- Absorption coefficient of the material is constant.
- Laser beam intensity distribution is Gaussian distribution.
- Consider the convection and radiation between the workpiece and the air.
- The material yields as per von Mises criterion.
- Plastic deformation does not cause volume change.
- The weight of the workpiece is negligible.
- Beam diameter is constant

3.2.2.1 Creating heat source

For the laser forming modelling throughout this thesis, the intensity distribution of the inward heat flux q_n was assumed to be a Gaussian distribution with an absorption coefficient (A) of 0.8 since in the experiments, the workpiece is coated with graphite, whose emissivity is ~0.8. The distribution of the intensity of the beam with a power P can be described with a Gaussian function, as shown in Equation 3.2.16, r is defined as the distance from the centre of the beam, ω_0 is the Gaussian beam radius at which the amplitude is $1/e^2$ (≈ 13.5%) of its value on the axis, and I_0 is maximum intensity at the centre of the beam at its waist as shown in Equation 3.2.17. So, the intensity of Gaussian distribution can be expressed by Equation 3.2.18.

$$I = I_0 \exp\left(-2\frac{r^2}{\omega_0^2}\right)$$

Equation 3.2.16

$$I_0 = \frac{2AP}{\pi\omega_0^2}$$

Equation 3.2.17

$$I = \frac{2AP}{\pi\omega_0^2}\exp\left(-2\frac{r^2}{\omega_0^2}\right)$$

Equation 3.2.18

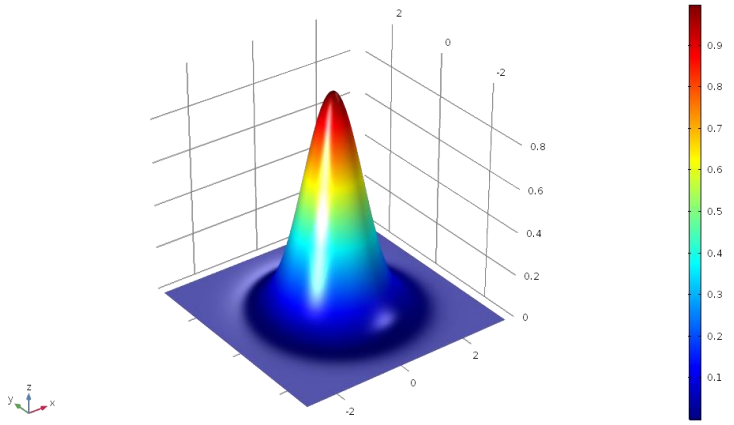

Figure 3.2.2 3D plot of Gaussian intensity distribution created in COMSOL

The inward heat flux q_n and the distance from the centre of the beam r_n in COMSOL can be expressed as:

$$q_n = \frac{2AP}{\pi\omega_0^2}\exp\left(-2\frac{r_n^2}{\omega_0^2}\right)$$

Equation 3.2.19

$$r_n = \sqrt{(x - x_n)^2 + (y - y_n)^2}$$

Equation 3.2.20

Using Equation 3.2.19 and Equation 3.2.20, the inward heat flux q_n can be expressed as:

$$q_n = \frac{2AP}{\pi\omega_0^2}\exp\left(-2\frac{(x - x_n)^2 + (y - y_n)^2}{\omega_0^2}\right)$$

Equation 3.2.21

where x_n and y_n are the coordinates for the beam in x and y-axis respectively.

There are three different studies with different scanning strategies in the FE modelling presented in this thesis. All the numerical simulations presented in this thesis were conducted with 500 W of power, 50mm/s as the velocity and 5mm for the beam

diameter, which is one of the parameters setting used in the experimental work. The dimension of the workpieces was 100×100×1.5mm and the material was mild steel S275. Coordinate origin is the corner of the workpiece. The validation of FE modelling was presented in the following subsection.

3.2.2.2 Determination of meshing and solving time steps

Meshing is one of the most memory-intensive steps when it comes to setting up and solving a finite element problem. For example, different design of the mesh will lead to different computational time [178]. There are four elements can be used to mesh the 3D geometries in COMSOL Multiphysics as shown in Figure 3.2.3.

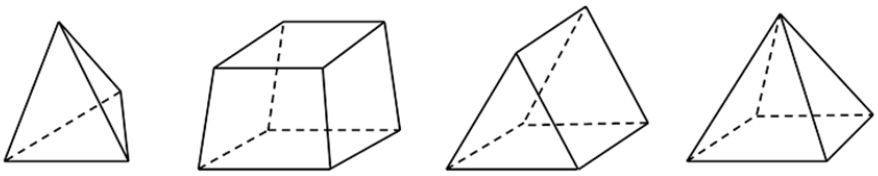

Figure 3.2.3 Images of different element types. From left to right: a tetrahedron, hexahedron, triangular prism, and pyramid [177]

Free meshing and swept meshing are the two most popular meshing methods in modelling. The free mesh automatically creates an unstructured mesh with tetrahedral elements, which is available for all types of geometries regardless of the shape of geometry. And, the swept meshing, which contains prism elements or hexahedral elements, starts at a source face and sweeps along to a target face (Figure 3.2.4) [177]. Each face about a subdomain that is to be operated on by the swept mesher is classified as either a source face, a target face, or a boundary face. The boundary faces are the faces linking the source and target face.

In addition to meshing, the solving time step also has a great impact on the accuracy and computational time of the modelling. In numerical simulation, since the difference equation that implements the integration algorithm is always an approximation of the exact solution of the differential equation, each step of the integration algorithm introduces truncation and rounding errors into the approximate solution. Therefore, in the unsteady numerical simulation, under the premise of ensuring stability, the selection of the time step needs to comprehensively consider the solving accuracy and time. Smaller time steps reduce truncation error but increase the number of computations and thus rounding errors; while larger time steps increase truncation error and often do not reflect changes in physical facts. However, the main error is the truncation error, so the time step should be small enough to reduce the truncation error and improve the accuracy of the simulation [179]. In order to determine the appropriate time step, the modelling was carried out with three different time steps 0.05s, 0.1s and 0.2s.

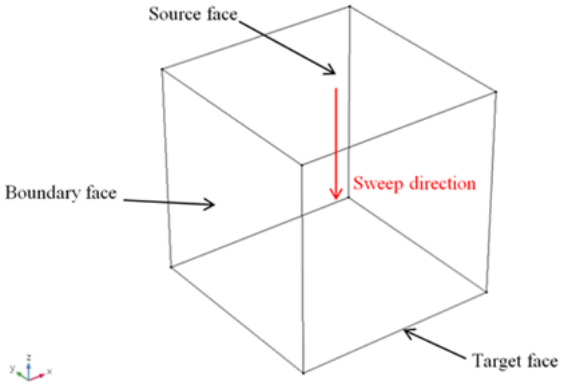

Figure 3.2.4 Schematic diagram of the sweep meshing

Therefore, based on the factors above, a simple modelling was used for determination of the meshing and solving time step. A laser beam was moving on a single scanning line 50mm to the free end of the plate with 1 pass along y-axis, as shown in Figure 3.2.5. Coordinate origin is bottom left corner of the plate. Thus, the coordinate x_n of the beam remains constant while the coordinate y_n changes with time (t) variant. The coordinate x_n of the beam is L/2, L is the length and width of the plate 100mm, and the coordinate y_n changes with time variant, single pass can be expressed as:

$$y_1 = v_0 t,$$

where v_0 is the processing speed.

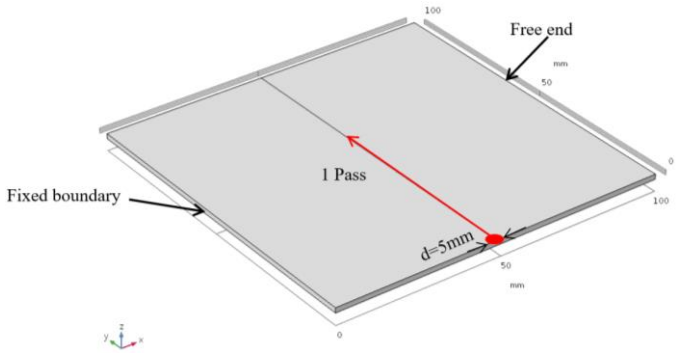

Figure 3.2.5 Schematic diagram of modelling of laser forming of a mild steel S275 plate with the dimensions of 100×100×1.5mm with single pass. Red arrow line represents the irradiation path and laser moving direction, Power 500W, Speed 50mm/s, Beam dia. 5mm

Figure 3.2.6 shows the free and swept meshing of the plate in the modelling. It can be noted that extremely fine mesh applied in the laser scanning region, in which the width of the dense band is equal the beam diameter 5mm, and coarse mesh for the remaining in order to avoid over-meshed and reduce the solving time.

Figure 3.2.7 shows the simulation results of the displacement at the free end of the plate in z-axis by using these two meshing methods after one pass. It can be found that the results obtained by these two meshing have a good agreement with each other. However, the simulation took 11 minutes to be solved by swept meshing and 17 minutes by free meshing. This is because swept meshing contains 17874 elements, while free meshing consists of 26149 elements. Compared with the free meshing, the swept meshing further reduces the number of elements, thereby reducing the size of the model and its computational complexity. In addition, it can be seen that there is a counter bending of the part due to the thermal expansion of the surface layer, resulting in a bending away from the laser beam at the beginning of the heating stage, which is consistent with TGM.

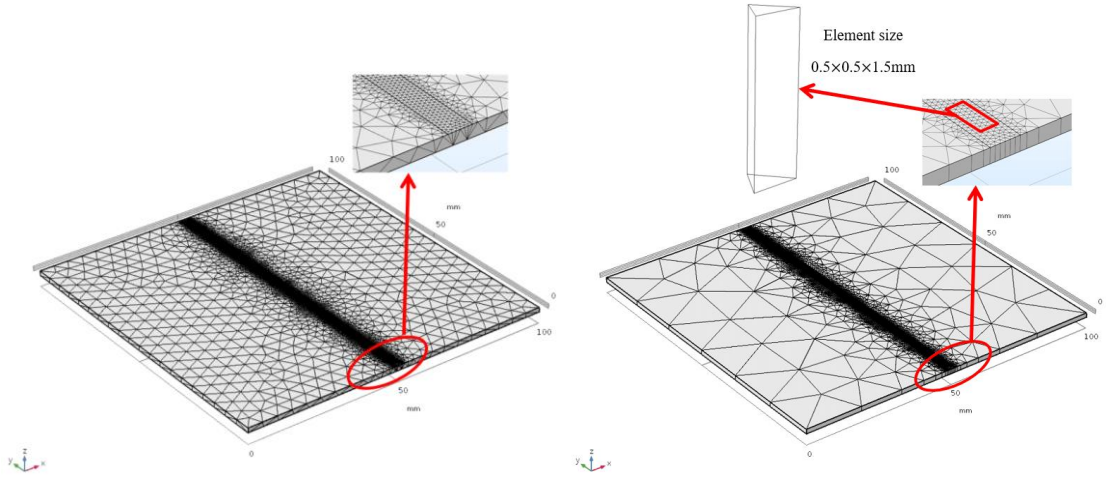

(a). Free meshing (b). Swept meshing

Figure 3.2.6 Meshing of the plate by using two different meshing in the modelling, (a). free meshing, (b). swept meshing

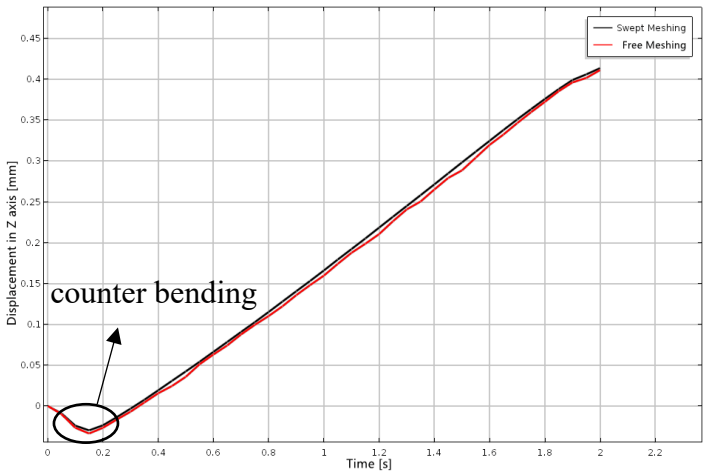

Figure 3.2.7 Simulation results of the displacement at the free end of the workpiece in z-axis by these two meshing methods after 1 pass

Figure 3.2.8 shows the simulation results of the displacement at the free end of the plate in z-axis by using three different solving time steps after one pass. It can be observed that almost the same displacement obtained by using the solving time steps of 0.05s and 0.1s, which is approximate 0.42mm (bending angle ~0.48°), and the computational time is 11mins55secs and 11mins respectively; however, the displacement is ~0.27mm (bending angle ~0.3°) by using the solving time step of 0.2s. which has agreement with the experimental result (0.5°), however, the bending angle was calculated as 0.3° at the time step of 0.2s.

It can be found that the simulation results obtained by using the solving time step of 0.05s and 0.1s are closer to the experimental result (0.5°) and so it is decided to use the solving time step of 0.1s and swept mesh for the following simulation.

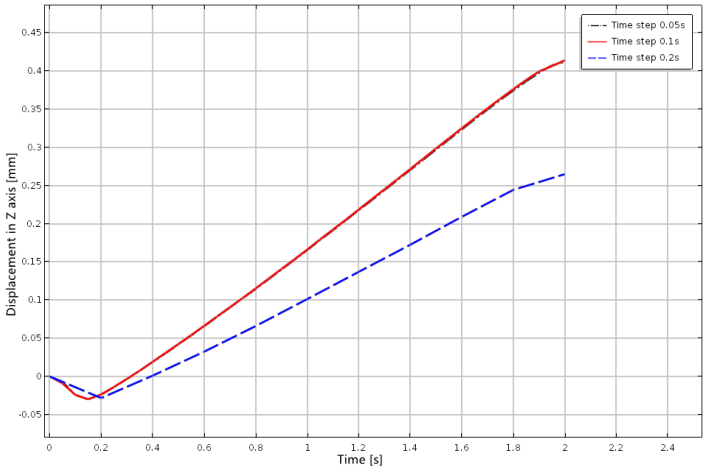

Figure 3.2.8 Simulation results of the displacement at the free end of the plate in z-axis by using three different solving time steps, 0.05s, 0.1s, 0.2s, after 1 pass

3.2.2.3 Validation of the modelling

The modelling presented in the previous section is only a preliminary determination of the meshing and solving time step, however, the result of a single pass scanning strategy is not enough to prove the authenticity of the modelling. Therefore, a multiple pass scanning strategy was used in the modelling presented in this section. The scanning position and processing parameters are the same as the single pass modelling. Figure 3.2.9 shows the arrangement for the modelling.

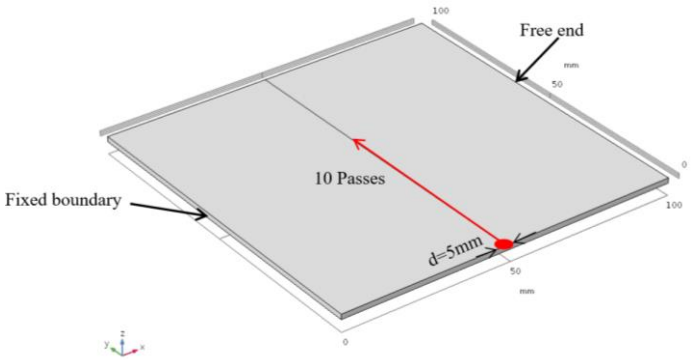

Figure 3.2.9 Schematic diagram of modelling of laser forming of a mild steel S275 plate with the dimensions of 100×100×1.5mm with 10 passes. Red arrow line represents the irradiation path and laser moving direction, Power 500W, Speed 50mm/s, Beam dia. 5mm

The coordinate x_n of the beam is L/2, L is the length and width of the workpiece 100mm, and the coordinate y_n changes with time variant, which can be expressed as:

$$Y_1 = v_0 t,\ y_2 = v_0(t - t_0),\ y_3 = v_0(t - 2t_0) \ldots, y_n = v_0(t - (n-1)t_0)$$

where n is the number of passes, t_0 is the single pass time

The validation of the modelling and experimental results of the cumulative bending angle after 10 passes are given in Figure 3.2.10. It can be found that there is a good agreement between the modelling and experimental result, which can provide theoretical support for experimental research. Therefore, the modelling will be used to analyse the effects of the scanning paths spacing on laser forming process for prediction of the scanning pattern in the following 3D laser forming investigation. The description and results of the modelling will be given in chapter 5. It is worth noting that the trend of modelling result is linear, and the cumulative bending angle is larger than the experimental results as the number of passes increases this could be attributed to the assumptions made in the modelling as mentioned before, such as the absorptivity of the material, material properties, and beam geometry are constant, which leads to the bending angle rate is the same for each pass. However, the trend of the experimental result is nonlinear, and the bending angle starts to fall-off after 6 passes this could be attributed to the decrease in energy fluence with increasing of the scanning passes in a real laser forming process, such as section thickening, variation of absorption, and change of the beam geometry, which result in the variation of the bending angle rate for each pass.

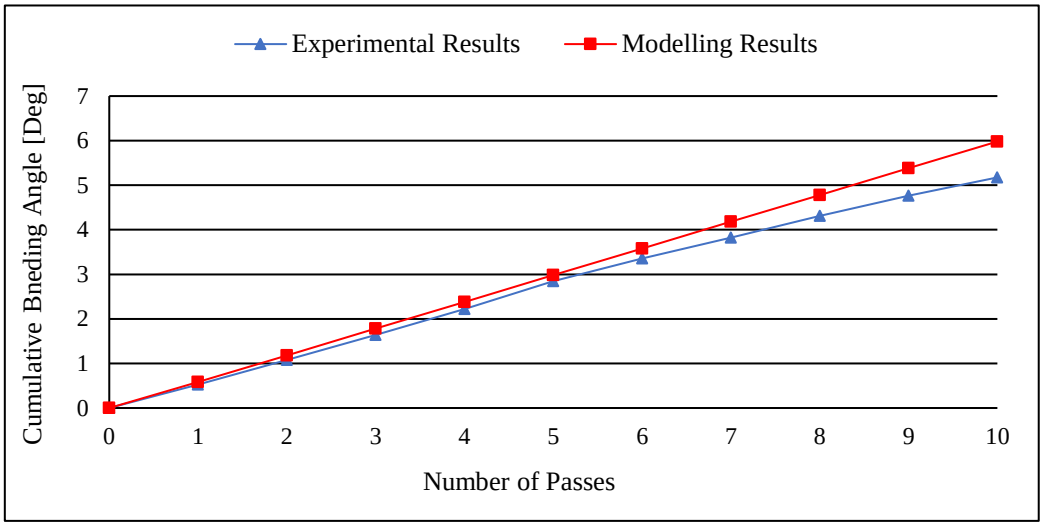

Figure 3.2.10 Modelling and experimental results of the cumulative bending angle after 10 passes

3.3 Laser Forming of Single Curved Shape

To date there has been a considerable amount of work carried out on two-dimensional laser forming, such as using multi-pass scanning strategies to produce a single curved shape. However, there is a limited understanding related to accuracy control the forming process to produce a target component.

It was concluded from earlier empirical studies that, a number of factors will affect the repeatability and reliability of laser forming process, such as residual stress history of the workpiece, material non-uniformity and process variability. Therefore, the aim of the first study presented in this thesis is to develop an advanced scanning strategy to improve the controllability of the process and produce a two-dimensional component independent of material and process variability.

There are a number of essential factors needed to be taken into account for control of the laser forming process, such as the current bending angle, the error between the current and the target bending angle, and the bending angle rate per pass, in which the

bending angle rate per pass is the most critical factor affecting forming accuracy[108], which can be controlled by varying process parameters such as the laser power, beam diameter and processing speed. However, for the laser system used throughout this thesis, the processing speed is the easiest variable to control and so it was decided to control the bending angle rate around the selection of process speed for development of this advanced scanning strategy.

In addition, the study is also to prove the manufacturing capabilities of the LF process at attempt was made to produce an actual car body component, which is linked to the Audi commercial project. The required 'U' shaped component with three different bending angles 20°, 40° and 60° from Audi AG was identified as an ideal candidate for laser forming. The experiments were conducted on mild steel DC01 with the dimensions of 200 × 100 × 0.89mm and AA6061-T6 with the dimensions of 200×100×1mm. The materials, test samples and requirements are all provided by Audi. The CAD drawings of the target shapes are shown in Figure 3.3.1. The 1.5kW PRC CO_2 laser described earlier was used throughout the process. The workpieces were held on the workbench using an edge clamping at 10mm from the constrained edge. There are two scanning lines on the workpiece, the 1st scanning line is 50mm away from the free end of the workpiece, and the 2nd scanning line is 100mm away from the 1st line, as depicted in Figure 3.3.2 and Figure 3.3.3. Initially the laser beam was applied to irradiate over the 1st line with multi-passes to bend region A to the target angle, and then moving the laser beam to the 2nd line for bending region B to the target angle.

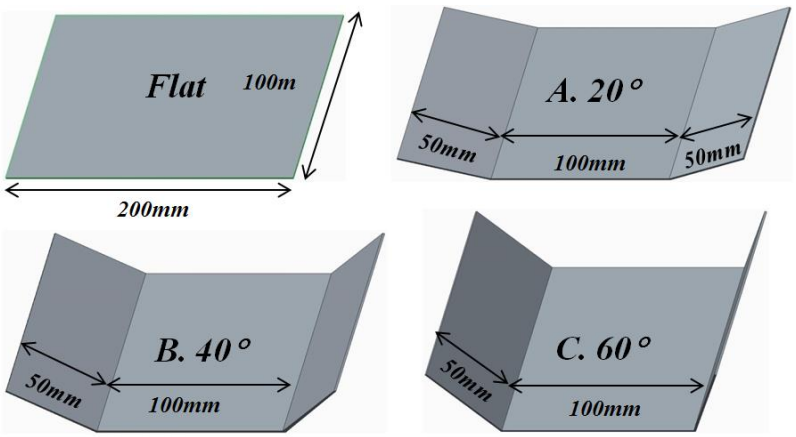

Figure 3.3.1 CAD drawings of the target shapes, "U" shape with 20°, 40° and 60° target bending angles

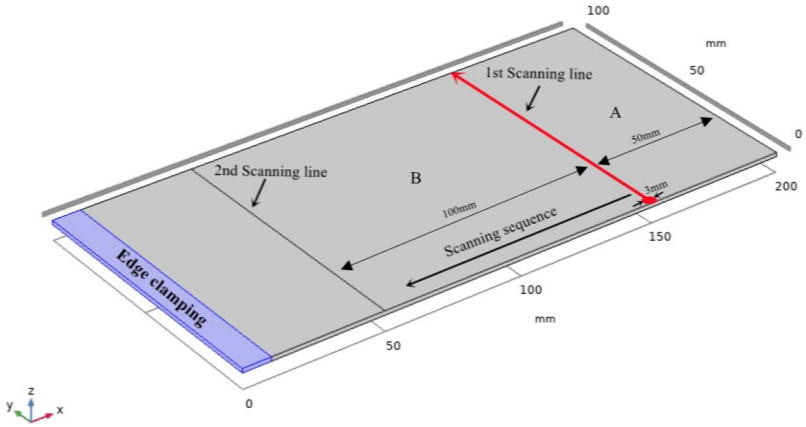

Figure 3.3.2 Schematic diagram of edge clamping arrangement with the component. Red arrow line represents irradiation path and direction

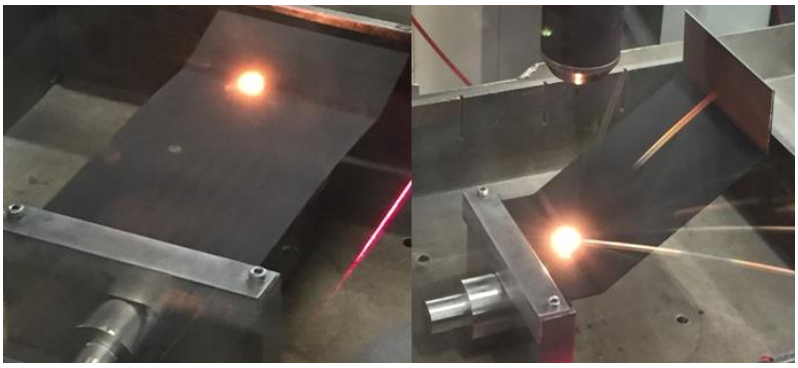

Figure 3.3.3 Experimental set up for laser forming of DC01 & AA6061-T6 with the size of 200×100×0.89mm and 200×100×1mm

The initial work of the study was to create the process map for the given materials mild steel DC01 and AA6061-T6. For mild steel DC01, the process map data using a 3mm beam diameter and a laser power of 400W in the speed range 30 to 50 mm/s. For AA6061-T6, the given parameters are a 3mm beam diameter, laser power of 500W and the speed range of 35 to 65mm/s. These process parameters for these two materials were taken from previous work within the group [15,169].

As mentioned, the target bending angles are 20°, 40° and 60°, thus the processing map for the given materials was created based on forming the maximum target bending angle of 60°. The workpieces were irradiated by a laser beam over the same track with multi-passes at a range of constant speed. The bending angle was measured after each pass and if the target bending angle was not achieved the process continues on the next pass. If the current bending angle was equal or greater than the target value, the process was terminated.

These values were then used to establish the relationship between scanning speed, error between the current bending and target angle, and bending angle rate for the given materials. It can provide a basis for selection of the scanning speed in development of the advanced scanning strategy. When the target angle has not been achieved in one pass, an appropriate scanning speed for the next pass can be selected based on both the bending angle rate and the error to the target angle.

The angle measurement accuracy of the system can be obtained to be about 0.125° according to the measuring range (100mm) and resolution (15μm) of the laser scanner. Due to this factor, the final bending angle can be considered as accurate when the

difference between the final bending angle and the target angle is within +/-0.125°. The details of this advanced scanning strategy are given in chapter 4.

3.4 Laser Forming of Double Curved Shape

For practical industrial applications, in addition to single curved shapes, most components have a double curved geometry, such as ship hulls, pillow shape, saddle shape etc. Therefore, it is necessary to consider 3D laser forming in order to advance the application of laser forming in the actual manufacturing environment.

Therefore, the second study presented in this thesis is to investigate 3D laser forming. The target component with a double curved shape (named it "ship hull shape") was given by a shipbuilding company, which was chosen for 3D laser forming investigation in this thesis, and the requirement is to form a ship hull shape with the deflection of 30mm at corner A&B and 20mm at corner C&D from a 100×100×1.5mm mild steel S275 plate. The CAD drawing of the target component can be seen in Figure 3.4.1. It is worth noting that the size (length, width, and thickness) of the ship hull of a real freighter is around 360000×64000×14mm [180]. The work presented in this section is also to demonstrate the potential application of laser forming in shipbuilding industry.

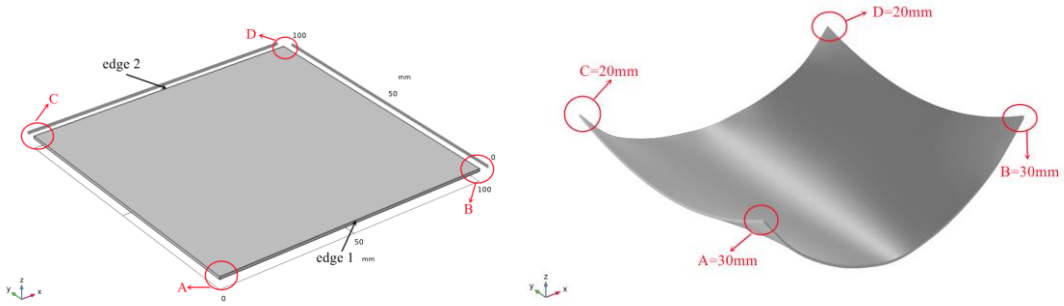

Figure 3.4.1 Laser forming of a ship hull shape with the deflection of 30mm at corner A&B and 20mm at corner C&D from a 100×100×1.5mm mild steel S275 plate

The procedure for this 3D laser forming investigation includes three parts. The initial work of the study is to create a process map for the given material mild steel S275 based around a short study of 2D bends as tools to help in the investigation of 3D laser forming. The second part is prediction of the scanning pattern based on the lines of constant height and the minimal principal strain field and verified by experiments. The final part is investigation of the scanning strategy, which is a very important factor in laser forming; different scanning strategies will lead to different thermal stress distribution during heating process and influence the final deformation. For a given shape with large deformation, a strategy of a one-off single pass would be extremely difficult to predict and control. A more sensible method of producing a target shape should be to increment towards it with a number of passes and taking surface measurements after each pass so as to have the ability to take account of any unwanted distortion or more forming required based on the error between the current formed shape and the target shape. A 3D laser sensor was employed to obtain the profile of the formed shape after each pass.

The experimental study was conducted on 100×100×1.5mm mild steel S275 using a 1.5 kW PRC CW CO_2 laser. A part of mild steel workpieces was used to create the process map for the given material via simple 2D bends and briefly investigate the effect of the varying a number of laser parameters on the laser forming process. The workpieces were held in place on the workstation table using an edge clamping for 2D bends as shown in Figure 3.4.2, and a centre clamping for 3D laser forming; this required a hole to be drilled in the centre of the workpiece for a bolt to pass through as shown in Figure 3.4.3. Although drilling the workpiece will lead to additional pre-stressing, fixing the plates was essential to avoid any unwanted movement, additionally by raising the workpiece off the work bench this alleviated any problems with the weight of the workpiece limiting the amount of forming available.

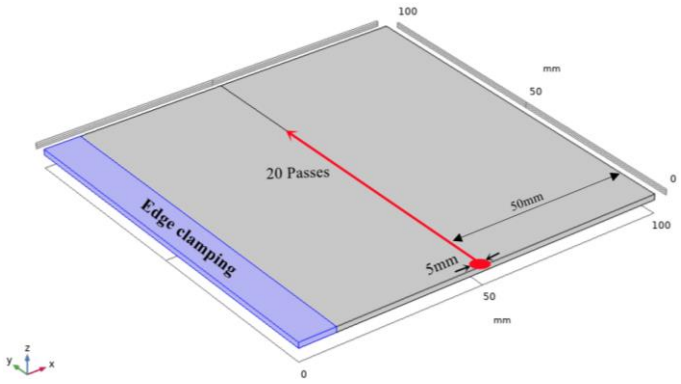

Figure 3.4.2 Schematic diagram of edge clamping arrangement with component 100×100×1.5mm. Red arrow line represents irradiation path and direction

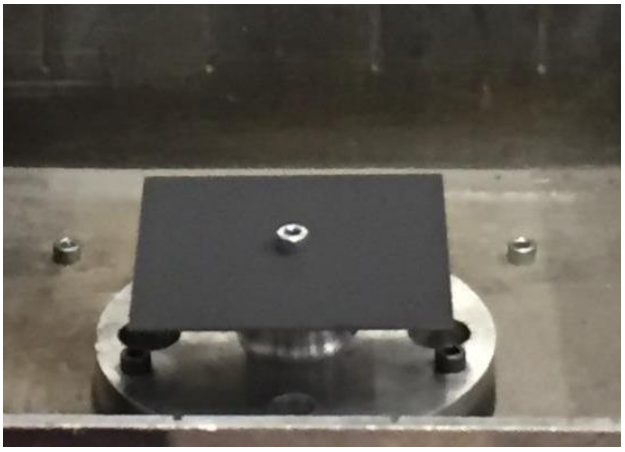

Figure 3.4.3 Centre clamping for 3D laser forming of the target ship hull shape from graphite coated 100×100×1.5mm mild steel S275

3.4.1 Determination of the Process Parameters

The first part of the study was a short work of 2D bends to create a process map for the given material mild steel S275. The samples were laser formed by multiple passes (up to 20 passes) over the same irradiation track using different parameters shown in Table 3.4.1. The choice of parameters used was taken from previous work within the group [15,169]. The bending angle was measured after each pass and converted into bending angle rate. These values are then used to produce a graph of laser power against processing speed for analysing the combined effects of these two parameters on bending characteristics of the workpiece and determining the appropriate energy parameters for 3D laser forming study.

Sample	Power [W]	Spot Dia. [mm]	Processing Speed [mm/s]				Number of Passes
			V_1	V_2	V_3	V_4	
1	500	5	30	40	50	60	20
2	600	5	30	40	50	60	20
3	800	5	30	40	50	60	20

Table 3.4.1 Processing parameters for creating the process map for the given material mild steel S275

3.4.2 Prediction of Scanning Pattern

The forming process of V-shaped component is comparatively simple and can be achieved by choosing appropriate heating position according to the bending requirements of a plate. However, for practical industrial applications, in addition to V-shaped workpieces, most workpiece shapes have a 3D geometry, and so one of the most important factors is to predict the heating paths.

In this part, the first step is to create the target shape, which is carried out using the large deformation FE modelling in COMSOL Multiphysics 5.2a. The displacement constraints are applied on the top surface of the flat sheet in the numerical modelling as a virtual stretching tool to stretch the flat plate to the target shape. The top surface of the flat sheet is decomposed into a group of 100 patches with 121 nodal points as shown in Figure 3.4.4, the displacement at these points correspond to the height of the target shape. The target shape with a full smooth surface can be obtained when the displacements of these points are interpolated in COMSOL as shown in Figure 3.4.5.

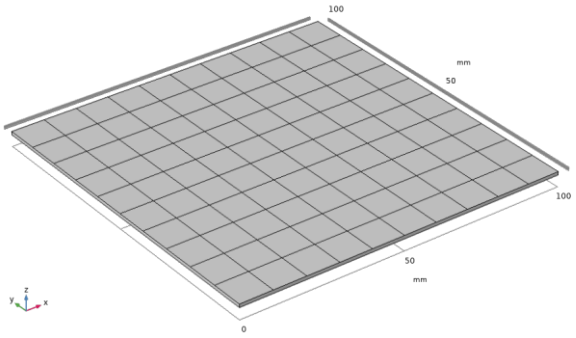

Figure 3.4.4 Flat sheet with 100 patches and 121 nodal points on the top surface

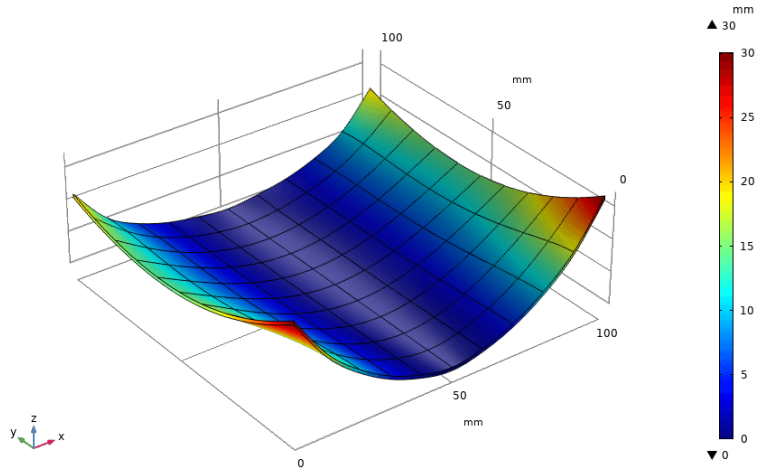

Figure 3.4.5 The defined target shape

Because in laser forming process the irradiation path about which a moment is generated should be stationary in space and bending parts either side will move instead thus a scan line or a location where a bend takes place about should always correspond to a line of constant height and vice versa [15], and the minimal principal strains occur in the direction perpendicular to a irradiation path [181].

Therefore, the lines of constant height of the target ship hull shape and the required minimal principal strain field at the upper surface of the target ship hull shape are used as a basis for prediction of the scanning patterns in this 3D laser forming investigation, which are obtained from the FE modelling as shown in Figure 3.4.6 and Figure 3.4.7.

In addition, for 3D laser forming the contour levels can be arbitrarily chosen to produce the 3D shapes, however on a continuous smooth surface the localised bend angles along the scanning lines should be small enough so as to not facet the surface significantly, which indicates another important factor that needs to be taken into account for prediction of the scanning pattern, as the number of contour levels selected or the spacing between adjacent scanning lines. The effect of the spacing between adjacent scanning lines on laser forming, such as deformation, temperature distribution and strain field, are analysed by FE modelling as mentioned before, which can provide a basis for the prediction of the scanning patterns.

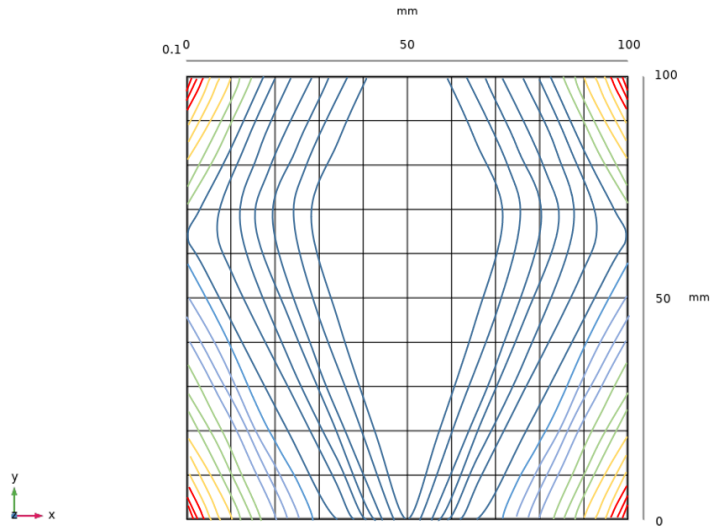

Figure 3.4.6 Contour lines of constant height of the target ship hull shape

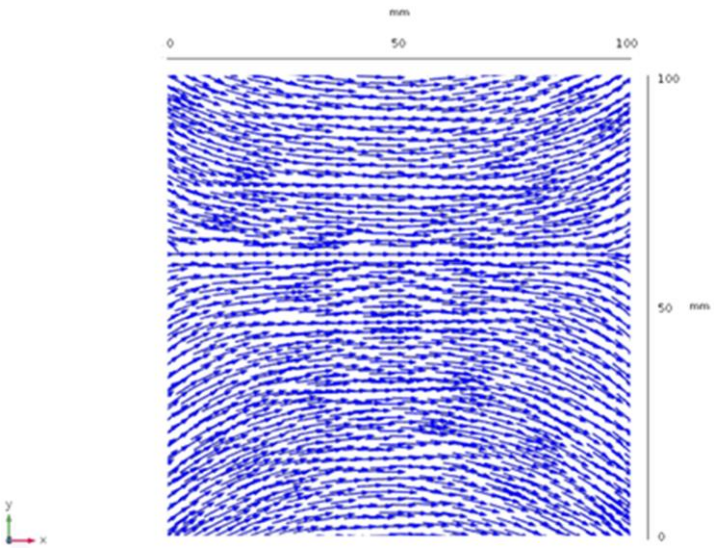

Figure 3.4.7 Vector plot of magnitude and orientation of minimum principal strain at the upper surface of the target ship hull shape (the length of a bar in the plot represents the magnitude, the arrow represents the orientation)

3.4.3 Determination of the Scanning Strategy

The key point of determination of the scanning strategy is to calculate the error between the formed shape and the target shape. The formed shape is measured by using a 3D laser sensor. The measurements from the 3D laser sensor are exported and saved as a STL file and imported into COMSOL to analyse the error between the current formed shape and the target shape. The error surface is obtained by subtracting the current formed surface away from the target shape through the “Join” function in COMSOL (target data – current formed measured data) as shown in Figure 3.4.9. The scanning strategy prediction is based on the error between the current formed shape and target shape, which could form the basis for a further scanning strategy.

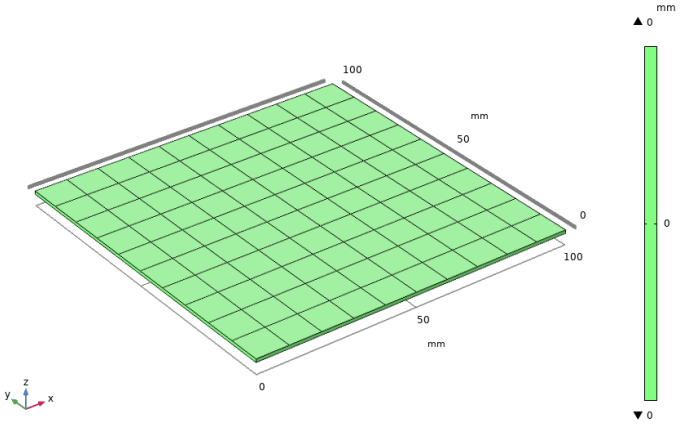

Figure 3.4.8 Measurement of the unformed flat sheet

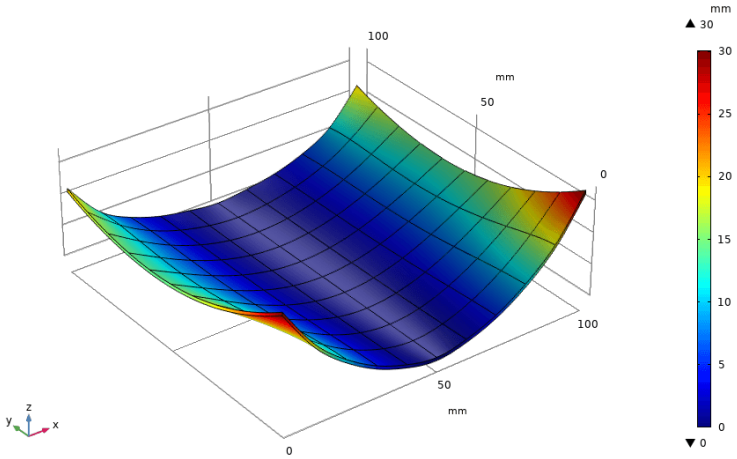

Figure 3.4.9 Error plot between the unformed flat sheet and the target shape

There were two scanning strategies used to produce the target shape and verified by two tests. The first scanning strategy prediction used in test 1 is based on the error between the current formed surface and target shape, a strategy of per pass monitoring is used to control the process. The control program will be terminated when the overall forming of the workpiece is equal or exceed the target shape. And the irradiation starts from outside to inside in order to keep the laser spot size constant. The purpose of first scanning strategy is to verify whether the predicted scanning pattern and the incremental error-based approach can produce a ship hull shape with a small degree of

error to the target shape.

The second scanning strategy prediction in test 2, such as positioning and sequencing of the irradiation, will be adjusted after each pass not only based on the error between the current formed surface and the target shape but also the deformation characteristics of the current part, such as that when the target shape is not formed within one pass, an appropriate scanning strategy for the next pass will be given by analysing the difference of the deflection of a number of points at 10mm steps along edge1 and 2 of the workpiece (Figure 3.4.10) between the current formed shape and the target shape.

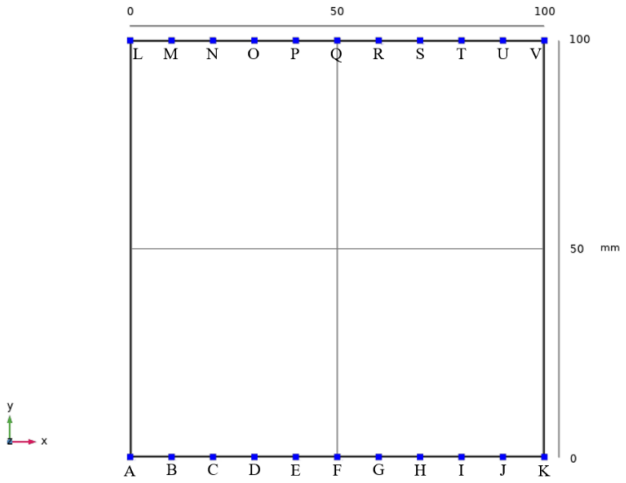

Figure 3.4.10 Measured points on edge 1 and edge 2 for prediction of the scanning strategy in test 2

As mentioned earlier, the final formed shape will be influenced by a number of factors, such as unknown residual stress distribution, variability in the absorption of the incident laser radiation and process variability. Therefore, the purpose of the second scanning strategy is to produce the target 3D shape independent of residual stress distribution and non-uniformity absorption of the laser radiation. Moreover, any unwanted distortion either caused by above two factors or process variability will be

taken into account and reduce the error to within +/- 0.5mm to the target shape. The control program will be terminated if the error between the current formed surface and target surface was within +/- 0.5mm so as to avoid any over-forming and asymmetry however small.

In addition, in the above two scanning strategies the forming rate was controlled by varying the scanning speed, such as that the scanning speed will be increased as the target shape approaches, which allows the workpiece to form in every decreasing increment to the target shape so as to reduce any risk of over-forming.

Chapter 4

Laser Forming of Single Curved Shape Results and Discussion

This chapter presents the results and discussion of the experimental studies into laser forming of single curved shape by using an advanced scanning strategy in two materials, mild steel DC01 and AA6061-T6.

The initial work of the study was to create the process map for the given materials, which can provide a basis for development of the advanced scanning strategy for improving the controllability of the process and producing a two-dimensional component independent of material and process variability. The details are presented in the following sections.

4.1 Creation of the Process Map

The initial work of the study is to create the process map for the given materials mild steel DC01 and AA6061-T6. For mild steel DC01, the process map data using a 3mm beam diameter and a laser power of 400W in the speed range 30 to 50 mm/s. For AA6061-T6, the given parameters are a 3mm beam diameter, laser power of 500W and the speed range of 35 to 65mm/s. As mentioned before, these process parameters were taken from previous work within the group.

The results of cumulative bending angle and bending angle per pass (bending angle rate) against number of passes for mild steel DC01 and AA6061-T6 are presented in Figure 4.1.1 to Figure 4.1.4. The repeatability tests for both materials are also conducted as shown in Figure 4.1.5 and Figure 4.1.6. These values were used to produce the relationship between processing speed, error between the current bending and target angle, and bending angle rate for the given materials as shown in Figure 4.1.7 and Figure 4.1.8.

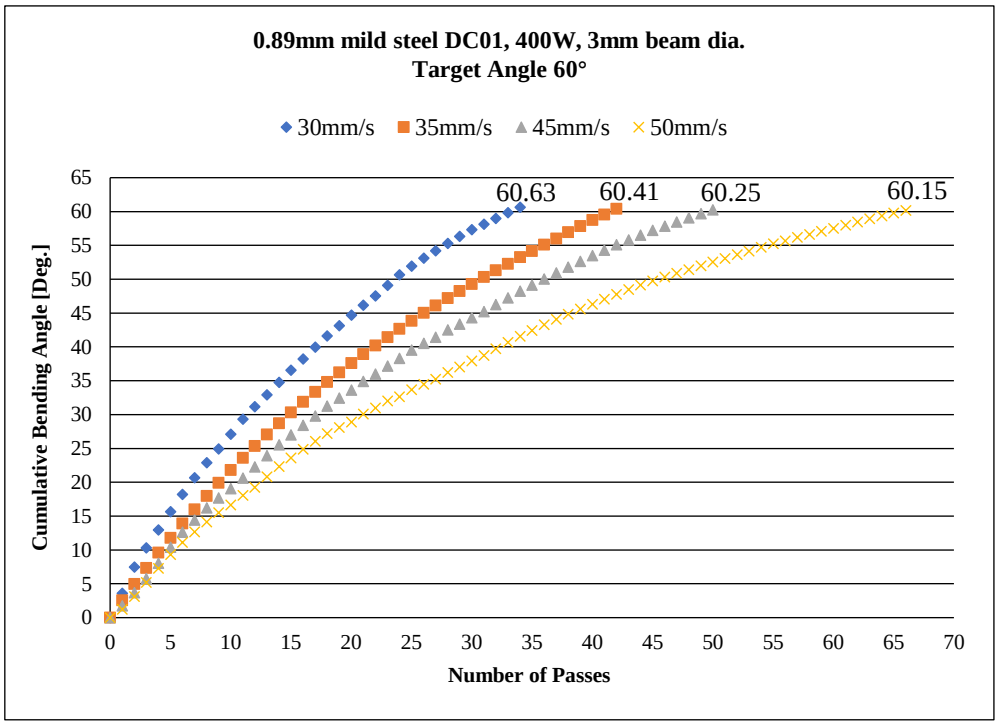

Figure 4.1.1 Cumulative bending angle against number of passes processed at 30mm/s, 35mm/s, 45mm/s, and 50mm/s for mild steel DC01, 60° target

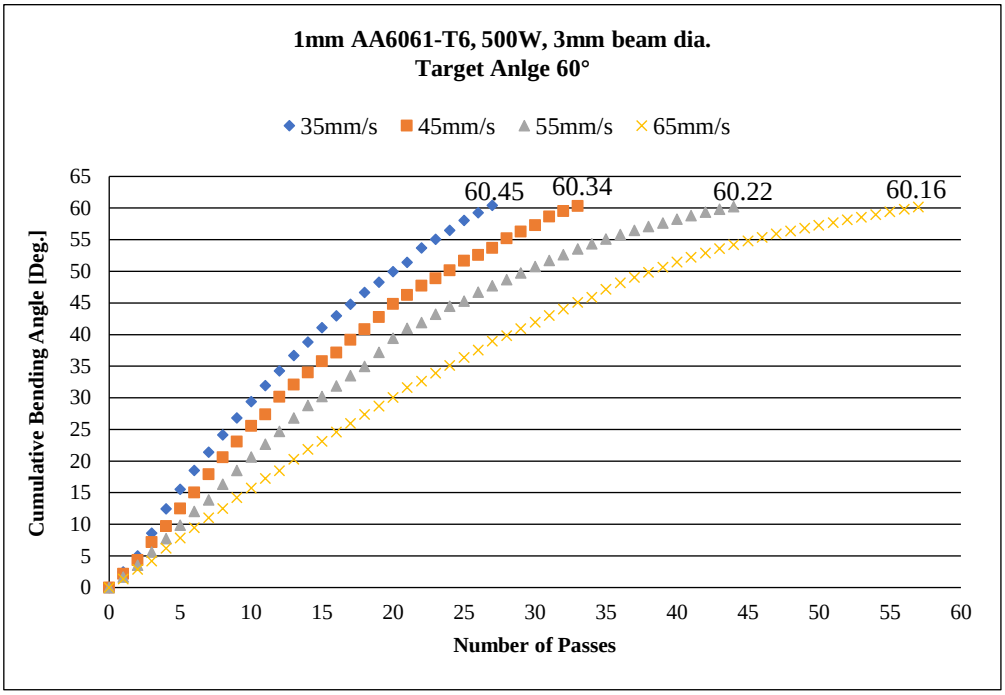

Figure 4.1.2 Cumulative bending angle against number of passes processed at 35mm/s, 45mm/s, 55mm/s, and 65mm/s for AA6061-T6, 60° target

From Figure 4.1.1 and Figure 4.1.2, it can be found that the final bending angles for both materials occurred a small degree of overshoot (0.15° to 0.63°). Although the magnitude of overshoot is small, it also exceeds 0.125° especially at the low speed. A possible reason to this may be that the constant processing speed was employed throughout the process, which would lead to a constant bending angle rate per pass, as the bending angle approached the target angle, if the current bending angle rate is greater than the difference between the current bending angle and the target angle, an overshoot will occur. For example, for mild steel DC01 (see Figure 4.1.1) the cumulative bending angle before the last pass is 59.82° at the processing speed of 30mm/s; if attempts to control the error of the final bending angle to within 0.125° of the target angle, the bending angle rate should be within 0.3° at last pass, however the actual bending angle rate is 0.81°, so the final bending angle has 0.63° overshoot.

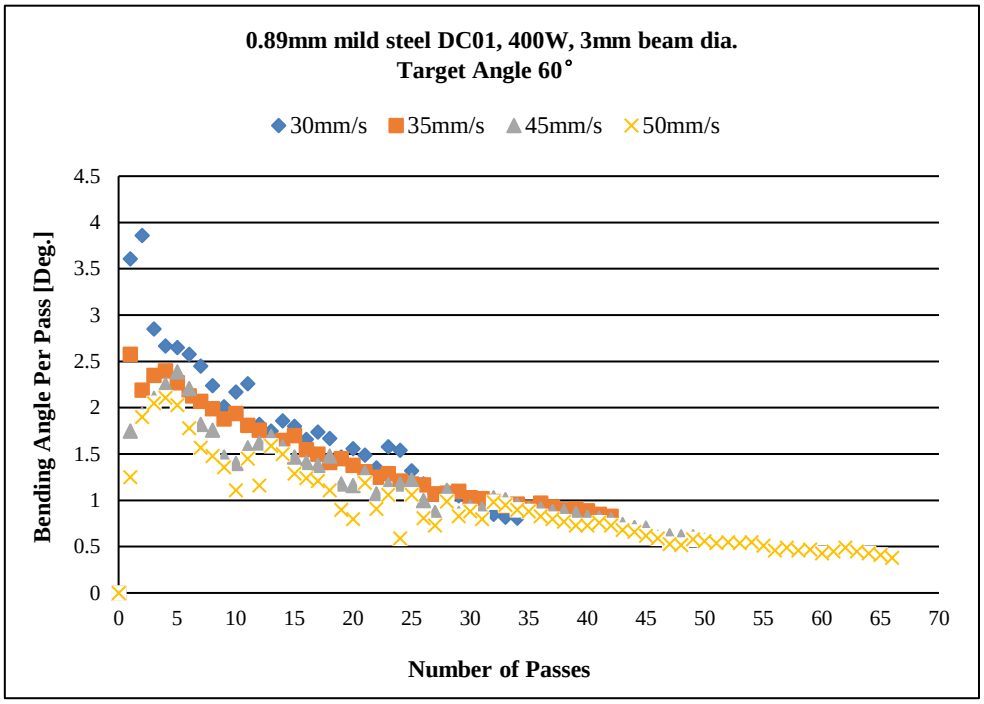

Figure 4.1.3 Bending angle per pass against number of passes processed at 30mm/s, 35mm/s, 45mm/s and 50mm/s for mild steel DC01

Figure 4.1.4 Bending angle per pass against number of passes processed at 35mm/s, 45mm/s, 55mm/s, and 65mm/s for AA6061-T6

As illustrated in Figure 4.1.3 and Figure 4.1.4 the bending angle rate for both materials present the similar trend, which starts at a high rate initially, and then drops off with increase of the number of passes especially at higher numbers of passes. This is attributed to a number of factors, such as strain hardening, section thickening, changes of geometry of the laser beam and degradation of the coating. Therefore, the number of passes is another important factor that needs to be considered in the laser forming process. As mentioned earlier, the degradation of the coating is dependent on the interaction time and the intensity of the laser beam. The high number of passes will increase the interaction time of the laser beam, which will lead to the degradation of the coating more seriously resulting in variation of absorption and heat transmission to the workpiece and reduction of the process reliability.

A repeatability test was performed using the same scanning strategy on ten additional samples for the given two materials respectively. A standard deviation between the ten samples for mild steel DC01 and AA6061-T6 can be seen in Figure 4.1.5 and Figure 4.1.6.

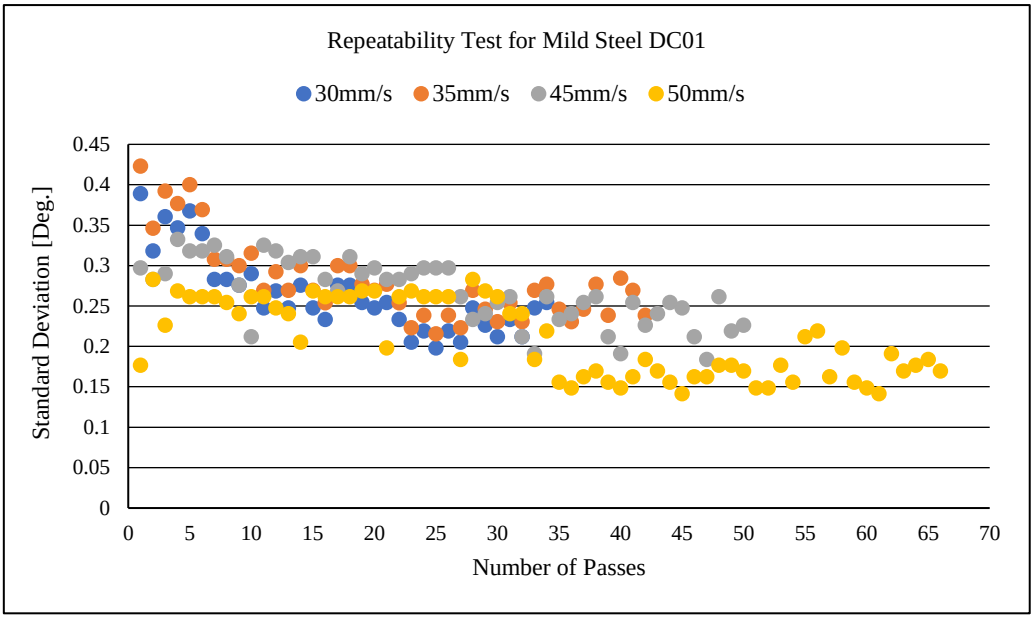

Figure 4.1.5 Repeatability Test for mild steel DC01

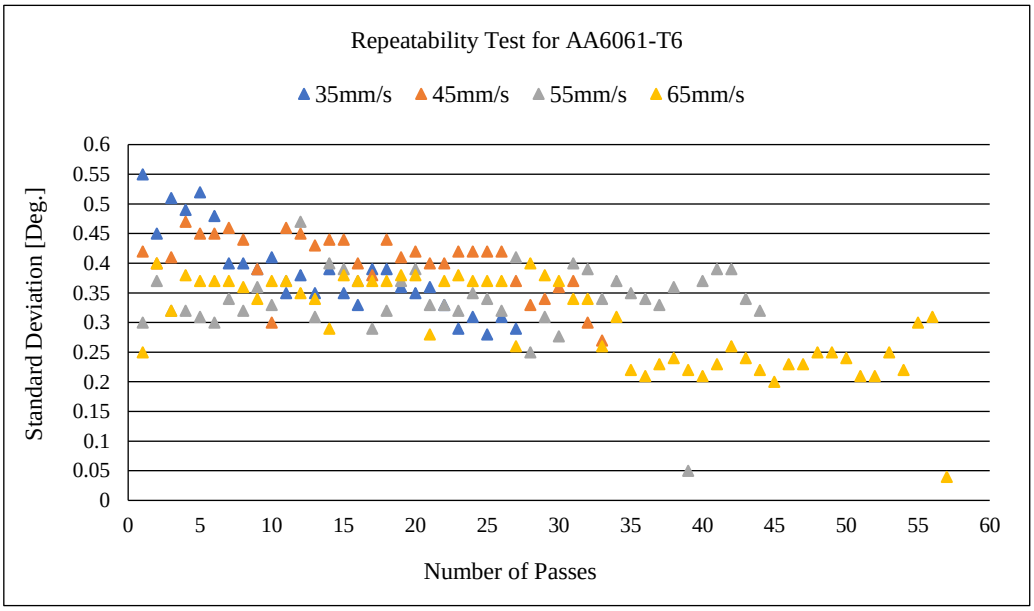

Figure 4.1.6 Repeatability Test for AA6061-T6

Figure 4.1.5 and Figure 4.1.6 show the standard deviation between the samples using the same scanning strategy for the given two materials respectively, which can be used to reflect the repeatability of the process. It can be observed that although a reasonable repeatability can be achieved using the same scanning strategy for these two materials, the variable nature of per pass still exists. This may be attributed to the

different residual stress distribution in the workpieces and the non-uniform thickness of the surface coating. It has been reported in some details by Edwardson et al. [70] that material factors such as differences in the residual stress history of a component can influence the repeatability of the laser forming process. Therefore, it is necessary to develop a new scanning strategy to improve the controllability of the process so as to produce a 2D bends component independent of material and process variability.

The residual stresses are the stresses that remain in an workpiece without external loading or thermal gradients, which are generated as a workpiece is stessed beyond its elastic limit resulting in plastic deformation [182].

In the laser forming process, the residual stresses are mainly generated by thermal variations, such as there is always a large difference in the cooling rate throughout the workpiece when it is cooled from a high temperature, which will result in localised variations in thermal contraction resulting in non-uniform stresses distribution throughout the workpiece [120].

During the laser forming process, the cumulative bending angle increase with increasing of the passes. However, the bending angle rate per pass decreases due to the different residual stress distribution in the workpiece after each pass, which can be explained by two possible reasons. A possible reason is that the flow stress increases due to the increased plastic strains with multiple passes. Another possible reason is that the recrystallization occurs repeatedly in the multi-pass process [120].

In addition, as mentioned earlier, the coatings are sprayed manually onto the surface to be irradiated for all the experiments in this thesis since an automatic

application is difficult to perform. Thus, the thickness of the coating layer can't be guaranteed uniform. Coatings not only absorb the laser energy, but also transport the released heat to the surface of the workpiece, hence the coating layers vary in thickness will lead to non-uniform of heat transmission to the surface of the workpiece resulting in reduction of the process efficiency.

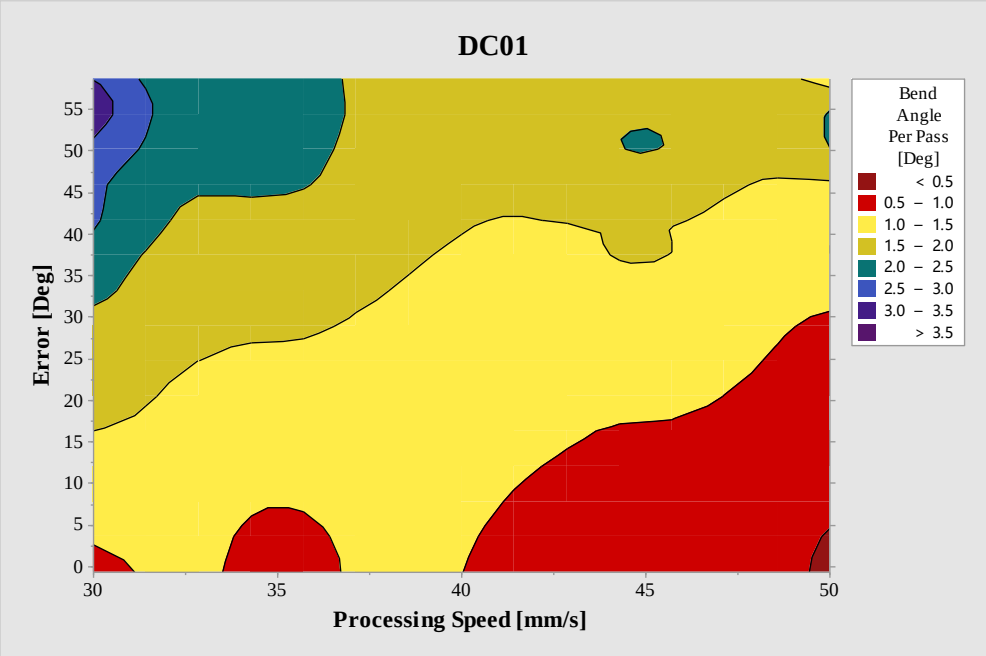

Figure 4.1.7 Process map for mild steel DC01

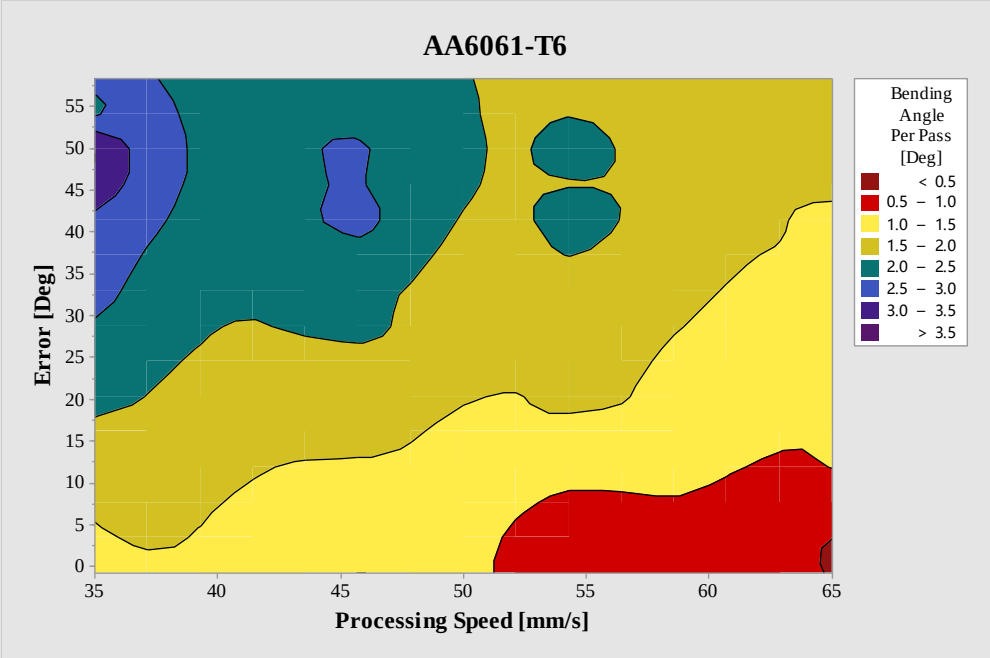

Figure 4.1.8 Process map for AA6061-T6

Figure 4.1.7 and Figure 4.1.8 present the relationship between processing speed (x-axis), error between the current bending and target angle (y-axis), and bending angle rate for the given materials it can be found that the given processing parameters gave a range of bending angle rate selection per pass from 0.5° to 3.5° in both materials. These data can provide a basis for selection of the processing speed in the followed study such as that when the target angle has not been achieved in one pass, an appropriate processing speed can be selected based on the bending angle rate and the error to the target angle for the next pass. The detailed description and results of the improved scanning strategy are presented in the following section.

4.2 Advanced Scanning Strategy

Control of the bending angle rate during the process is the key point in this work. The concept was that the forming process was not only to monitor the current bending angle but also to control the bending angle rate or how many degrees per pass are required based on the error between the current and target bending angle in order to control of the forming accuracy. Initially the workpiece was scanned at an optimum speed, measure the bending angle, compare it to the target angle and make a selection of an appropriate processing speed for the next pass according to the error between the current and the target bending angle. As the target angle approaches the process speed increases to reduce the bending angle rate in order to slowly move towards the target angle so as to avoid any significant overshoot. For example, when the error between current and target angle is small, the bending angle rate should be less than or equal to the required bends to avoid overshoot. In addition, as mentioned before the the angle measurement accuracy of the system is about 0.125° thus the control program will be terminated as the error between the current and target bending angle was within 0.125° so as to avoid any overshoot however small.

The result of the first improved scanning strategy for mild steel DC01 at laser forming up to the target angle of 20° is shown in Figure 4.2.1.

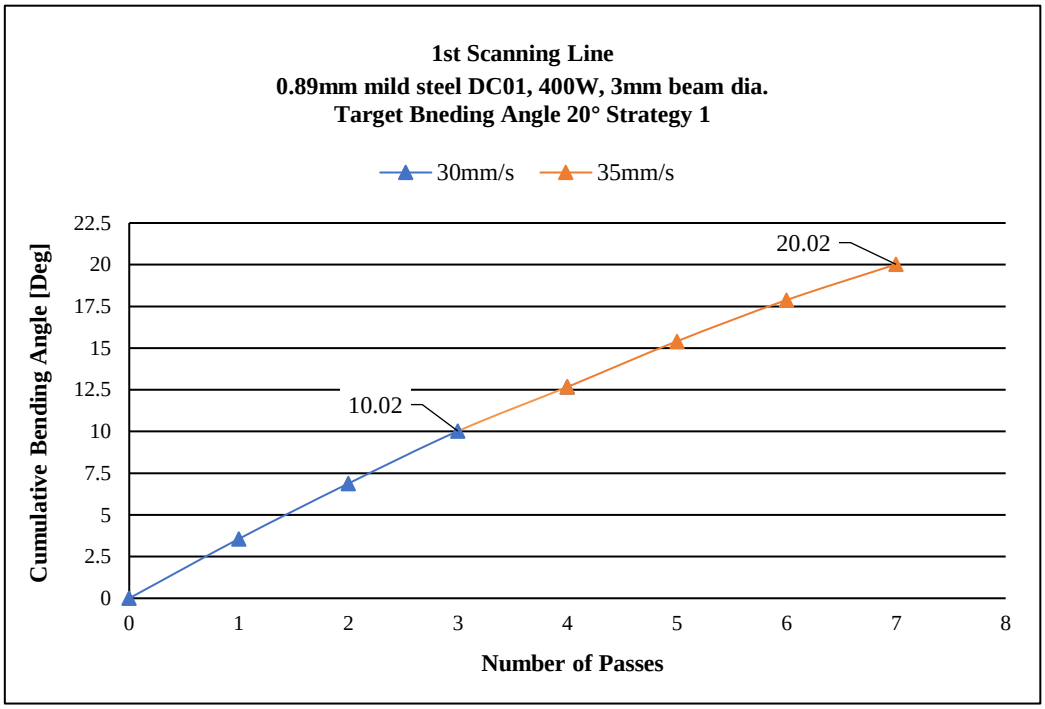

Figure 4.2.1 Laser forming of mild steel DC01, 20° target, 1st scanning line, scanning strategy 1

In the first scanning strategy for the target bending angle of 20°, a relatively low processing speed of 30mm/s was used at the initial passes to obtain the initial high bending rate. Once the current bending angle exceeded 10°, the processing speed was increased to 35mm/s for the subsequent passes until the error to target bending angle is within 0.125°. It can be seen from Figure 4.2.1 that the final bending angle has been produced reasonably accurately within the accuracy of the measurement system and the control program was terminated after pass 7, however, it can be observed that the bending angle rate is still very high when approaching the target angle and it seems to be just a coincidence resulting in an accurate final bending angle without significant overshoot. This may be due to use of only one speed step and the increase of the second speed was only 5mm/s. The second speed was implemented from pass 3 to 7, it can be found that the fall off in bending angle increase per pass is subtle. An improvement to

the first scanning strategy was made in order to solve this problem that was to introduce more speed increases during the processing and to employ relative high speed for the last few passes when approaching the target angle so as to reduce the bend angle rate significantly to improve controllability of the process. The results of the second scanning strategy for the target bending angle of 20° are shown in Figure 4.2.2 to Figure 4.2.4.

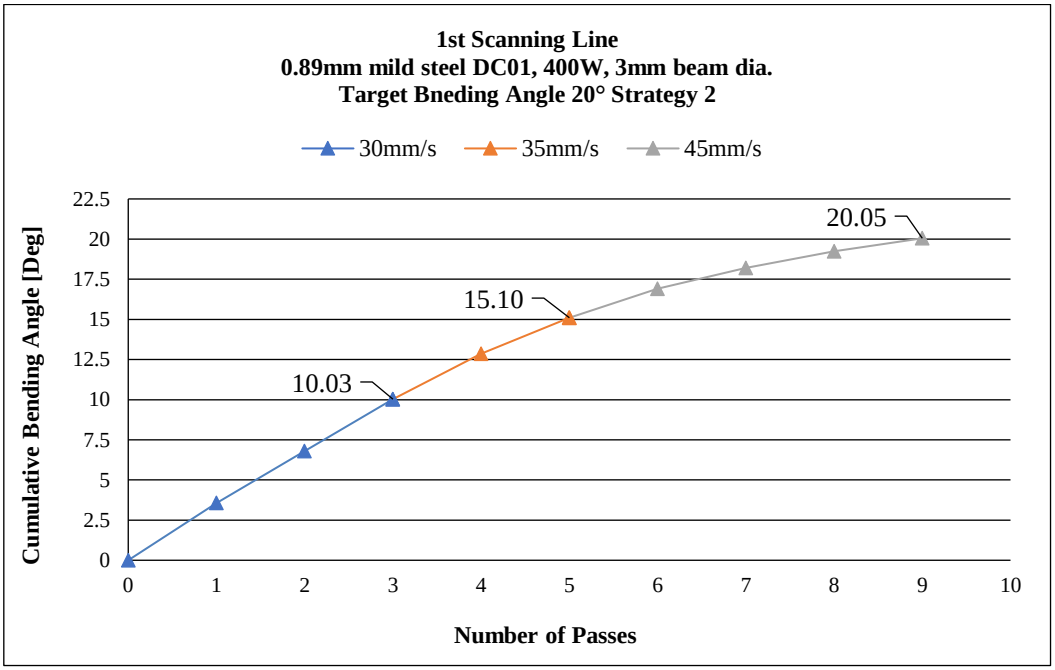

Figure 4.2.2 Laser forming of mild steel DC01, 20° target, 1st scanning line, scanning

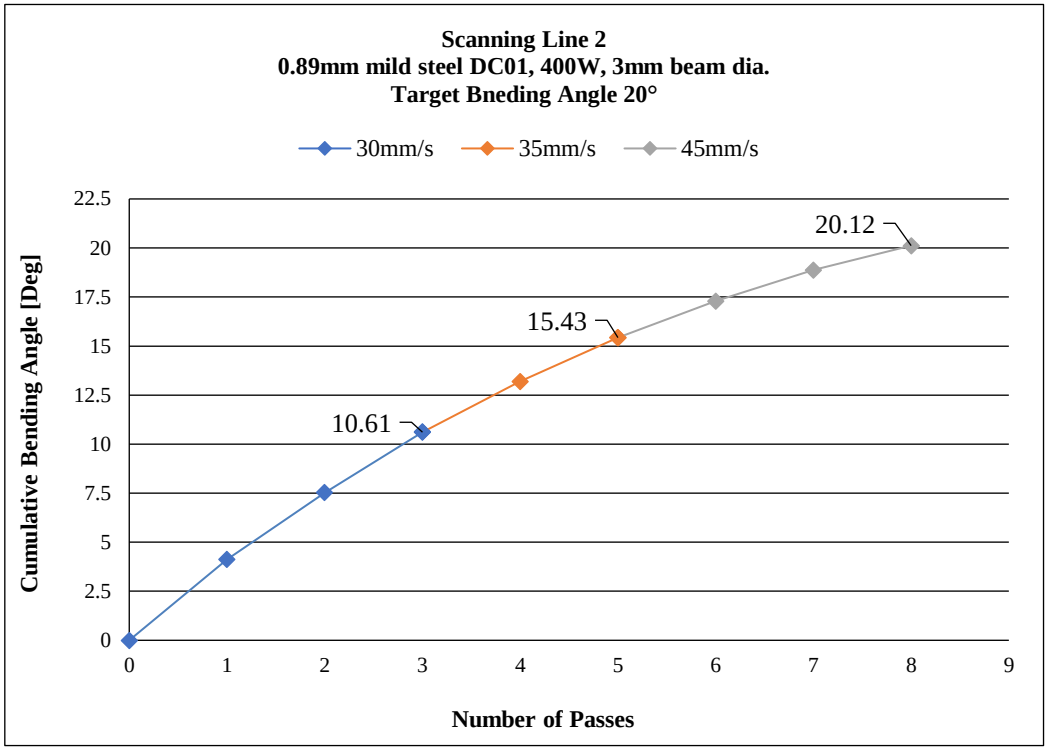

Figure 4.2.3 Laser forming of mild steel DC01, 20° target, 2nd scanning line, scanning strategy 2

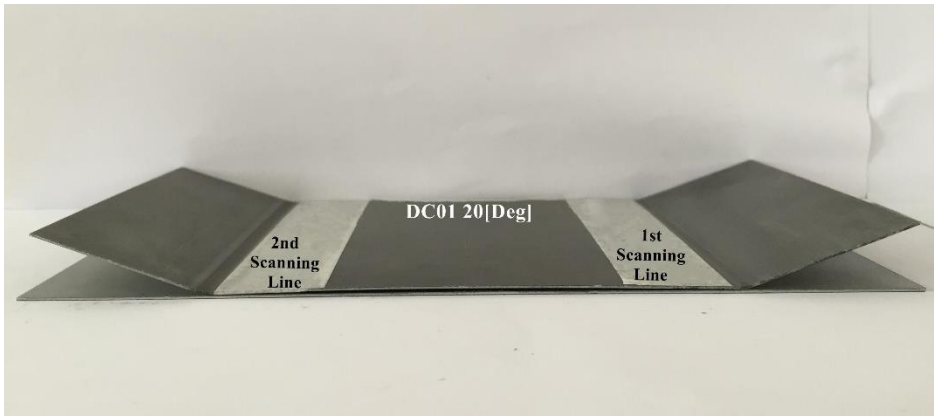

Figure 4.2.4 Mild steel DC01 final formed "U" shape component with 20° bending angle

It can be seen from above figures that there were 3 processing speeds employed for the second scanning strategy, as the same for the first scanning strategy the high bending angle rate speed of 30mm/s and 35mm/s were used for initial few passes to achieve a bending angle over 10° and 15°, once the bending angle was within 5° of the target the processing speed was increased up to 45mm/s for the last few passes, the drop

off in bending angle increase per pass can be seen clearly from pass 5 to the end. It can be seen that the error between the final bending angle and target angle has been reduced to 0.05° and 0.12° on the 1st and 2nd scanning line respectively by using this scanning strategy.

The method of improving the forming accuracy has been preliminarily verified in the laser forming of target bending angle of 20°. In order to prove that this method can be used to control the forming accuracy of any positive bending angle, the results of the scanning strategy using 40° and 60° as the target angle are shown in Figure 4.2.5 to Figure 4.2.10.

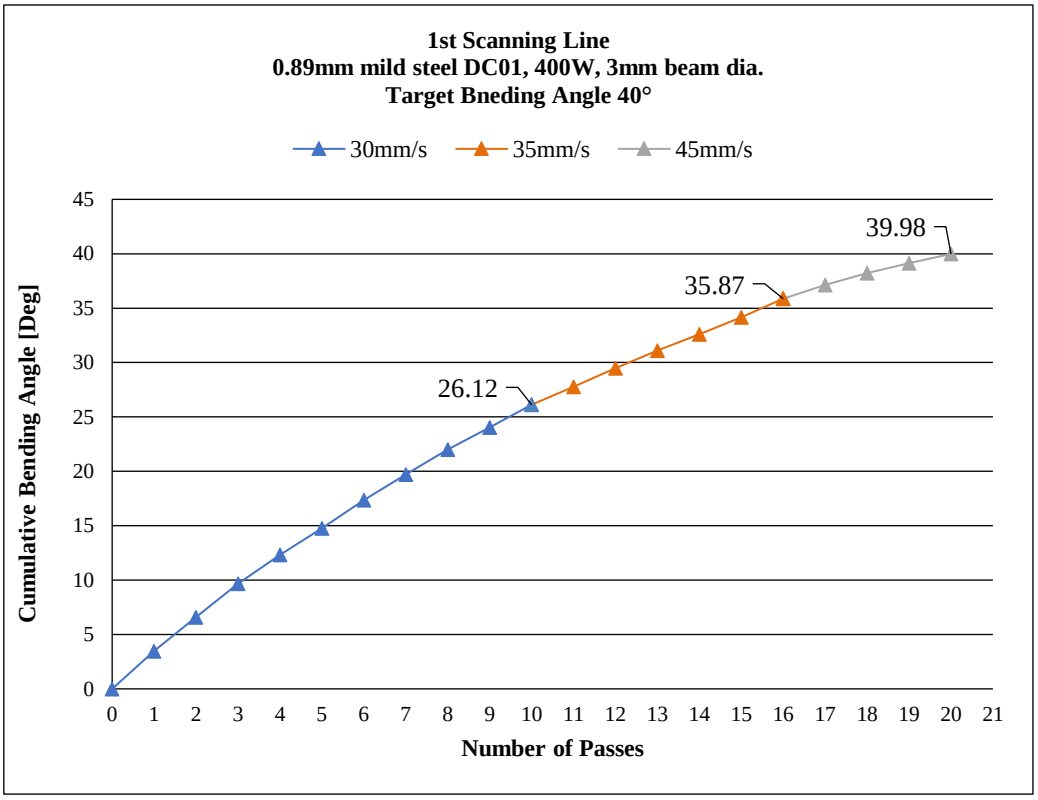

Figure 4.2.5 Laser forming of mild steel DC01, 40° target, 1st scanning line, scanning strategy 2

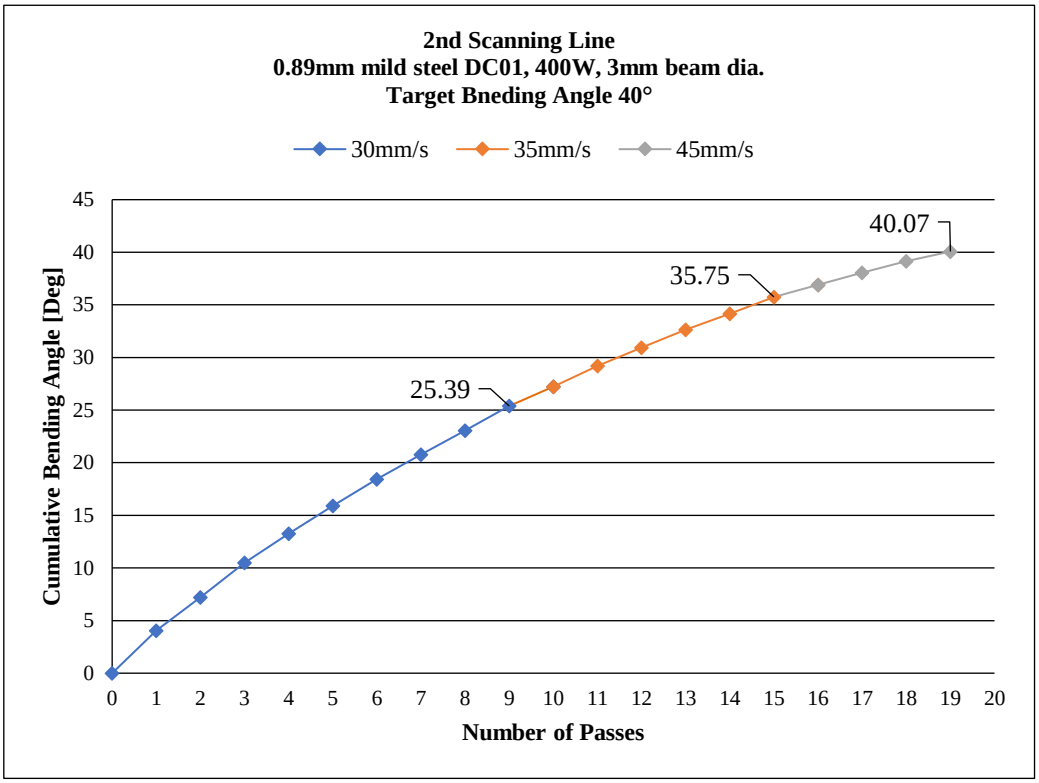

Figure 4.2.6 Laser forming of mild steel DC01, 40° target, 2nd scanning line, scanning strategy 2

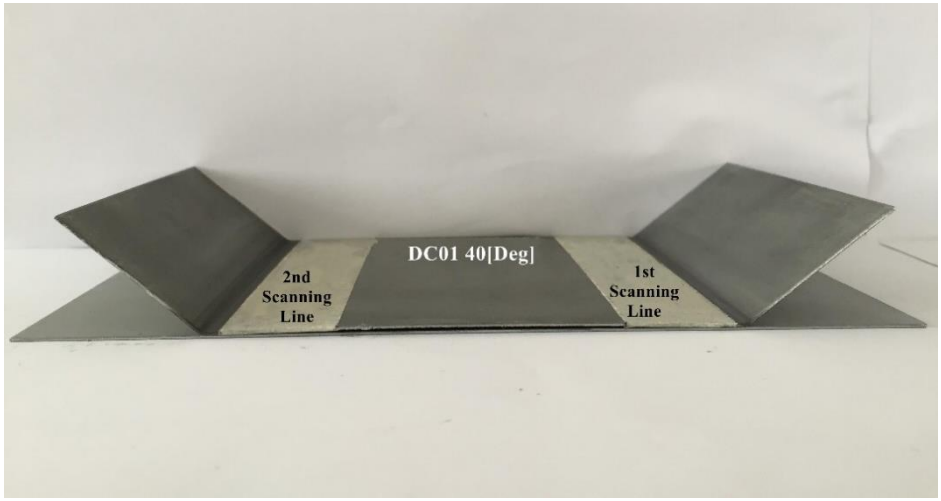

Figure 4.2.7 Mild steel DC01 final formed "U" shape component with 40° bending angle

It can be seen in Figure 4.2.5 and Figure 4.2.6 that the scanning strategy for achieving the target angle of 40° is similar with the scanning strategy for the target angle of 20°. In this scanning strategy, the processing speed of 30mm/s was used for the initial few passes to obtain the high bending rate. Once the target angle approaches

within 15° and 5°, the processing speed was successively increased to 35mm/s and 45mm/s. And the control program was terminated when the current bending angle was within 0.125° of the target angle. It can be found that the error between the final bending angle and the target angle is 0.02° and 0.07° on the 1st and 2nd scanning line respectively.

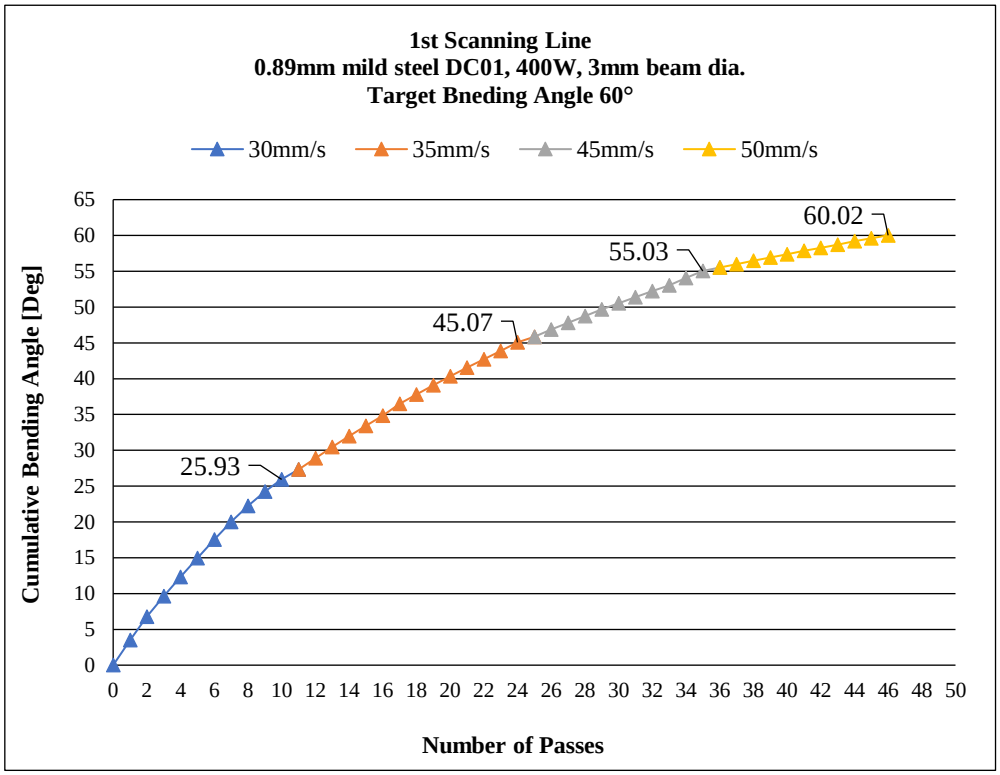

Figure 4.2.8 Laser forming of mild steel DC01, 60° target, 1st scanning line, scanning strategy 2

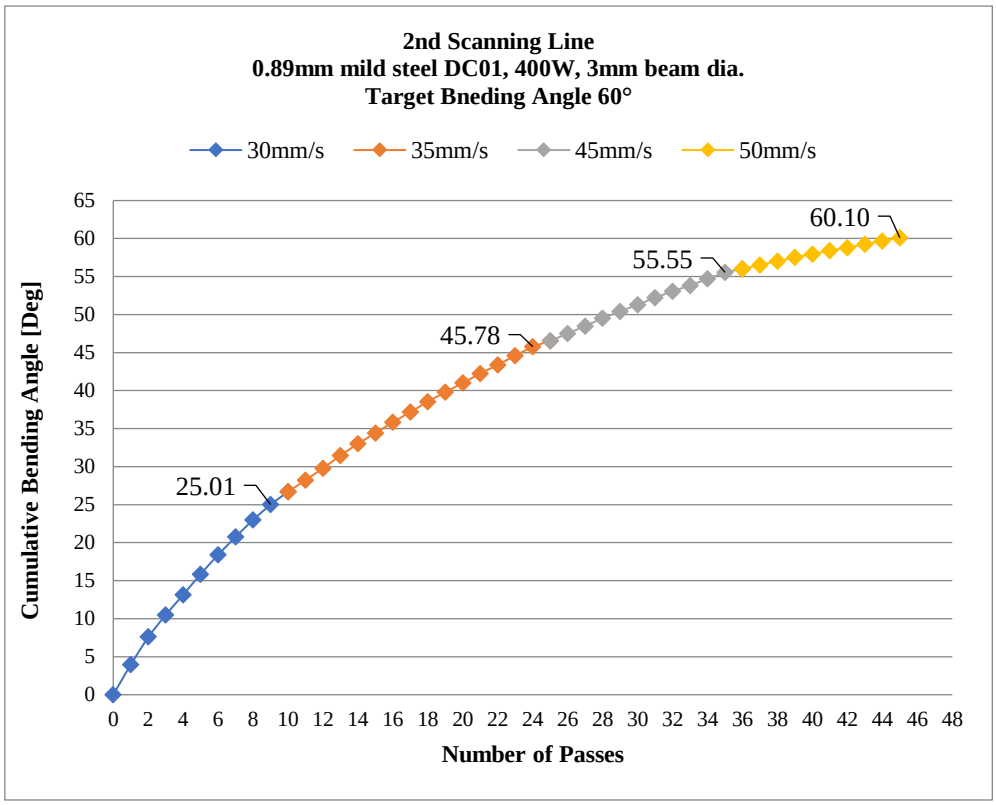

Figure 4.2.9 Laser forming of mild steel DC01, 60° target, 2nd scanning line, scanning strategy 2

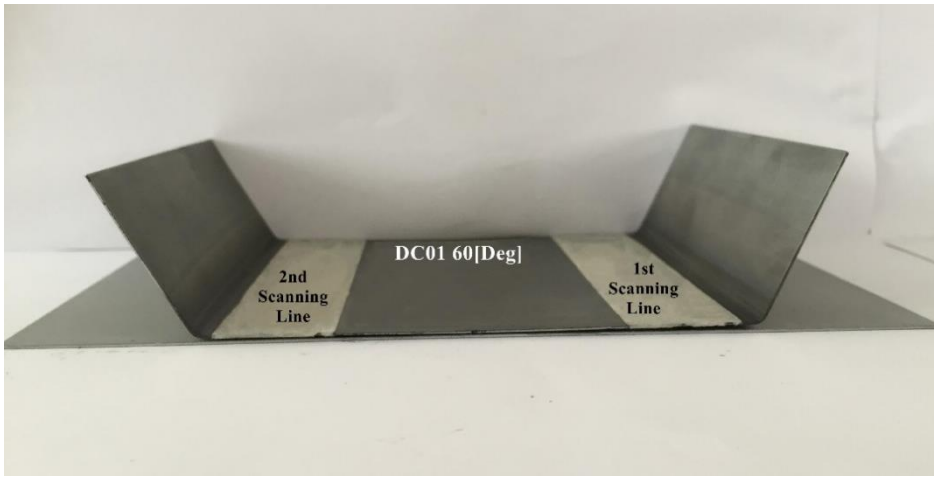

Figure 4.2.10 Mild steel DC01 final formed "U" shape component with 60° bending angle

Figure 4.2.8 to Figure 4.2.10 present the results of the scanning strategy at laser forming up to the target angle of 60°. Compared with the scanning strategies used in achieving the target angle of 20° and 40°, there were 4 processing speeds introduced in

this strategy for achieving the target angle.

In this scanning strategy, the processing speeds of 30mm/s was used for the initial few passes until the bending angle exceeds 25°, and then when the error between the current bending angle within 35° and 15° from the target angle, the processing speed was increased sequentially to 35mm/s and 45mm/s. Once the difference between the current bending angle and target angle was within 5° the processing speed was increased up to 50mm/s for the last few passes in order to control the process with a great deal of accuracy. It can be found that the error between the final bending angle and the target angle was successfully controlled within 0.125° through this scanning strategy.

In order to prove the versatility of this method of controlling the accuracy of laser forming, a study was conducted on the 200×100×1mm AA6061-T6 in this section. According to the successful work on mild steel DC01, the concept of setting the scanning strategies used to produce the target angles in this material is similar to that in the study of mild steel DC01. In this material, two speed increases were used for the target angles of 20°, and three speed increases for the target angles of 40° and 60°. The processing speeds of 35mm/s was used for the initial multi-pass to achieve a high bending rate, and then the processing speed was increased sequentially to 45mm/s, 55mm/s and 65mm/s based in the error between the current and target bending angle so as to reduce any risk of overshoot. The results of the scanning strategies for laser forming of the AA6061-T6 workpiece to the target angle of 20°, 40° and 60° are shown in Figure 4.2.11 to Figure 4.2.19.

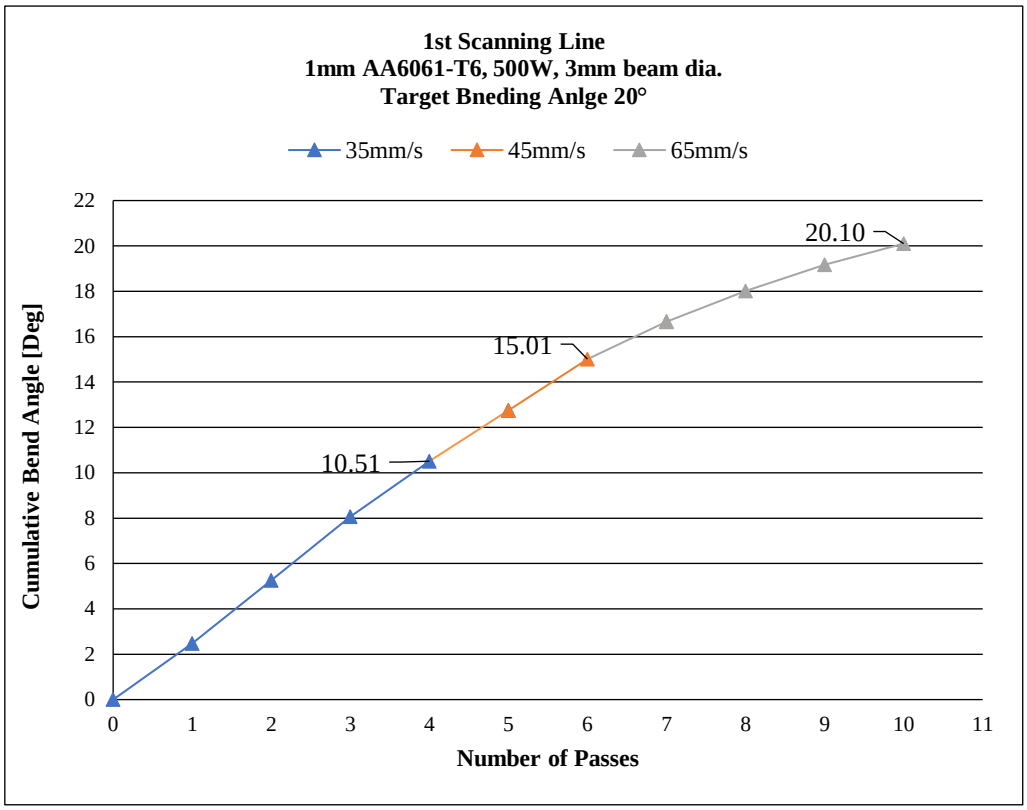

Figure 4.2.11 Laser forming of AA6061-T6, 20° target, 1st scanning line, scanning strategy 2

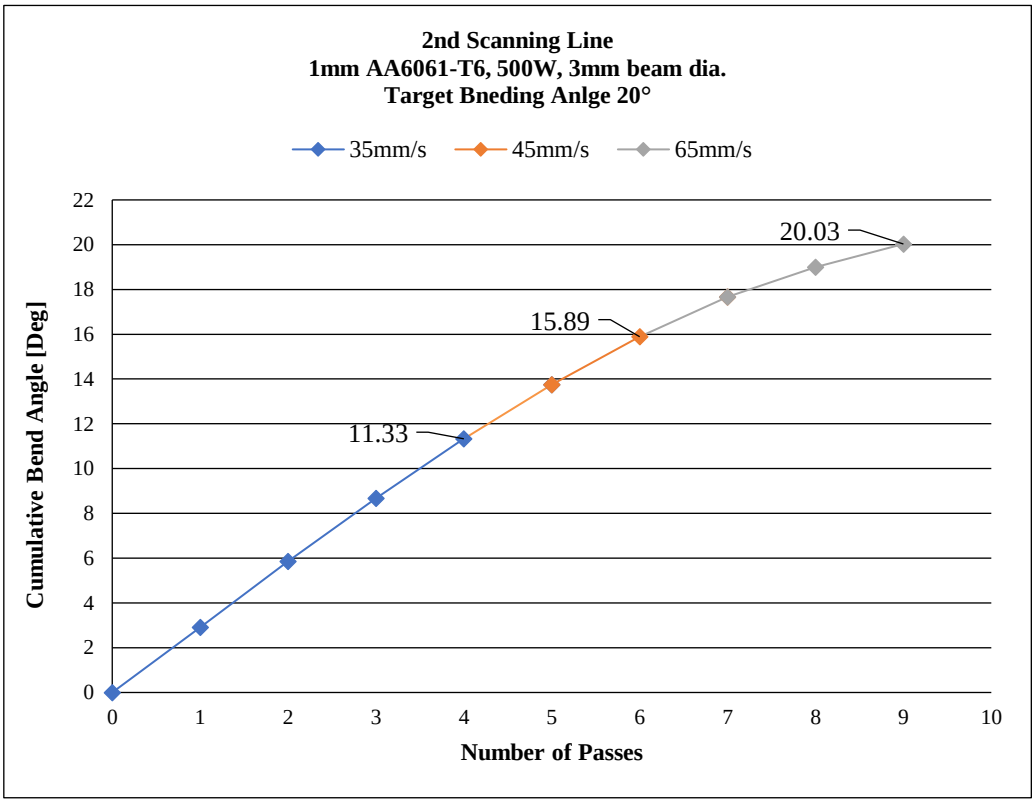

Figure 4.2.12 Laser forming of AA6061-T6, 20° target, 2nd scanning line, scanning strategy 2

Figure 4.2.13 AA6061-T6 final formed "U" shape component with 20° bending angle

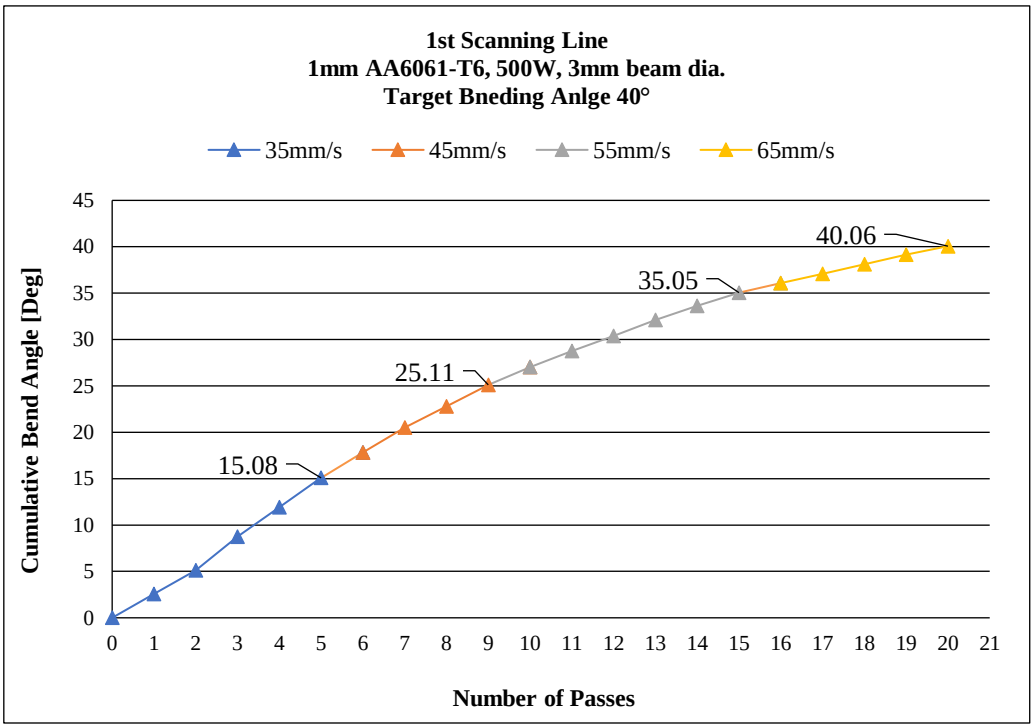

Figure 4.2.14 Laser forming of AA6061-T6, 40° target, 1st scanning line, scanning strategy 2

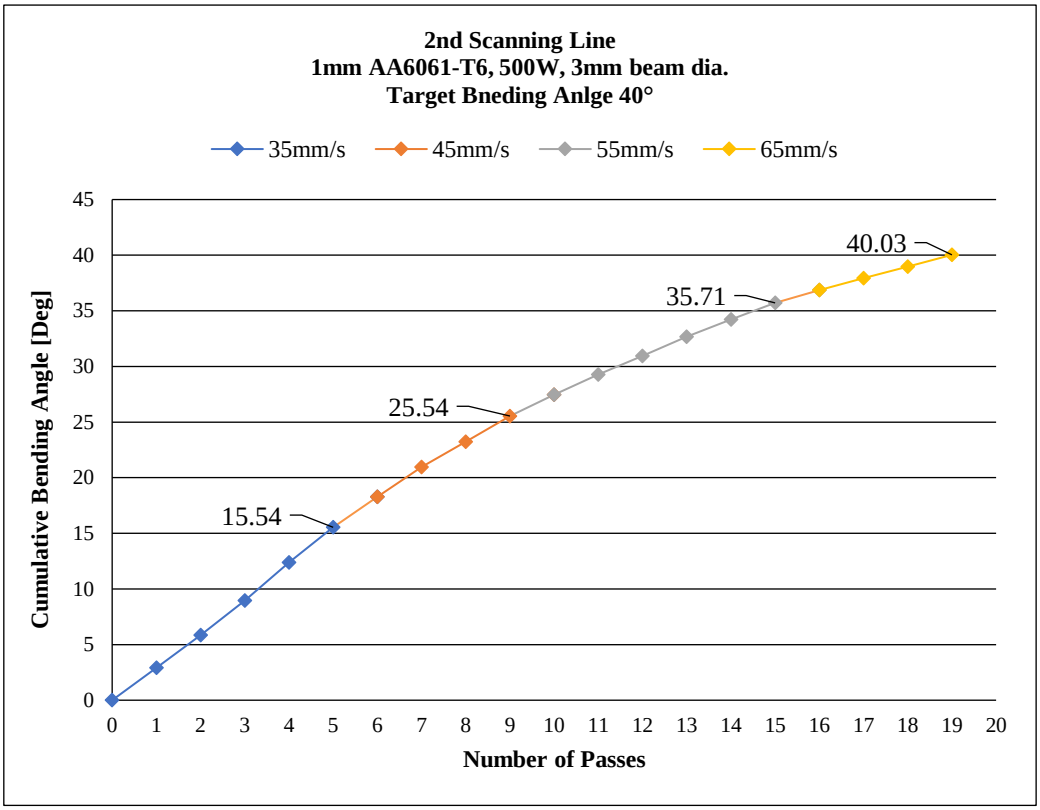

Figure 4.2.15 Laser forming of AA6061-T6, 40° target, 2nd scanning line, scanning strategy 2

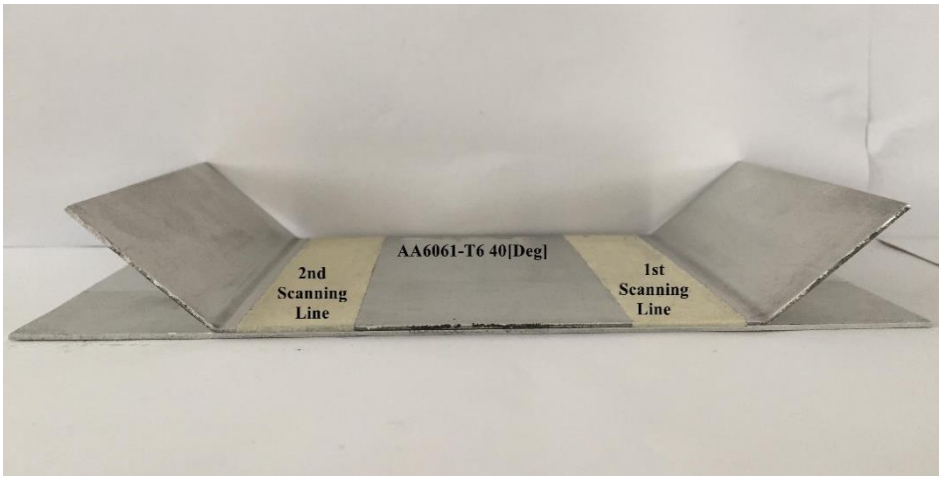

Figure 4.2.16 AA6061-T6 final formed "U" shape component with 40° bending angle

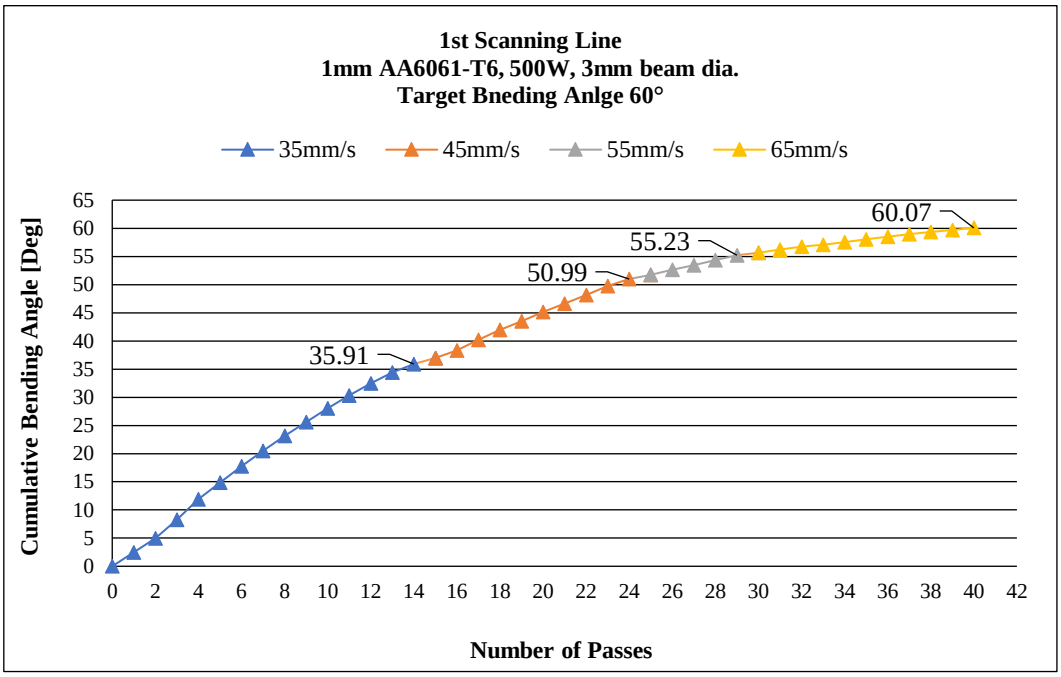

Figure 4.2.17 Laser forming of AA6061-T6, 60° target, 1st scanning line, scanning strategy 2

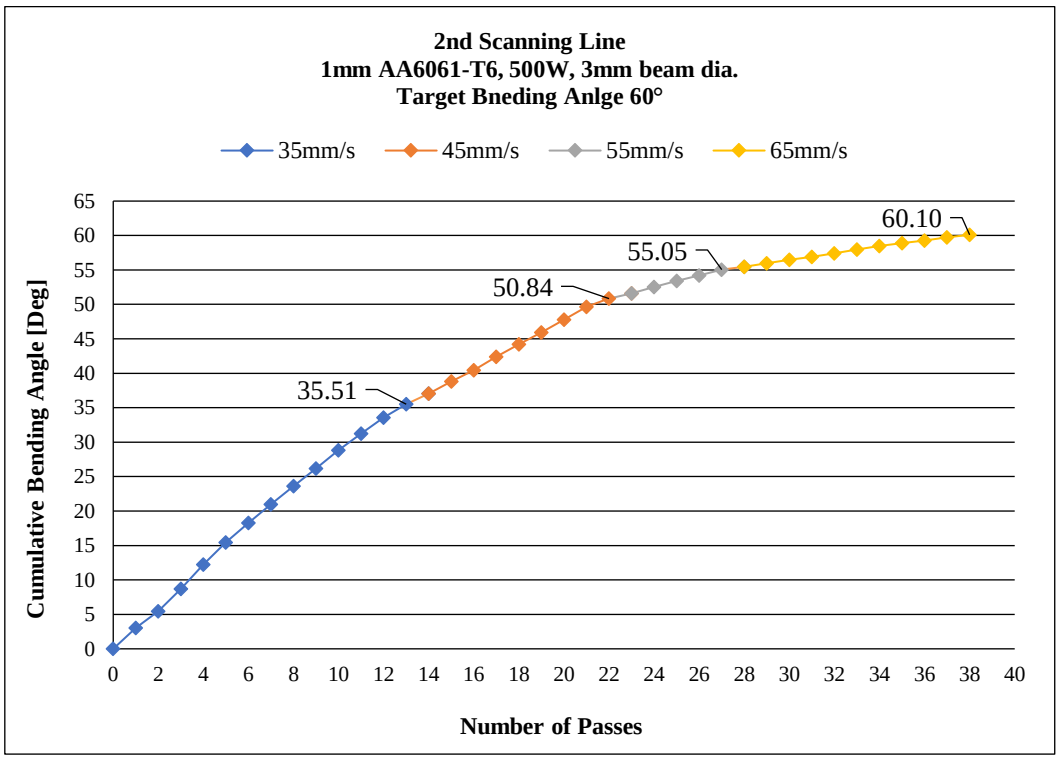

Figure 4.2.18 Laser forming of AA6061-T6, 60° target, 2nd scanning line, scanning strategy 2

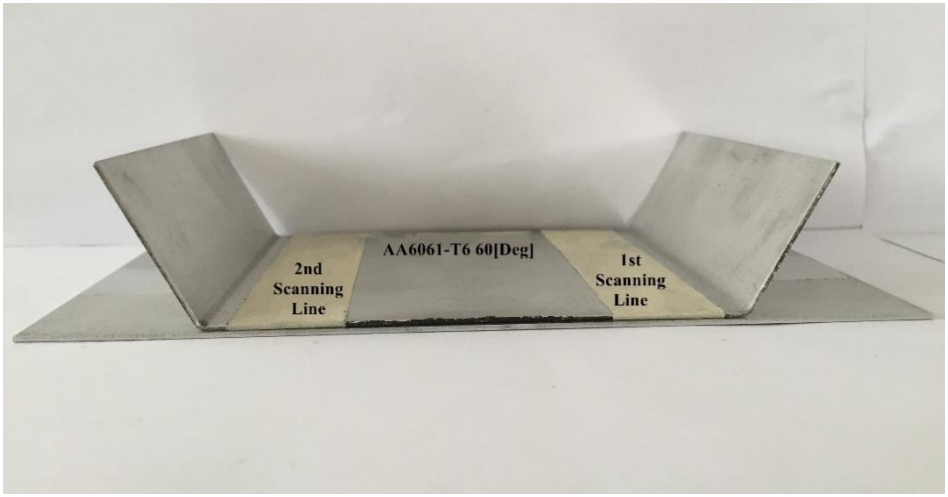

Figure 4.2.19 AA6061-T6 final formed “U” shape component with 60° bending angle

As can be seen from the above figures, by using the method of controlling the bending angle rate during the forming process, a considerable accurate two-dimensional aluminum component has also been successfully produced. And the errors of all the final bending angles were reduced to within 0.125° to the target angles.

Comparing the results from section 4.1 and 4.2, it can be seen that a large target bending angle can be achieved with less irradiation passes at a constant low processing speed, but the forming accuracy might be difficult to control due to the high bending angle rate. However, although the forming accuracy can be possible to be improved with a constant higher processing speed, more irradiation passes are required to achieve the target angle, which may reduce the reliability of the process. However, using the improved scanning strategy presented in section 4.2 can not only improve the forming accuracy but also reduce the number of scanning passes, which can reduce the effects of multiple passes such as strain hardening so as to improve the reliability of the process.

The results in this chapter demonstrate that the forming accuracy can be improved through control of the bending angle rate during the process via varying the processing speed. It has the potential to produce a two-dimensional component independent of residual stress history and material non-uniformity and take account of unwanted distortion, perhaps brought about by these two factors or process variability. The process can be controlled with a great deal of accuracy by the introduction of more speed steps with much higher processing speeds as the target angle approaches. In this feedback (closed loop) control system, the target bending angle, the desired minimum error, a set of incremental scanning speeds, and the maximum number of passes were set as input values, and the current bending angle and bending angle difference were set as the output values. Moreover, the accuracy of the measurement system used for feedback control (closed loop control) also influences the accuracy of the forming process since the higher the accuracy of the measurement system and measuring method, the more accurate measuring results of the bending produced in the workpiece.

In addition, the study presented in this chapter does demonstrate the potential manufacturing capabilities of the laser forming process for producing the single curved component, which provides the capability to produce or alter the shape of the component easily only through changing the process parameters or the scanning strategy without the need of expensive and inflexible hard tooling, this is a major advantage of the process over conventional forming technologies.

Chapter 5

Laser Forming of Double Curved Shape Results and Discussion

This chapter presents the results and discussion of experimental studies into laser forming of double curved shape, which includes creation of the process map for the given material (mild steel S275) used in this study, prediction of the scanning pattern, and determination of the scanning strategy to produce the target ship hull shape.

The study of laser forming of single curved components presented in chapter 4 has shown that laser forming has a great deal of potential capabilities in manufacturing. However, for practical industrial applications, in addition to single curved shapes, most components have a double curved geometry. Therefore, in order to advance the application of laser forming in the actual manufacturing environment, it is necessary to consider 3D laser forming.

5.1 Determination of the Process Parameters

This section presents the results and discussions of a short study of 2D bends, which includes the effect of the varying a number of laser parameters on the laser forming process and creating of the process map for the given material mild steel S275 and analysing the combined effects of laser power and processing speed on bending characteristics of the workpiece such as the bending angle rate.

The process map for the given material mild steel S275 was created by using the experimental results from 2D bends of 100×100mm coupons in 1.5mm thickness. The samples were laser formed by multiple passes (up to 20 passes) over the same irradiation track using different parameters. The bending angle was measured after each pass and converted into bending angle per pass (bending angle rate). These values are then used to plot a line of best fit to give a visual approximation of the effect of varying both laser power and processing speed on the bending characteristics of the workpiece as shown in Figure 5.1.1. The various lines indicate contours where on that line is it possible to produce a bending angle per pass of the indicated value and above the line a value of over the indicated value but below the next given contours value is produced. Therefore, the area defined by these contours corresponds to the 'formability' of the given material, giving an indication of how applicable laser forming is to the material.

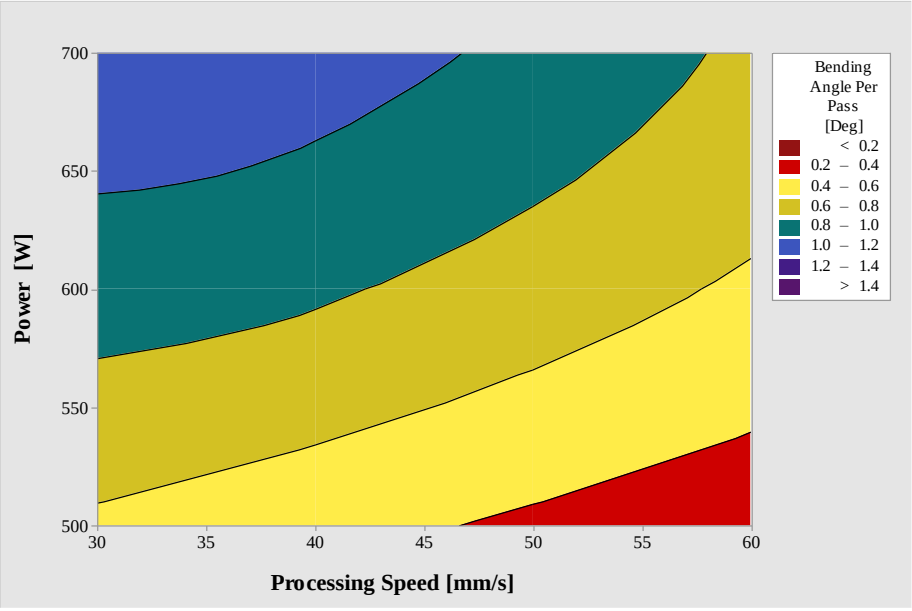

Figure 5.1.1 Combined effect of laser power and processing speed on bending angle rate

From Figure 5.1.1 it can be found that the bending angle rate can be controlled by varying either the laser power or the processing speed such as that the bending angle rate increases with increasing of laser power, however, the relationship between the processing speed and the bending rate is inversely proportional. A possible reason for this is that either increasing of the laser power or decreasing the processing speed (longer the interaction time of the laser beam) will cause a rise in the temperature on the top surface of the material. The elevated surface temperature will result in an increased temperature gradient through the thickness of the material and reducing the flow stress of the material, especially for materials with lower thermal conductivity as mild steel. This leads to larger plastic stresses being induced in the top surface of the sample than in the lower surface, which leads in turn to a greater bending angle. However, excessively high temperature will increase the risk of damage to the surface of the material. It can be seen from Figure 5.1.2 that the surface of the material has been damaged under the power of 800W and the processing speed of 30mm/s after 20 passes.

Figure 5.1.2 Mild steel S275, 1.5mm thickness ,5mm Beam Dia., 800W, 30mm/s, surface condition after 20 passes

As can be seen from the processing map data, the data range of 5mm beam diameter and laser power of 500W gave a bend angle rate selection between 0.2° and 0.8° in the processing speed range 30 to 60 mm/s, thus these parameters were selected for the followed 3D laser forming study since no damage to the surface of the material and fine controllability of the process are the two important factors needed to be taken into account in laser forming.

5.2 Prediction of Scanning Pattern

The results and discussions of prediction of the scanning pattern are presented in this section, which is mainly focus on the effect of the spacing between adjacent scanning lines on laser forming.

As mentioned before, the lines of constant height and the minimal principal strain field are used as a basis for prediction of the scanning patterns in this 3D laser forming investigation. And for 3D laser forming the contour levels can be arbitrarily chosen to produce the 3D shapes, however on a continuous smooth surface the localised bend angles along the scanning lines should be small enough so as to not facet the surface significantly, which indicates another important factor that needs to be taken into account for prediction of the scanning pattern, as the number of contour levels selected or the spacing between adjacent scanning lines. The effect of the spacing between adjacent scanning lines on laser forming, such as deformation, temperature distribution and strain field, are analysed by numerical simulation, which can provide a basis for the prediction of the scanning patterns. The discussion and results are given below.

To analyze the effect of the path spacing on the laser forming process, numerical simulations were conducted with 500 W of power, 50 mm/s as the processing speed and 5mm for the spot diameter (d) according to the scanning paths shown in Figure 5.2.1, where the scanning line spacing S=d/2, d, 2d, 3d and 4d, respectively. The dimensions of the plate were 100×100×1.5mm.

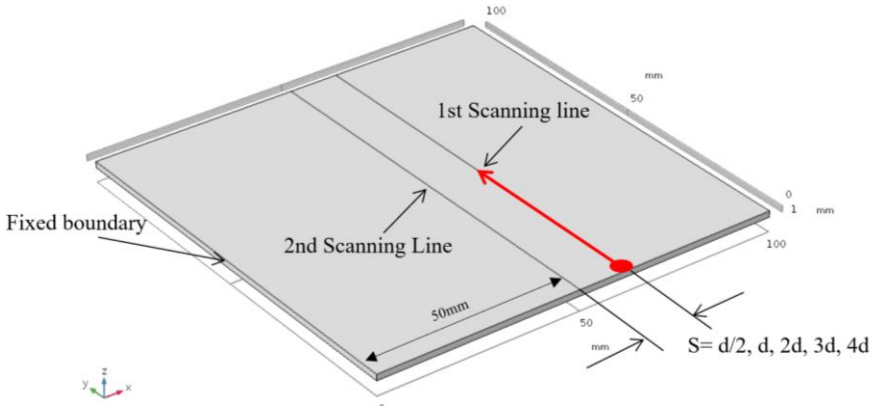

Figure 5.2.1 Schematic figure of path spacing in laser forming processes

Figure 5.2.2 shows the numerical results of the deformation of the plate in Z direction. As can be seen from the results, the bending deformation is different as the path spacing varies. A continuous curved line near the heating line can be obtained when the path spacing is smaller or equal to a beam diameter 5 mm, but the bending section is changed into a curved line then to a straight line and back to a curved line with increasing of the scanning line spacing. However, the given ship hull shape has a continuous smooth surface, thus, the smaller scanning line spacing should be chosen to acquire the continuous deformation, which can effectively raise the forming accuracy of the plate in the laser forming. In addition, it can be found that for a smaller path spacing, the displacement at the free end of the plate is greater than that of a larger path spacing. A possible reason for this may be that a hot plate is easier to be formed than a

cold one [68]. From Figure 5.2.3 to Figure 5.2.7 it can be found that the smaller spacing between the scanning lines the more heat is retained in the plate, which will also result in reducing the yield stress of the material.

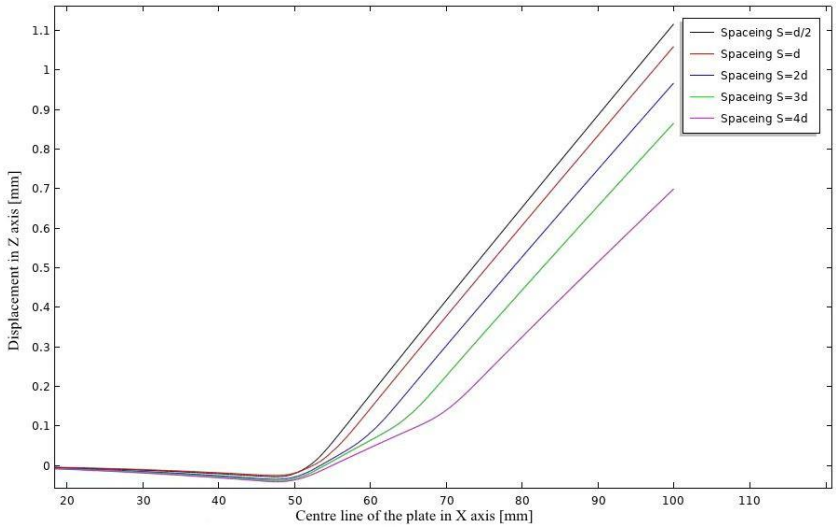

Figure 5.2.2 The effect of path spacing on the displacement at the free end of the workpiece, single pass, t=4.2s

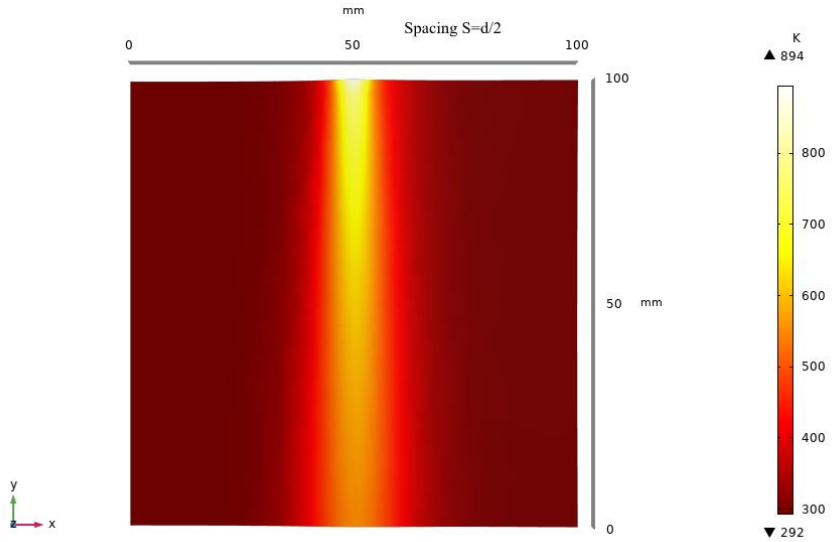

Figure 5.2.3 Effect of path spacing on temperature distribution path spacing of d/2, single pass, t=4.2s

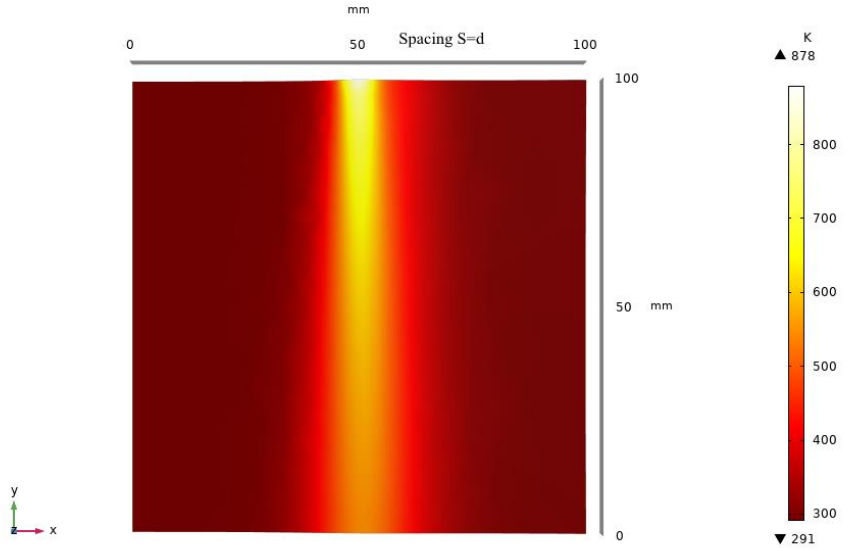

Figure 5.2.4 Effect of path spacing on temperature distribution path spacing of d, single pass, t=4.2s

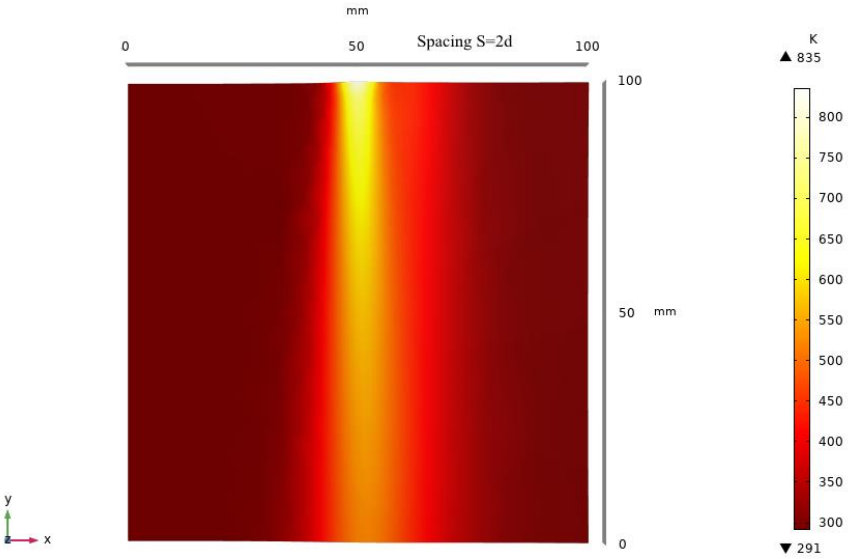

Figure 5.2.5 Effect of path spacing on temperature distribution path spacing of 2d, single pass, t=4.2s

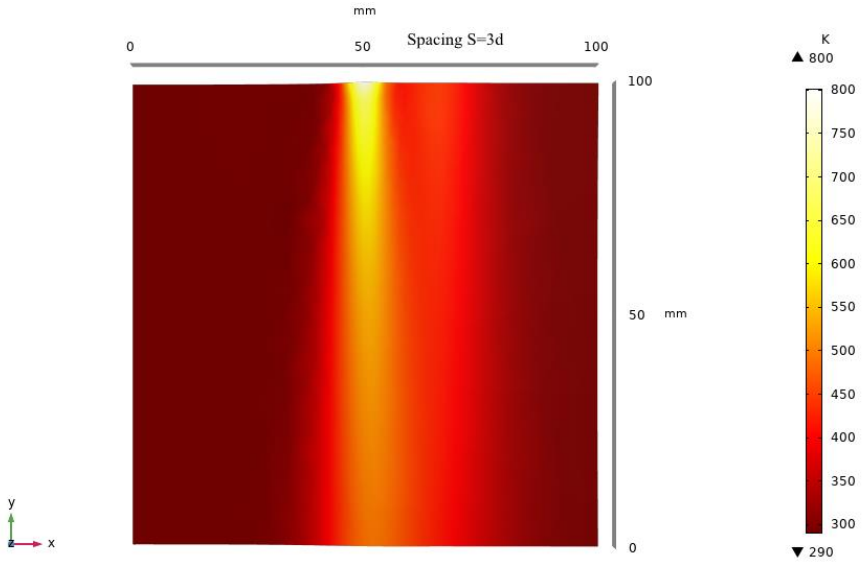

Figure 5.2.6 Effect of path spacing on temperature distribution path spacing of 3d, single pass, t=4.2s

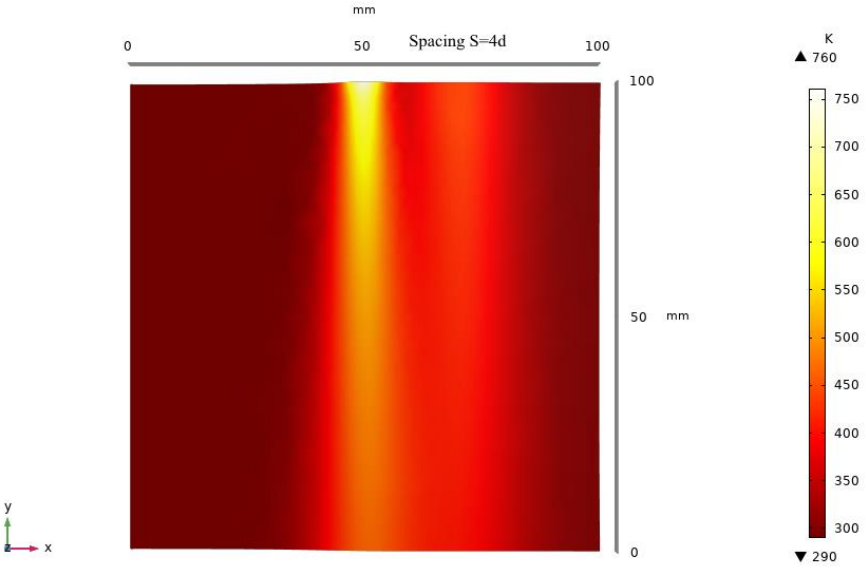

Figure 5.2.7 Effect of path spacing on temperature distribution path spacing of 4d, single pass, t=4.2s

Figure 5.2.8 to Figure 5.2.12 shows the numerical results of the minimal principal strain in X direction with the different scanning lines spacing under the same process parameters. The minimal principal strains generated in laser forming are mainly concentrated in the laser spot heating zone. It can be observed that when the path

spacing is less than the spot diameter, the strain fields between the heating paths interfere with each other because the minimal principal strain near the second heating line already exists before the second heating, but the continuous plastic strain can be obtained as shown in Figure 5.2.8. As can be seen from Figure 5.2.9 to Figure 5.2.12 the influence zone of the strain fields between the heating lines decreases with increasing of the scanning line spacing, which means that the interaction between the adjacent heating paths can be possible to be avoid with increasing of the scanning line spacing and the deformation of the plate can be considered as a superposition of a single scan, but it leads to the strain fields being discontinuous. However, the target ship hull shape presented in this thesis has a smooth continuous surface, thus a continuous strain field is needed.

Moreover, it can be observed that the peak minimal principal strains generated on the second scanning line are larger than that on the first scanning line for the different scanning lines spacing. This is mainly due to the fact that at the end of the process the temperature near the second scanning line cannot be cooled to the initial temperature because of the short time interval, which leads to the temperature along the second scanning line being higher than that in the first as illustrated in Figure 5.2.13 to Figure 5.2.17 and so the temperature difference between the two scans results in the different strain fields of every scan. In addition, it can be noted that for a smaller path spacing, the peak minimal principal strains of the two scan lines are higher than the larger path spacing, which is also an important reason for the reduction of the displacement at the free end of the plate with increasing of the scan spacing.

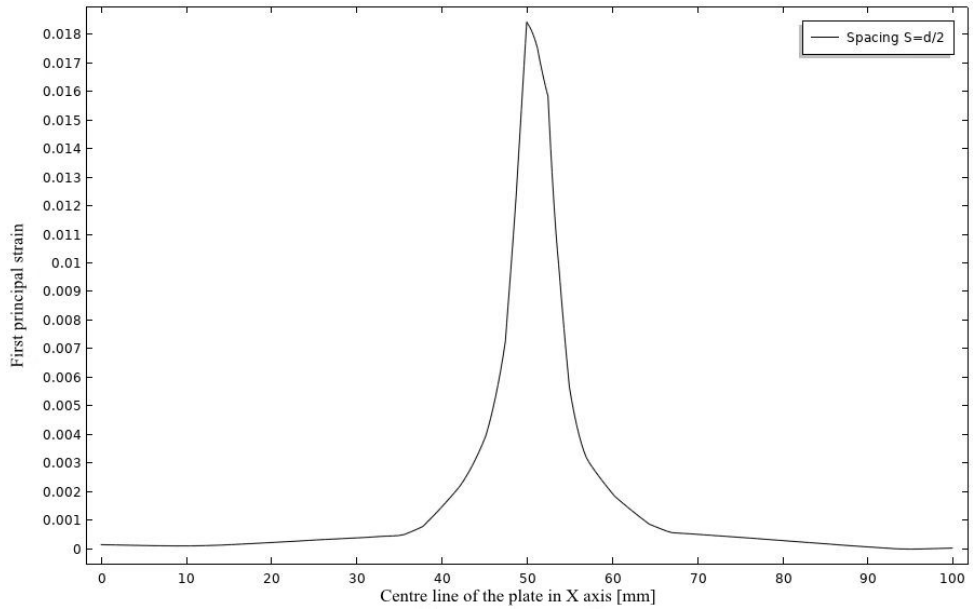

Figure 5.2.8 Effect of path spacing on minimal principal strain in the X direction path space of d/2, single pass, t=4.2s

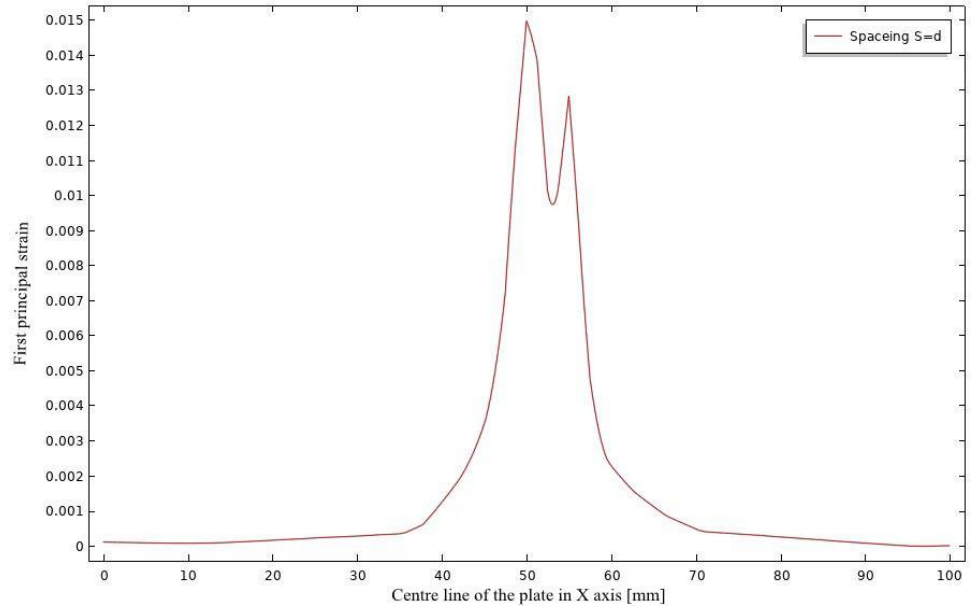

Figure 5.2.9 Effect of path spacing on minimal principal strain in the X direction path space of d, single pass, t=4.2s

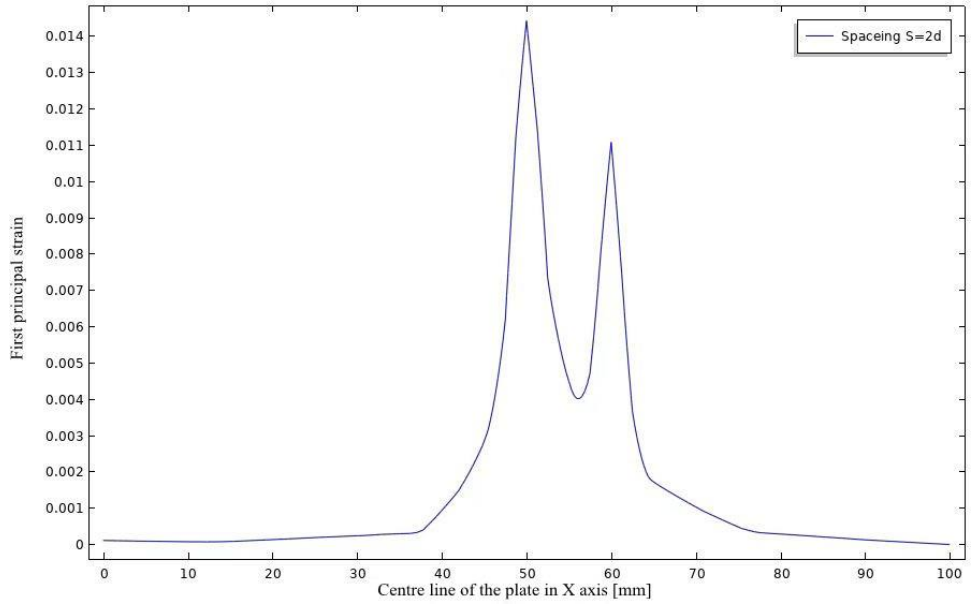

Figure 5.2.10 Effect of path spacing on minimal principal strain in the X direction path space of 2d, single pass, t=4.2s

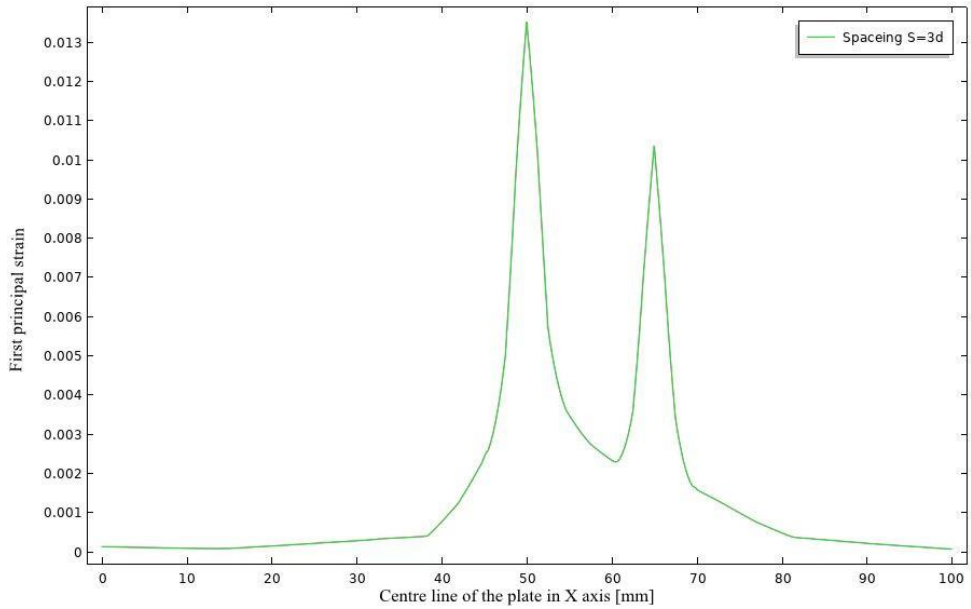

Figure 5.2.11 Effect of path spacing on minimal principal strain in the X direction path space of 3d, single pass, t=4.2s

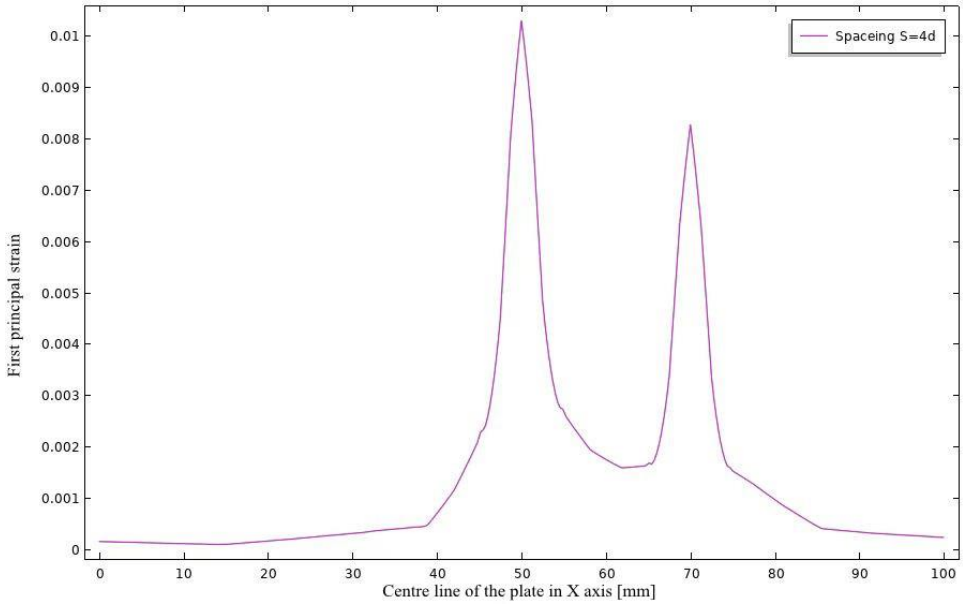

Figure 5.2.12 Effect of path spacing on minimal principal strain in the X direction path space of 4d, single pass, t=4.2s

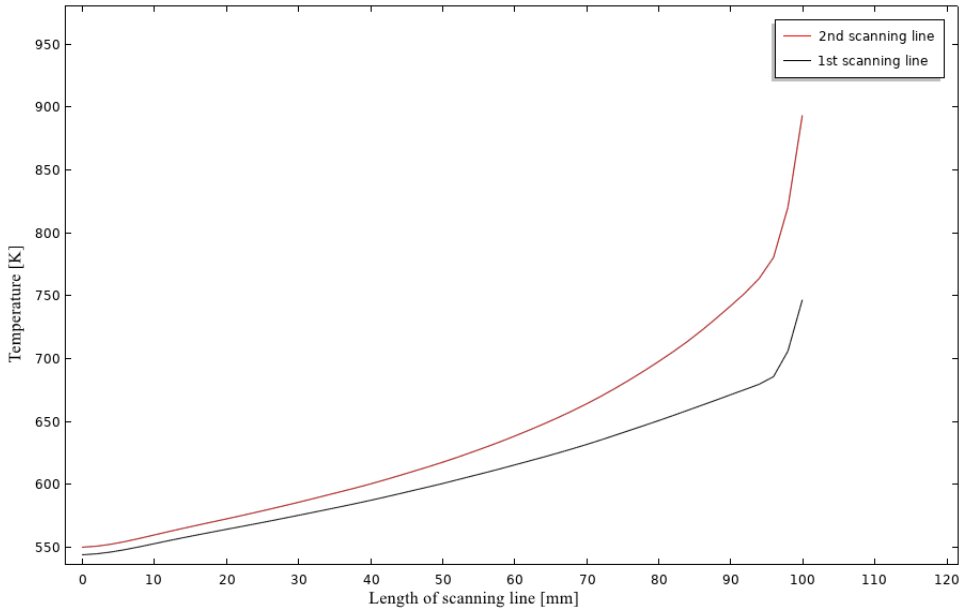

Figure 5.2.13 Effect of path spacing on temperature along scanning lines at the end of the process d/2, single pass, t=4.2s

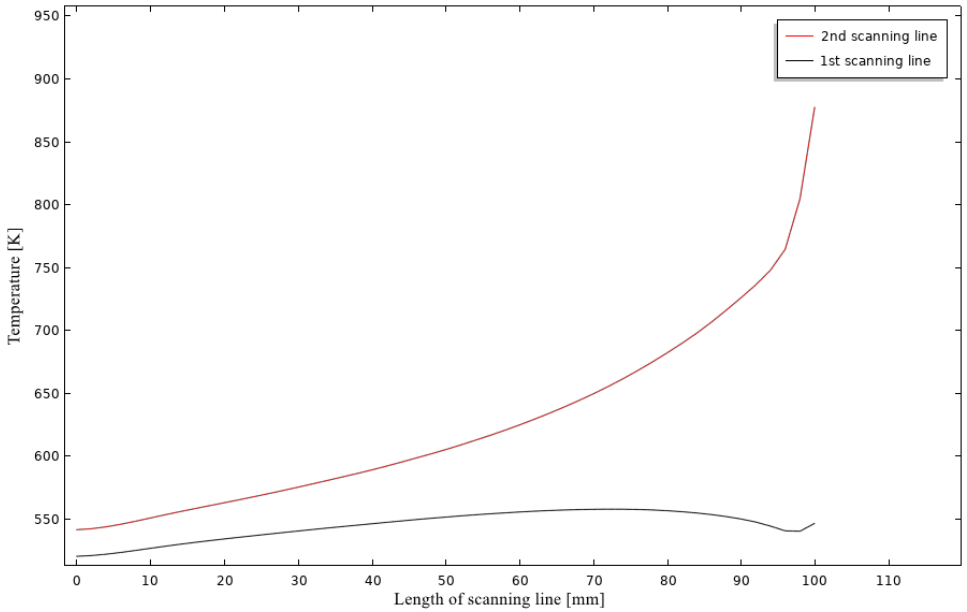

Figure 5.2.14 Effect of path spacing on temperature along scanning lines at the end of the process d, single pass, t=4.2s

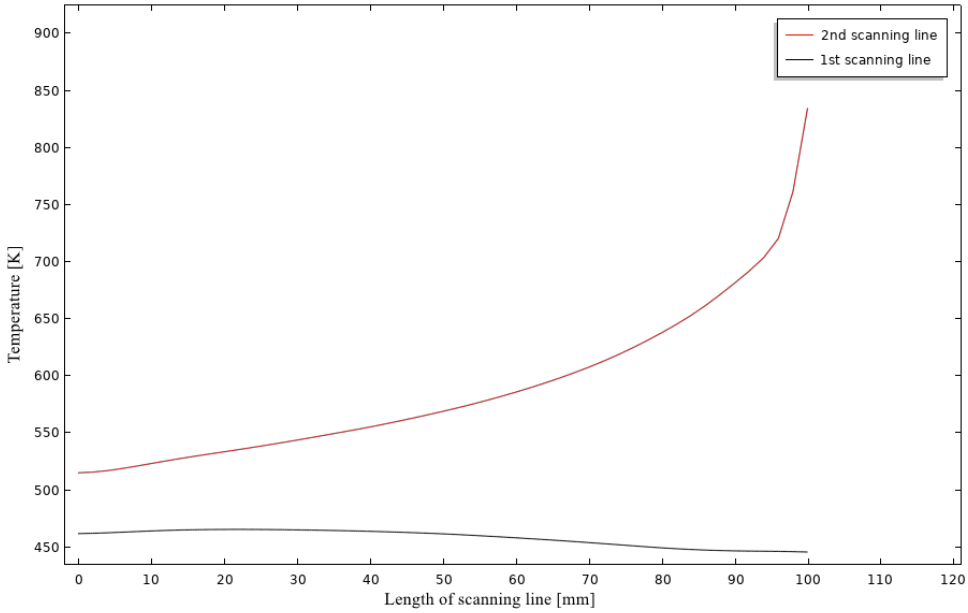

Figure 5.2.15 Effect of path spacing on temperature along scanning lines at the end of the process 2d, single pass, t=4.2s

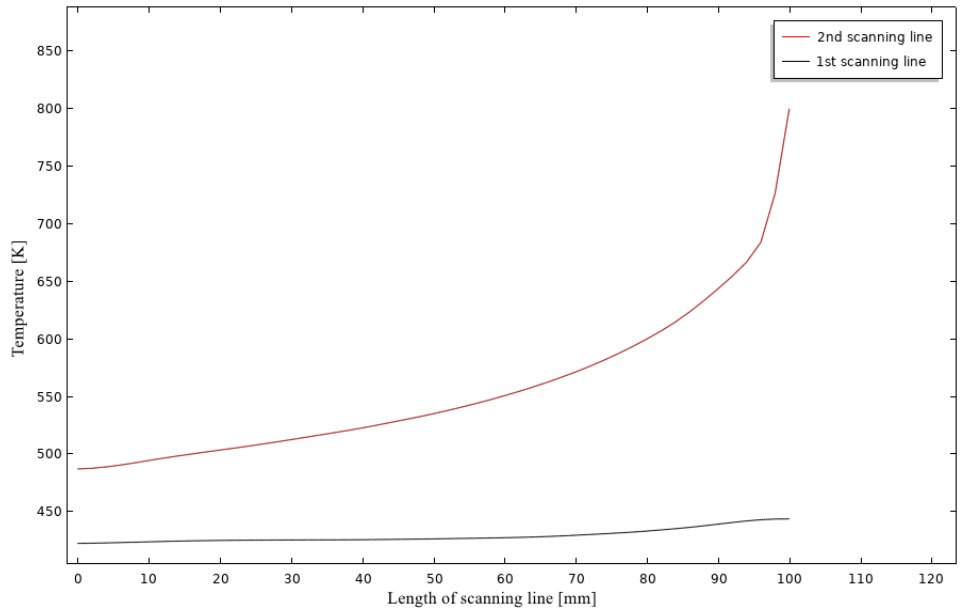

Figure 5.2.16 Effect of path spacing on temperature along scanning lines at the end of the process 3d, single pass, t=4.2s

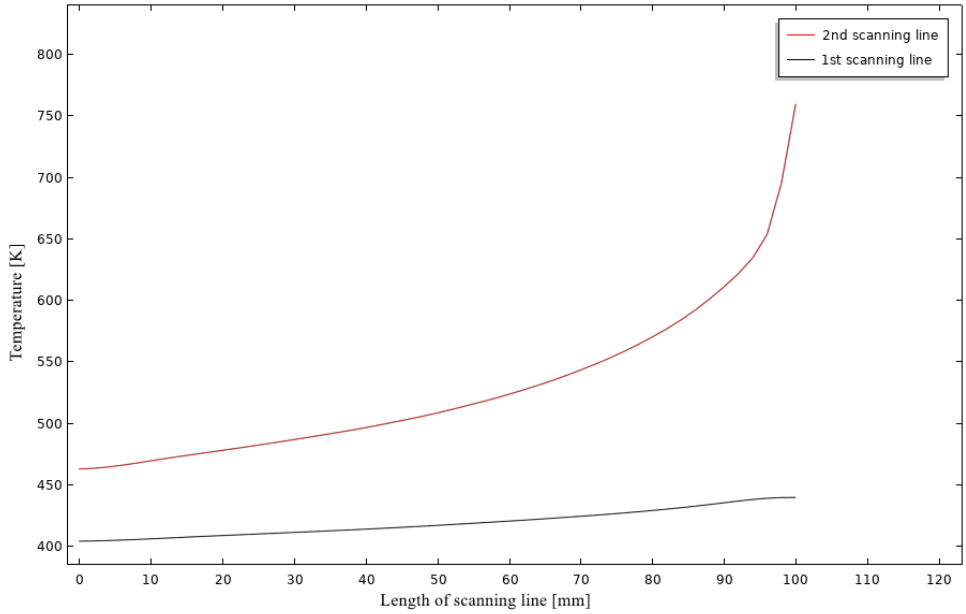

Figure 5.2.17 Effect of path spacing on temperature along scanning lines at the end of the process 4d, single pass, t=4.2s

The target ship hull shape has a geometry symmetrical along the y-axis and asymmetrical along the x-axis, which can be regard as a cross combination of two part-cylinders symmetrically along the y-axis and bending along the diagonal as can be seen in Figure 5.2.18, thus the plate is divided into four independent irradiation areas and

assume that the scanning pattern can be multiple straight scanning lines as similar to scanning pattern used for producing the part-cylinder.

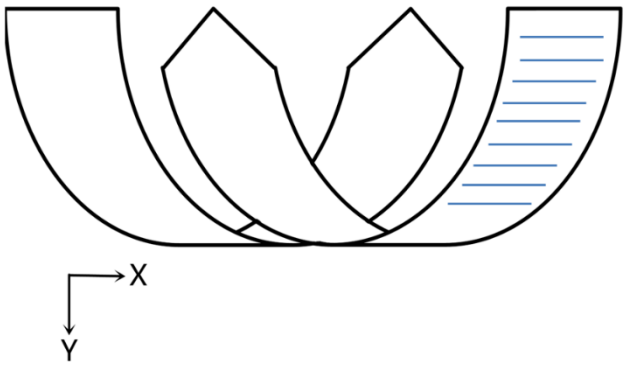

Figure 5.2.18 Cross combination of two part-cylinders symmetrically along the y-axis

As mentioned before, a scanning line should always correspond to a line of constant height, and from Figure 3.4.6 presented in section 3.4.2 it can be found that the lines of constant height of the target ship hull shape are linear around the four corners and gradually becoming curved lines towards the centre. Thus, the scanning pattern for producing the given shape should consist of straight lines near the four corners and curved lines close to the center. However, there are some changes made to the center scanning lines such as that the curved scanning lines are replaced with multiple straight scanning lines. Next, using a numerical simulation to demonstrate that the simple straight scanning line can also be used to produce the target shape without being completely consistent with the line of constant height. Figure 5.2.19 presents the lines of constant height of a target deformation. Figure 5.2.20 presents the numerical simulation result of laser forming of this target shape under 500W power, 5mm beam diameter and 50mm/s processing speed, in which the black arrow lines present the minimal principal strain distribution and orientations, the colour curved lines present

the lines of constant height and red arrow line presents the laser scanning path. It can be seen that the scanning path is normal to the minimum principal strain orientation and a shape corresponding to the lines of constant height of the target shape can be produced by straight line irradiation path.

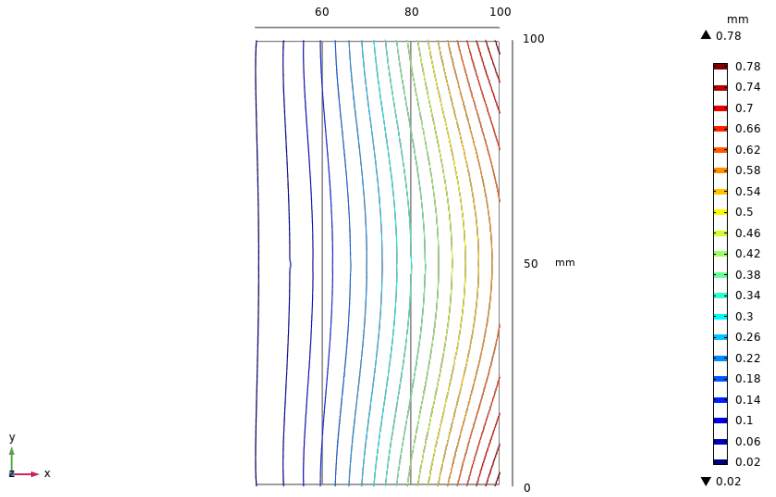

Figure 5.2.19 Contour lines of constant height of a target deformation at z-axis

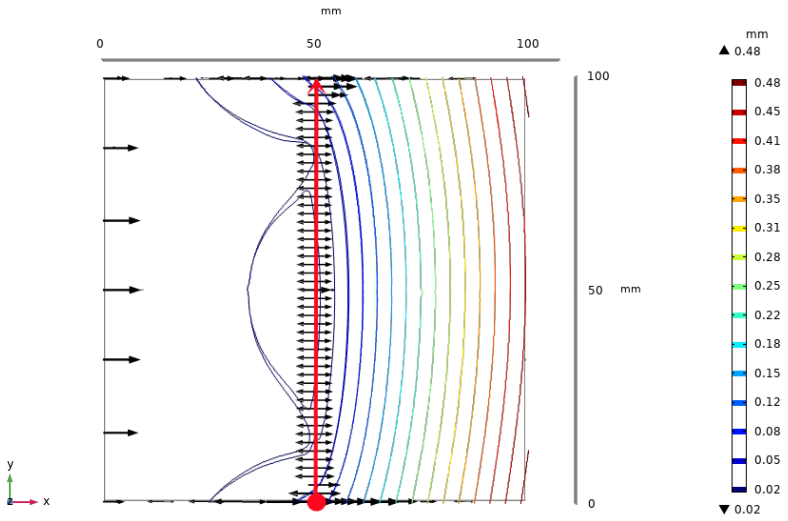

Figure 5.2.20 Numerical simulation of a target deformation at z-axis

Another reason to modify the center scanning lines is that if the scanning lines close to the center are consistent with the contour lines close to the center, which will cause the simultaneous deformation of corner A and D or corner B and C (four corners on the plate have been identified in Figure 3.4.1), so it is difficult to achieve forming of the four corners independently and the forming accuracy is difficult to control.

Therefore, the prediction of the scanning pattern for producing the target ship hull shape can be seen in Figure 5.2.21 according to the factors above. In addition, it was decided to set the spacing between the two scanning lines to half of the diameter (2.5mm) according to the numerical simulation results of the influence of the scanning line spacing on laser forming. The red arrow lines represent the irradiation paths and the laser moving direction. It can be seen that the irradiation area by the scanning pattern corresponds to the deformed area indicated by the contour lines of constant height of the given ship hull shape.

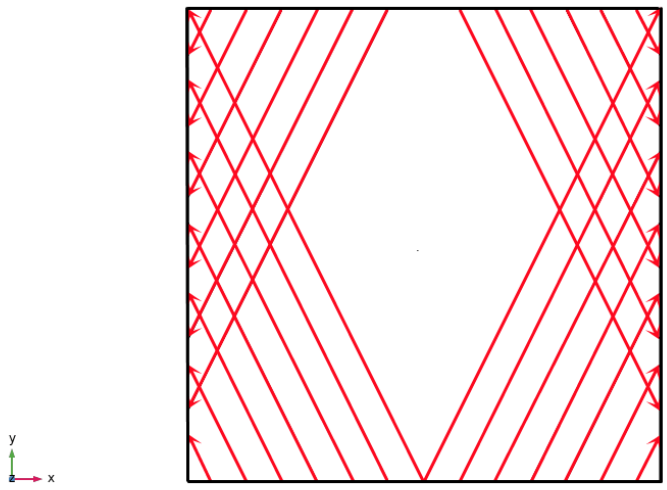

Figure 5.2.21 Prediction of the scanning pattern for producing the target ship hull shape

5.3 Determination of the Scanning Strategy

This section presents the results and discussions of two scanning strategies for producing the given ship hull shape.

The first scanning strategy used in test 1 is used to verify the feasibility of the predicted scanning pattern and the incremental error-based approach, which can be regarded as a basic scanning strategy. The second scanning strategy is a modified strategy based on the first one, of which the purpose is to produce the target 3D shape independent of residual stress distribution and non-uniformity absorption of the laser radiation and to take account of any unwanted distortion either caused by above two factors or process variability and reduce the error to within +/- 0.5mm to the target shape. The results of these two scanning strategies are given in the following sub sections.

5.3.1 Basic Scanning Strategy

The first scanning strategy prediction used in test 1 is based on the overall error between the current formed surface and target shape, the processing will be terminated when the whole of the workpiece is equal or exceed the target shape, which can be regarded as a basic scanning strategy used to verify the feasibility of the predicted scanning pattern and the incremental error-based approach. And the irradiation sequence is from outside to inside in counterclockwise as shown in Figure 5.3.1. As mentioned before, the plate was divided into four independent irradiation areas, thus the direction of rotation is not important that will not influence the forming results. The results after each pass

are presented below.

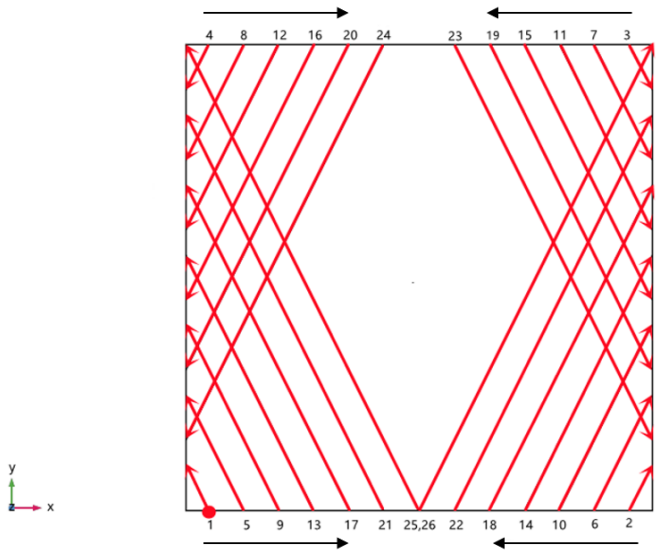

Figure 5.3.1 The first scanning strategy, irradiation sequence is from outside to inside in counterclockwise

Pass 1

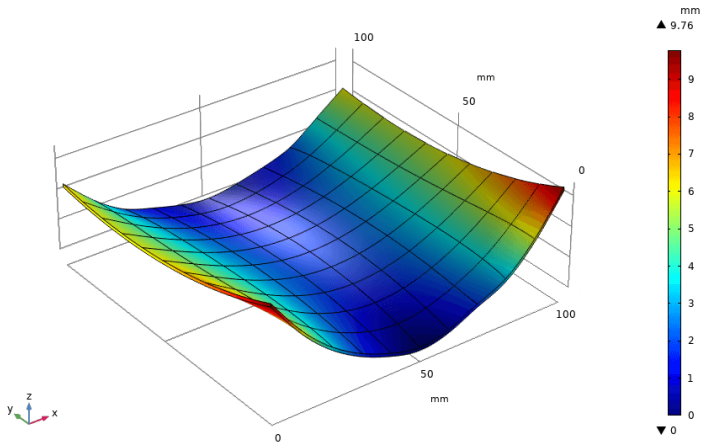

Figure 5.3.2 Current formed shape after Pass 1, 5mm beam diameter, 500W and 30mm/s speed. Maximum forming ~9.76mm

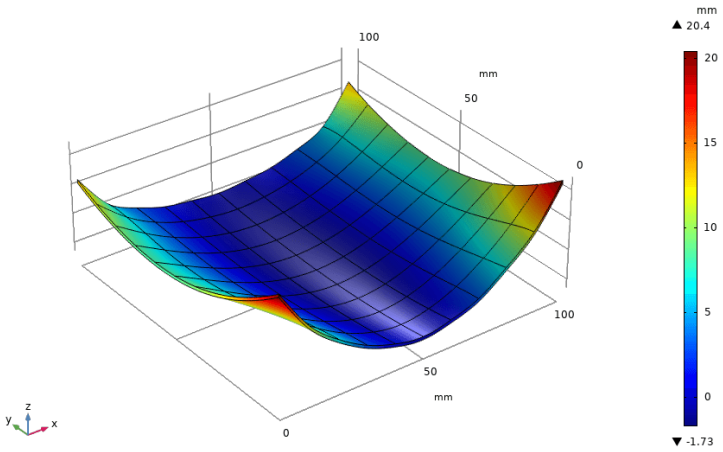

Figure 5.3.3 Error surface between the formed surface after pass 1 and the target shape, ~20.4mm maximum error to the target shape

In pass 1, all scanning lines were irradiated at the speed of 30mm/s. It can be seen from Figure 5.3.2 to Figure 5.3.3 that a shape resembling the target shape has been formed after the first irradiation pass with a maximum deflection of ~9.76mm. Figure 5.3.3 presents the errors between the current formed surface and target shape after pass 1, it can be observed that after pass 1 the maximum error between the current formed surface and the target shape is +20.4mm, which means that more forming is required to achieve the target shape. However, it can be noted that the shrinkage (-1.73mm) occurred around the centre; this is where the work piece is clamped. A possible reason for this is that the restriction of the clamp causes the stress concentration during the thermal deflection of the plate, which results in shrinkage around the centre. An addition irradiation pass (pass 2) was carried on after pass 1 for achieving more forming.

Pass 2

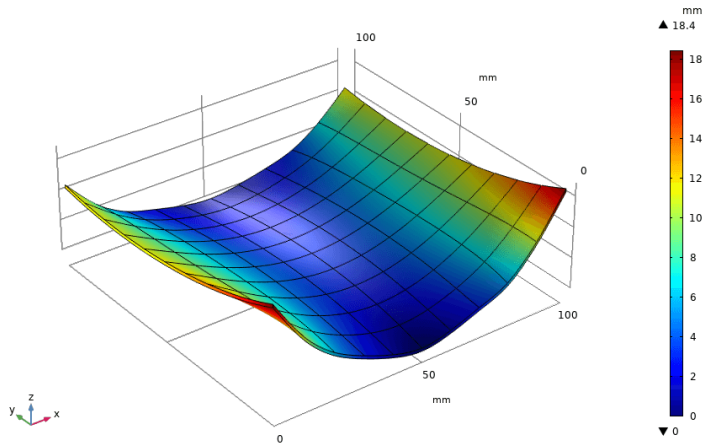

Figure 5.3.4 Current formed shape after Pass 2, 5mm beam diameter, 500W and 40mm/s speed. Maximum forming ~18.4mm

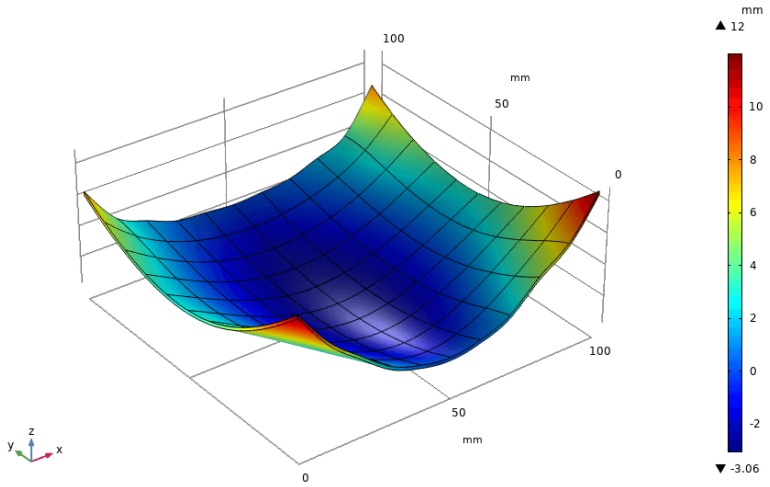

Figure 5.3.5 Error surface between the formed surface after pass 2 and the target shape, ~12mm maximum error. Error surface gives a prediction for the next pass

For pass 2 the processing speed was increased to 40mm/s in order to decrease the increments to its target shape. It can be seen from the results after pass 2 presented in Figure 5.3.4 and Figure 5.3.5 that a ship hull shape component with the maximum deflection ~18.4mm was formed, and the maximum error between the formed surface and the target shape is +12 and -3.06mm.

Pass 3

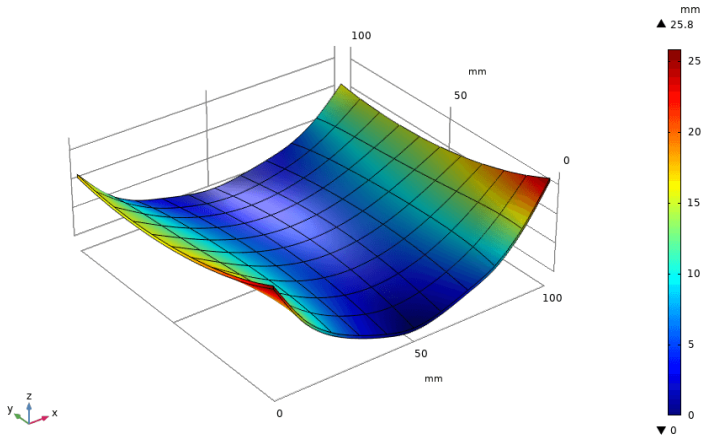

Figure 5.3.6 Current formed shape after Pass 3, 5mm beam diameter, 500W and 50mm/s speed. Maximum forming ~25.8mm

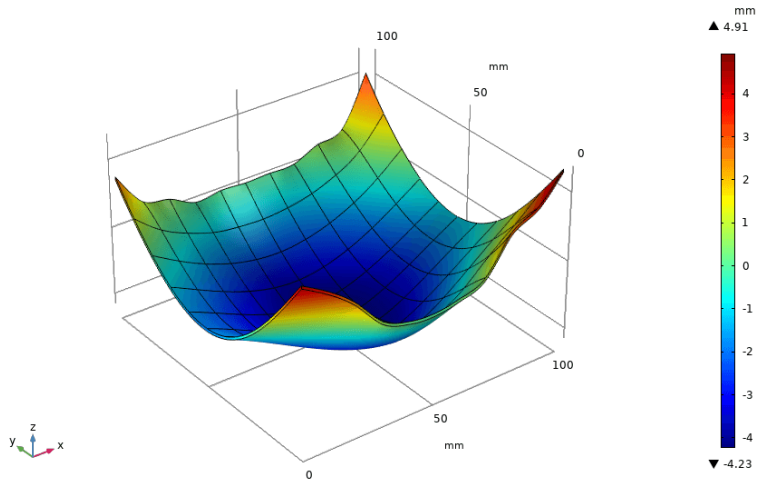

Figure 5.3.7 Error surface between the formed surface after pass 3 and the target shape, ~4.91mm maximum error. Error surface gives a prediction for the next pass

For pass 3 the processing speed was increased to 50mm/s to further reduce the forming rate, it can be seen from the results after pass 3 that a considerable amount of forming of ~25.8mm (Figure 5.3.6) has been achieved and a reasonable symmetrical state was maintained. And the error between the current formed surface and the target final shape is +4.91 and -4.23mm (Figure 5.3.7), thus the speed was increased to

60mm/s for the last two passes as the target approached. The results of the last two passes can be seen in Figure 5.3.8 to Figure 5.3.11.

Pass 4

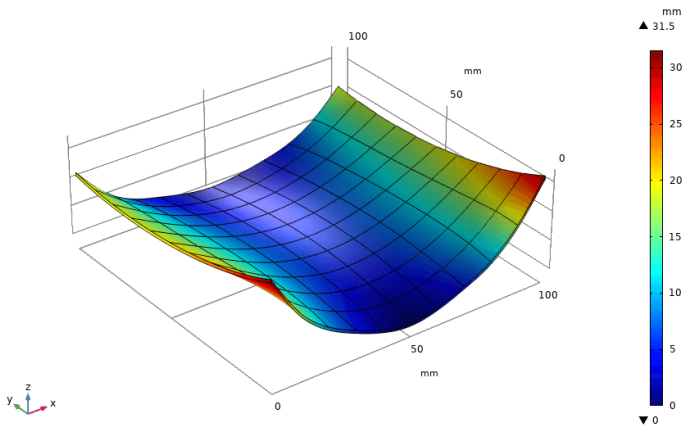

Figure 5.3.8 Current formed shape after Pass 4, 5mm beam diameter, 500W and 60mm/s speed. Maximum forming ~31.5mm

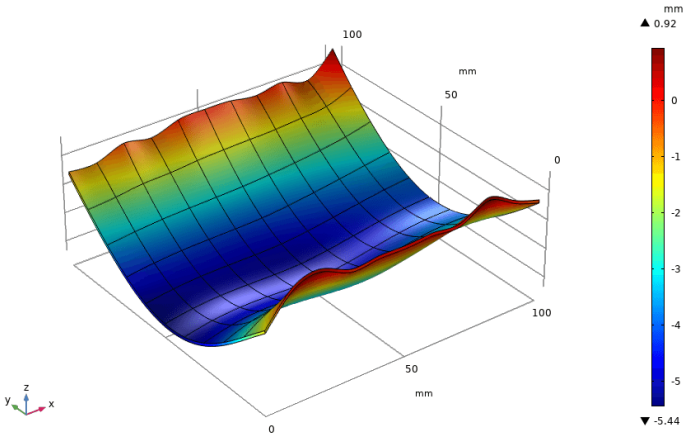

Figure 5.3.9 Error surface between the formed surface after pass 4 and the target shape, ~0.92mm maximum error. Error surface gives a prediction for the next pass

Pass 5

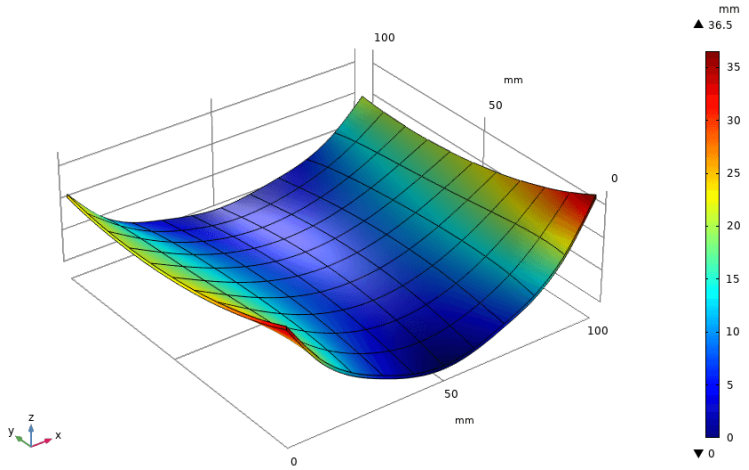

Figure 5.3.10 Current formed shape after Pass 5 (final pass), 5mm beam diameter, 500W and 60mm/s speed. Maximum forming ~36.5mm

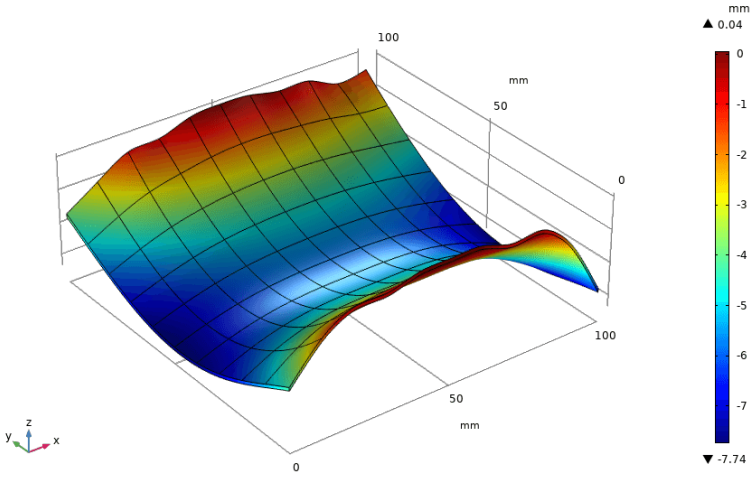

Figure 5.3.11 Error surface between the formed surface after pass 5 and the target shape, the whole of the final shape occurred maximum amount of ~7.74mm over-forming

From the error plot after each pass above, it can be seen that after pass 3 a slight over-forming has occurred towards the edges and after pass 4 most area on the workpiece has over formed, only local areas are below the target shape. However, as mentioned before, the processing will be terminated when the overall forming of the

workpiece is equal or exceed the target shape and so pass 5 was performed. After pass 5 the forming of whole of the final formed shape exceeded the target shape (Figure 5.3.11) and so the processing was terminated.

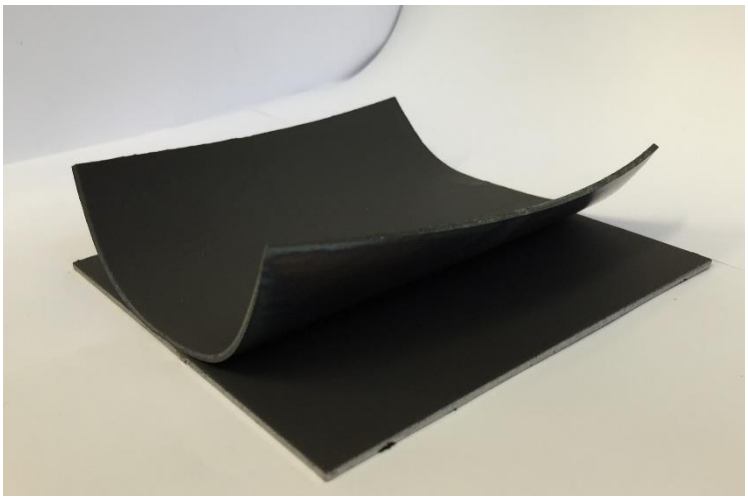

Figure 5.3.12 Final formed shape by using the scanning strategy in test 1

Repeatability Test

A repeatability test was performed using this strategy on another plate; the results are given in Figure 5.3.13 and Figure 5.3.14.

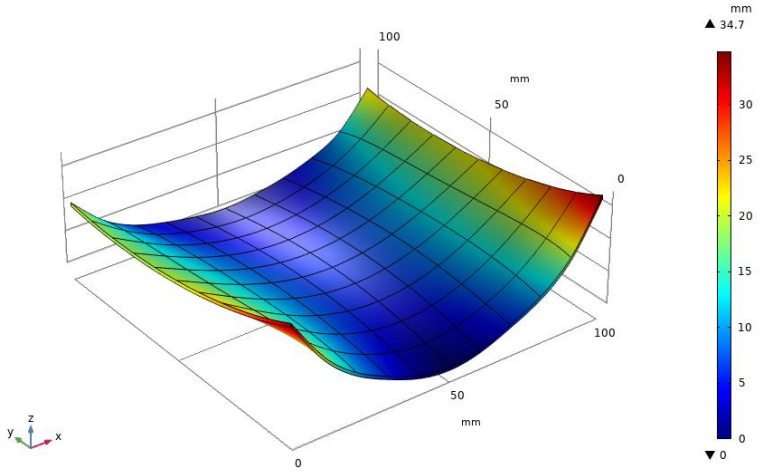

Figure 5.3.13 A repeatability test forming result by using the same scanning strategy. Maximum forming ~34.7mm

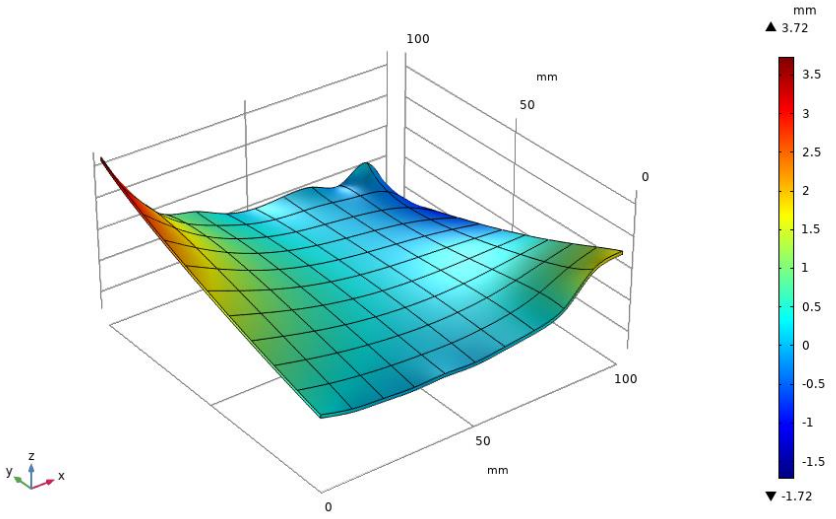

Figure 5.3.14 Comparison between the final formed surfaces by using the same scanning strategy with maximum error of ~3.72mm

The results of the repeatability tests show that a reasonable repeatability can be achieved using the same scan strategy, the maximum difference between the samples is 3.72 and -1.72mm.

As can be seen from the results of test 1 above, a smooth contoured ship hull shape has been formed by using of this scanning pattern based on the lines of constant height and minimal principal strain distribution of a target shape. This could potentially be a relatively straightforward approach to predict the scanning pattern in 3D laser forming for a given shape. And a component within the error of -7.74mm of the target shape has been produced by using an iterative scanning strategy based on the error between the current formed and the target shape.

However, there is a weakness in this scanning strategy such as that all scan lines were irradiated for each pass, and the influence of each scan line on the rest of the plate was not taken into account, which resulted in over-forming, especially in the area close to the edges since the scanning paths in the center of the plate will cause the outer edge

to be deflected.

And it can be noted that the scanning paths are created symmetrical along y-axis, so theoretically the formed shape or the error distribution after each pass should have a symmetrical state along the y-axis, however, it can be seen from the errors plot after each pass that the errors are distributed asymmetrically along y-axis. This is due to a number of factors such as unknown residual stresses distribution of the workpiece, variability in the absorption of the incident laser radiation, and the asymmetric nature of the laser forming process itself. However, the asymmetry of the laser forming process is difficult to be avoided by using of the current single optical path system unless a dual optical path system is implemented for parallel processing.

In addition, it can be found for the error plot after each pass that the amount of shrinkage was increased after each pass. A possible reason for this is that the scanning sequency was from outside to inside in this scanning strategy, which resulted in stresses building towards the centre of the work piece. For this case the workpiece would be formed normally initially and as the irradiation paths moved towards the centre a buildup of stresses would increase towards the centre a force is exerted onto the clamp eventually causing the shrinkage around the centre of the workpiece. This effect will increase with each line passes and the amount of shrinkage will be increased with increasing of the irradiation passes. However, forming from the centre out perhaps can reduce this effect. When forming from the inside out the strains caused by this effect though initially restricted by the clamp build up outwards and are free to move. The next test will verify this.

Improvements to the basic scanning strategy were made in the next test (test 2) in order to solve the problems reflected in test 1.

5.3.2 Modified Scanning Strategy

The incremental error-based approach and the scanning pattern used in previous test has been proven to be of use in producing the given ship hull shape. As the basic pattern is correct another method of creating the irradiation strategy for the given ship hull shape will have to have the same pattern but with different distribution.

However, a weakness in the basic scanning strategy used in test 1 is without considering of influence of forming at each scan line on the rest of the plate. And, another reason for over-forming in the previous test perhaps was that during forming the focal position remained static, which resulted in the part moving towards the focus as it was formed, especially at the outer scanning paths. This would reduce the beam size and increase the intensity of the beam so as to affect the amount of forming and increase the possibility of damage. However, it is difficult to completely solve this issue with the current laser forming system unless a height controller or an automatic focusing system is integrated in the system to keep a constant beam spot on the workpicce.

In the previous test the scanning strategy prediction was only based on the overall error between the current formed surface and the target surface after each pass, while in this test, the scanning strategy, such as positioning and sequencing of the irradiation, will be adjusted after each pass not only based on the error plot but also the deformation

characteristics of the current part, such as that when the target shape is not formed within one pass, an appropriate scanning strategy for the next pass will be given by analysing the difference of the deflection of a number of points at 10mm steps along edge1 and 2 between the current formed shape and the target shape.

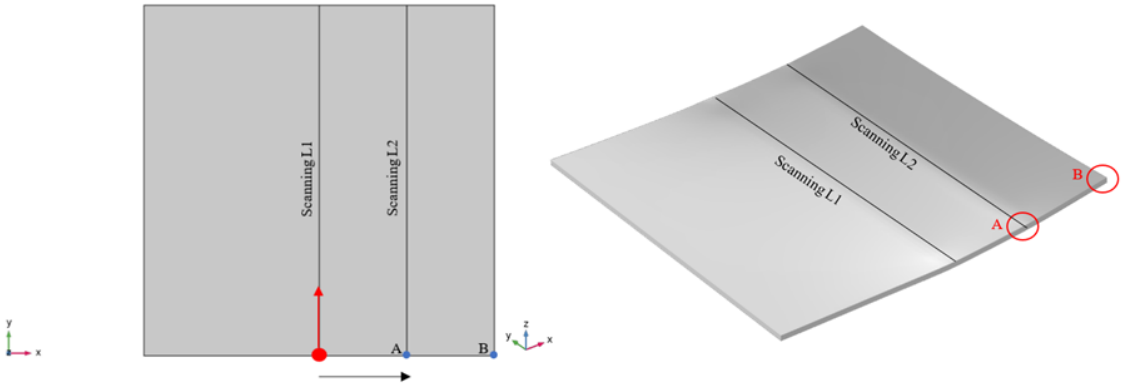

Figure 5.3.15 Schematic of selection of scanning line for producing a target double bends shape

In laser forming process the point about which a moment is generated is on the scanning line and should be stationary in space and bending legs either side will move instead. Figure 5.3.15 presents the forming of a double bends shape from a square flat surface. It can be noted that there are two measured points A and B, if the deflection of the measured point A arrives the target value the scanning line 1 no longer needs laser irradiation in the next pass, and if the deflection of the measured point B arrives the target value the scanning line 1 & 2 no longer needs laser irradiation in the next pass. It is thought that this should be the case for the selection of the scanning line in the modified scanning strategy. In the modified scanning strategy, the measured points on edge1 and 2 correspond to the starting points of the scanning lines.

The basic concept of the modified scanning strategy is that the scanning lines close to the centre of the plate will be irradiated in the initial passes for achieving the maximum amount of forming from inside to outside, while leaving the last few passes on the outer scanning lines for the fine adjustment of forming on the outer edges so as to reduce any risk of over-forming. The detailed description of the modified scanning strategy was presented in the following part, based on the same target shape in the previous test.

Therefore, a modified scanning strategy was created in this test in order to produce the target shape independent of residual stress distribution and non-uniformity absorption of the laser radiation and to take account of any unwanted distortion either caused by above two factors or process variability. The purpose of this test is to reduce the error to within +/- 0.5mm to the target shape, namely, it is decided to terminate the control program if the difference between the current formed surface and target surface was within 0.5mm so as to avoid any over-forming and asymmetry however small.

Pass1

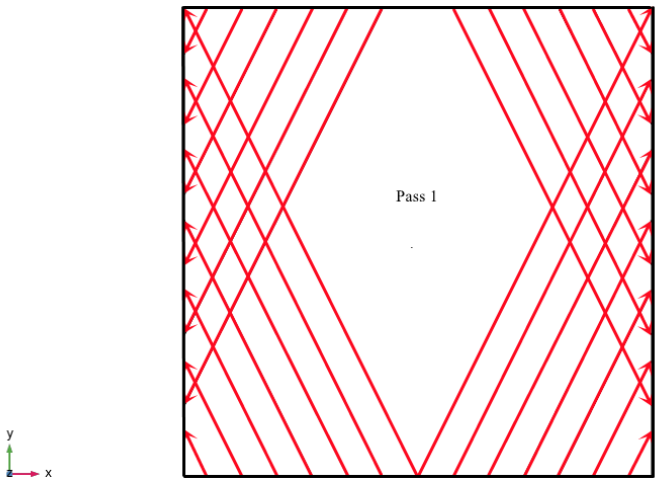

Figure 5.3.16 The first scanning strategy for pass1 in test 2

The first scanning strategy performed for the first pass was the same as in the previous test, all scanning lines were irradiated at the speed of 30mm/s, and the irradiation started from the outside moving towards the centre to keep the laser spot with a consistent diameter throughout pass 1.

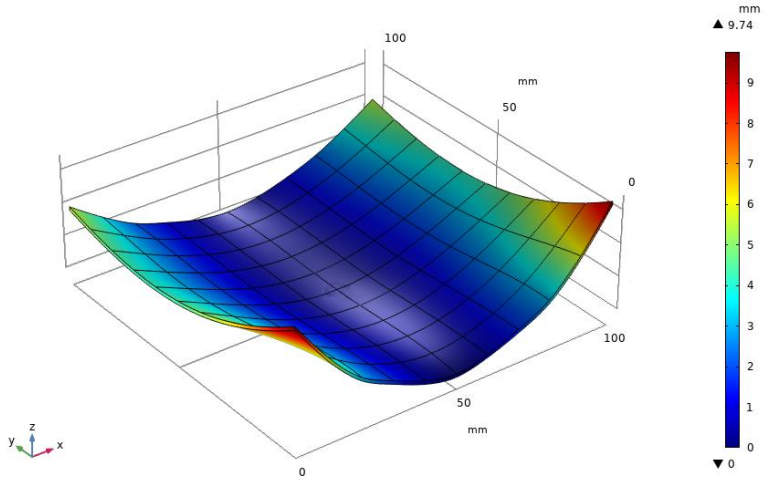

Figure 5.3.17 Current formed shape after Pass 1, 5mm beam diameter, 500W and 30mm/s speed. Maximum forming ~9.74mm

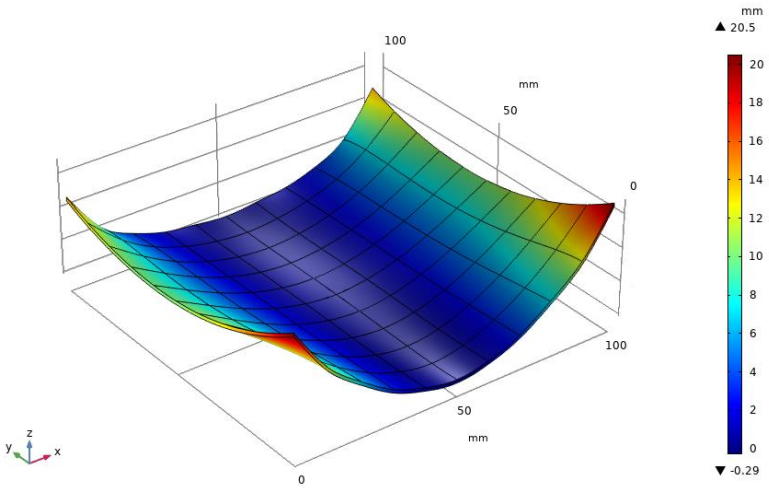

Figure 5.3.18 Error surface between the formed surface after pass 1 and the target shape, ~20.5mm maximum error

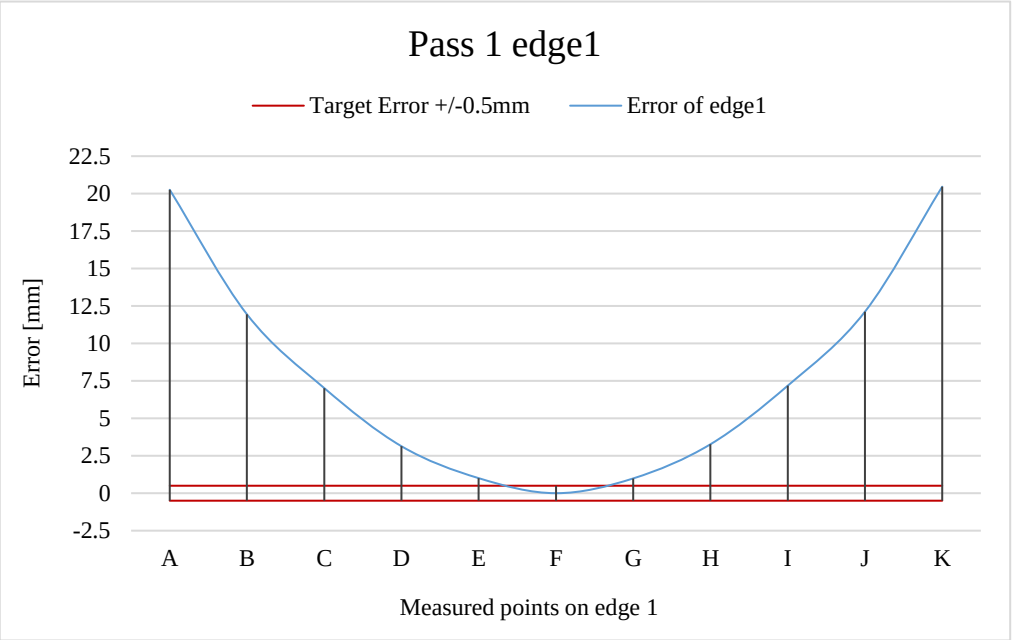

Figure 5.3.19 Comparison of the measured points on edge1 between formed surface after pass 1 and target shape. Error of the points gives a prediction for the next pass

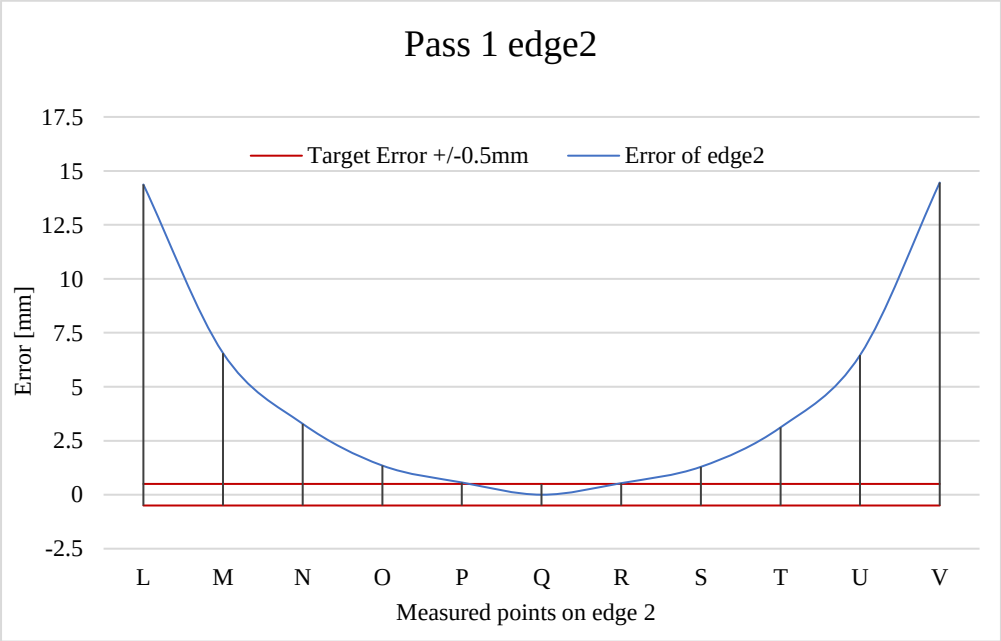

Figure 5.3.20 Comparison of the measured points on edge2 between formed surface after pass 1 and target shape. Error of the points gives a prediction for the next pass

From the forming result of pass1 above (Figure 5.3.17), it can be seen that the target surface was already taking form at this shallow formed state with the maximum amount of forming ~9.74mm, which was similar to the result of the first pass in the test 1. And from the error between the current formed surface after pass 1 and the target shape (Figure 5.3.18 to Figure 5.3.20), it can be seen that over-forming has not occurred and the error of the measured points on edge1 and 2 are greater than 0.5mm to the target. However, it can be noted that the error at the points close to the centre on edge2 is extremely close to 0.5mm, which means that if additional irradiation applied on the centre scanning lines, the error of these points is possible to be reduced to within 0.5mm since the forming rate on next pass will be reduced.

Therefore, a second pass was performed to form the workpiece towards the target shape at the speed of 40mm/s to decrease the forming rate. As discussed earlier, the irradiation lines close to the centre of the workpiece will cause a deflection of the outer edges and so the irradiation on the outer scanning lines was reduced in pass 2 to reduce the forming on the outer edges. The scanning strategy for pass 2 is shown in Figure 5.3.21.

Pass 2

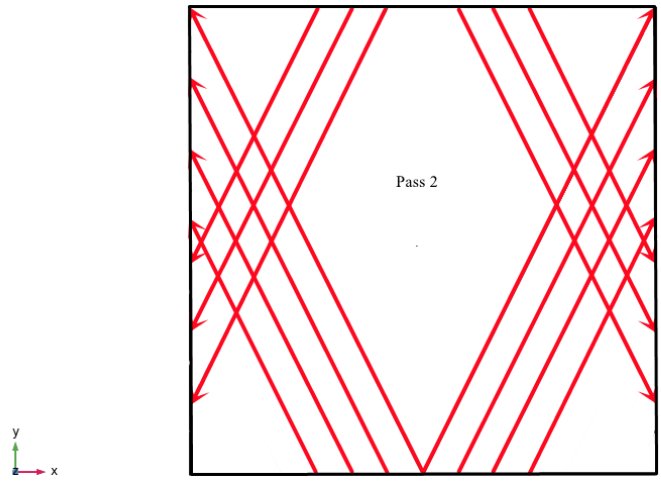

Figure 5.3.21 The second scanning strategy for pass2 in test 2

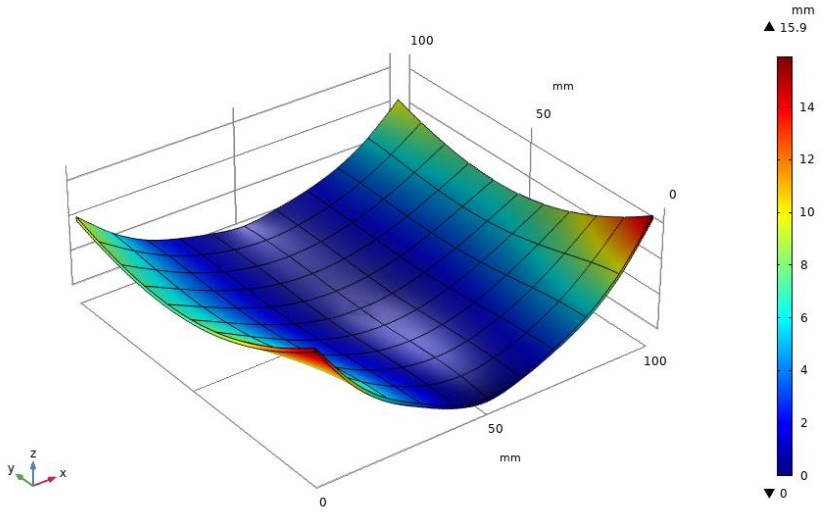

Figure 5.3.22 Current formed shape after Pass 2, 5mm beam diameter, 500W and 40mm/s speed. Maximum forming ~16mm

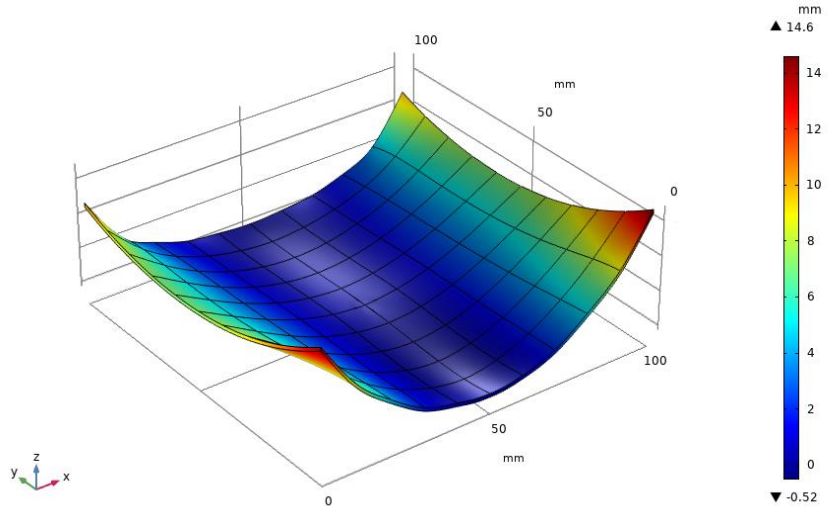

Figure 5.3.23 Error surface between the formed surface after pass 2 and the target shape, ~14.6mm maximum error

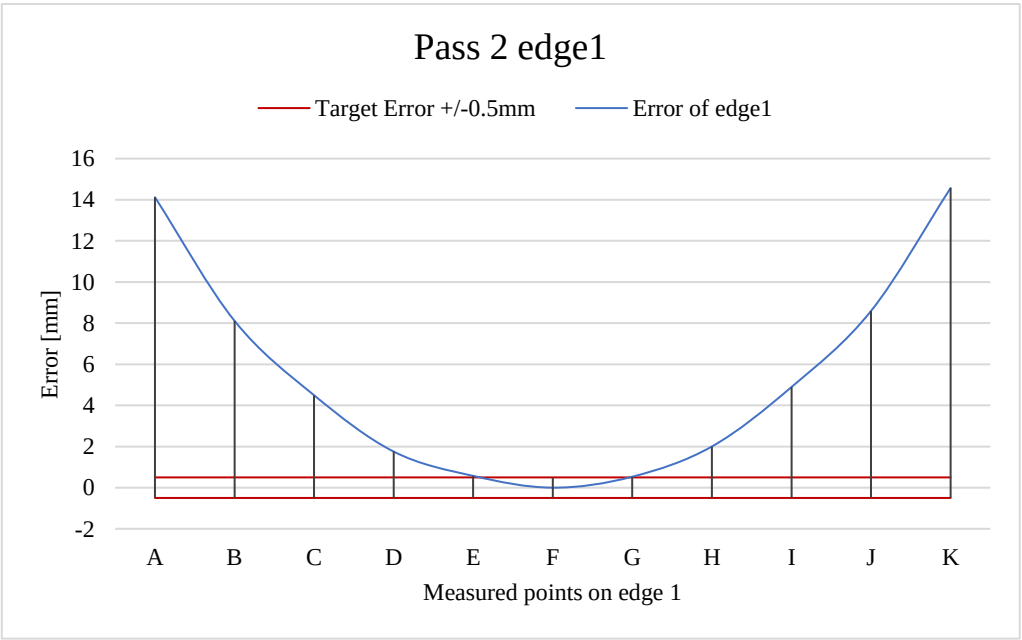

Figure 5.3.24 Comparison of the measured points on edge1 between formed surface after pass 2 and target shape. Error of the points gives a prediction for the next pass

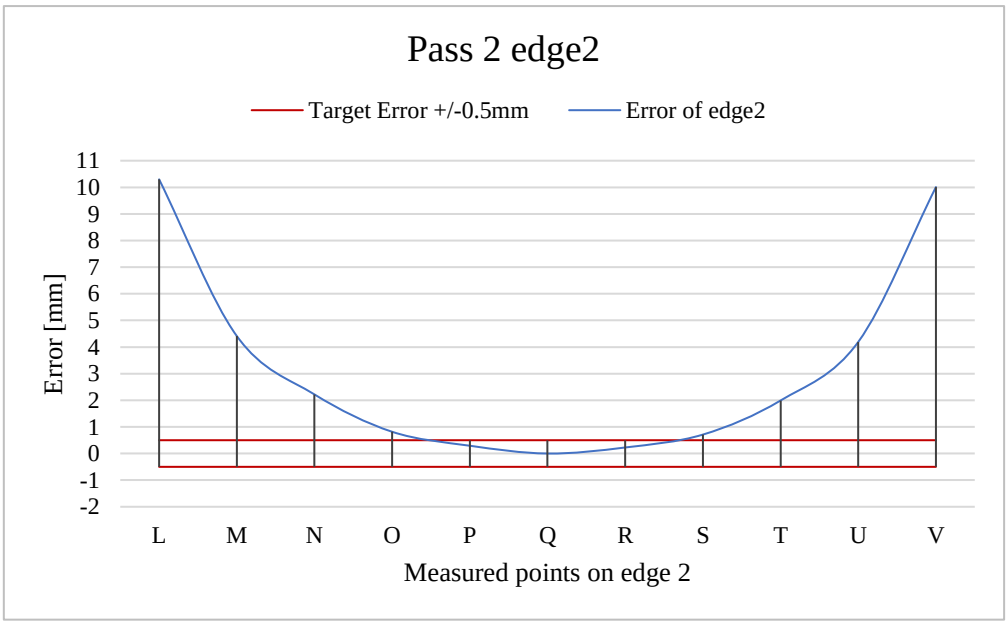

Figure 5.3.25 Comparison of the measured points on edge2 between formed surface after pass 2 and target shape. Error of the points gives a prediction for the next pass

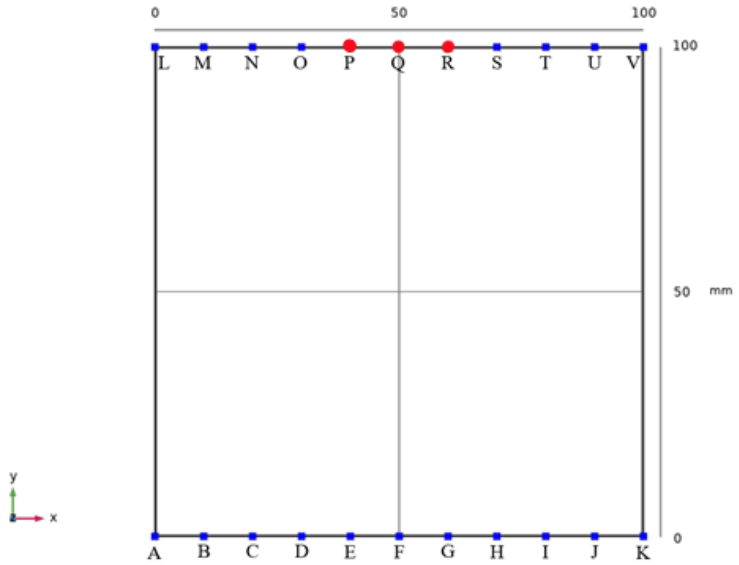

Figure 5.3.26 The error of three points on edge 2 has been reduced to within 0.5mm after pass 2 (the points in Red indicate the error is within +/-0.5mm to the target; the points in Blue indicate the error is out of +/-0.5mm to the target)

Figure 5.3.22 shows the formed shape after pass 2, it can be seen that a reasonable symmetrical ship hull shape was formed with the maximum deflection of ~16mm. The forming rate was decreased comparing with the result of pass 2 in test 1.

Figure 5.3.24 to Figure 5.3.26 show the difference of the measured points on edge1 and 2 between the current formed surface and the target shape after pass 2. It can be seen that the error at the points close to the centre on edge2 (point P & R in red colour) are reduced to within 0.5mm to the target and the remaining points are still greater than 0.5mm. In addition, the error at the points close to the centre on edge1 (point E & G) are reduced extremely close to 0.5mm and the remaining points are still greater than 0.5mm. Therefore, the scanning strategy for pass 3 was adjusted to reduce the irradiation on the central scanning lines on the workpiece as shown in Figure 5.3.27, and processing speed was kept the same as in pass 2 according to the current forming rate (~0.43 to ~6mm on edge1 and ~0.3 to 4mm on edge2).

Pass 3

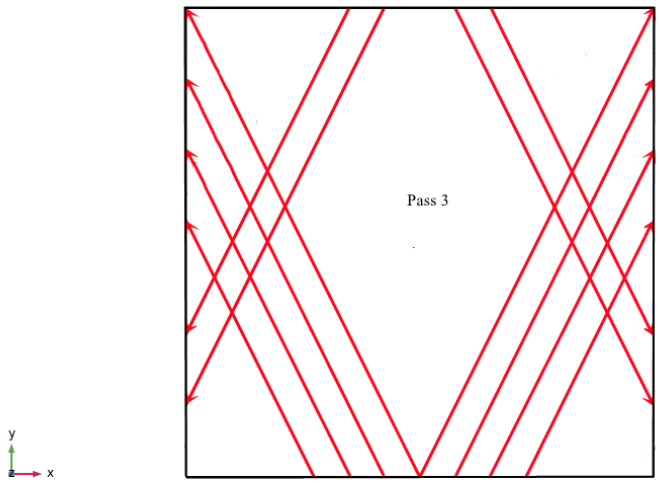

Figure 5.3.27 The third scanning strategy for pass3 in test 2

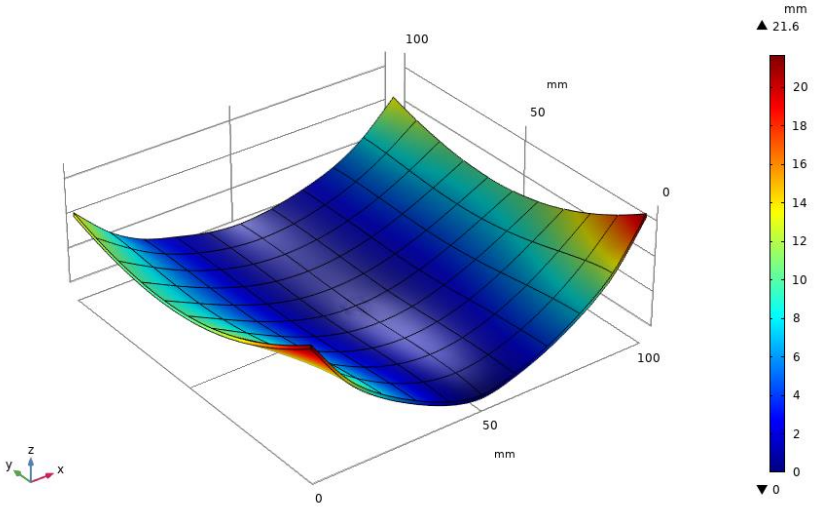

Figure 5.3.28 Current formed surface after Pass 3, 5mm beam diameter, 500W and 40mm/s speed. Maximum forming ~21.6mm

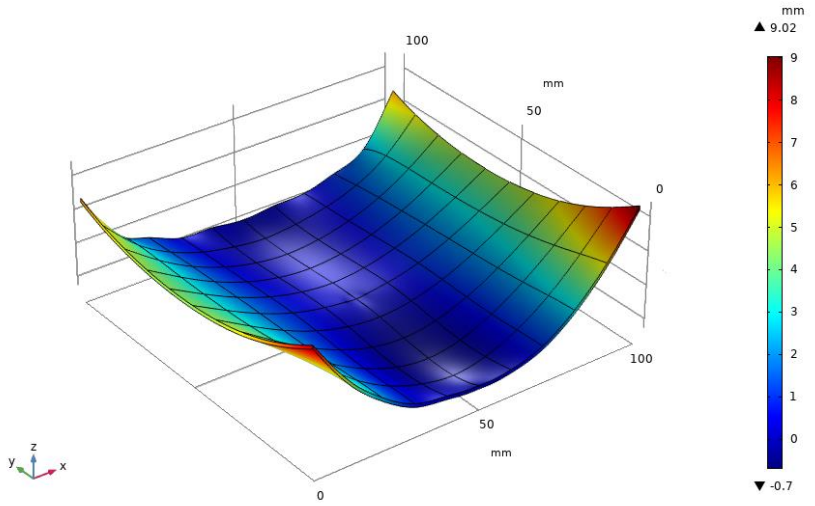

Figure 5.3.29 Error surface between the formed surface after pass 3 and the target shape, ~9.02mm maximum error

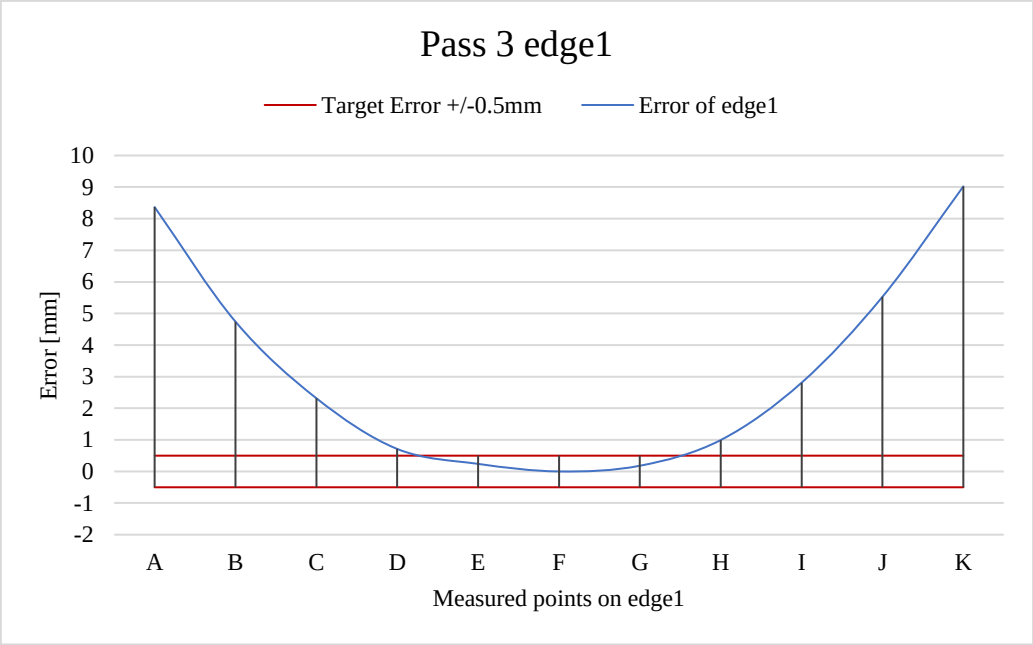

Figure 5.3.30 Comparison of the measured points on edge1 between formed surface after pass 3 and target shape. Error of the points gives a prediction for the next pass

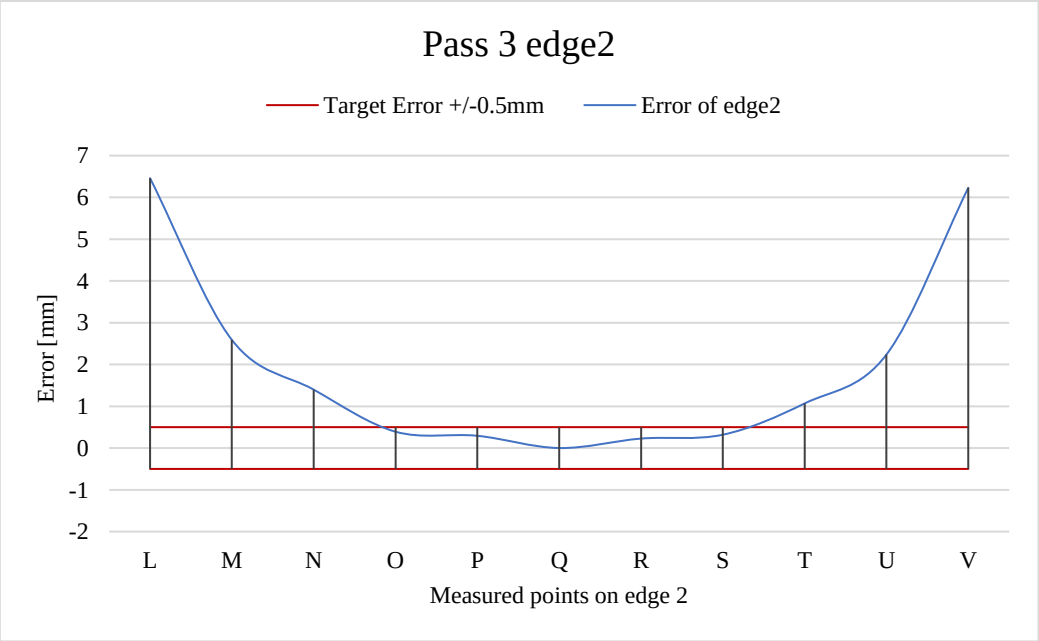

Figure 5.3.31 Comparison of the measured points on edge2 between formed surface after pass 3 and target shape. Error of the points gives a prediction for the next pass

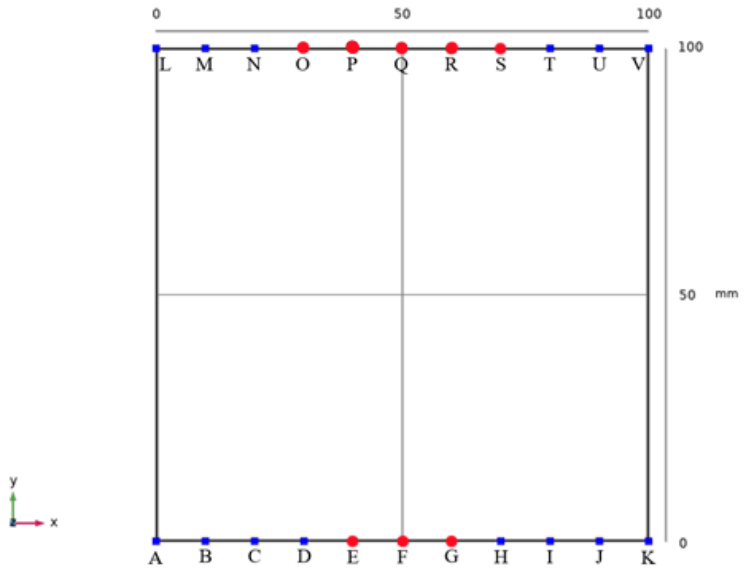

Figure 5.3.32 The error of three points on edge1 and five points on edge2 has been reduced to within 0.5mm after pass 3

After pass 3, a ship hull shape with the maximum deflection of ~21.6mm was achieved (Figure 5.3.28) and over-forming has not occurred as can be seen from the error surface between the current formed surface and the target shape (Figure 5.3.29). In addition, it can be seen from Figure 5.3.30 to Figure 5.3.32 that the error of more points closed to the centre on edge1 and 2 are reduced to within 0.5mm to the target. Therefore, the scanning strategy for the next pass (pass 4) was adjusted to further reduce the irradiation on the scanning lines close to the centre and increase the irradiation on the specific outer scanning lines and processing speed was increased to 50mm/s to further decrease the forming rate as shown in Figure 5.3.33.

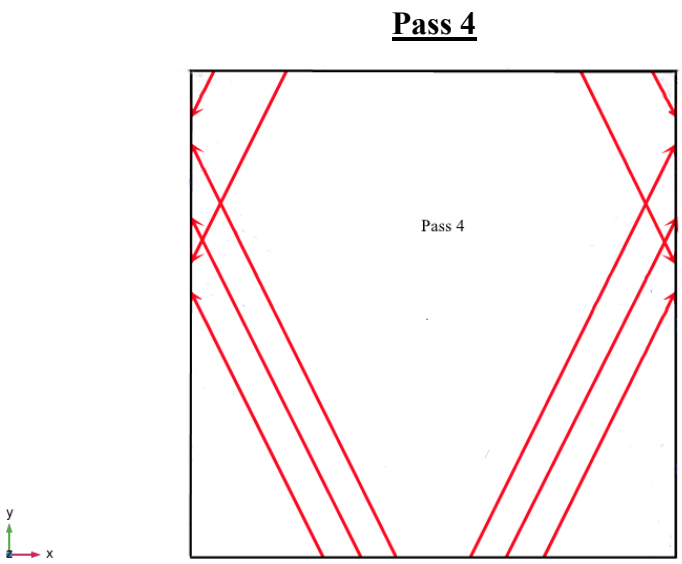

Figure 5.3.33 The fourth scanning strategy for pass4 in test 2

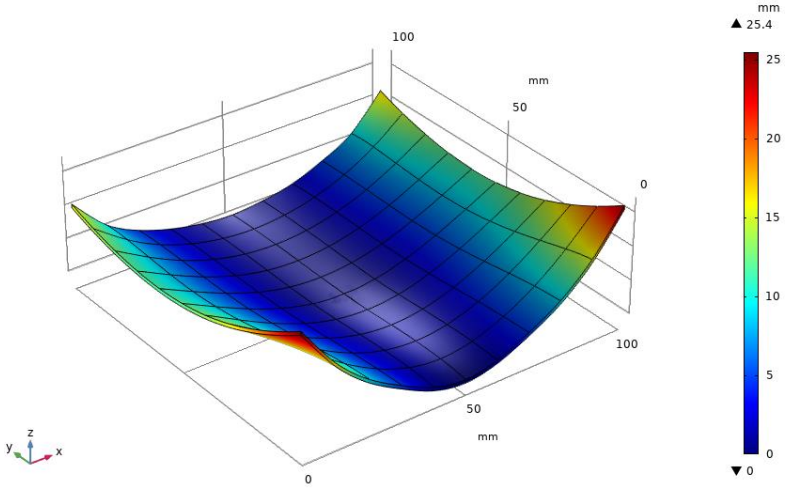

Figure 5.3.34 Current formed shape after Pass 4, 5mm beam diameter, 500W and 50mm/s speed. Maximum forming ~25.4mm

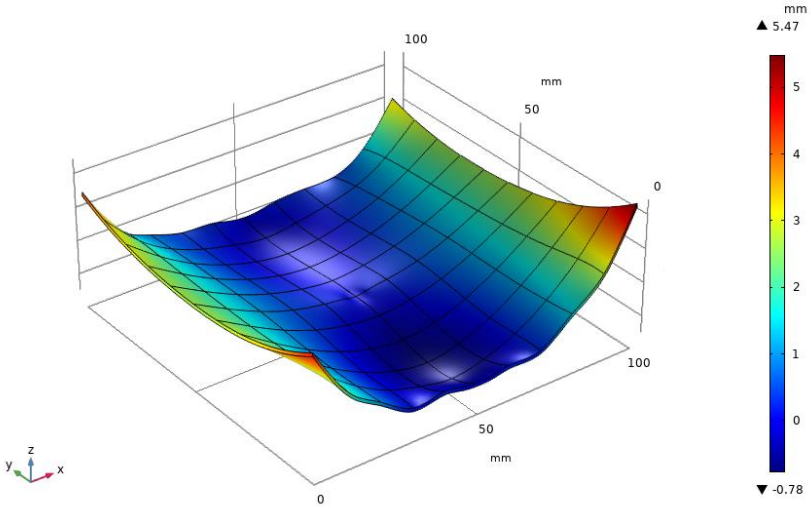

Figure 5.3.35 Error surface between the formed surface after pass 4 and the target shape, ~5.47mm maximum error

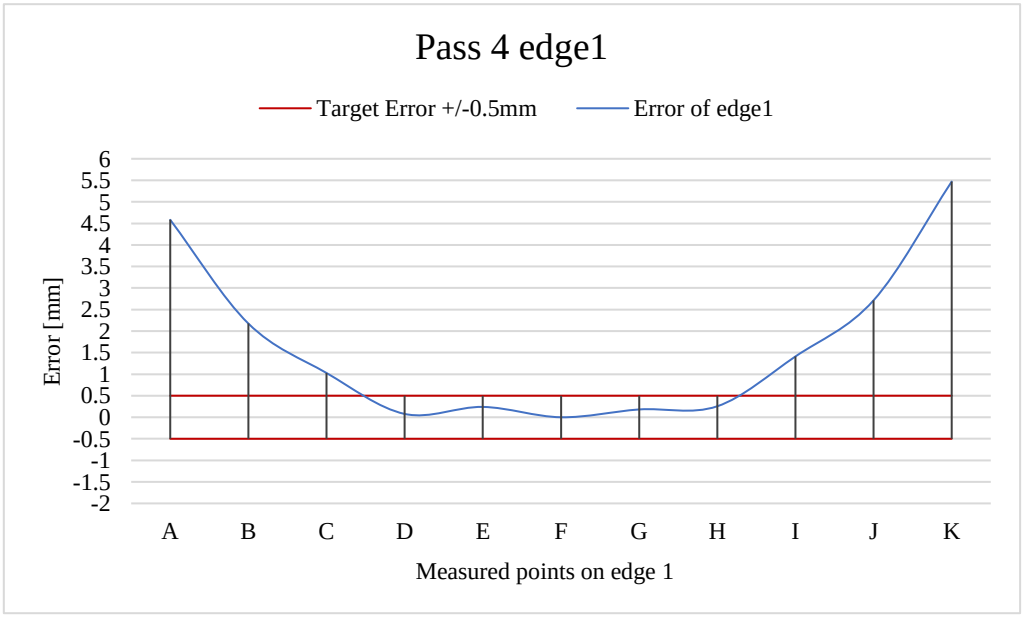

Figure 5.3.36 Comparison of the measured points on edge1 between formed surface after pass 4 and target shape. Error of the points gives a prediction for the next pass

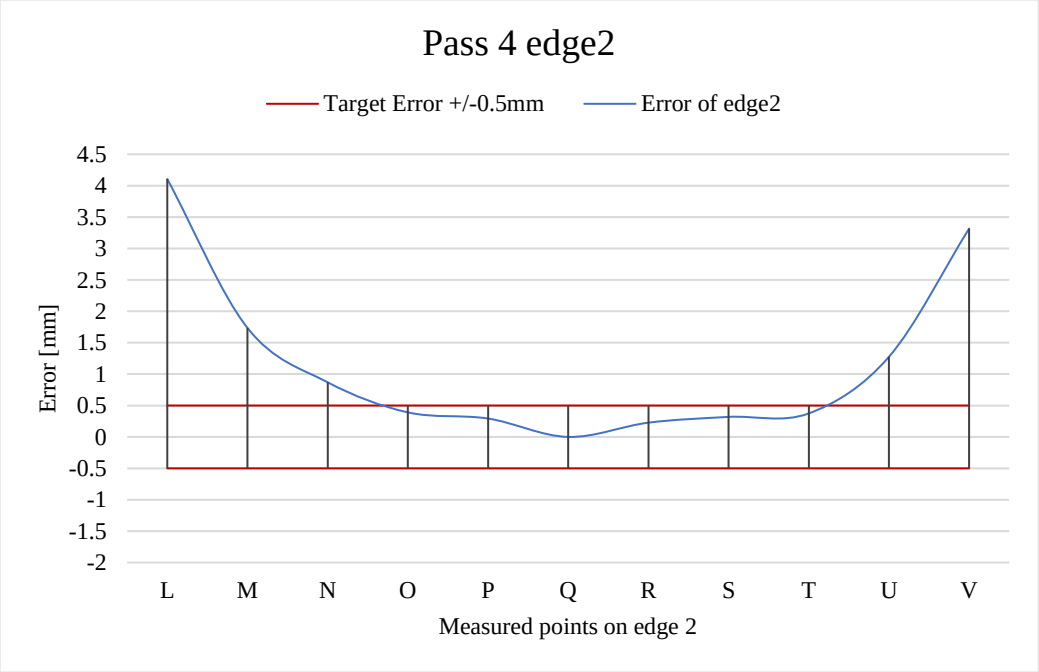

Figure 5.3.37 Comparison of the measured points on edge2 between formed surface after pass 4 and target shape. Error of the points gives a prediction for the next pass

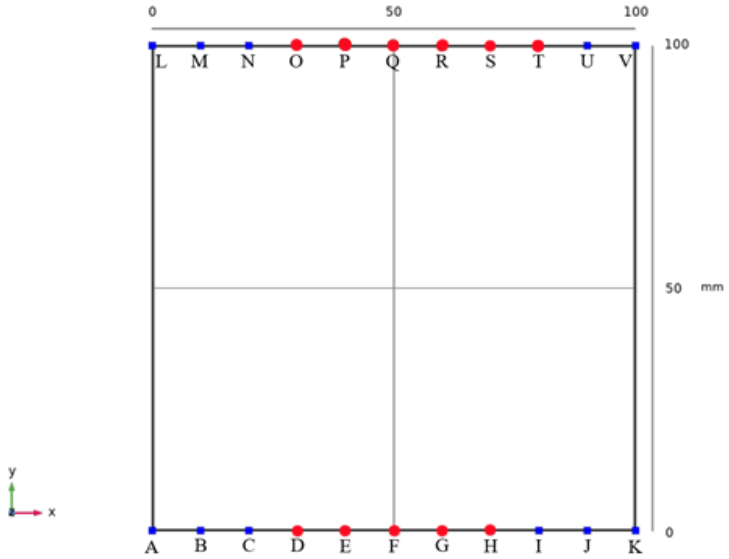

Figure 5.3.38 The error of five points on edge1 and six points on edge2 has been reduced to within 0.5mm after pass 4

As can be seen from the results after pass 4 above, the maximum amount of forming is increased to ~25.4mm (Figure 5.3.33) and the error between the current formed surface and the target shape is +5.47 and -0.78mm (Figure 5.3.34). From Figure

5.3.36 to Figure 5.3.38 it can be observed that the errors at point D & H on edge1, error at point T on edge 2 are reduced to within 0.5mm to the target, while the error at point N, which is symmetrical to point T along y-axis, exceeds 0.5mm. A usable scanning strategy for pass 5 was given based on the results of pass 4 as shown in Figure 5.3.39.

Pass 5

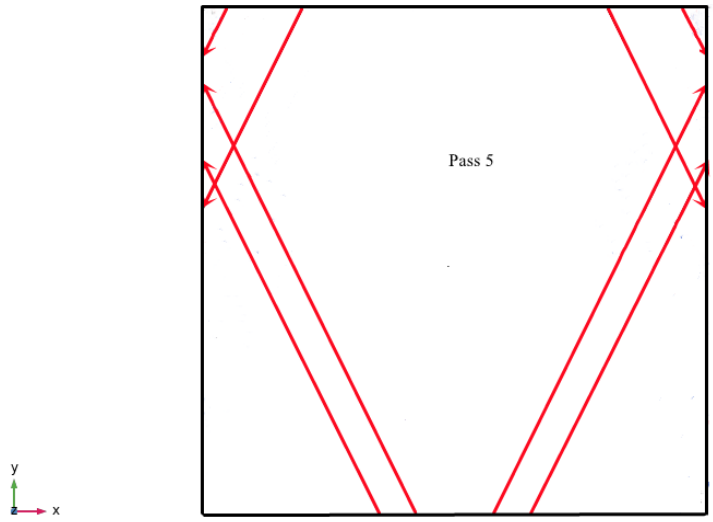

Figure 5.3.39 The fifth scanning strategy for pass5 in test 2

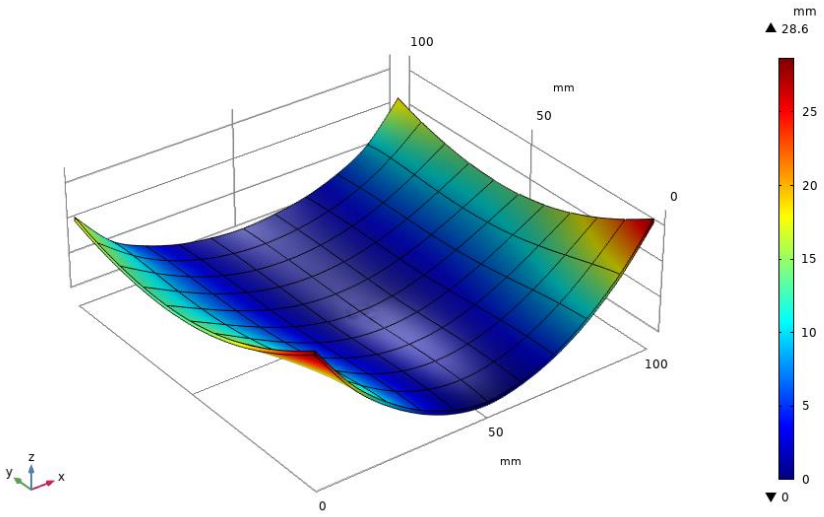

Figure 5.3.40 Current formed shape after Pass 5, 5mm beam diameter, 500W and 50mm/s speed. Maximum forming ~28.6mm

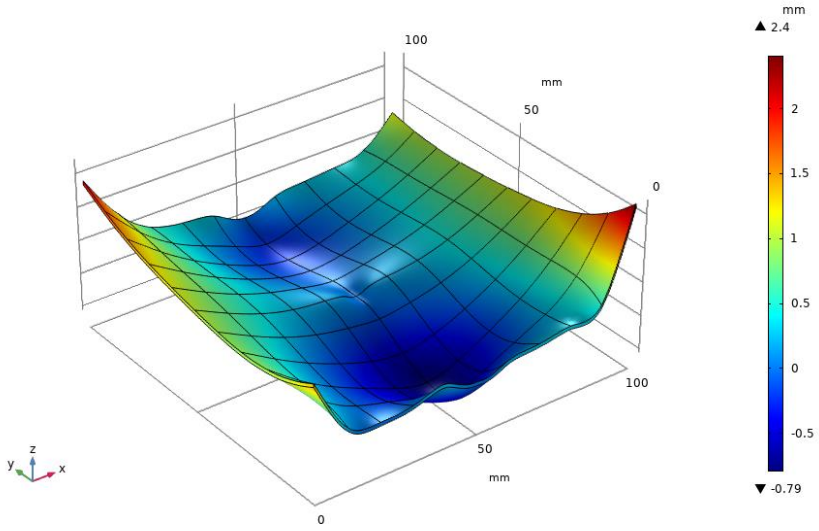

Figure 5.3.41 Error surface between the formed surface after pass 5 and the target shape, ~2.4mm maximum error

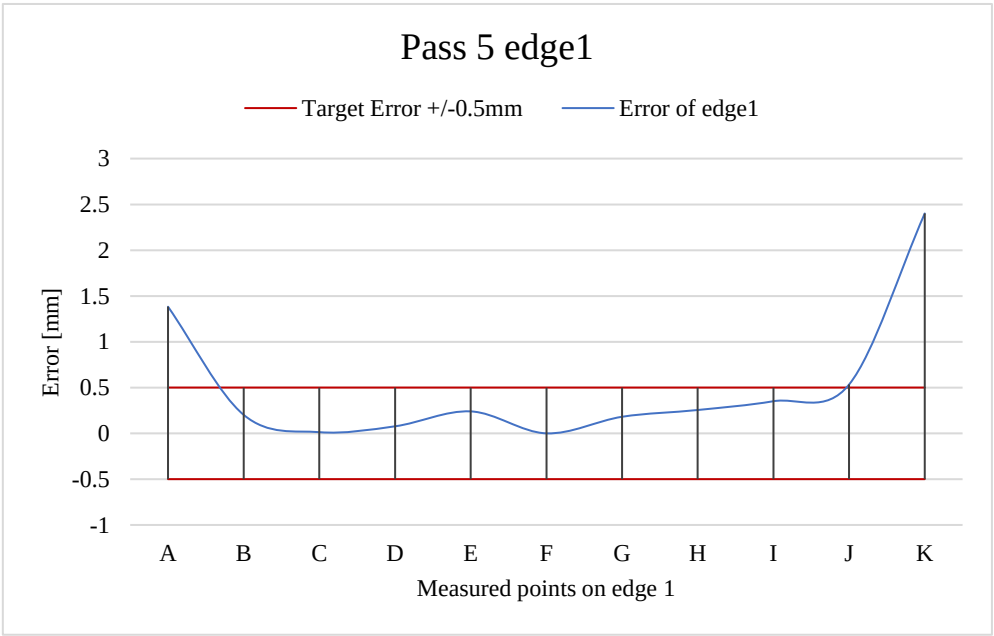

Figure 5.3.42 Comparison of the measured points on edge1 between formed surface after pass 5 and target shape. Error of the points gives a prediction for the next pass

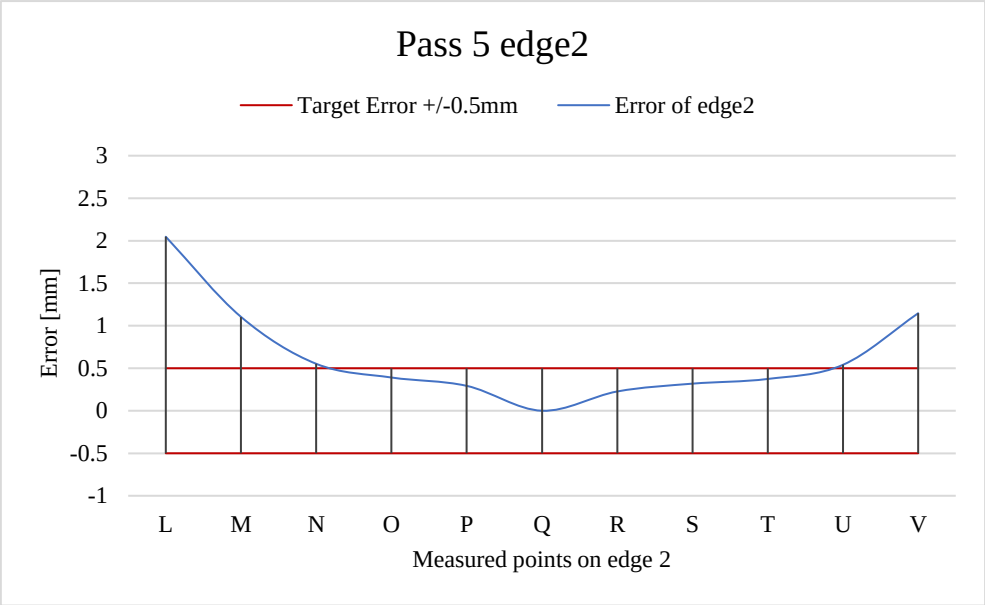

Figure 5.3.43 Comparison of the measured points on edge2 between formed surface after pass 5 and target shape. Error of the points gives a prediction for the next pass

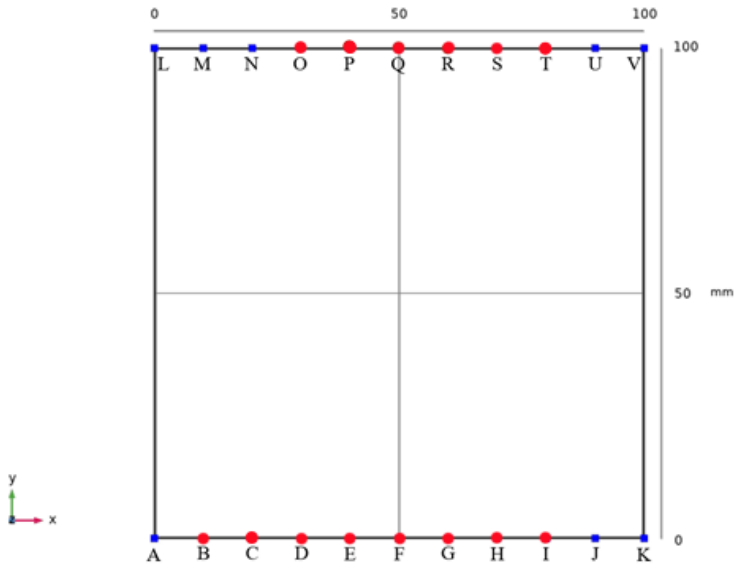

Figure 5.3.44 The error of eight points on edge1 and six points on edge2 has been reduced to within 0.5mm after pass 5

After pass 5, the error between the current formed surface and the target shape is +2.4 and -0.79mm (Figure 5.3.41). In addition, it can be seen from Figure 5.3.42 to Figure 5.3.44 that the error of most of the points on edge1 are reduced to within 0.5mm, and only the errors at the points close to the corner are still greater than 0.5mm, which

means that more forming was required in the area close to the two corners on edge1 thus the irradiation for the next pass was mainly on the outer scanning lines on edge1 and the processing speed was increased to 60mm/s as the target shape approached. The scanning strategy for pass 6 is presented in Figure 5.3.45.

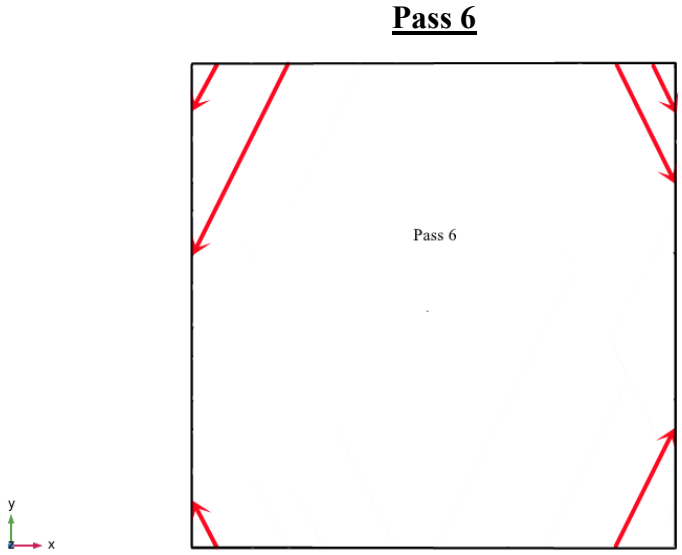

Figure 5.3.45 The sixth scanning strategy for pass6 in test 2

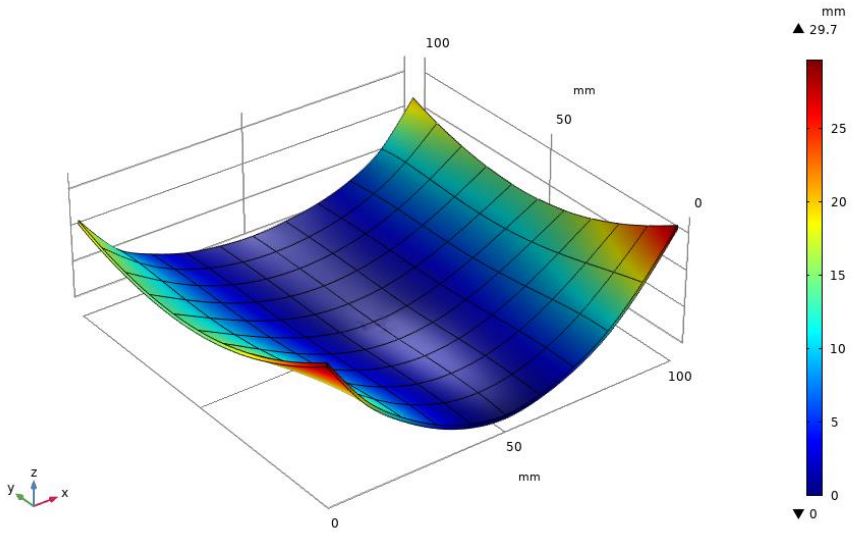

Figure 5.3.46 Current formed shape after Pass 6, 5mm beam diameter, 500W and 60mm/s speed. Maximum forming ~29.7mm

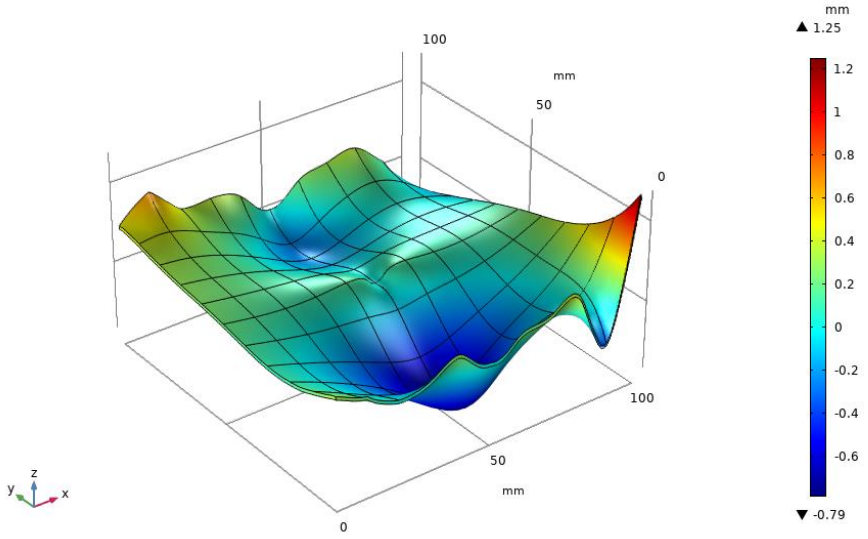

Figure 5.3.47 Error surface between the formed surface after pass 6 and the target shape, ~1.25mm maximum error

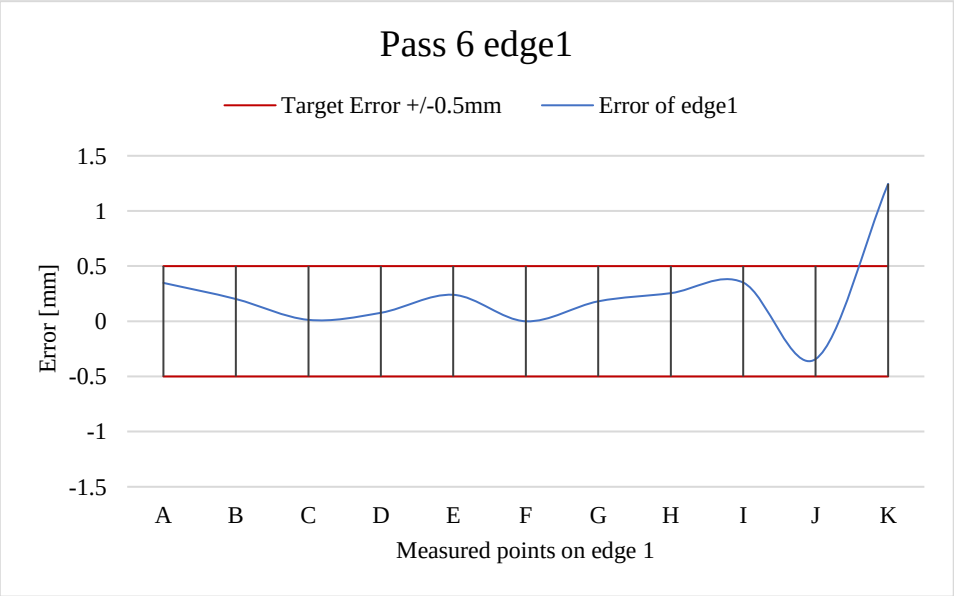

Figure 5.3.48 Comparison of the measured points on edge1 between formed surface after pass 6 and target shape. Error of the points gives a prediction for the next pass

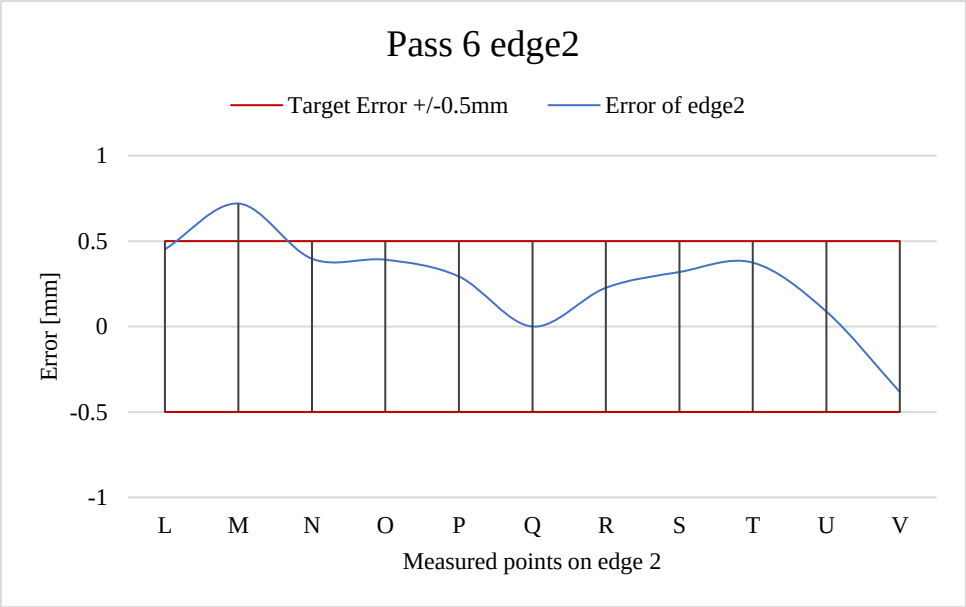

Figure 5.3.49 Comparison of the measured points on edge2 between formed surface after pass 6 and target shape. Error of the points gives a prediction for the next pass

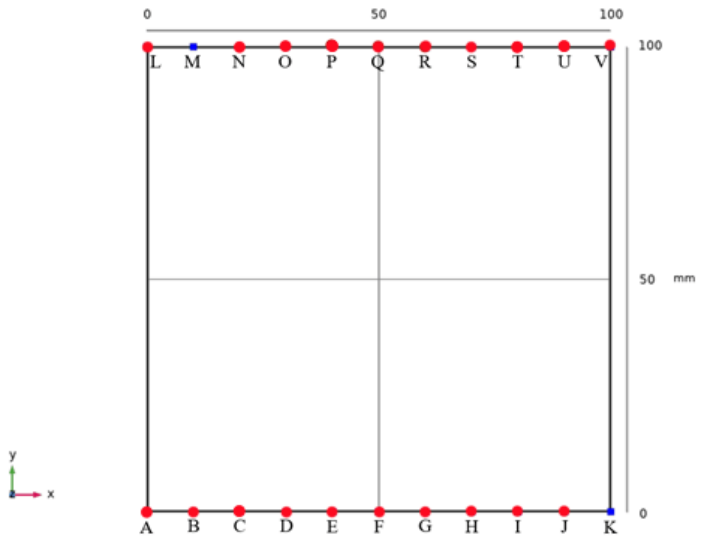

Figure 5.3.50 Only 2 points close to the corner on edge1 and 2 exceed the target after pass 6

After pass 6, it can be seen from Figure 5.3.46 that the current formed component with a maximum amount of forming ~29.7mm has been achieved, which is extremely close to the target shape. However, as can be seen from Figure 5.3.47 the error between the current formed surface and the target shape is +1.25 and -0.79mm, which means

that the local area on the plate still has the error greater than 0.5mm to the target shape especially in the area close to corner B and C (the four corners on the plate have been defined earlier as shown in Figure 3.4.1). And from Figure 5.3.48 to Figure 5.3.50 it can be observed that only two points (point K & M) on edge1 and 2 have an error greater than 0.5mm and the remaining points have been reduced to within +/-0.5mm. Therefore, the irradiation is only required on the specific locations in the next pass attempts to reduce the error in the local area to within +/-0.5mm as shown in Figure 5.3.51.

Pass 7

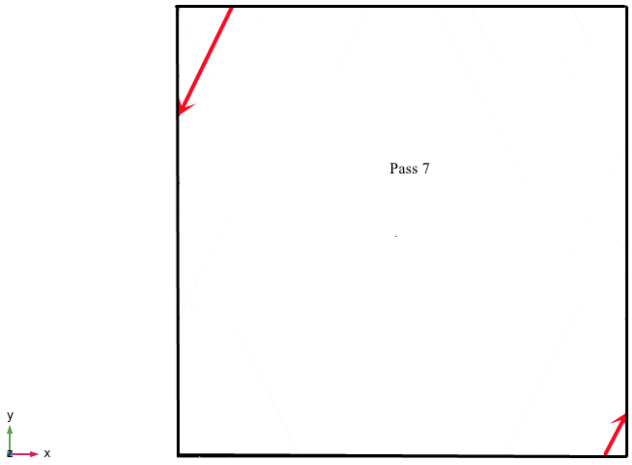

Figure 5.3.51 The final scanning strategy for final pass (pass7) in test 2

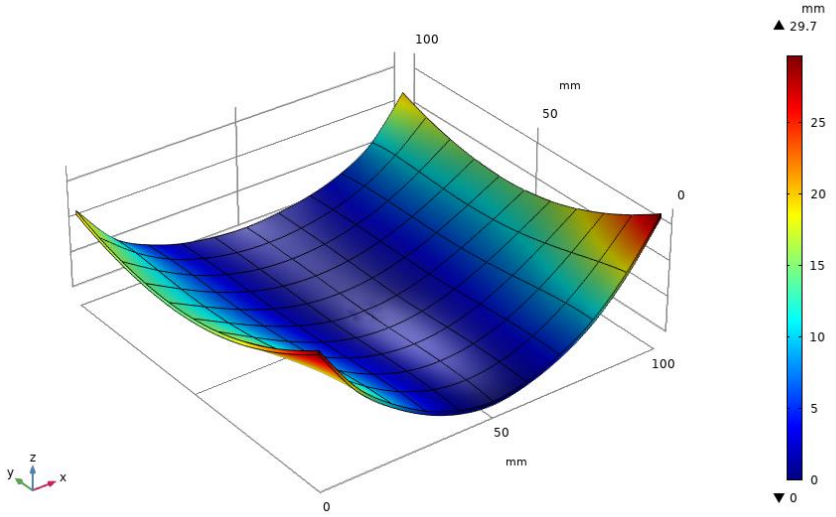

Figure 5.3.52 Current formed shape after Pass 7, 5mm beam diameter, 500W and 60mm/s speed. Maximum forming ~29.7mm

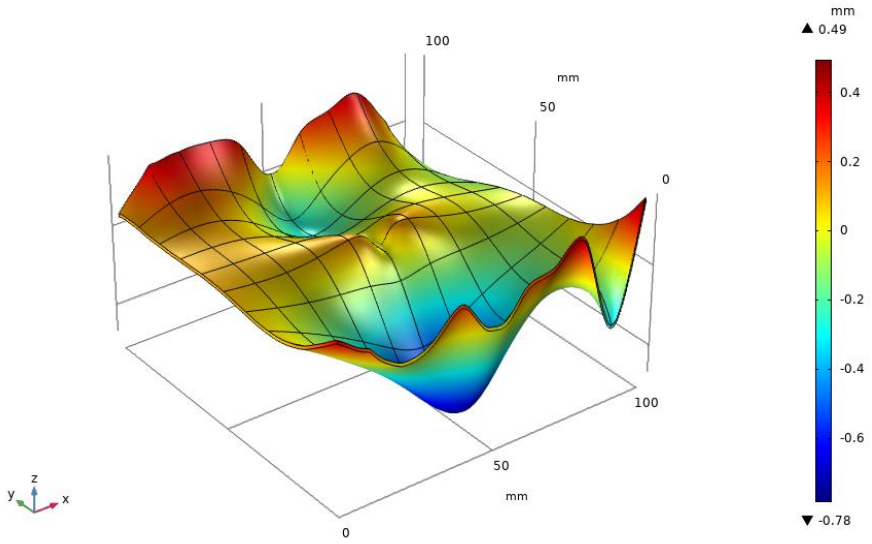

Figure 5.3.53 Error surface between the formed surface after pass 7 and the target shape, maximum error 0.49mm and -0.78mm

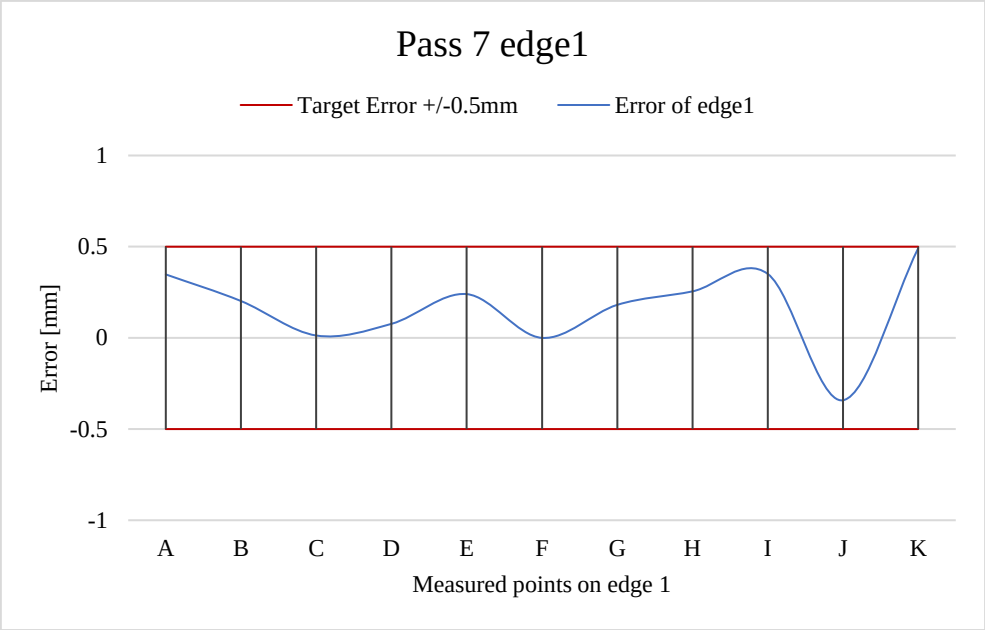

Figure 5.3.54 Comparison of the measured points on edge1 between formed surface after pass 7 and target shape

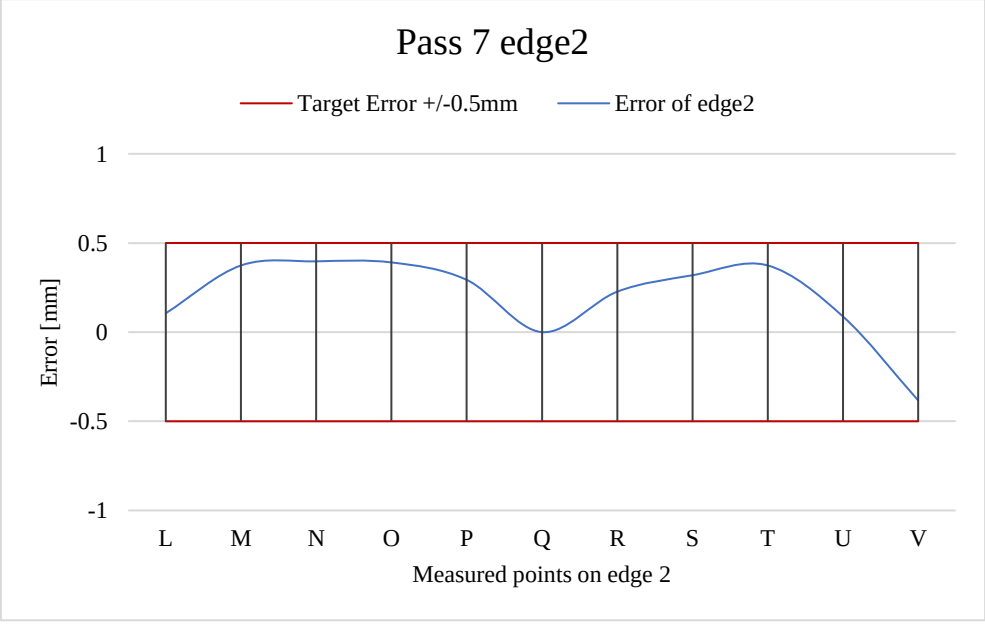

Figure 5.3.55 Comparison of the measured points on edge1 between formed surface after pass7 and target shape

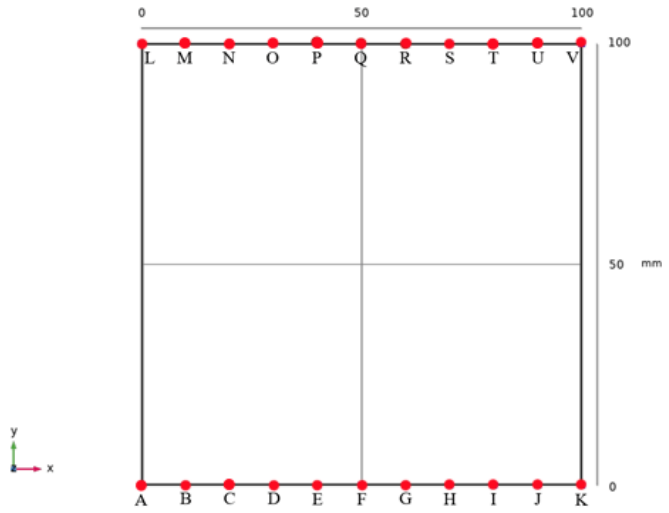

Figure 5.3.56 All points on edge1 and 2 within +/-0.5mm the target after pass7

From the results of the final pass (pass 7) above, it can be seen that the modified scanning strategy used in this test successfully produced a symmetrical ship hull shaped component with the maximum error of +0.49 and -0.78mm to the target shape (Figure 5.3.53). And the errors of the all-measured points on edge1 and 2 between the final formed surface and the target shape are reduced to within +/-0.5mm (see Figure 5.3.54 to Figure 5.3.56). Compared with the results achieved by the irradiation strategy used in test1, the accuracy has been greatly improved. In addition, as can be seen from the error plot after each pass, through irradiating from inside to outside it has been possible to reduce the traverse shrinkage around the centre, however, there is still a slight shrinkage at the front and rear part of the workpiece.

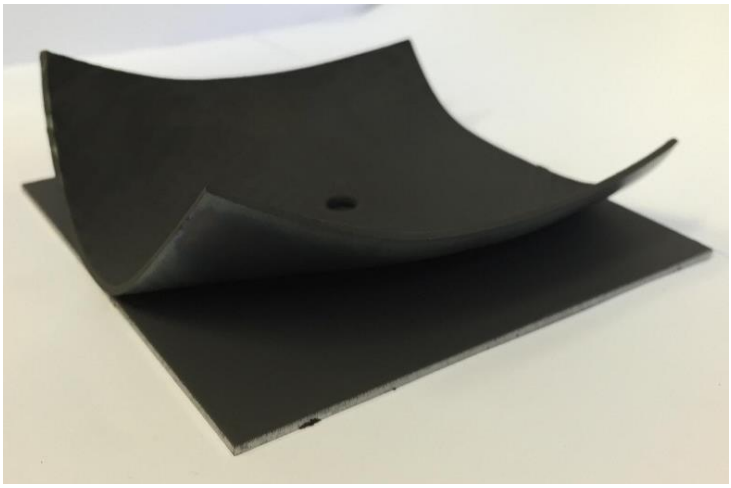

Figure 5.3.57 Final formed shape by using the modified scanning strategy in test 2

Repeatability Test

In order to determine the repeatability of this scanning strategy, another two samples were processed by using the same approach. The results are shown in Figure 5.3.58 to Figure 5.3.61. It can be seen that the maximum difference between the samples is 1.54mm, which shows better repeatability of the process comparing with the scanning strategy using in test1. In addition, according to the results of the repeatability tests in test1 and 2, it can be observed that the largest variation occurs towards the outer edges, this suggest that the larger the displacement induced by laser forming will reduce repeatability since in laser forming of a 3D shape the accuracy of the area close to the outer edges is more difficult to control than the area close to the centre.

Sample2

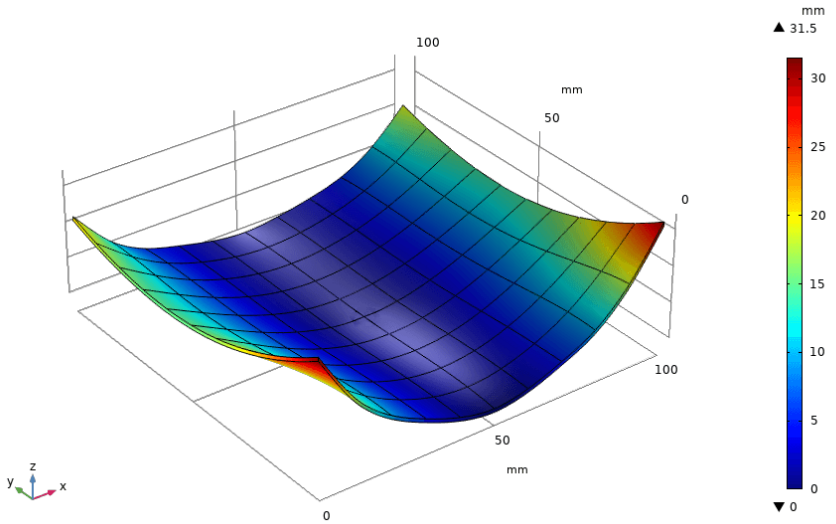

Figure 5.3.58 A repeatability test forming result of sample 2 by using the same scanning strategy, Maximum forming ~31.5mm

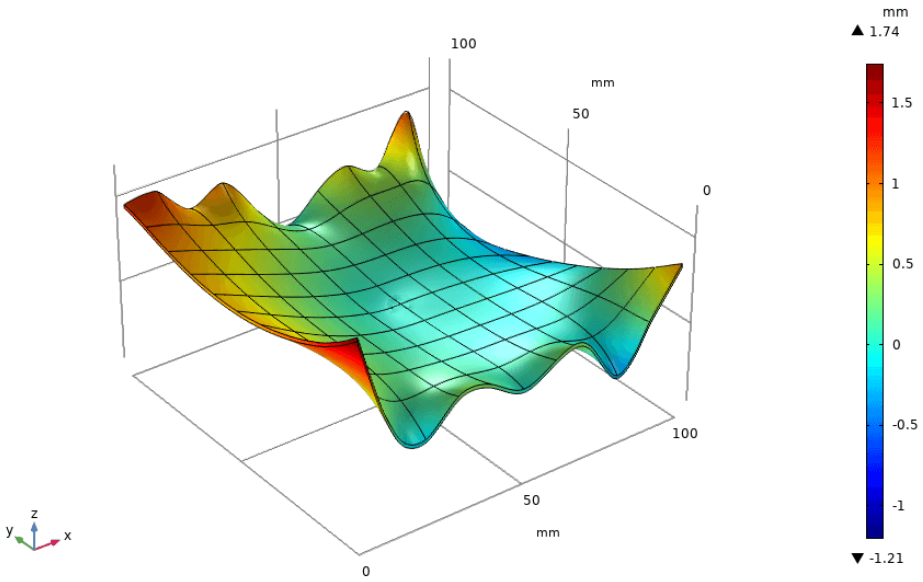

Figure 5.3.59 Comparison of the final formed shape between sample1 and sample2 by using the same scanning strategy with maximum error of ~1.74mm and -1.21

Sample3

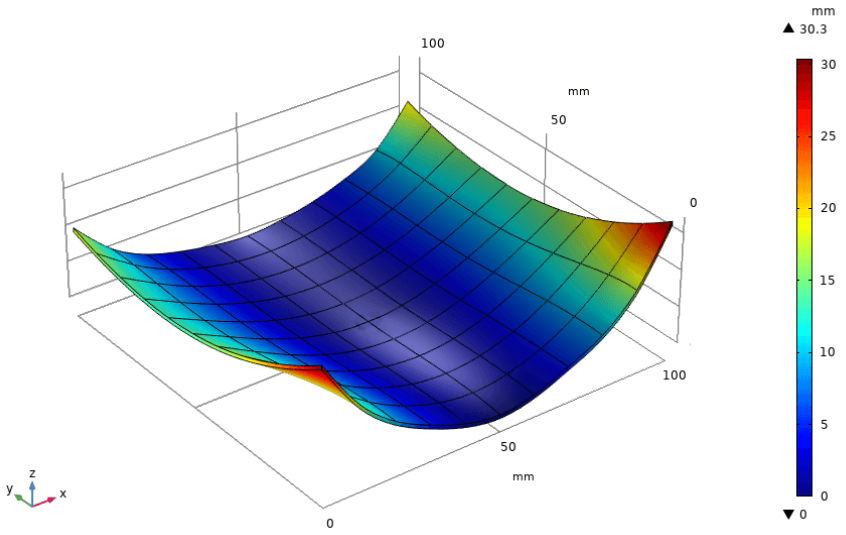

Figure 5.3.60 A repeatability test forming result of sample 3 by using the same scanning strategy, Maximum forming ~30.3mm

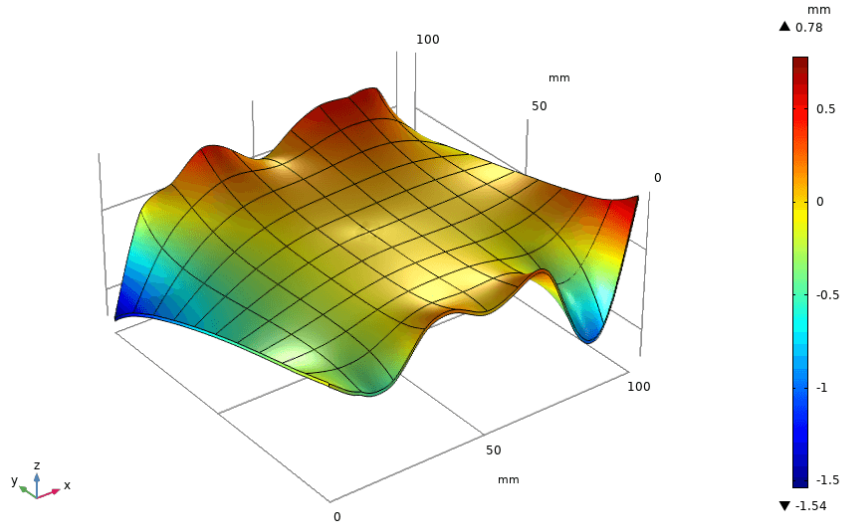

Figure 5.3.61 Comparison of the final formed shape between sample1 and sample3 by using the same scanning strategy with maximum error of ~0.78mm and -1.54

Overall, for laser forming of a given 3D shape, using scan patterns based on lines of constant height and minimal principal strain distribution has been shown possible to produce useful results. Using an iterative approach, based on the error between the current and target shape it has been possible to produce a component in increments towards the target shape without significant over-forming across the whole surface.

Providing over-forming has not occurred on the first pass it has been possible to iterate towards the final shape, by increasing the processing speed to reduce the forming rate and adjusting the scanning strategy for the deformation characteristics of the current part. It has the potential to produce a final component independent of residual stress distribution and material non-uniformity and to take account of unwanted distortion either brought about by these two factors or process variability.

A number of limitations of 3D laser forming have been identified from the process trials for the given shape. Firstly, it is possible to over form the target shape by some degree. Controlling the forming rate by varying the processing speed based on the amount of forming is possible to reduce the over-forming. Secondly, another limitation is that the accuracy across the whole surface is difficult to control due to the influence on the rest of the plate of each forming line. In addition, the forming lines at the centre of the plate will cause a deflection of the outer edges and so the amount of forming near the outer edges must be reduced to reduce any risk of over-forming in the area close to the outer edges.

An addition limitation is that during forming the focal position remain static. This means that as sections formed, especially at the side edges, the workpiece moved into

focus. This will decrease the spot size affecting the amount of forming here, increasing the intensity, and increasing the possibility of damage. Combined with an irradiation path that starts from the outside moving towards the centre the laser spot will have a consistent diameter only in the first pass and the geometry of the beam will be changed in the subsequence passes. However, it is difficult to completely solve this issue with the current laser forming system unless a height controller or an automatic focusing system is integrated in the system to keep a constant laser spot on the workpiece.

Using the modified scanning strategy is possible to reduce the risk of over-forming, such as that the scanning lines close to the centre of the plate are irradiated in the initial passes for achieving the maximum amount of forming from inside to outside, while leaving the last few passes on the outer scanning lines for the fine adjustment of forming on the outer edges. And another solution to this might be to over form to some degree on the outer edges of the plate and then turn the plate over to bend the outer edges back to the required deformation. However, it is difficult to achieve this process under current experimental conditions unless a visual positioning system is integrated in the system, since the workpiece is difficult to fix back into the original coordinate system, or a 6 degrees of freedom platform is employed. Further work is needed to verify this.

A potential and noval method of scanning strategy prediction has been developed based on analysing the difference of the deflection of a number of points on the plate. The energy distribution within the scanning strategy can be given by the processing map of the given material, which gives a potential predictive capability to a control system. However, as discussed earlier, the single pass implementation of this would be

computationally intense and cannot take into account material non-uniformity and residual stresses. The method developed here used the predictive COMSOL model to give an initial scanning strategy based on a required geometry. When the geometry is not formed within one pass, an incremental adaptive approach can then be used for subsequent passes, utilising the error between the current and target geometry (difference of the deflection of a number of points on the plate) to give a new scan strategy. Thus, any unwanted distortion due to material variability can be accounted for. The forming rate and distribution of the magnitude of forming across the surface can be controlled by the scanning speed based on the factors above and the amount of forming required so as to avoid overshoot. A strategy of per pass monitoring and controlling the process was considered.

In the future, an intelligent predictive system will be developed based on the Knowledge-Based Systems, neural networks or thermo-mechanical models and combined with an advanced, highly tuned process model / control algorithm, which will be coupled with the sensors to provide accurate controlled feedback and achieve predictability. It can provide an incremental or even real time closed loop method of accurate 3D laser forming, based on the current part characteristics independent of material variability e.g., residual stress. The study presented in this chapter does also demonstrate that laser forming could be utilised as a direct manufacturing tool in an industrial environment.

Chapter 6

Conclusion

6.1 Laser Forming of Single Curved Shape

This investigation was to develop an advanced scanning strategy to improve the controllability of the process and produce a two-dimensional component independent of material and process variability.

There are a number of conclusions from the work presented in here, these include:

- A large target bending angle can be achieved with less irradiation passes at a constant low processing speed, but the forming accuracy might be difficult to control due to the high bending angle rate. However, although the forming accuracy can be possible to be improved with a constant higher processing speed, more irradiation passes are required to achieve the target angle, which may reduce the reliability of the process.
- When forming a larger target bending angle, using an relative low speed in the initial passes, measuring the bending angle, comparing it to the target angle and make a selection of an appropriate processing speed for the next pass according to the error between the current and the target bending angle, as the target angle approaches the process speed increases to reduce the bending angle rate slowly

move towards the target angle, which can not only improve the forming accuracy but also reduce the number of irradiation passes

- The forming accuracy can be improved through control of the bending angle rate during the process via varying easily controlled the processing speed and it has the potential to produce a two-dimensional component independent of material and process variability.
- The process can be controlled with a great deal of accuracy by the introduction of more speed steps with much higher processing speeds as the target angle approaches. In addition, the accuracy of the measurement system used for feedback control also influences the accuracy of the forming process since the higher the accuracy of the measurement system and measuring method, the more accurate measuring results of the bending produced in the workpiece.
- The study does demonstrate the potential manufacturing capabilities of the laser forming process for producing the single curved component, which provides the capability to produce or alter the shape of the component easily only through changing the process parameters or the scanning strategy without the need of expensive and inflexible hard tooling, this is a major advantage of the process over conventional forming technologies. The automobile components with three different bending angles have been produced reasonably accurately.

6.2 Laser Forming of Double Curved Shape

The purpose of the investigation was to produce the target 3D shape independent of residual stress distribution and non-uniformity absorption of the laser radiation and to take account of any unwanted distortion either caused by above two factors or process variability and reduce the error to within a small degree to the target shape.

There are a number of conclusions from the work presented in here, these include:

- For a smaller path spacing, the displacement at the free end of the plate is greater than that of a larger path spacing. A possible reason for this may be that for the smaller spacing between the scanning lines the more heat is retained in the plate as can be seen, which will result in reducing the yield stress of the material, in that a hot plate is easier to form than a cold one.
- When the path spacing is less than the spot diameter, the strain fields between the heating paths interfere with each other because the minimal principal strain near the second heating line already exists before the second heating, but the continuous plastic strain can be obtained. The influence zone of the strain fields between the heating lines decreases with increasing of the scanning line spacing, which means that the interaction between the adjacent heating paths can be possible to be avoid with increasing of the scanning line spacing and the deformation of the plate can be considered as a superposition of a single scan, but it leads to the strain fields being discontinuous. However, to raise the forming accuracy of the plate, a continuous strain field is needed.

- For laser forming of a given 3D shape, using scan patterns based on lines of constant height and minimal principal strain distribution has been shown possible to produce useful results. However, the scanning pattern does not need to be completely consistent with the lines of constant height of the given shape, only the irradiated area of the scanning pattern corresponds to the deformed area indicated by the contours line of the given shape.
- Providing over-forming has not occurred on the first pass it has been possible to iterate towards the final shape, by increasing the processing speed to reduce the forming rate and adjusting the scanning strategy for the deformation characteristics of the current part, such as analysing the error of the deflection of the points at the edges. It has the potential to produce a accurate final component independent of residual stress distribution and material non-uniformity and to take account of unwanted distortion either brought about by these two factors or process variability.
- A number of limitations of 3D laser forming have been identified from the process trials for the given shape. Firstly, it is possible to over form the target shape by some degree. Controlling the forming rate by varying the processing speed based on the amount of forming is possible to reduce the over-forming.
- Secondly, another limitation is that the accuracy across the whole surface is difficult to control due to the influence on the rest of the plate of each forming line. In addition, the forming lines at the centre of the plate will cause a deflection of the outer edges and so the amount of forming near the outer edges must be reduced to reduce any risk of over-forming in the area close to the outer edges.

- An additional limitation is that during forming the focal position remain static. This means that as sections formed, especially at the side edges, the workpiece moved into focus. This will decrease the spot size affecting the amount of forming here, increasing the intensity, and increasing the possibility of damage. Combined with an irradiation path that starts from the outside moving towards the centre the laser spot will have a consistent diameter only in the first pass and the geometry of the beam will be changed in the subsequence passes. However, it is difficult to completely solve this issue with the current laser forming system unless a height controller or an automatic focusing system is integrated in the system to keep an constant laser spot on the workpiece.
- Using the modified scanning strategy is possible to reduce the risk of over-forming, such as that the scanning lines close to the centre of the plate will be irradiated in the initial passes for achieving the maximum amount of forming from inside to outside, while leaving the last few passes on the outer scanning lines for the fine adjustment of forming on the outer edges.
- The study demonstrates the potential of the laser forming process to produce accurate repeatable 3D surfaces in a controlled way. This suggests that laser forming could be utilised as a direct manufacturing tool in an industrial environment. Providing the desired and the current surfaces can be realized in a virtual way, a scan strategy can be predicted to give the final shape.

6.3 Further Work

A number of recommendations for further research have arisen from this work and these are:

- Investigate the use of laser wavelengths that require no absorptive coatings The variability of absorptive coatings used in the work in this thesis demonstrates that they should not be used if possible. In addition, the application and removal of the coatings constitutes additional process steps in an industrial process and an environmental hazard, by not using them an improvement in efficiency can be achieved. Research is recommended into the use of shorter laser wavelengths that do not require absorptive coatings in order to improve the industrial viability of the process.
- Use of dual optical path system or scan optics to remove the asymmetric nature of the process – As a follow on from the previous recommendation the use of dual optical path has the potential to realise parallel processing in a rapid segmented fashion, offering the ability to evenly distribute the incident energy rather than a single optical. This has great potential for 3D laser forming process, particularly for large area forming were the temporal effects of using a single point source are magnified.
- A 6 degrees of freedom platform is needed to be employed in the laser forming process to ensure the incident laser beam is always perpendicular to the irradiated region or using of fiber delivery laser with robot to further improve the flexibility of the laser forming process.

- A height controller or an automatic focusing system should be integrated in the system to keep a constant laser spot on the workpiece during the process.
- Intelligent predictive systems, perhaps based on Knowledge-Based Systems (KBS), neural networks or thermo-mechanical models can achieve predictability through a knowledge of the material (including its stress history) combined with a developed, highly tuned process model / control algorithm. In an adaptive system the use of sensors to provide accurate controlled feedback coupled with the development of intelligent control software e.g., neural network, provides an incremental or even real time closed loop method of accurate 3D laser forming, based on the current part characteristics independent of material variability e.g., residual stress.
- Further investigation is required to determine the effects of post forming of heat treatment on 3D laser formed components and therefore the amount of residual stress that occurs in a laser formed part. Further investigation is also needed in the study of the effect clamping arrangement has on creating residual stresses

References

[1] J. Magee, K. G. Watkins and W. M. Steen, "Advances in Laser Forming," *Journal of Laser Applications,* pp. 235-246, 1998.

[2] F. C. Campbell, Elements of metallurgy and engineering alloys, Materials Park, Ohio: ASM International, 2008.

[3] M. Geiger, "Synergy of Laser Material Processing and Metal Forming," *CIRP Annals,* vol. 43, no. 2, pp. 563-570, 1994.

[4] M. Geiger and F. Vollertsen, "The Mechanisms of Laser Forming," *CIRP Annals,* vol. 42, no. 1, pp. 301-304, 1993.

[5] F. Vollertsen, "Forming, Sintering and Rapid Prototyping," in *Handbook of the Eurolaser Academy*, New York, Springer, 1998, pp. 357-453.

[6] J. Lawrence, M. Schmidt and L. Li, "The forming of mild steel plates with a 2.5 kW high power diode laser," *International Journal of Machine Tools and Manufacture,* vol. 41, no. 7, pp. 967-977, 2001.

[7] J. D. Majumdar, A. K. Nath and I. Manna, "Studies on laser bending of stainless steel," *Materials Science and Engineering: A,* vol. 385, no. 1-2, pp. 113-122, 2004.

[8] W. Maher, K. Tong, C. Bampton, M. Bright and J. Woote, "Laser forming of titanium and other metals is useable within metallurgical constraints," in *Proceedings of ICALEO'1998*, Florida, 1998.

[9] J. Shackel, J. Sidhu and P. B. Prangnell, "The metallurgical implications of laser forming Ti-6Al-4V sheet," in *Proceedings of ICALEO'2001*, Florida, 2001.

[10] J. Magee, K. G. Watkins and W. M. Steen, "Laser Bending of High Strength," *Journal of Laser Applications,* vol. 10, no. 4, pp. 149-155, 1998.

[11] J. Magee, K. G. Watkins, W. M. Steen, R. L. Cooke and J. Sidhu, "Development of an Integrated Laser Forming Demonstrator System for the Aerospace Industry," in *Proceedings of ICALEO'98*, Orlando, 1998.

[12] S. P. Edwardson, K. G. Watkins, G. Dearden and J. Magee, "Generation of 3D Shapes Using a Laser Forming Technique," in *Proceedings of ICALEO'2001*, Jacksonville, 2001.

[13] J. Magee, S. P. Edwardson, P. French, G. Dearden and K. G. Watkins, "Laser Forming of Aerospace Alloys," in *Society of Automotive Engineers*, Seattle, 2001.

[14] N. B. Dahotre and S. P. Harimkar, Laser Fabrication and Machining of Materials, New York: Springer, 2008.

[15] S. P. Edwardson, "A Study into the 2D and 3D Laser Forming of Metallic," University of Liverpool, Liverpool, 2004.

[16] W. M. Steen, Laser Material Processing, New York: Springer, 2010.

[17] C. Vásquez-Ojeda and J. Ramos-Grez, "Bending of stainless steel thin sheets by a raster scanned low power CO2 laser," *Journal of Materials Processing Tech,* vol. 209, no. 5, pp. 2641-2647, 2009.

[18] F. Vollertsen and Sakkiettibutra, "Different types to use laser as a forming tool," *Physics Procedia,* p. 193–203, 2010.

[19] J. M. Dutta and I. Manna, "Laser material processing," *International materials reviews,* vol. 56, no. 5-6, pp. 341-388, 2011.

[20] K. Alexander, "Laser Assisted Forming Techniques," in *XVI International Symposium on Gas Flow, Chemical Lasers, and High-Power Lasers*, Gmunden, 2007.

[21] M. Safari and J. Joudaki, "Recent Advances in the Laser Forming Process: A Review," *Metals,* vol. 10, no. 11, pp. 1472-1491, 2020.

[22] T. Pretorius, "Laser Forming," in *The Theory of Laser Materials Processing*, Springer, 2009, p. 281–314.

[23] Y. j. Shi, Z. q. Yao, H. Shen and J. Hu, "Research on the mechanisms of laser forming for the metal plate," *International Journal of Machine Tools and Manufacture,* vol. 46, no. 12-13, pp. 1689-1697, 2006.

[24] F. Vollertsen and M. Rodle, "Model for the temperature gradient mechanism of laser bending," in *Proceedings of the LANE'94*, 1994.

[25] M. Merklein, T. Hennige and M. Geiger, "Laser forming of aluminium and aluminium alloys-microstructural investigation," *Journal of Materials Processing Tech,* vol. 115, no. 1, pp. 159-165, 2001.

[26] Z. Hu, R. Kovacevic and M. Labudovic, "Experimental and numerical modeling of buckling instability of laser sheet forming," *International Journal of Machine Tools & Manufacture,* vol. 42, no. 13, pp. 1427-1439, 2002.

[27] R. Kant and S. N. Joshi, "Numerical simulation of laser bending of magnesium alloy AZ31B using FEM," in *Proceeding of the International Conference IDDRG 2012*, 2012.

[28] W. Li and Y. L. Yao, "Numerical and Experimental Investigation of Convex Laser Forming Process," *Journal of Manufacturing Processes,* vol. 3, no. 2, pp. 73-81, 2001.

[29] A. N. Thomsen, "Laser Forming of Sheet metal," Alborg University, Alborg, 2020.

[30] X. y. Wang, X. p. Ma, Z. h. Li and R. Wang, "A Study of Thickening Phenomenon in Laser Bending Zone of a Metal Laminated Plate," *Procedia CIRP,* pp. 454-459, 2016.

[31] W. Li and Y. L. Yao, "Laser bending of tubes: mechanism, analysis and prediction," *Journal of Manufacturing Science and Engineering,* vol. 123, no. 4, p. 674–681, 2001.

[32] F. Vollertsen, I. Komel and R. Kals, "The laser bending of steel foils for microparts by the buckling mechanism-a model," *Modelling and Simulation in Materials Science and Engineering,* pp. 107-119, 1995.

[33] G. Dearden and S. P. Edwardson, "Some recent developments in two-and three-dimensional laser forming for 'macro' and 'micro' applications," *Journal of Optics A: Pure and Applied Optics,* vol. 5, no. 4, pp. 8-15, 2003.

[34] S. P. Edwardson, K. G. Watkins, G. Dearden and J. Magee, "3D Laser Forming of Saddle Shapes," in *LANE*, Erlangen, 2001.

[35] T. Hennige, S. Holzer, F. Vollertsen and M. Geiger, "On the working accuracy of laser bending," *Journal of Materials Processing Technology,* vol. 71, no. 3, pp. 422-432, 1997.

[36] Y. Shi, H. Shen, Z. Yao, J. Hu and L. Xia, "Application of similarity theory in the laser forming process," *Computational Materials Science,* vol. 37, no. 3, p. 323–327, 2006.

[37] M. S. Jamil, M. A. Sheikh and L. Li, "A study of the effect of laser beam geometries on laser bending of sheet metal by buckling mechanism," *Optics & Laser Technology,* vol. 43, no. 1, pp. 183-193, 2011.

[38] S. S. Chakraborty, H. More and A. K. Nath, "Laser forming of a bowl shaped surface with a stationary laser beam," *Optics and Lasers in Engineering,* vol. 77, pp. 126-136, 2016.

[39] H. Shen, "Mechanism of laser micro-adjustment," *Journal of Physics D: Applied Physics,* vol. 41, no. 24, pp. 1-19, 2008.

[40] Y. j. Shi, Y. c. Liu, P. Yi and J. Hu, "Effect of different heating methods on deformation of metal plate under upsetting mechanism in laser forming," *Optics & Laser Technology,* vol. 44, no. 2, pp. 486-491, 2012.

[41] R. Karwa, Heat and Mass Transfer, Singapore: Springer, 2020.

[42] S. S. Chakraborty, H. More, V. Racherla and A. K. Nath, "Modification of bent angle of mechanically formed stainless steel sheets by laser forming," *Journal of Materials Processing Technology,* vol. 222, pp. 128-141, 2015.

[43] R. Kant, S. N. Joshi and U. S. Dixit, "Research issues in the laser sheet bending process," in *Materials Forming and Machining*, Elsevier, 2016, p. 73–97.

[44] G. f. Chen and X. f. Xu, "Experimental and 3D Finite Element Studies of CW Laser Forming of Thin Stainless Steel Sheets," *Journal of Manufacturing Science and Engineering,* vol. 123, no. 1, pp. 66-73, 2001.

[45] S. c. Wu and J. s. Zheng, "An experimental study of laser bending for sheet metals," *Journal of Materials Processing Technology,* vol. 110, no. 2, pp. 160-163, 2001.

[46] H. S. Hsieh and J. Lin, "Thermal-mechanical analysis on the transient deformation," *International Journal of Machine Tools & Manufacture,* vol. 44, no. 2-3, pp. 191-199, 2004.

[47] R. Kant and S. N. Joshi, "Finite element simulation of laser assisted bending with moving mechanical load," *International Journal of Mechatronics & Manufacturing,* vol. 6, no. 4, pp. 351-366, 2013.

[48] V. Paunoiu, E. A. Squeo, F. Quadrini, C. Gheorghies and D. Nicoara, "Laser Bending of Stainless Steel Sheet Metals," *International Journal of Material Forming,* vol. 1, no. 1, pp. 1371-1374, 2008.

[49] Z. Ji and S. c. Wu, "FEM simulation of the temperature field during the laser forming of sheet metal," *Journal of Materials Processing Technology,* vol. 74, no. 1-3, pp. 89-95, 1998.

[50] A. K. Kyrsanidi, T. B. Kermanidis and S. G. Pantelakis, "Numerical and experimental investigation of the laser forming process," *Journal of Materials Processing Technology,* vol. 87, no. 1-3, pp. 281-290, 1999.

[51] W. Li and Y. L. Yao, "Numerical and experimental study of strain rate effects in laser forming," *Journal of Manufacturing Science and Engineering,* vol. 122, no. 3, p. 445–451, 2000.

[52] M. Barletta, L. Casamichele and V. Tagliaferri, "Line bending of Al2O3 coated and uncoated aluminium thin sheets," *Surface & Coatings Technology,* vol. 201, no. 3-4, pp. 660-673, 2006.

[53] S. Safdar, L. Li, M. A. Sheikh and Z. Liu, "The Effect of Nonconventional Laser Beam Geometries on Stress Distribution and Distortions in Laser Bending of Tubes," *Journal of Manufacturing Science and Engineering,* vol. 129, no. 3, pp. 592-600, 2007.

[54] M. A. Sheikh and L. Li, "Understanding the effect of non-conventional laser beam geometry on material processing by finite-element modelling," *Journal of Mechanical Engineering Science,* vol. 224, no. 5, pp. 1061-1072, 2010.

[55] M. S. Jamil, M. A. Sheikh and L. Li, "A Numerical Study of the Temperature Gradient Mechanism in Laser Forming Using Different Laser Beam Geometries," *Lasers in Engineering,* vol. 22, no. 5, pp. 413-428, 2012.

[56] S. P. Edwardson, J. Griffiths, G. Dearden and K. G. Watkins, "Temperature Gradient Mechanism: Overview of the Multiple Pass Controlling Factors," *Physics Procedia,* p. 53–63, 2010.

[57] D. j. Wu, G. y. Ma, X. y. Wang and S. Liu, "Experiments and simulation on laser bending of silicon sheet with different thicknesses," *Applied Physics A,* vol. 101, no. 3, pp. 517-521, 2010.

[58] P. Cheng, Y. j. Fan, J. Zhang and Y. L. Yao, "Laser Forming of Varying Thickness Plate—Part II: Process Synthesis," *Journal of Manufacturing Science & Engineering,* vol. 128, pp. 642-650, 2006.

[59] S. P. Edwardson, K. R. Edwards, J. D. Griffiths and G. Dearden, "Laser forming: Overview of the controlling factors in the temperature gradient mechanism," *Journal of Mechanical Engineering Science,* vol. 224, no. 5, pp. 1031-1040, 2010.

[60] J. Griffiths, S. P. Edwardson, G. Dearden and K. G. Watkins, "Finite Element modelling of laser forming at macro and micro scales," *Physics Procedia,* pp. 371-380, 2010.

[61] R. Kant and S. N. Joshi, "Thermo-mechanical studies on bending mechanism, bend angle and edge effect during multi-scan laser bending of magnesium M1A alloy sheets," *Journal of Manufacturing Processes,* vol. 23, pp. 135-148, 2016.

[62] K. C. Lee and J. Lin, "Transient deformation of thin metal sheets during pulsed laser forming," *Optics & Laser Technology,* vol. 34, no. 8, pp. 639-648, 2002.

[63] E. G. Zahrani and A. Marasi, "Modeling and optimization of laser bending parameters via response surface methodology," *Journal of Mechanical Engineering Science,* vol. 227, no. 7, pp. 1577-1584, 2013.

[64] D. J. Chen, S. C. Wu and M. Q. Li, "Studies on laser forming of Ti–6Al–4V alloy sheet," *Journal of Materials Processing Technology,* vol. 152, no. 1, pp. 62-65, 2004.

[65] P. Cheng, Y. L. Yao, C. Liu, D. Pratt and Y. j. Fan, "Analysis and Prediction of Size Effect on Laser Forming of Sheet Metal," *Journal of Manufacturing Processes,* vol. 7, no. 1, pp. 28-41, 2005.

[66] Y. Shi, J. Hu and C. Dong, "Analysis of the geometric effect on the forming accuracy in laser forming," *Journal of Engineering Manufacture,* vol. 225, no. 10, pp. 1792-1800, 2011.

[67] G. Chen, X. Xu, C. C. Poon and A. C. Tam, "Experimental and numerical studies on microscale bending of stainless steel with pulsed laser," *Journal of Applied Mechanics,* vol. 66, no. 3, p. 772–779, 1999.

[68] S. P. Edwardson, E. Abed, K. Bartkowiak and G. Dearden, "Geometrical influences on multi-pass laser forming," *Journal of Physics D: Applied Physics,* vol. 39, no. 2, p. 382, 2006.

[69] C. Carey, W. J. Cantwell, G. Dearden, K. R. Edwards, S. P. Edwardson, J. D. Mullett, C. J. Williams and K. G. Watkins, "Effects of laser interaction with graphite coatings," in *Proceedings of the Laser Assisted Net Shape Engineering*, Erlangen, 2007.

[70] S. P. Edwardson, E. Abed, C. Carey, K. R. Edwards, G. Dearden and K. G. Watkins, "Factors influencing the bend per pass in multi-pass laser forming," in *Proceedings of Laser Assisted Net Shape Engingeering*, Erlangen, 2007.

[71] A. Chehrghani, M. J. Torkamany, M. J. Hamedi and J. Sabbaghzadeh, "Numerical modeling and experimental investigation of TiC formation on titanium surface pre-coated by graphite under pulsed laser irradiation," *Applied Surface Science,* vol. 258, no. 6, p. 2068–2076, 2012.

[72] K. Singh, A. K. Ray, S. N. Joshi and U. S. Dixit, "Effect of lime and graphite grease coatings on the absorptivity of mild steel sheet in line heating by CO2 laser," in *Proceedings of national conference on recent advancements in mechanical engineering*, Kanpur, 2013.

[73] P. P. Dutta, U. S. Dixit and K. Kalita, "Experimental investigation on laser bending of mild steel coated with black enamel paint," in *Proceedings of national conference on manufacturing: Vision for Future*, Kanpur, 2013.

[74] S. S. Gautam, S. K. Singh and U. S. Dixit, "Laser Forming of Mild Steel Sheets Using Different Surface Coatings," in *Lasers Based Manufacturing*, New Delhi, 2015.

[75] A. Bejan and K. D. Allan, Heat Transfer Handbook, New Jersey: WILEY, 2003.

[76] Y. j. Guan, S. Sun, G. q. Zhao and Y. g. Luan, "Finite element modeling of laser bending of pre-loaded sheet metals," *Journal of Materials Processing Technology,* vol. 142, no. 3, pp. 400-407, 2003.

[77] Y. j. Guan, S. Sun, G. q. Zhao and Y. g. Luan, "Influence of material properties on the laser-forming process of sheet metals," *Journal of Materials Processing Technology,* vol. 167, no. 1, pp. 124-131, 2005.

[78] J. Cheng and L. Yao, "Cooling Effects in Multiscan Laser Forming," *Journal of Manufacturing Processes,* vol. 3, no. 1, pp. 60-72, 2001.

[79] F. Lambiase, A. Ilio and A. Paoletti, "An experimental investigation on passive water cooling in laser forming process," *International Journal of Advanced Manufacturing Technology,* vol. 64, no. 5-8, pp. 829-840, 2013.

[80] R. Kant and S. N. Joshi, "Numerical Simulation of Multi-pass Laser Bending Processes using Finite Element Method," in *IRAM*, India, 2013.

[81] H. Shen, M. l. Ran, J. Hu and Z. q. Yao, "An experimental investigation of underwater pulsed laser forming," *Optics and Lasers in Engineering,* vol. 62, pp. 1-8, 2014.

[82] J. Magee and L. J. De Vin, "Process planning for laser-assisted forming," *Journal of Materials Processing Technology,* vol. 120, no. 1-3, pp. 322-326, 2002.

[83] A. H. Roohi, M. H. Gollo and H. M. Naeini, "External force-assisted laser forming process for gaining high bending angles," *Journal of Manufacturing Processes,* vol. 14, no. 3, pp. 269-276, 2012.

[84] F. Bammer, T. Schumi and B. Holzinger, "A Diode-Laser-System for Laser-AssistedBending of Brittle Materials," *Advances in Optical Technologies,* vol. 2011, pp. 1-4, 2011.

[85] S. Mueller, B. Kruck and P. Baudisch, "LaserOrigami: laser-cutting 3D objects," in *Conference on Human Factors in Computing Systems*, 2013.

[86] A. Gisario, M. Barletta and S. Venettacci, "Improvements in springback control by external force laser-assisted sheet bending of titanium and aluminum alloys," *Optics & Laser Technology,* vol. 86, pp. 46-53, 2016.

[87] A. J. Birnbaum, P. Cheng and Y. L. Yao, "Effects of Clamping on the Laser Forming Process," *Journal of Manufacturing Science and Engineering,* vol. 129, no. 6, pp. 1035-1044, 2007.

[88] R. Kant and S. N. Joshi, "Analysis of Sheet-holding Methods in Laser Bending Process," in *3rd Asian Symposium on Materials & Processing*, Chennai, 2012.

[89] J. Hu, H. Xu and D. Dang, "Modeling and reducing edge effects in laser bending," *Journal of Materials Processing Tech,* vol. 213, no. 11, pp. 1989-1996, 2013.

[90] G. Thomson and M. Pridham, "Material property changes associated with laser forming of mild steel components," *Journal of Materials Processing Tech,* vol. 118, no. 1-3, pp. 40-44, 2001.

[91] S. Jaap, Fatigue of Structures and Materials, London: Springer, 2008.

[92] P. J. McGrath and C. J. Hughes, "Experimental fatigue performance of laser-formed components," *Optics & Lasers in Engineering,* vol. 45, no. 3, pp. 423-430., 2007.

[93] J. Cheng and Y. L. Yao, "Microstructure integrated modeling of multiscan laser forming," *Journal of Manufacturing Science and Engineering,* vol. 124, no. 2, p. 379–388, 2002.

[94] Y. j. Fan, Z. s. Yang, P. Cheng, K. Egland and L. Yao, "Investigation of Effect of Phase Transformations on Mechanical Behavior of AISI 1010 Steel in Laser Forming," *Journal of Manufacturing Science and Engineering,* vol. 129, no. 1, pp. 110-116, 2007.

[95] G. J. Cheng, D. Pirzada and Z. Ming, "Microstructure and mechanical property characterizations of metal foil after microscale laser dynamic forming," *Journal of Applied Physics,* vol. 101, no. 6, pp. 345-360, 2007.

[96] F. c. Liu , X. Lin, M. h. Song and W. w. Zhao, "Effect of intermediate heat treatment temperature on microstructure and notch sensitivity of laser solid formed Inconel 718 superalloy," *Journal of Wuhan University of Technology-Mater. Sci.,* vol. 26, no. 5, p. 908–913, 2011.

[97] I. A. Palani, S. Naikwad, R. Padmanabhan, S. Shanmugam and H. Natu, "Parametric Investigation in Laser Forming of 8mm FE-410 Plate Using High Power CO2 Laser and Its Bend Angle Prediction," *Materials today: proceedings,* vol. 2, no. 4-5, pp. 2013-2021, 2015.

[98] H. Shen, J. Hu and Z. Q. Yao, "Cooling Effects in Laser Forming," *Materials Science Forum,* pp. 663-665, November 2010.

[99] R. Kant and U. Dixit, "State of the art and experimental investigation on edge effect in laser bending process," in *Proceedings of the National Conference on Recent Advances in Mechanical Engineering*, Pauri, 2013.

[100] J. c. Bao and Y. L. Yao, "Study of Edge Effects in Laser Bending," in *ASME International Mechanical Engineering Congress and Exposition*, Tennessee, 1999.

[101] J. c. Bao and Y. L. Yao, "Analysis and Prediction of Edge Effects in Laser Bending," *Journal of Manufacturing Science & Engineering,* vol. 123, no. 1, pp. 53-61, 2001.

[102] M. S. Jamil, Z. Samad, M. A. Sheikh and A. M. Najib, "Influence of non-conventional beam profile on edge effects in laser forming of AISI 304 stainless steel plate," *The International Journal of Advanced Manufacturing Technology,* vol. 104, p. 1593–1601, 2019.

[103] G. C. Jha, A. K. Nath and S. K. Roy, "Study of edge effect and multi-curvature in laser bending of AISI 304 stainless steel," *Journal of Materials Processing Tech,* vol. 197, no. 1-3, pp. 434-438, 2008.

[104] H. Shen, J. Hu and Z. Yao, "Analysis and control of edge effects in laser bending," *Optics and Lasers in Engineering,* vol. 48, no. 3, p. 305–315, 2010.

[105] M. Safari and M. Farzin, "A study on laser bending of tailor machined blanks with various irradiating schemes," *Journal of Materials Processing Technology,* vol. 214, no. 1, pp. 112-122, 2014.

[106] Y. Shi, X. Lu, Y. Liu and P. Yi, "Forming accuracy analysis of plate in multiscanning laser bending process," *Journal of Process Mechanical Engineering,* vol. 227, no. 3, p. 225–228, 2013.

[107] H. Shen and J. Hu, "Controlling edge effects in laser bending," *Applied Mechanics and Materials,* vol. 271, p. 1521–1525, 2013.

[108] F. Vollertsen, "An Analytical Model for Laser Bending," *Lasers in Engineering,* vol. 2, pp. 261-276, 1994.

[109] C. L. Yau, K. C. Chan and W. B. Lee, "Laser bending of lead frame materials," *Journal of Materials Processing Technology,* vol. 82, no. 1, p. 117–121, 1998.

[110] F. Lambiase, "An analytical model for evaluation of bending angle in laser forming of metal sheets," *Journal of materials engineering and performance,* vol. 21, no. 10, p. 2044–2052, 2012.

[111] Y. Shi, H. Shen, Z. Yao and J. Hu, "An analytical model based on the similarity in temperature distributions in laser forming," *Optics and lasers in engineering,* vol. 45, no. 1, pp. 83-87, 2007.

[112] T. Ueda, E. Sentoku, K. Yamada and A. Hosokawa, "Temperature measurement in laser forming of sheet metal," in *CIRP Annals*, 2005.

[113] M. H. Gollo, S. M. Mahdavian and H. M. Naeini, "Statistical analysis of parameter effects on bending angle in laser forming process by pulsed Nd:YAG laser," *Optics and Laser Technology,* vol. 43, no. 3, p. 475–482, 2011.

[114] A. Eideh, U. S. Dixit and R. Echempati, "A Simple Analytical Model of Laser Bending Process," in *Lasers Based Manufacturing*, Springer, 2015, pp. 1-15.

[115] H. G. Woo and H. S. Cho, "Three-dimensional temperature distribution in laser surface hardening processes," *Journal of Engineering Manufacture,* vol. 213, no. 7, p. 695–712, 1999.

[116] P. J. Cheng and S. C. Lin, "An analytical model for the temperature field in the laser forming of sheet metal," *Journal of Materials Processing Technology,* vol. 101, no. 1, p. 260–267, 2000.

[117] Z. H. Shen, S. Y. Zhang, J. Lu and X. W. Ni, "Mathematical modeling of laser induced heating and melting in solids," *Optics and laser technology,* vol. 33, no. 8, p. 533–537, 2001.

[118] Y. Shi, H. Shen, Z. Yao and J. Hu, "Temperature gradient mechanism in laser forming of thin plates," *Optics and Laser Technology,* vol. 39, no. 4, p. 858–863, 2007.

[119] V. Kumar and U. S. Dixit, "Selection of process parameters in a single-pass laser bending process," *Engineering Optimization,* vol. 50, no. 9, p. 1–16, 2018.

[120] Z. Hu, M. Labudovic, H. Wang and R. Kovacevic, "Computer simulation and experimental investigation of sheet metal bending using laser beam scanning," *International Journal of Machine Tools and Manufacture,* vol. 41, no. 4, pp. 589-607, 2001.

[121] F. Vollertsen, M. Geiger and W. M. Li, "FDM and FEM simulation of laser forming: a comparative study," in *Proceedings of the fourth international conference on technology of plasticity*, Beijing, 1993.

[122] X. R. Zhang and X. Xu, "Laser bending for high-precision curvature adjustment of microcantilevers," *Applied Physics Letters,* vol. 86, no. 2, 2005.

[123] S. Safdar, L. Li, M. A. Sheikh and Z. Liu, "Finite element simulation of laser tube bending: Effect of scanning schemes on bending angle, distortions and stress distribution," *Optics and Laser Technology,* vol. 39, no. 6, p. 1101–1110, 2007.

[124] S. Holzer, H. Arnet and M. Geiger, "Physical and numerical modelling of the buckling mechanism," in *Proceedings of the LANE*, Erlangen, 1994.

[125] G. N. Labeas, "Development of a local three-dimensional numerical simulation model for the laser forming process of aluminium components," *Journal of materials processing technology,* vol. 207, no. 1, p. 248–257, 2008.

[126] B. S. Yilbas and S. S. Akhtar, "Laser bending of metal sheet and thermal stress analysis," *Optics and Laser Technology,* vol. 61, p. 34–44, 2014.

[127] I. Pitz, A. Otto and M. Schmidt, "Simulation of the laser beam forming process with moving meshes for large aluminium plates," *Physics Procedia,* p. 363–369, 2010.

[128] G. Yu, K. Masubuchi, T. Maekawa and N. M. Patrikalaki, "FEM Simulation of laser forming of metal plates," *Journal of Manufacturing Science and Engineering,* vol. 123, no. 3, p. 405–410, 2001.

[129] X. R. Zhang, G. Chen and X. Xu, "Numerical simulation of pulsed laser bending," *Journal of Applied Mechanics,* vol. 69, no. 3, p. 254–260, 2002.

[130] L. Zhang, E. W. Reutzel and P. Michaleris, "Finite element modeling discretization requirements for the laser forming process," *International Journal of Mechanical Sciences,* vol. 46, no. 4, p. 623–637, 2004.

[131] J. Hu, D. Dang, H. Shen and Z. Zhang, "A finite element model using multi-layered shell element in laser forming," *Optics and Laser Technology,* vol. 44, no. 4, p. 1148–1155, 2012.

[132] M. Barletta, A. Gisario and S. Guarino, "Hybrid forming process of AA6108 T4 thin sheets: modelling by neural network solutions," *Journal of Engineering Manufacture,* vol. 223, no. 5, p. 535–545, 2009.

[133] P. J. Cheng and S. C. Lin, "Using neural networks to predict bending angle of sheet metal formed by laser," *International Journal of Machine Tools and Manufacture,* vol. 40, no. 8, p. 1185–1197, 2000.

[134] V. Dragos, V. Dan and R. Kovacevic, "Prediction of the laser sheet bending using neural network," in *IEEE International Symposium on Circuits and Systems*, Geneva, 2000.

[135] G. Casalino and A. D. Ludovico, "Parameter selection by an artificial neural network for a laser bending process," *Journal of Engineering Manufacture,* vol. 216, no. 11, p. 1517–1520, 2002.

[136] K. Maji, D. K. Pratihar and A. K. Nath, "Analysis and synthesis of laser forming process using neural networks and neuro-fuzzy inference system," *Soft Computing,* vol. 17, no. 5, p. 849–865, 2013.

[137] K. Maji, D. K. Pratihar and A. K. Nath, "Laser forming of a dome shaped surface: Experimental investigations, statistical analysis and neural network modeling," *Optics and Lasers in Engineering,* vol. 53, p. 31–42, 2014.

[138] K. Maji, D. K. Pratihar and A. K. Nath, "Analysis of pulsed laser bending of sheet metal using neural networks and neuro-fuzzy system," *Journal of Engineering Manufacture,* vol. 228, no. 9, p. 1015–1026, 2014.

[139] J. A. Pérez, M. González and D. Dopico, "Adaptive neurofuzzy ANFIS modeling of laser surface treatments," *Neural Computing and Applications,* vol. 19, no. 1, p. 85–90, 2010.

[140] S. Jovic, S. Makragic and M. Jovanovic, "Parameters influence of laser forming on shaped surface by soft computing technique," *International Journal for Light and Electron Optics,* vol. 142, p. 451–454, 2017.

[141] J. G. Cheng and Y. L. Yao, "Process synthesis of laser forming by genetic algorithm," *International Journal of Machine Tools and Manufacture,* vol. 44, no. 15, p. 1619–1628, 2004.

[142] Y. Du, X. Wang and J. Silvanus, "Improved BP network to predict bending angle in the laser bending process for sheet metal," in *Intelligent Systems Design and Applications*, Springer, 2010, p. 839–843.

[143] R. Aster, Parameter Estimation and Inverse Problems, Amsterdam: Elsevier, 2019.

[144] A. Eideh and U. S. Dixit, "A robust and efficient inverse method for determining the thermal parameters during laser forming," in *Proceedings of National Conference of Recent Advancements in Mechanical Engineering*, 2013.

[145] G. Romer and J. Meijer, "Inverse calculation of power density for laser surface treatment," in *Annals of the CIRP*, 2000.

[146] H. K. Kim and S. I. Oh, "Evaluation of heat transfer coefficient during heat treatment by inverse analysis," *Journal of Materials Processing Technology,* vol. 112, pp. 157-165, 2001.

[147] P. L. Woodfield, M. Monde and Y. Mitsutake, "On estimating thermal diffusivity using analytical inverse solution for unsteady one-dimensional heat conduction," *International Journal in Heat and Mass transfer,* vol. 50, p. 1202–1205, 2007.

[148] A. Shidfar, B. Jazbi and M. Alinejadmofrad, "Inverse estimation of pulse parameters of a time-varying laser pulse to obtain desired temperature at the material surface," *Optics and Laser Technology,* vol. 44, p. 1675–1680, 2012.

[149] A. Mishra and U. S. Dixit, "Determination of thermal diffusivity of the material, absorptivity of the material and laser beam radius during laser forming by inverse heat transfer," *Journal of Machining and Forming Technology,* vol. 5, no. 3-4, pp. 208-226, 2013.

[150] W. Xu, L. C. Zhang and X. Wang, "Laser bending of silicon sheet: absorption factor and mechanisms," *Journal of Manufacturing Science and Engineering,* vol. 135, no. 6, 2013.

[151] C. Liu and Y. L. Yao, "Optimal and robust design of the laser forming process," *Journal of Manufacturing Processes,* vol. 4, no. 1, p. 52–66, 2002.

[152] F. Pukelsheim, Optimal Design of Experiments, Society for Industrial and Applied Mathematics, 2006.

[153] J. Kim and S. J. Na, "Development of irradiation strategies for free curve laser forming," *Optics & Laser Technology,* vol. 35, no. 8, p. 605–611, 2003.

[154] H. Shen, Y. Shi and Z. Yao, "Laser Forming of Plates Using Two Sequent Scans of Different Intervals," *Journal of Mechanical Engineering Science,* vol. 220, no. 4, pp. 507-511, 2006.

[155] G. Thomson and M. Pridham, "A feedback control system for laser forming," *Mechatronics,* vol. 7, no. 5, p. 429–441, 1997.

[156] J. Kim and S. J. Na, "Feedback control for 2d free curve laser forming," *Optics & Laser Technology,* vol. 37, no. 2, p. 139–146, 2005.

[157] J. Kim and S. J. Na, "3D laser-forming strategies for sheet metal by geometrical information," *Optics & Laser Technology,* vol. 41, no. 6, p. 843–852, 2009.

[158] R. Goldman, "Curvature formulas for implicit curves and surfaces," *Computer Aided Geometric Design,* vol. 22, no. 7, p. 632–658, 2005.

[159] C. Liu, Y. L. Yao and V. Srinivasan, "Optimal process planning for laser forming of doubly curved shapes," *Journal of manufacturing science and engineering,* vol. 126, no. 1, pp. 1-9, 2004.

[160] H. Gao, G. Sheikholeslami, G. Dearden and S. P. Edwardson, "Development of scan strategies for controlled 3d laser forming of sheet metal components," *Physics Procedia,* p. 286–295, 2016.

[161] H. Gao, G. Sheikholeslami, G. Dearden and S. P. Edwardson, "Reverse analysis of scan strategies for controlled 3d laser forming of sheet metal," *Procedia Engineering,* p. 369–374, 2017.

[162] H. Shen, W. Zhou and H. Wang, "Laser forming of doubly curved plates using minimum energy principle and comprehensive strain control," *International Journal of Mechanical Sciences,* vol. 145, p. 42–52, 2018.

[163] H. Shen, H. Wang and W. Zhou, "Process modelling in laser forming of doubly-curved sheets from cylinder shapes," *Journal of Manufacturing Processes,* vol. 35, p. 373–381, 2018.

[164] L. Yang, M. Wang, Y. Wang and Y. Chen, "Dynamic analysis on laser forming of square metal sheet to spherical dome," *The International Journal of Advanced Manufacturing Technology,* vol. 51, no. 5-8, p. 519–539, 2010.

[165] M. Safari and M. Farzin, "Experimental investigation of laser forming of a saddle shape with spiral irradiating scheme," *Optics & Laser Technology,* vol. 66, p. 146–150, 2015.

[166] M. H. Gollo, G. Nadi, M. Mehdi and M. Abbaszadeh, "Experimental and numerical study of spiral scan paths on cap laser forming," *Journal of Laser Applications,* vol. 27, no. 1, pp. 1-9, 2015.

[167] E. Abed, S. P. Edwardson, G. Dearden and K. G. Watkins, "Geometrical based control method for 3d laser forming," in *Laser Assisted Net Shape Engineering*, Erlangen, 2007.

[168] J. Magee, "Laser Forming of Aerospace Alloys," University of Liverpool, Liverpool, 1999.

[169] E. Abed, "Modelling and Experimental Investigation of 3D Laser Forming of Metallic Components," University of Liverpool, Liverpool, 2007.

[170] C. Carey, "Laser Forming of Fibre Metal Laminates," University of Liverpool, Liverpool, 2009.

[171] J. D. Griffiths, "Modelling of Laser Forming at Macro and Micro Scales," University of Liverpool, Liverpool, 2012.

[172] A. E. Siegman, "How to Measure Laser Beam Quality," Stanford University, California, 1997.

[173] F. Brueckner, R. Mirko, M. Müller and F. Marquardt, "Enhanced manufacturing possibilities using multi-materials in Laser Metal Deposition," *Journal of Laser Applications,* vol. 30, no. 3, 2018.

[174] W. Material, "EN 10130 DC01 Steel 1.0330+ZE Material Data Sheet Equivalent, Properties," 2022. [Online]. Available: https://www.theworldmaterial.com. [Accessed 12 April 2021].

[175] J. Hirsch, B. Skrotzki and G. Gottstein, Aluminium Alloys: The Physical and Mechanical Properties, Weinheim: Wiley-VCH, 2008.

[176] P. V. Steels, "S235, S275 and S355 Structural Steels," 2018. [Online]. Available: https://www.azom.com. [Accessed 15 April 2021].

[177] COMSOL, "Comsol Multiphysics User´s Guide VERSION 5.2a," 2016. [Online]. [Accessed 25 April 2021].

[178] C. Allison, "Meshing in FEA: Introduction to meshing," 18 March 2020. [Online]. Available: https://onscale.com/. [Accessed 15 April 2021].

[179] L. Yuan and Z. Tong, "Analysis of Influence of Time Step on Numerical Simulation Using Finite Volume Method," *China Academic Journal Electronic Publishing House,* vol. 3, pp. 117-120, 2009.

[180] Raunek, "The Ultimate Guide to Ship Sizes," 22 February 2022. [Online]. [Accessed 20 April 2022].

[181] C. Liu and Y. L. Yao, "FEM-Based Process Design for Laser Forming of Doubly Curved Shapes," *Jounal of Manufacturing Processes,* vol. 7, no. 2, pp. 109-121, 2005.

[182] TWI, "WHAT IS RESIDUAL STRESS," 2022. [Online]. Available: https://www.twi-global.com. [Accessed 15 April 2022].

[183] W. Material, "EN 10130 DC01 Steel 1.0330+ZE Material Data Sheet Equivalent, Properties," 2022. [Online]. Available: https://www.theworldmaterial.com/din-en-10130-dc01-steel-1-0330-material-datasheet/#DC01_Meaning_and_Definition. [Accessed 12 April 2022].

[184] TWI, "WHAT IS RESIDUAL STRESS?," 2022. [Online]. Available: https://www.twi-global.com/technical-knowledge/faqs/residual-stress. [Accessed 15 April 2022].

[185] L. Yuan and Z. Tong, "Analysis of Influence of Time Step on Numerical Simulation Using Finite Volume Method," *China Academic Journal Electronic Publishing House,* vol. 3, pp. 117-120, 2009.

[186] J. Hirsch, B. Skrotzki and G. Gottstein, Aluminium Alloys: The Physical and Mechanical Properties, 1st ed., Weinheim: Wiley-VCH, 2008.

[187] Pressure Vessel Steels, "S235, S275 and S355 Structural Steels," 2018. [Online]. Available: https://www.azom.com/article.aspx?ArticleID=15176. [Accessed 15 April 2022].

[188] Raunek, "The Ultimate Guide to Ship Sizes," 22 February 2022. [Online]. Available: https://www.marineinsight.com/. [Accessed 20 April 2022].

[189] W. g. Li, X. h. Zhang, H. b. Kou and R. z. Wang, "Theoretical prediction of temperature dependent yield strength for metallic materials," *International Journal of Mechanical Sciences,* vol. 105, pp. 273-278, 2016.

[190] F. Pukelsheim, Optimal Design of Experiments, Philadelphia: Society for Industrial and Applied Mathematics, 2006.

[191] A. E. Siegman, "How to MeasureLaser Beam Quality," Stanford University, California, 1997.

[192] H. Shen, Y. j. Shi and Z. q. Yao, "Numerical simulation of the laser forming of plates using two simultaneous scans," *Computational Materials Science,* vol. 37, no. 3, pp. 239-245, 2006.

[193] S. S. Chakraborty, K. Maji, V. Racherla and A. K. Nath, "Investigation on laser forming of stainless steel sheets under coupling mechanism," *Optics & Laser Technology,* vol. 71, pp. 29-44, 2015.

[194] U. S. Dixit, S. N. Joshi and R. Kant, "Laser forming systems: a review," *International Journal of Mechatronics and Manufacturing Systems,* vol. 8, no. 3-4, pp. 160-205, 2015.

[195] V. I. Mazhukin, M. G. Lobok and I. Smurov, "Transient effects in pulsed laser," *Applied Surface Science,* vol. 253, no. 19, pp. 7744-7748, 2007.

[196] R. Kant, S. N. Joshi and U. S. Dixit, "An integrated FEM-ANN model for laser bending process with inverse estimation of absorptivity," *Mechanics of Advanced Materials and Modern Processes,* vol. 1, no. 6, pp. 1-12, 2015.

[197] "Studies on laser forming of Ti–6Al–4V alloy sheet," *Journal of Materials Processing Technology,* vol. 152, no. 1, pp. 62-65, 2004.

[198] K. Samm, M. Terzi, A. Ostendorf and J. Wulfsberg, "Laser-assisted micro-forming process with miniaturised structures in sapphire dies," *Applied Surface Science,* vol. 255, no. 24, pp. 9830-9834, 2009.

[199] A. Gisario, M. Barletta, C. Conti and S. Guarino, "Springback control in sheet metal bending by laser-assisted bending: Experimental analysis, empirical and neural network modelling," *Optics and Lasers in Engineering,* vol. 49, no. 12, pp. 1372-1383, 2011.

[200] J. Liu, S. Sun and Y. j. Guan, "Numerical investigation on the laser bending of stainless steel foil with pre-stresses," *Journal of Materials Processing Technology,* vol. 209, no. 3, pp. 1580-1587, 2009.

[201] L. Chao and Y. L. Yao, "Optimal and Robust Design of the Laser Forming Process," *Journal of Manufacturing Processes,* vol. 4, no. 1, pp. 52-66, 2002.

[202] R. Kant, S. N. Joshi and U. S. Dixit, "State of the Art and Experimental Investigation on Edge Effect in Laser Bending Process," in *National Conference on Recent Advancement in Mechanical Engineering*, Nirjuli, 2013.

[203] E. G. Zahrani and A. Marasi, "Experimental investigation of edge effect and longitudinal distortion in laser bending process," *Optics & Laser Technology,* vol. 45, pp. 301-307, 2013.

[204] P. P. Dutta, U. S. Dixit and K. Kalita, "A strategy for achieving accurate bending by multi-pass laser line heating," *International Journal of Mechatronics and Manufacturing Systems,* vol. 10, no. 4, p. 277–298, 2017.

[205] M. Van Elsen, M. Baelmans, P. Mercelis and J. P. Kruth, "Solutions for modelling moving heat sources in a semi-infinite medium and applications to laser material processing," *International Journal of heat and mass transfer,* vol. 50, no. 23, p. 4872–4882, 2007.

[206] K. Maji, S. S. Chakraborty, D. K. Pratihar and A. K. Nath, "Inverse analysis and multi-objective optimization of coupling mechanism based laser forming process," *Sadhana,* vol. 45, no. 8, pp. 1-16, 2020.